Dynamics And Control Of

A Two Link Flexible Planar Manipulator

by

Songping Yu, B. Eng., M.Sc.Eng.

A Thesis

Submitted to the School of Graduate Studies

in Partial Fulfilment of the Requirements

for the Degree

Doctor of Philosophy

McMaster University

Dynamics And Control Of

A Two Link Flexible Planar Manipulator

DOCTOR OF PHILOSOPHY (1994) McMaster University
(Mechanical Engineering) Hamilton, Ontario

TITLE: Dynamics and Control of A Two Link Flexible Planar Manipulator

AUTHOR: Songping Yu, B. Eng. (Jilin University of Technology)
M.Sc.Eng. (University of New Brunswick)

SUPERVISOR: Professor M.A. Elbestawi

NUMBER OF PAGES: xvi, 201

To My Wife

ACKNOWLEDGEMENTS

I would like to thank Dr. M.A. Elbestawi for his guidance and for suggesting the research topic. I would also like to extend my appreciation and gratitude to all members of my supervisory committee for their interest in my work and their helpful comments.

Special thanks go to the Department of Mechanical Engineering at McMaster University for providing me with financial support throughout the duration of my thesis work. The help of their technical staff, J. Verhaegh, D. Schick, and R. Lodewyks, is very much appreciated.

ABSTRACT

A lightweight manipulator has many desirable features. The structural flexibility associated with lightweight manipulators often results in mechanical vibrations and consequently leads to long settling times and position inaccuracy. The aim of the current study is to investigate the dynamics of a two degree of freedom manipulator with elastic joints and very flexible arms and develop a proper control strategy. The dynamic model of the manipulator is derived with the Lagrangian formulation and the assumed-modes approach. The eigenvalues and eigen-functions of the flexible arms are determined by the transfer matrix method. The dynamic effects of friction at the joints, gear backlash within the actuation, and internal structural damping of the arms are all considered. The derived theoretical model is verified by experiments.

The parametric analysis is designed to examine the effects of the major system parameters on the dynamic performance of the manipulator. The dynamic interactions between the members of the manipulator are also investigated.

The power balancing technique is extended for distributed parameter systems and a new approach for model order reduction of nonlinear systems is

proposed. Using the derived power elements of the original system states as a criterion, the model reduction is performed in the original physical coordinates. The proposed technique is applied to the manipulator. It is found that the bending vibrations of the flexible link are dominated by its first two natural modes. The contributions of the higher modes are negligible.

A model reference adaptive control algorithm originally developed by Sobel is modified and used for the control of the manipulator with an unknown payload. It is shown that the modification improves the algorithm's performance significantly. Computer simulations are performed to examine the algorithm's properties and select proper values for the gain matrices. Real-time testing is implemented to validate the theoretical analysis. It is found that the proposed algorithm provides satisfactory performance of the closed-loop system.

Table Of Contents

List Of Figures

Figure Page

List Of Tables

Chapter 1

INTRODUCTION

Traditional robots have been designed for "rigidity" with short arms and heavy structure, which significantly restrict their range of applications. Lightweight manipulators with lower arm cost, higher motion speed, better energy efficiency, safer operation, and improved mobility are highly desirable. However, lightweight construction of manipulator often results in increased structural flexibilities and consequently leads to long settling times and position inaccuracy. The increased flexibilities must be considered in the design of control systems in order to properly account for the dynamic flexible vibrations and static deflections.

The dynamic modelling and performance control of flexible manipulators have been an active research field in recent years. A large amount of research work has been done in the area. The flexibilities of a manipulator are considered from the non-rigidity of power transmission chain at joints and the distributed structural elasticity of arms. Due to the complexity of the problem, the structural patterns of flexible manipulators have been intentionally classified into three basic categories: manipulators with flexible joint(s), manipulators with flexible link(s), and

manipulators with both flexible joint(s) and link(s). The majority of the research so far has concentrated on the first two structural patterns.

For the dynamic modelling, the elastic joint of a manipulator is usually approximated by a linear torsional spring and its flexible arm is regarded as a slender Euler-Bernouli beam. Having the same degree of freedom, a manipulator with flexible links features a much more complex dynamic model than the one with non-rigid joints, and the model's order is also much higher. This is why the structure patterns of flexible link manipulator under research are still limited to one or two degrees of freedom, while many results on multi-flexible-joint manipulators have been reported. Some research efforts have been made on a manipulator with multi-flexible-links, or on those with both joint and link flexibilities. Usually they are limited to numerical simulations.

The manipulator considered in the current study is a flexible planar manipulator with two degrees of freedoms. It consists of two non-rigid joints and two flexible links. The objective of the study is to investigate the dynamic characteristics of the manipulator, control its lateral vibrations, and ultimately optimize its performance. The research work consists of dynamic modelling, model verification, parametric analysis, model linearization, model order reduction, control strategy development, control simulations, and real-time testing. The development of the experimental facility hardware is also a part of the research.

The thesis consists of eight chapters. Chapter 2 presents a literature review of the research area under consideration. Various dynamic modelling techniques and control algorithms are discussed and summarized. The theoretical dynamic

equations of the manipulator are derived in Chapter 3. The dynamic effects of the link's internal structural damping, the backlash between the driving gears, and the dry friction at the joints are all considered in the derived model. The experimental verification of the derived model is presented in Chapter 4, which includes the design and development of the experiment facility hardware. Model verification is performed by comparing the dynamic simulation results with the experimental data. Chapter 5 reports the results of a parametric analysis of the manipulator main design variables. The effects of the system parameters on the manipulator's dynamics and the dynamic interactions between the members of the manipulator are investigated. In Chapter 6, the nonlinear dynamic equations of the manipulator derived in Chapter 3 are first linearized. A new method for model order reduction of nonlinear dynamic systems is then developed and applied to the manipulator. It is found that the first two vibration modes of each link dominate its bending motions and the contributions of higher vibration modes are negligible. Chapter 7 addresses the control issues of the manipulator. A model reference adaptive algorithm is used to control the lateral vibrations. The algorithm's performance is evaluated through numerical simulations. The real-time testing is conducted to validate the simulation results. The thesis is concluded in Chapter 8. The major contributions of the current study and some recommendations for further research are outlined.

LITERATURE REVIEW

2.1 Introduction

There is a large body of research results available in the open literature related to flexible manipulators. The structural patterns of the flexible manipulators under research vary from case to case, and the proposed control techniques are widely scattered. So far, most of research has concentrated on flexible manipulators with relative simple structures such as one link flexible manipulators having uniform cross-section. Very little efforts has been reported which deals with flexible manipulators with more complex structures. This chapter will give a comprehensive literature review of the area, which includes dynamic modelling techniques, model reduction methods, control strategies, and on-line parameter estimation algorithms.

Starting with the next section, the dynamic modelling techniques applied to flexible manipulators are discussed. Different model order reduction methods are examined in Section 2.3. In Section 2.4, the proposed control strategies are

reviewed. The on-line parameter estimation algorithms developed for flexible manipulators are summarized in Section 2.5. Other aspects of flexible manipulators are covered by Section 2.6. Some concluding remarks are given in Section 2.7.

2.2 Dynamic Modelling

Many modelling techniques have been proposed in the literature to investigate the dynamic characteristics of flexible manipulators, such as the Lagrangian-Euler assumed-modes method, the Newton-Euler formulation [1,2], the Timoshenko beam theory [1], the recursive lumped mass/spring approximation [69], and Kane's method [27]. The Lagrangian-Euler assumed-modes method is one of the most popular techniques. Considering the flexible arm as a Euler-Bernoulli beam, the natural frequencies and mode shapes of the arm are determined under certain boundary conditions. The dynamic equations are derived on the energy conservation basis. For manipulators with flexible joint(s), the dynamic modelling is based on approximating the non-rigid joint as a linear torsional spring. The dynamic equations are usually developed with the Lagrangian formulation.

2.2.1 Manipulators With Flexible Joint(s)

Marino and Nicosia [3] developed a dynamic model for a manipulator with $N+1$ rigid links and N flexible joints. Friction effects and viscous phenomena were neglected. The equations of motion were given as:

$$B(^1q)\,\ddot{q} + a(^1q, {}^1\dot{q}) + e(^2q) = \begin{bmatrix} u \\ -u \end{bmatrix} \tag{2.1}$$

The term $e(^2q)$ is in the form of $(0, \ldots, 0, k_1q_{N+1}, \ldots, k_Nq_{2N})$, which accounts for the joint flexibility. If the joints are rigid ($k_i=\infty$, $i=1, \ldots, N$), the equations of motion can be obtained by imposing the constraint $^2q(t)=0$ for $t>0$, where $^2q = (q_{N+1}, \ldots, q_{2N})$, denotes the elastic displacement of an actuated link with respect to its actuator.

Spong [4] modelled the elastic joints of robotic manipulators as linear torsional springs and derived the dynamic equations by using the Lagrangian formulation. It was assumed that the motion of the rotor is a pure rotation with respect to an inertial frame and the rotor/gear inertia is symmetric about the rotor axis of rotation.

2.2.2 Manipulators With Flexible Link(s)

The majority of the research in the field has concentrated on this case. With the Lagrangian-Euler assumed-modes method, the dynamic models of one link flexible manipulators having uniform cross-section can be derived and the linearized version of the original nonlinear equations can be expressed in the form of [5 - 16]

$$\left.\begin{aligned} \dot{x} &= Ax + Bu \\ y &= Cx \end{aligned}\right\} \tag{2.2}$$

where x is the state variable vector, y is the output vector, and u is the system input. The model (2.2) is only capable of fitting the first finite number of infinite natural modes of a flexible link. The effects of the higher natural modes are assumed to be negligible. The method of determining the proper truncation of the

infinite natural modes is an important aspect of the dynamic analysis, which significantly affects the model's accuracy. Most of the models existing in the literature only include the first two or three vibration modes. Increasing the vibration modes included in the analysis certainly improves the model accuracy, but it also increases the model's order and complicates the corresponding controller design.

Using the same method, Kojima [17] derived a dynamic model for a one link flexible robot arm with variable cross-section. The internal viscous damping effect of the link was considered. It was pointed out that the variable cross-section arms have some favourable characteristics such as high structure strength, vibration suppression and small amount of inertia. An issue on the length changing of a flexible link undergoing deflection was raised by Oakley and Cannon [18]. When the assumed-modes method is used to model the bending deflection of a flexible link, the mode shapes are generally described as the function of the distance x along an undeflected axis and x is assumed to range from zero to the projected length of the deflected arm (of length L) onto the undeflected axis. Under this approximation, the endpoint may actually appear to go outside the workspace. A solution of assuming that the mode shapes depend on the arc length of the deflected axis was proposed and it was verified through numerical simulations.

The dynamic model of a spherical co-ordinate robot with the last link being very flexible was developed by Chalhoub [19]. The assumed-modes method was applied to describe the bending deflection of the arm and the Lagrangian formulation was used to derive the unconstrained equations of motion. The

kinematic constraints associated with a leadscrew were introduced to investigate the behaviour of a leadscrew driven flexible robot arm in the presence of the coulomb friction and the self locking condition. The length of the part of the second arm (flexible) protruding from the first arm was assumed being constant for the simplicity of the model.

Naganathan and Soni [20] applied the finite element technique to model a spatial manipulator with link flexibility. The model obtained accounts for the effects of rotatory inertia, shear deformation, and the effects of the gross nonlinear motion. The flexible arm was modelled using the Timoshenko theory and the finite element scheme was developed using Galerkin's technique.

A general discussion of the dynamic modelling of flexible manipulators with the Lagrangian assumed-modes approach was presented by Nicosia et al. [21]. The properties of the dynamic model, such as controllability, were examined. Low and Vidyasagar [22] reported the dynamic analysis results of flexible manipulators with open and closed chain mechanisms. Only the last link of the manipulators was considered to be flexible. The dynamic equations were obtained with the Lagrangian equation and several different robot structures were examined.

The derivation of the transfer function for a single flexible link was investigated by Wang and Vidyasagar [23]. It was found that if the output is defined as the net tip deflection, the relative degree of the transfer function is not well-defined as the number of modes approaches infinity. A new approach was proposed to overcome this drawback by defining the output as the rigid body deflection minus the elastic deflection. The relative degree of the transfer function obtained with the new approach is independent of the number of the modes used.

Based on the Newton-Euler inverse algorithm, an iterative scheme for the inverse dynamics of a multi-link elastic robot was developed by Bayo et al. [24] with the finite element technique. The iterative solution scheme relies on the local linearization of the robot trajectory, which was carried out in the frequency domain. An inverse dynamic algorithm in the time domain for a flexible manipulator was proposed in [25]. The numerical simulations were conducted for a single link flexible robot. The extension of the algorithm to a multi-link flexible manipulator was discussed.

Using the Euler-Lagrangian formulation and the Newton-Euler technique, Cyril et al. [26] performed the dynamic modelling of a manipulator with the distributed link flexibility. Both bending and torsional motions were considered. The advantages and the disadvantages of both methods were summarized. Neither numerical simulation nor experimental investigation were conducted to verify the discussion.

Everett [27] extended Kane's method for the derivation of the dynamic equations for flexible manipulators. Only the general modelling procedure was presented. Using the assumed-modes approach in conjunction with Kane's dynamic equation, Oakley and Cannon [28] derived the dynamic model for a two-link flexible manipulator. A different method of representing the spatial mode shapes of the manipulator, called the system modes representation, was described. The theoretical model was verified with experimental results.

Yuh et al. [29] performed dynamic modelling of a flexible link with a prismatic driving joint. The assumed-modes approach and the Lagrangian formulation were used. The flexible arm was considered as a cantilever beam with

a changing length. The model was verified experimentally. The exact modelling of a flexible slewing link was presented by Bellezza et al. [30]. Two different boundary conditions, pseudo-clamped and pseudo-pinned, were considered and an experimental verification was presented.

With an equivalent rigid link system (ERLS), the dynamic equations of a single-link flexible manipulator were obtained in [31] by using the finite element technique. The Lagrangian equation was applied and the joint variable and nodal displacements were chosen as the generalized coordinates. The model was verified experimentally. The concept of ERLS was also used by Chang and Hamilton to perform the kinematic [32] and dynamic [33] analysis of flexible manipulators. The ERLS was used to separate the rigid-body dynamics from the flexible structural dynamics. The finite element technique and the Lagrangian formulation were utilized.

The dynamic equations of a rotating flexible beam were obtained by Choura et al. [34] with the Lagrangian assumed-modes approach. The effects of the rotating speed on the dynamic model were investigated. It was concluded that the "simple-flexure" model should suffice for control applications when the maximum speed of rotation is kept below the first natural frequency of flexure.

2.2.3 Manipulators With Both Link And Joint Flexibility

There are several papers which deal with modelling the dynamic characteristics of flexible manipulators in a more general sense. Fukuda and Arakawa [35] considered the dynamics of a link which vibrates both transversely

and torsionally. The torsional vibration of robotic arms may be caused by the fact that the centre of gravity of a payload deviates from the axial centre of the arm. With the assumed-modes approach for both the torsional vibrations and the transverse deflections, the dynamic equations of the link were developed.

Applying the finite element technique, Dado and Soni [36] obtained a dynamic model which includes joint flexibility and link flexibility. The links experience bending in two planes as well as axial and torsional vibrations. The link's cross-section was considered to vary linearly along the axis. The effects of gear train, shaft inertia, shaft flexibility, and bearing's dry friction were all included by the model.

Low and Vidyasagar [37] presented a systematic approach of applying the Lagrangian equation to derive the equations of motion for robotic manipulators with elastic links. The formulation is based on expressing the kinetic and potential energies of a manipulator system in terms of the generalized coordinates. In the case of flexible links, the mass distribution and flexibility are taken into account. The dynamic equations of a two-link planar manipulator with one rigid link and one elastic link were developed as an example.

Lin and Yuan [38] derived a dynamic model for a flexible robotic manipulator by the Lagrangian-Euler assumed-modes approach. The model fits both the link's bending deflection and the joint's torsional vibration. The deformation of a link from its rigid body position was expressed by a homogeneous 4x4 transformation matrix composed of the summation of the link's assumed modes. The joint flexibility was approximated by a linear torsional spring with known characteristics.

Dado and Soni [39] presented a finite element technique to perform the forward and inverse dynamic analysis of elastic manipulators. The flexible link was modelled with line elements and the elastic joint was regarded as a linear torsional spring. Yang and Donath [40] reported their simulation results on the dynamic modelling of a two link robotic manipulator with both link and joint flexibility. Based on the assumption of small angle rotation for the joints and small bending deflection of the links, the dynamic equations were derived with the use of the Lagrangian formulation. The effect of the internal structural damping was not considered.

2.2.4 Modelling Of Internal Structural Damping And Gear Backlash

Several papers, which concentrate on the damping features of cantilever beams, are reviewed here. Baker et al. [41] introduced both the internal and external damping effects into the dynamic equations of a thin cantilever beam with free transverse vibrations. The internal damping was regarded as viscous and the external air damping coefficient was defined as the function of air density, surface area normal to the flow, and air drag coefficient. The internal damping problem in cantilever beams was also discussed by Zhang [42]. The damping was considered to be proportional and a concrete model of a flexible beam with end mass and internal damping was developed.

Kataoka et al. [43] conducted both an experimental investigation and a numerical simulation study on the backlash effects on the forced torsional vibrations of a two degree of freedom system. Based on the contact force being

considered as piece-wise continuous, the dynamic equations were derived. The simulation results were in agreement with experimental data.

The coefficient of restitution in vibro-impact system was interpreted as viscous damping by Hunt and Crossley [44] . The relation between the coefficient of restitution, impact speed and damping ratio was presented.

2.3 Model Reduction

Dynamic models for flexible manipulators are usually complex and of high order. A lower order model which retains the dominant features of the system is highly desirable for control purposes. The model order reduction itself is a large research area and considerable literature has been published. This section only discusses several popular approaches and their flexible manipulator related applications.

Various model reduction techniques have been proposed in the literature. Several popular ones include the balanced realization [45, 46], the Hankel norm optimal approximation [47], and the modal cost analysis [48]. Both the balanced realization and the Hankel norm optimal approximation are singular value based techniques. The balanced realization technique derives the reduced order model by truncating the weaker portion of the system from the reachability and observability point of view, while the Hankel norm optimal approximation approach obtains a lower order model by minimizing the Hankel norm error between the original system model and the reduced order model. The basic idea of the modal cost analysis is to decompose a norm of the response into contributions

from each co-ordinate of the original system and to find co-ordinates that contribute a small amount.

The balanced realization technique was applied to a one link flexible manipulator by Hastings et al. [49]. It was found that the dominant part of the dynamics for the flexible arm can be represented by three modes: the rigid mode and the first two flexible ones. With the modal cost analysis method, Tsujisawa and Book [50] performed the derivation of a reduced order model for a RALF (robotic arm, large and flexible) robot. It was shown that the reduced model, which consists of the first two modes of each link, is optimal from the control point of view. The reduced order model was evaluated by comparisons between the frequency responses and the model cost analysis results.

Fowler [51] presented a general discussion on the model reduction of systems described by ordinary differential equations. The reduction method was based on the partition of the state space into two orthogonal subspaces. The distance between the original and reduced systems is measured by an error norm corresponding to the energy. The optimal Hankel model reduction technique for non-minimum phase system was considered by Safonov et al. [52].

2.4 Control Strategies

The performance control of flexible manipulators plays a crucial role in the development of lightweight robots. The structural flexibilities associated with lightweight manipulators cause mechanical vibrations and lead to long setting time and position inaccuracy. The primary objective of the research in the area is to

control the mechanical vibrations of the manipulator and improve its positioning accuracy. However, the nonlinearity of the dynamic model and the non-colocated system structure make the control of flexible manipulators a very challenging research problem. Various control techniques have been proposed in the literature. Some popular approaches are reviewed in this section.

2.4.1 Optimal Control

Optimal control has been widely applied in the flexible manipulator area. It possesses the following desirable features [11]:

a. Optimal control can easily handle the uses of multiple sensors for feedback. It can also address the multi-input, multi-output control of a linearized dynamic model for a multi-link flexible robot.

b. An optimal controller permits trade-offs between endpoint speed of response, damping and available actuator power.

The selection of the performance index or the cost function of an optimal control algorithm directly determines the controller's performance. Usually, the cost function is defined on the basis of the performance requirements of the system, the desired control energy consumption, and other considerations. The control is "optimal" only in the sense of the pre-defined cost function.

Rovner and Cannon [53] reported their implementation of a Linear Quadratic Gaussian (LQG) control with a real time estimator on a very flexible one-link manipulator. The performance index of the LQG control consists of the weighted tip position and the weighted tip rate. The closed-loop bandwidth is

largely determined by the amount of weight placed on the tip rate. The final performance of the controller was evaluated in terms of step response. It was found that as the payload increases, the overshot becomes worse and the settling time is longer. Oakley and Cannon [18] also used a LQG algorithm for the endpoint control of a two-link manipulator with a very flexible forearm. The major consideration in the cost function was the endpoint performance and the control power consumption. By minimizing the cost function subject to the linearized state equations, the regulator gain matrix was determined. The performance of the manipulator with the LQG control was compared with the performance of a PD controller subject to tracking the commanded trajectory. It was shown that the manipulator performance was significantly improved by the LQG algorithm.

Emphasizing the smoothness of the control input, Carusone et al. [12] designed an optimal controller to perform the end-effector tracking control of a structurally flexible manipulator. The system performance with the proposed control strategy was evaluated through the end-effector tracking a square trajectory. The effects of structural flexibility, control robustness, and higher speed performance control were investigated.

Cannon and Schmitz [11] implemented endpoint control of a one-link flexible robot with an optimal control algorithm. Some interesting results were found. Good stability and response can be achieved for the flexible robot under the condition that a good model of the system is available, and the system is always conditionally stable. The achievable response time is physically limited by the wave propagation through the length of system members.

Tip position control of a flexible, single link manipulator was carried out by Ramakrishnan [15] using an optimal control algorithm. The cost function was defined as

$$J=\frac{1}{K_f}\left\{\sum_{K=0}^{K_f-1}\left[(y_K-y_K^{ref})^2+\mu u_K^2\right]+(y_{K_f}-y_{K_f}^{ref})^2\right\} \tag{2.3}$$

where K_f is the total number of samples, y_K is the beam tip position at the Kth sample, μ is the input weighing factor, and u_K is the input at the Kth sample. The parameters of the manipulator were determined experimentally. The controller was designed based on the estimated parameters. Experimental testing was carried out and the effectiveness of the algorithm was confirmed

An optimal regulator was developed by Hastings [16] for a one link flexible manipulator. Two controllers were derived respectively for the model which only counts the first flexible mode and the one counting the first two flexible modes. The robustness and payload sensitivity of both controllers were examined theoretically and evaluated experimentally. Barbieri and Figueroa [54] proposed an optimal control algorithm for a redundant flexible planar manipulator. The manipulator consists of four links, the first one being flexible and the last three being rigid. Two optimal control strategies were developed. Their study was restricted to numerical simulations.

A LQR control scheme with strain and joint angle feedback was implemented by Yuan et al. [55] on a large flexible manipulator with a parallel linkage driver. The algorithm was based on a simplified model that accounts for the constraints of the parallel linkage kinematically rather than through constraint forces. Schmitz [56] reported his results on the PD control and LQR control of a

planar manipulator with an elastic forearm. The nonlinear terms of the dynamic equations were examined and the control performance's assessment steps were summarized. An H_2-optimal control algorithm was designed for a single link flexible joint robot by Wang and Liu [57]. The quadratic performance index was defined in the frequency domain. Both numerical simulations and experimental testing were conducted.

An optimal control algorithm, which minimizes a quadratic cost function of the predicted output errors and the control increment, was developed for a single-link flexible arm by Cetinkunt and Wu [58]. The discrete-time root locus was applied to find the proper weighting parameters for the PI function. The noise rejection capability of the algorithm was investigated. Alder and Rock [59] developed a LQR algorithm to control a flexible robotic manipulator with an unknown dynamic payload, a pendulum. Numerical simulations of the control accounting for both static and dynamic payload were performed.

2.4.2 Sliding Mode Control

Sliding mode control, also called the variable structural control (VSC), is a nonlinear control technique. It utilizes a high speed switching control law to drive the plant's state trajectory onto a specified and user-chosen surface in the state space and to maintain the plant's state trajectory on this surface for all subsequent time. The surface is called a switching surface since if the state trajectory of the plant is "above" the surface a control path has one gain, and a different gain if the

trajectory drops "below" the surface. The plant dynamics restricted to this surface represent the controlled system's behaviour.

The application of the sliding mode technique on flexible manipulators was reported by Yeung and Chen [17]. The control design was carried out in two steps: using a sliding control to force the system into the sliding motion in an arbitrarily short time; once in the sliding motion, the system response was designed by a pole placement technique. The sliding control was derived to achieve robust feedback linearization of the highly nonlinear dynamic equations of a flexible robot. It was concluded that the sliding control technique has the following advantages: the controller is robust against parameter variations; load forecast is not needed; accurate knowledge of the plant parameters is not necessary; the design procedure is simple; the cost of implementing the control law is low; and no parameter estimation is necessary.

A variable structure control algorithm was developed for a robotic manipulator with two flexible links by Nathan and Singh [60]. The dynamic model was derived with the assumed-modes method and only the first two vibration modes of the flexible arm were included in the model. Based on VSC theory, a discontinuous joint angle control law was developed to make the trajectory attracted towards a pre-defined hypersurface in state space and then slide along it. In order to control the elastic oscillations of the links, a stabilizer was designed with a pole placement technique.

2.4.3 Adaptive Control

The basic idea in adaptive control is to estimate the uncertain plant parameters (or equivalently, the corresponding controller parameters) on-line based on the measured system signals, and use the estimated parameters in the control input computation. An adaptive control can thus be regarded as a control system with on-line parameter estimation.

Meldrum and Balas [61] derived both adaptive and non-adaptive model reference control algorithms for a one-link flexible manipulator. Only numerical simulations were conducted. Yuan and Book [62] performed direct adaptive control of flexible arms with a model reference control scheme. A controllable stable system which is related to the plant was chosen as the reference model to specify the desired system performance. The separation principle was applied to decouple the model into a linear part and an uncertain part. The robustness of the algorithm to the uncertainties was theoretically analyzed.

A so-called decentralized adaptive control was developed for a two degrees of freedom flexible manipulator by Yuan et al. [63]. The control input consists of two parts. The first part was derived from model reference control. And the second part was designed to compensate the uncertainties in the dynamic model. The error dynamics were proven to be uniformly bounded by the Lyapunov criterion. Both numerical simulations and experimental verification were carried out.

2.4.4 Composite Control

Since a single control technique hardly provides satisfactory performance of flexible manipulators, combining two or more control strategies together to perform flexible manipulator control has been proposed by several researchers [3, 8, 9, 64]. Considering a complex dynamic system such as a flexible manipulator as the superposition of several simpler subsystems and designing a proper controller for each subsystem, the composite control algorithm has been developed as an effective approach for the flexible manipulator control.

Fan and Castelazo [9] derived a composite algorithm consisting of a PID scheme and an optimal controller to implement force control for a flexible manipulator. Its philosophy is based on the PID algorithm's capability for eliminating the steady state error through properly selecting gain, and the optimal controller's efficiency in improving the transient response of a system. The combination of these two controllers produces an algorithm which provides satisfactory transient response performance without any steady state error.

Simulation results of a flexible arm control were reported by Lee et al. [65]. The control process was divided into two stages: coarse control and fine control. The fine controller was designed with the pole placement technique. The control scheme shifts from coarse control to fine control as soon as pre-defined conditions are satisfied.

A composite control algorithm was applied to control a multi-link robotic manipulator with elastic joints by Lin et al. [66]. The control input consists of three parts: one for the linearization of the dynamic equations, one containing the

PID state feedback signals, and one derived to ensure the system's stability by the second method of Lyapunov. Numerical simulation on the model of a six degrees of freedom Cincinnati Milacron T3-776 industrial robot with six compliant joints was carried out.

In [67] and [68], Lin and Yuan presented an approach for the control of flexible robot arms on the basis of differential geometric nonlinear control theory and the linear quadratic regulator algorithm. The control scheme was separated into two parts: The first part, which was derived by the differential geometric structure algorithm, is a globe external linearization and decouples nonlinear feedback law for nominal trajectory tracking. The second part was synthesized by combining LQR and servo-compensator techniques. It is a robust linear time-invariant stabilization and error correcting feedback control designed for active damping of elastic vibrations and for robustness to uncertainty in system parameters.

Tip position control of a flexible arm was implemented by Rattan et al. [69]. The control scheme consists of an inner loop and an outer loop. The inner loop controller was designed to control the motor and to remove the effects of friction at the joints. The outer loop was used to control the tip position of the arm with a feedforward term. The flexible link was simplified as a lumped mass system for dynamic modelling convenience.

One of the popular composite control approaches for flexible manipulators is the singular perturbation technique. The basic idea of the technique can be described as follow. The motion of a flexible manipulator can be considered as the superposition of the rigid motion (called the slow subsystem) produced by joint

variables and the elastic motion (called the fast subsystem) caused by the flexibility of the structure. Neglecting the distributed flexibility of the structure, the dynamic model for the slow subsystem can be easily derived. With the use of the elastic forces and their time derivatives as the state variables, the model for the fast subsystem is developed with the application of the singular perturbation theory. The corresponding control design is performed in two steps [3]: first, a slow feedback controller is designed in order to solve the tracking problem for the slow subsystem model; then a fast feedback controller is developed to stabilize the fast reduced model on an equilibrium manifold which depends on the choice of the slow controller. The attractive feature of this strategy [8] is that the slow controller can be designed on the basis of well-established control schemes for rigid manipulators. The fast controller can be synthesized as a linear state feedback control with the slow state variables acting as parameters.

Marino and Nicosia [3], Siciliano [70] and Siciliano and Book [8] applied this technique to implement flexible manipulator control. Marino and Nicosia mainly dealt with the control implementation of a manipulator with flexible joints. A PID control algorithm was used for both the slow and fast subsystems. The bending flexibility of arms was considered by Siciliano and Book. With a PID controller for the slow motion, an optimal fast controller was designed to minimize a cost function, which was defined as a function of the slow state variables.

The key issue for the success of the singular perturbation technique [8] is the assumption of the robot's weak structural flexibility so as to preserve the time scale separation. If this assumption does not quite stand, the use of integral

manifolds was proposed [4] to obtain a more accurate slow subsystem. This slow subsystem accounts for the effect of flexibility up to a certain level.

Spong [4] developed a control scheme for an elastic joint robot by using the singular perturbation technique and the concept of integral manifold. The integral manifold was defined to describe the dynamics of the rigid manipulator in state space and was made to be invariant under the solutions of the flexible joint system with a corrective control concept. A composite control algorithm, which consists of a fast subsystem controller and a slow subsystem controller, was produced to improve the robot performance.

Mills [71] proposed a composite control algorithm for the control of a robotic manipulator with flexible joints during constrained motion task execution using the singular perturbation technique. The algorithm consists of two sub-schemes respectively for the slow and fast subsystem dynamics. The slow subsystem controller is comprised of a corrective controller which uses the concept of an integral manifold to compensate for flexibility effects and a rigid control law.

2.4.5 Other Control Techniques

A new control technique, namely pointwise control, was proposed by Chassiakos and Bekey [13] for a flexible manipulator. The basic idea of the method is to supplement torque control at the joints by the application of force pulses at specific points along the structure. The control law was developed from a quadratic optimization criterion. Based on the same criterion, an algorithm for the

optimization of the actuator's locations was developed and the optimal locations of the actuators were determined.

A torque-wheel actuator located at the tip of a flexible arm was used by Montgomery et al. [72] to suppress the vibrations of a flexible link. A sliding mass method was proposed by Jumarie [73] to improve the performance of flexible robotic manipulators. The control effort consists of acting on both the sliding masses and the joint torques in a suitable way. The control scheme was designed in the sense of optimization with respect to the defined performance index. The study was restricted to general discussions.

With the finite element technique, the effects of distributed passive [74] and active [75] actuators on elastic robot structures were studied by Tzou and Wan. The distributed passive viscoelastic actuator is a layer of viscoelastic polymer directly attached to flexible arms and automatically dissipates the vibration energy of the flexible links. The active distributed sensor and controller are a layer, or multi-layer, of piezoelectric polymer attached to the controlled element. By utilizing direct and converse piezoelectric characteristics, respectively, the integrated piezoelectric sensor/controller can monitor the vibration, and constrain the undesired vibration by injecting high voltages. Their study rested on numerical simulations.

Tsujio [76] presented an approach to perform feedforward control of a flexible manipulator with an inverse dynamic analysis. The principle of this approach is the utilization of the inverse dynamics of a rigid manipulator for calculating the flexible robot's driving force. The desired trajectory was warped to an imaginary trajectory using the trajectory of the flexible manipulator. The

imaginary trajectory was applied as an input to the inverse dynamic model of the rigid manipulator and the driving forces were calculated using an iterative algorithm. It was shown that a feedback controller is required with the application of the proposed technique in order to suppress the vibration of the structure. The inverse dynamic analysis was performed on the dynamic equations with over-damping or the quasi-static model. The simulation study suggested that the convergence of the algorithm occurs with two to three repetitions, and the driving force which produces the desired trajectory can be obtained in a precise manner. One problem with the inverse dynamic analysis is the sensitivity of the solution to changes of the system parameters.

Korolov and Chen [7] developed a robust controller, which accounts for imperfect knowledge of the link's natural frequencies for a one-link flexible robot arm. The robust control law was given as:

$$p(\hat{x}) = k\hat{x} + P_e(\hat{x}) \tag{2.4}$$

where $\hat{x}$ is the state estimate provided by a reduced order observer, k is determined by solving the Riccati equation. The "uncertainty" is described by the nonlinear term $P_e(\hat{x})$. The reduced order observer was designed to be independent of the system control input.

Zalucky and Hardt [77] designed a mechanism to correct the elastic deflection of the flexible manipulator's arm by using a hydro-actuator to transfer the outer link's bending deflection to the inner link and keep the outer link's bending deflection be zero. The hydro-actuator was controlled through a servo valve and the bending of the outer link was sensed by an optical displacement sensor.

Asada et al. [78, 79, 80] presented several papers which deal with the performance control of flexible robots with an inverse dynamics algorithm. A special co-ordinate system, called the virtual rigid link coordinates (VRLC), was proposed to derive the dynamic model of a flexible manipulator. The implementation can be divided into three steps: first determine the virtual rigid link motion, followed by the computation of the dynamic link deformations relative to the virtual rigid links, and then determine the actuator torques. The boundary conditions of the flexible arms with respect to the VRLC were assumed to be the ones of a simply supported beam. In [81], the necessary conditions permitting driving torques to be non-diverging and non-oscillatory were discussed. The trajectory control of flexible robot arms with an inverse dynamics feedforward loop based on the VLCS system was reported in [82].

A passive control idea for a single flexible link was proposed by Wang and Vidyasagar [83]. It was demonstrated that with an appropriately selected output variable, the transfer function of a single flexible link can be considered to be passive. According to the passivity theorem, any strictly passive controller with finite gain will result in an L_2-stable system. A controller was designed as an example and its experimental results were presented. They also studied the dynamic model properties for a class of manipulators with a single flexible link [84, 85]. It was shown that the input-output equations are only feedback linearizable if the output variables are chosen appropriately. However, the nonlinear dynamics made unobservable by this feedback are not asymptotically stable. It was concluded that feedback linearization techniques are not appropriate for this class of manipulators. A controller and observer design technique was

proposed. By transforming the state space equations of these manipulators into an equivalent set of equations which are almost linear, a nonlinear state feedback controller was designed based only on the linear part of the transformed system equations. An observer was developed in which the estimated states converge to the actual states exponentially. It was demonstrated that combining the observer with the controller results in a system which is input-output stable in a local sense.

The control performance of two flexible manipulators, one fabricated from aluminium and one from composite laminates, was compared through the step response of the systems to a commanded angular position, and the results were reported by Choi [86]. Both of the manipulators were controlled by a PID scheme. It was shown that the manipulator fabricated from composite materials has superior performance characteristics such as faster settling time, small input torque and smaller overshoot relative to the one made from aluminium.

A nonlinear feedback control algorithm for flexible manipulators was proposed by Castelazo and Lee [87]. The feedback loop uses the products of the state variables to obtain a lightly damped system at the beginning of a step response and a more heavily damped system when close to the steady state position. It results in faster rise and settling times than those obtained with an optimal linear controller while maintaining a comparable amount of control effort.

2.5 Parameter Estimation Techniques

The Recursive Least Squares (RLS) algorithm is an effective tool for the on-line parameter estimation. With the given model structure, the least squares estimates of the parameters are determined by minimizing the sum of the squared differences between the predicted outputs and the measured plant outputs. Rovner and Cannon [53] applied an RLS algorithm to implement the on-line identification of the transfer function for a very flexible one link manipulator. The algorithm was derived both in the time domain and in the frequency domain. In order to evaluate the estimation accuracy, the estimated results were compared with a "baseline" model, which was obtained by a Solartron Frequency Response Analyzer. It was found that the unmodified RLS estimator gives a very heavy weighting to the higher frequency region. The minimization of the sum of the squared errors resulted in a transfer function with a too large high-frequency gain. The estimated model was improved by using a filter to counteract the emphasis on the high frequency fit. The sequence of errors passes through the filter before being minimized. To reduce the order of the identified transfer function and increase the estimation accuracy and efficiency, the transfer function was divided into the product of the known and unknown dynamics. Prefiltering the input and output data by the known part of the transfer function, the number of the estimate parameters was efficiently reduced. A recursive least squares algorithm was also used by Yurkovich et al. [88] to estimate the parameters of an ARMA model for a two link flexible manipulator. Based on the estimated parameters, PID and auto-tuning control schemes were developed.

Assuming that the deflection of a flexible link caused by higher vibration modes is negligible, Wang and Hsu [10] determined the first vibration natural frequency of the link from the link's slope sensor signal. This frequency was the only parameter to be identified. With pole placement control, this simple estimation technique provided satisfactory adaptive control performance for the prescribed flexible system.

State space observers or predictors are often used as on-line estimators in adaptive control algorithms. Through a proper design, the prediction errors can be asymptotically forced to zero. Hashimoto et al. [89] used an observer in their proposed adaptive scheme. It was theoretically demonstrated that the designed control law forces the plant output to converge to the desired output as time increases.

A model reference method was used to experimentally estimate the parameters of a flexible link and a motor system by Ramakrishnan [15]. It was found that the sampling time selection is critical to the accuracy of the estimated parameters. Slower sampling, in general, gives more accurate estimates. Also the friction can cause the misconvergency of the estimation. However, if Coulomb friction torque is included in the system model, the accuracy of the estimation is improved.

Morimoto et al. [90] used a modal analysis technique to estimate the transfer function of a flexible robot arm. The effects of gravity, centrifugal, and Coriolis forces were all neglected. The control algorithm was designed based on the inverse dynamics and was verified experimentally.

A SISO discrete Hammerstein model was used by Krzyzak [91] to identify the deflection of a flexible robotic arm. A Hammerstein system consists of two cascaded subsystems: a nonlinear, memoryless subsystem followed by a dynamic linear subsystem. The parameters of the dynamic linear subsystem were identified by the correlation calculation and the nonlinearity of the nonlinear, memoryless subsystem was recovered through a Hermite series regression estimate. The convergence and the convergent rates of the algorithm were discussed.

System identification algorithms for a one-link flexible manipulator with an unknown payload were discussed by Chen and Menq [92]. Three on-line identification schemes, the standard recursive least squares method, a least squares with known information lumped, and an average modified gradient method, were examined and compared. It was found that the least squares based methods are sensitive to unmodelled dynamics, while the average gradient method shows significant improvement in counteracting unmodelled dynamics.

Cetinkunt and Wu [93] proposed to use a lattice filter for the real-time parameter estimation of a one arm flexible robot. The lattice filter was considered to be particularly suitable for identifying the parameters of a mechanical system with distributed flexibility since the order of the filter may be tuned on-line as the task condition requires. The filter was implemented for the predictive adaptive control of a flexible one arm robot.

2.6 Other Aspects On The Topic

Whitney et al. [94] presented a progress report to summarize the theoretical and practical results on the integration of the design and control aspects of manipulator arms for industrial or space applications. The relationships between task specifications, gross motions, fine motions, actuator type and location, size and strength of structural members, control servos and strategies, and overall design evaluation were discussed. In [95], Chretien presented a exclusive discussion on the experimental setup for the study of flexible structure's active controls. The issues include the setup requirements, the mechanical dimensioning, and an architecture survey on SECAFLEX. SECAFLEX is a experimental facility which was built in house to experimentally investigate the various aspects of the mechanical flexible structure controls and joint torque controls.

The experimental determination of model parameters was performed by Cannon and Schmitz [11] and Nebot et al. [5]. Using sinusoidal signals with various frequencies to excite the system, the required parameters were determined by direct measurements or calculations based on the sensor's output data. The assumption of the effects of the higher vibration modes on the arm's deflection being negligible was made.

Vidyasagar and Morris [96] analyzed the dynamic model of Euler-Bernoulli beams from the standpoint of controller design. It was concluded that a distributed parameter system described by an undamped Euler-Bernoulli equation cannot be stabilized by any finite-dimensional controller, i.e. any controller which can be described by an ordinary differential equation with constant coefficients. Also,

such a system cannot even be stabilized by a controller which can be synthesized using adders, multipliers, integrators and delays. A similar result applies even if viscous damping is included in the model. It was also pointed out that this negative result should be interpreted as the commentary on the limitations of the Euler-Bernoulli model, rather than on the control of a real beam. In [97], Morris and Vidyasagar showed that if a Rayleigh damping model is used, a finite-dimensional controller can be designed to move the closed loop system poles essentially as far to the left in the complex plane as desired. The result also holds for certain hysteresis damping models.

Rivin [98] used the finite element technique to explore the manipulator arm design for high stiffness and low inertia by the composition of different materials. Computer simulations were performed to formulate the optimal proportions for design and to develop an effective and reliable joint between various materials without adding much weight to the link.

Nebot and Lee [99] presented a paper to discuss the experimental setup for a single link flexible manipulator. A detailed sensor design was given and estimation techniques were provided. The performance limitations of joint variable-feedback controllers for flexible manipulators were discussed in [100] by Cetinkunt and Book. Both fine motion control and gross motion control algorithms were examined.

The effects of a link's flexibility on the dynamic stability of a two link flexible manipulator were investigated by Chiou and Shahinpoor [101]. It was assumed that the end-effector of the robot is in contact with the environment and the contact point is locked. A stability analyses was carried out by computing the

eigenvalues of the linearized system. It was concluded that the system stability is sensitive to the variation of the force sensor's stiffness. Reducing the sensor stiffness makes the system more stable. As far as the stability is concerned, the flexibility of the first link is dominant.

A trajectory planner for a one link flexible manipulator was proposed by Serna and Bayo [102]. The approach was based on the solution to the inverse dynamics problem for flexible manipulators in the frequency domain and was formulated as the optimization of the settling time subject to maximum torque and high frequency content constraints.

A special transmission mechanism, which relocates the torque actuation point and modifies a flexible arm to a minimum phase system, was developed by Park and Asada [103]. With the use of an outer hub, which is connected directly to the motor shaft, the torque exerted by the motor is transmitted to the point of torque actuation by means of a couple of cables, which were assumed to be massless. The arm is free to rotate about the joint axis. Experimental verifications were carried out.

A general discussion on the dynamic modelling and control algorithm for a deformable and compliant N-link robotic system was presented by Cotsaftis [104]. Dynamic modelling was based on the Euler-Bernouilli slender beam theory and the Lagrangian formulation. Four different control schemes, direct control, adaptive control, robust control, and function control, were examined.

2.7 Summary

Various approaches to implement the dynamic modelling and performance control of flexible manipulators have been reviewed. The major difficulties in the field can be summarized into the following four aspects:

1. Dynamic modelling. A flexible manipulator is a distributed parameter mechanical system and possesses an infinite number of natural vibration modes. The dynamic modelling of such a system is always based on certain assumptions. Moreover, some nonlinear phenomena, such as gear backlash, structural damping, and friction, associated with flexible manipulators cannot be precisely described. The obtained mathematical dynamic equations of the system are the result of the trade-off between the model's accuracy and its complexity.
2. Model order reduction. The mathematical model of a flexible manipulator is usually nonlinear, complex and of high order. It is difficult to use such a model directly for controller development. A simplified lower order model with adequate accuracy is highly desirable. To date, most of the model reduction techniques are developed for linear dynamic systems. Very few can be applied on nonlinear ones.
3. Control Strategies. The control theory for a linear time-invariant system is well-established. Nonlinear dynamic systems lack effective control algorithms. For flexible manipulators, due to the nonlinear dynamic feature, non-colocated structure (non-minimum phase), inaccurate mathematical

model, uncertain payload, and varying system parameters, the development of a proper control algorithm becomes more challenging.

4. Estimation techniques. The adaptation of a control algorithm requires the real time estimation of the system parameters. Due to the computer's speed limitation, an estimator is required to provide accurate estimating results with acceptable computation. In addition, a good estimation algorithm should be insensitive to the noise and the type of excitations.

DYNAMIC MODELLING

3.1 Introduction

The manipulator considered in this study is a two degrees of freedom flexible manipulator, which operates on a horizontal plane, as shown in Figure 3.1. It consists of two flexible links and two elastic joints. Two flexible arms are connected in series and the second arm is carried by the first one. Two DC motors are used to provide the driving force for the system and an elastic joint connects the driving motor with the driven link. The dynamics of the system are assumed to be independent of the gravity force and the arm's torsional deformation is considered to be zero. Referring to Figure 3.1, a local two dimensional coordinate system is assigned to each arm, and the coordinate's origin is located at the arm's driving joint. The arm's bending deflection with respect to its local coordinate is denoted by w. The relative joint angle rotation is given as θ.

The dynamic modelling of the manipulator is implemented in two major steps: (i) determination of the arms' eigenvalues and mode shapes and, (ii)

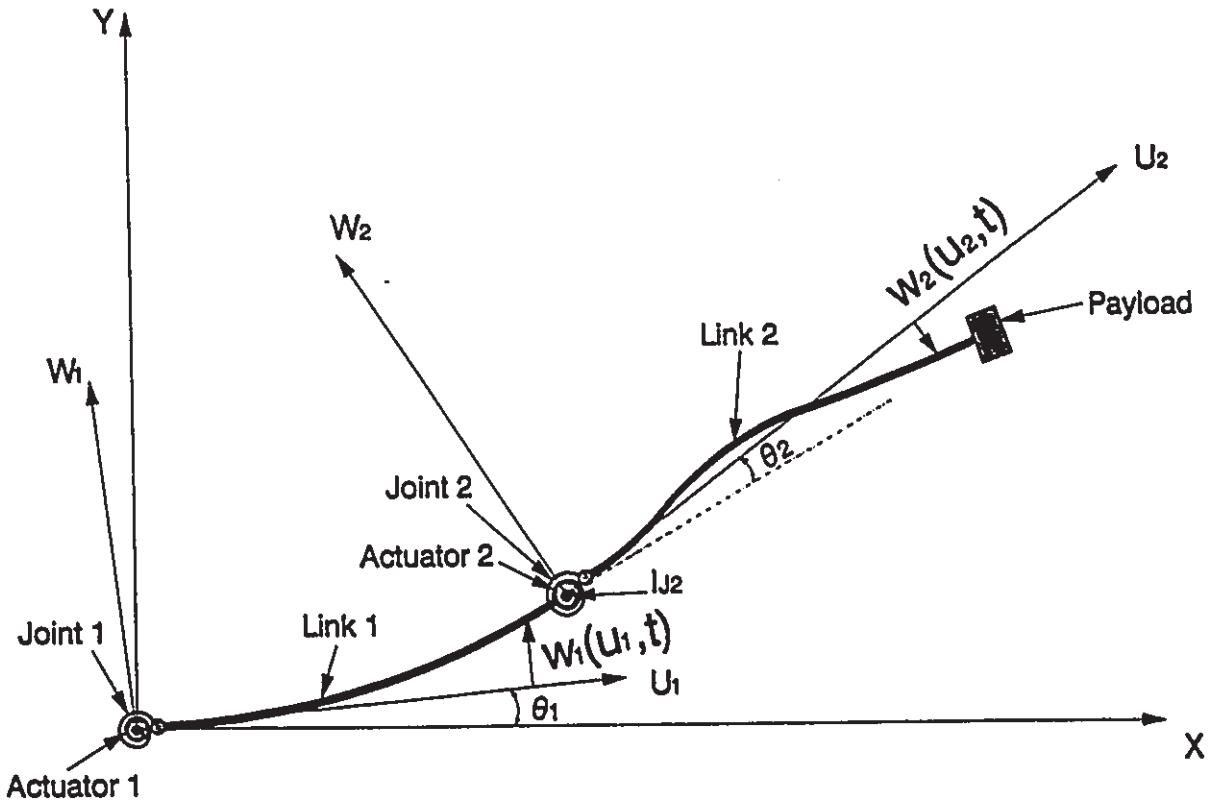

Figure 3.1 Two Link Manipulator With Link and Joint Flexibilities

derivation of the system dynamic equations. The eigenvalues and the mode shapes of the arm are obtained using the transfer matrix method, and the system's dynamic equations are derived using the Lagrangian equation. The arm's internal structural damping, backlash between driving gears, and friction torques at the joints are all modelled and their effects on the system dynamics are considered.

3.2 Arm's Eigenvalues

In the experimental setup the friction torque at the joints cannot be eliminated completely. The non-zero friction at the ends of the link significantly affects the eigenvalues of the arm and complicates its boundary conditions. The physical connection between the link and the joint results in the beam cross-section being non-uniform. Although both arms of the manipulator are geometrically slender and mechanically flexible, the traditional Bernoulli-Euler's beam model has some difficulties of handling them due to the friction effects in the boundary conditions and the step variation of the cross-section. An alternative technique is suggested in the following.

The transfer matrix method [105] is the matrix systemization of Myklestad's procedure and can effectively model beams with complicated boundary conditions and nonlinear cross-section variations. By dividing each portion of the beam with a constant cross-section area into N small sections and representing each small section with a point mass, a concentrated mass momentum of inertia, and a massless elastic beam, the manipulator arm with three different cross sectional areas can be approximated as shown in Figure 3.2. The mass and momentum

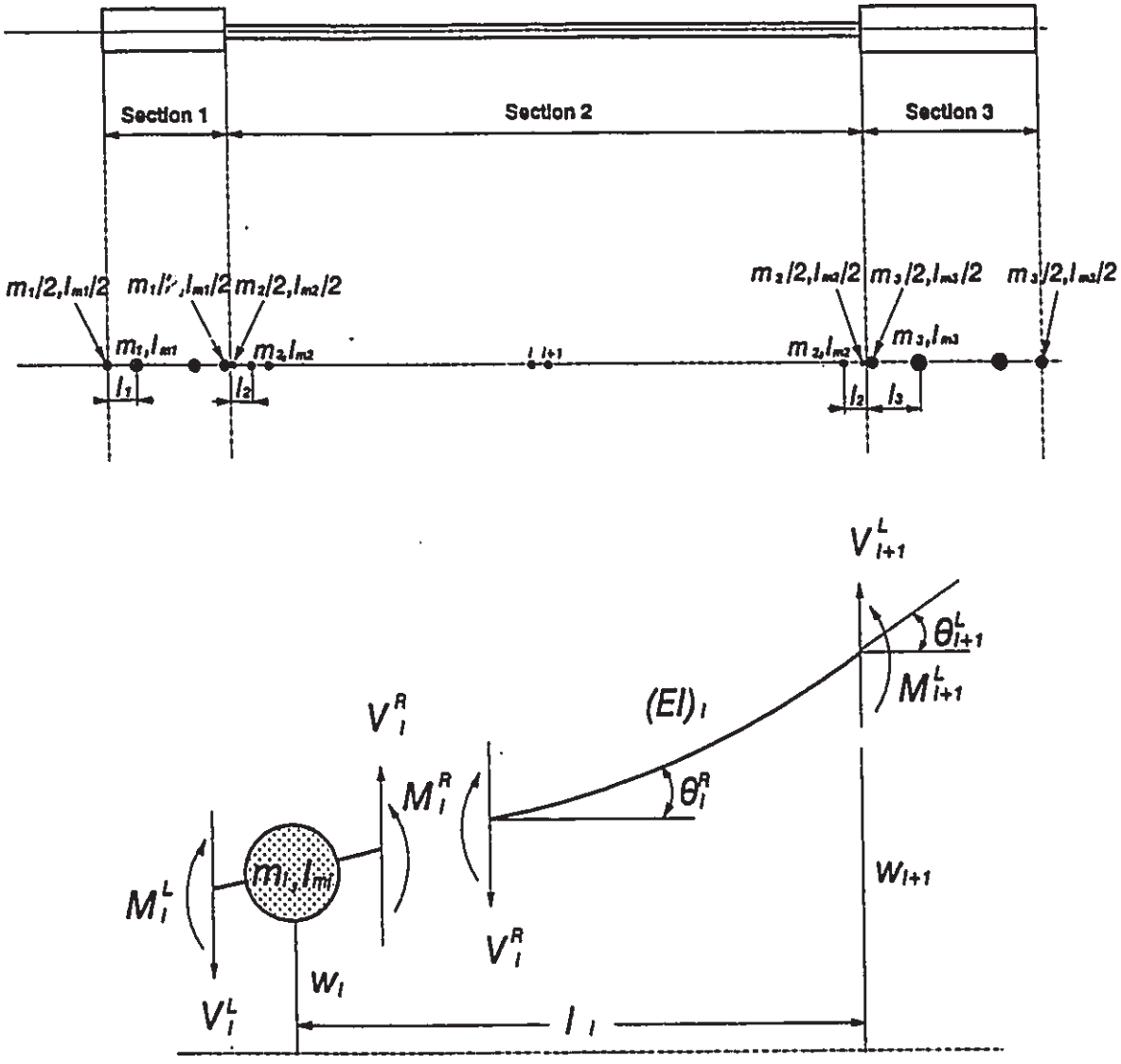

Figure 3.2 Approximation of Continuous Beam

values at the two boundary points of each portion are equal to half of the corresponding values at its interior points. One portion of the arm is connected rigidly with its neighboring portion. Four variables: shear V, moment M, slope θ , and deflection w, are used to describe the dynamic states of the arm along each point. The relations between the variables at the point i and those at the point $i+1$ can be derived as follows:

Referring to Figure 3.2, we have

$$V_{i+1}^{L} = V_i^{R} \tag{3.1a}$$

$$M_{i+1}^{L} = M_i^{R} - V_i^{R} \times l_i \tag{3.1b}$$

$$\theta_{i+1}^{L} = \theta_i^{R} + M_{i+1}^{L} \times (\frac{l}{EI})_i + V_{i+1}^{L} \times (\frac{l^2}{EI})_i \tag{3.1c}$$

$$w_{i+1}^{L} = w_{i+1}^{R} + \theta_i^{R} \times l_i + M_{i+1}^{L} \times (\frac{l^2}{2EI})_i + V_{i+1}^{L} \times (\frac{l^3}{6EI})_i \tag{3.1d}$$

where l_i is the length of the ith section and $(EI)_i$ is the stiffness of the ith elastic beam. Rearrange equations (3.1) into the matrix form

$$\begin{Bmatrix} -V \\ M \\ \theta \\ w \end{Bmatrix}_{i+1}^{L} = \begin{bmatrix} 1 & 0 & 0 & 0 \\ l & 1 & 0 & 0 \\ \frac{l^2}{2EI} & \frac{l}{EI} & 1 & 0 \\ \frac{l^3}{6EI} & \frac{l^2}{2EI} & l & 1 \end{bmatrix}_i \begin{Bmatrix} -V \\ M \\ \theta \\ w \end{Bmatrix}_i^{R} \tag{3.2}$$

where the 4x4 square matrix is called the field matrix. Also

$$V_i^{R} = V_i^{L} - m_i \times \omega^2 \times w_i \tag{3.3a}$$

$$M_i^{R} = M_i^{L} + I_{mi} \times \omega^2 \times \theta_i \tag{3.3b}$$

$$\theta_i^{R} = \theta_i^{L} \tag{3.3c}$$

$$w_i^{R} = w_i^{L} \tag{3.3d}$$

or

$$\begin{Bmatrix} -V \\ M \\ \theta \\ w \end{Bmatrix}_i^{R} = \begin{bmatrix} 1 & 0 & 0 & m \times \omega^2 \\ 0 & 1 & I_m \times \omega^2 & 0 \\ 0 & 0 & 1 & 0 \\ 0 & 0 & 0 & 1 \end{bmatrix}_i \begin{Bmatrix} -V \\ M \\ \theta \\ w \end{Bmatrix}_i^{L} \tag{3.4}$$

The square matrix in equation (3.4) is known as the point matrix. Substituting equation (3.4) into equation (3.2), we have

$$\begin{Bmatrix} -V \\ M \\ \theta \\ w \end{Bmatrix}^{L}_{i+1} = \begin{bmatrix} 1 & 0 & 0 & 0 \\ l & 1 & -I_m\omega^2 & ml\omega^2 \\ \frac{l^2}{2(EI)} & (\frac{l}{EI}) & 1-\omega^2(\frac{I_m l}{EI}) & \omega^2(\frac{ml^2}{2EI}) \\ \frac{l^3}{6EI} & \frac{l^2}{2EI} & l-\omega^2(\frac{I_m l}{2EI}) & 1+\omega^2(\frac{ml^3}{6EI}) \end{bmatrix}_i \begin{Bmatrix} -V \\ M \\ \theta \\ w \end{Bmatrix}^{L}_{i} \qquad (3.5)$$

where ω is the vibration frequency of the arm and the square matrix is the transfer matrix, which is the product of the field matrix and the point matrix. Recursively using the transfer matrix, we can easily obtain the following equation, which relates the boundary conditions at the two ends of the link.

$$\begin{Bmatrix} -V \\ M \\ \theta \\ w \end{Bmatrix}^{R}_{N} = \begin{bmatrix} t_{11} & t_{12} & t_{13} & t_{14} \\ t_{21} & t_{22} & t_{23} & t_{24} \\ t_{31} & t_{32} & t_{33} & t_{34} \\ t_{41} & t_{42} & t_{43} & t_{44} \end{bmatrix} \begin{Bmatrix} -V \\ M \\ \theta \\ w \end{Bmatrix}^{L}_{1} \qquad (3.6)$$

The above square matrix is denoted as T and every element of T is a function of the variable ω. The values of ω which satisfy the above equation are the natural frequencies of the arm. For each arm of the manipulator, one end is driven by the actuator (called the support end) and another end is connected to the second arm or carries a payload (called the far end). The boundary conditions at the far end can be approximated as a free-end with an equivalent mass momentum of inertia and a point mass. At the support end, due to friction, the boundary conditions are between clamped and pinned-free. Due to the nonlinear characteristics of friction, a so-called "switch mechanism" is used to approximate its effect. First with the assumption of the support end being clamped, an ω value which satisfies the clamped boundary conditions is calculated. This value is used to calculate the corresponding required minimum torque at the support end. If the required torque

cannot be provided by the friction, the assumption of the clamped end is invalid. Accordingly, the algorithm is switched to the case where the boundary conditions of the displacement are zero and the absolute value of the torque is equal to the friction torque at the support end. A new ω which satisfies the redefined boundary conditions is calculated. This ω is then accepted as one of the system's natural frequencies. With the use of the arm's physical properties, the corresponding eigenvalue of the arm can be easily calculated. Changing the searching range and repeating the same procedure, the desired number of the arm eigenvalues are obtained. The magnitude of the friction torques at the joints was measured experimentally. The eigenvalue determination is done separately for each arm.

Although the transfer matrix method is effective for eigenvalue determination of the arms, it fails to provide an analytical expression for the mode shape functions of the links. Instead, a set of discrete data which represents the corresponding mode shape can be obtained. With a least squares estimation algorithm the discrete data set is compressed into a mathematical expression. The structure of the expression is assumed to have the following form, which is a general expression for all the Euler-Bernoulli beam's mode shape functions.

$$\psi(u) = C_1\sin(\beta u) + C_2\sinh(\beta u) + C_3\cos(\beta u) + C_4\cosh(\beta u) \qquad (3.7)$$

where the constants *C1*, *C2*, *C3*, and C_4 are estimated; β is the eigenvalue of the arm.

The adequacy of the proposed method and the correctness of its program code are verified by comparing the results of the transfer matrix method with the analytic solutions of the Euler-Bernoulli beam model for the cases of a uniform

beam with pinned and clamped boundary conditions. The differences between the results of these two methods in this case are less than 0.05%.

3.3 Internal Structural Damping Of Arms

With the assumption of the internal structural damping of the arms being viscoelastic, its dissipation function can be defined as [17]

$$V_D = \frac{1}{2}\int_0^{L_1} C_{a1} I_1 \left(\frac{\partial}{\partial t}\left(\frac{\partial^2 w_1(u_1,t)}{\partial u_1^2} \right) \right)^2 du_1 + \frac{1}{2}\int_0^{L_2} C_{a2} I_2 \left(\frac{\partial}{\partial t}\left(\frac{\partial^2 w_{21}(u_2,t)}{\partial u_2^2} \right) \right)^2 du_2 \quad (3.8)$$

with

$$C_{a1} = \xi_1 L_1^2 \sqrt{\frac{A_1 E_1}{I_1}} \qquad \text{and} \qquad C_{a2} = \xi_2 L_2^2 \sqrt{\frac{A_2 E_2}{I_2}}$$

where ξ_1 and ξ_2 are the damping ratios for the first and second arm, respectively. L_1 is the length of the first arm and L_2 is the length of the second arm.

3.4 Backlash Effects

The kinetic energy loss due to the impact of the two members of the system is considered. The kinetic energy loss rate is indirectly defined by the coefficient of restitution. For a limited range of low impact velocity and for most materials within a linear elastic range, the coefficients of restitution can be given as [44]

$$e = 1 - \zeta |v_i|$$

where ζ has a value of between 0.08-0.32 sec/m and v_i is the relative impact speed. Assuming the velocities of the two impacting bodies being p_1 and v_1 before collision and p_2 and v_2 after collision, we have the following set of equations:

$$m_1 p_1 + m_2 v_1 = m_1 p_2 + m_2 v_2 \quad (3.9a)$$

$$e = \frac{p_2 - v_2}{v_1 - p_1} \quad (3.9b)$$

The total kinetic energy loss of the two impacting subjects (of mass m_1 and m_2), over a single-impact sequence, is

$$\Delta E_K = \frac{1}{2}m_1 p_1^2 + \frac{1}{2}m_2 v_1^2 - \frac{1}{2}m_1 p_2^2 - \frac{1}{2}m_2 v_2^2 \tag{3.10}$$

with backlash clearance of d_b. The dissipation function can be approximated as:

$$V_B = \frac{1}{2}\frac{\Delta E_K}{\Delta t} \tag{3.11}$$

with

$$\Delta t = \frac{1}{2}\left(\frac{d_b}{p_1 - v_1} + \frac{d_b}{v_2 - p_2}\right) = \frac{(1+e)d_b}{2e(p_1 - v_1)}$$

For the manipulator, the backlash clearance exists between a pair of actuating gears at the joint. Its magnitude is defined here as the driven gear's maximum free rotation angle with the driving gear being fixed, and was determined experimentally through the optical encoders.

3.5 Friction

The nonlinear friction phenomenon at the joint is approximated as shown in Figure 3.3. The friction torque is considered to be independent of the system variables and time. Damper C_1 represents the damping effects of the motor and damper C_2 represents the energy dissipation resulting from the backlash. J_1 is the rotor's mass momentum of inertia and I_{h1} is the mass momentum of inertia of the arm's hub. The flexible joint is represented as K_1 and the motor actuation torque is τ. The friction torque is expressed by T_f.

With consideration of the friction being dry, T_f can be defined by the following equation:

$$T_f = \begin{cases} T_s & \dot{\theta} < 0.0 \\ -T_s < T_f < T_s & \dot{\theta} = 0.0 \\ -T_s & \dot{\theta} > 0.0 \end{cases} \qquad (3.12)$$

and T_s is the static friction torque, having different value for each joint. The above equation is used to describe the friction phenomena at the both joints.

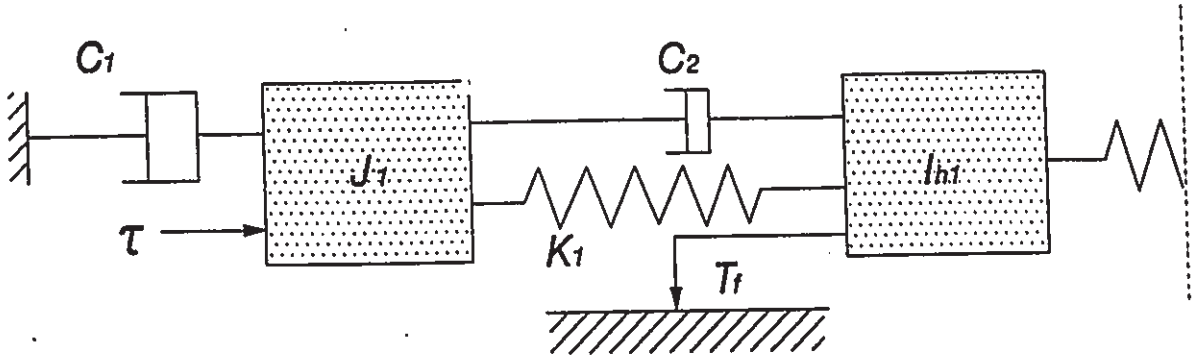

Figure 3.3 Approximation of Friction Effect

3.6 Dynamic Equations

Using the Lagrangian-Euler assumed-modes approach, the actual bending deformation of each arm is a superposition of its natural modes. That is

$$w_1(u_1, t) = \sum_{i=1}^{M} \psi_{1i}(u_1)\varphi_{1i}(t) \qquad (3.13a)$$

$$w_2(u_2, t) = \sum_{i=1}^{M} \psi_{2i}(u_2)\varphi_{2i}(t) \qquad (3.13b)$$

The contributions from the vibration modes higher than mode M are considered to be small and negligible.

With respect to the assigned coordinate systems shown in Figure 3.1, the globe coordinates of a point at link 1 can be expressed as

$$x_1(u_1, t, \theta_1) = u_1 \cos\theta_1 - w_1(u_1, t) \sin\theta_1 \qquad (3.14a)$$

$$y_1(u_1, t, \theta_1) = u_1 \sin\theta_1 + w_1(u_1, t) \cos\theta_1 \qquad (3.14b)$$

The velocity of the point is

$$v_1(u_1,t,\theta_1)=\sqrt{\dot{x}_1^2+\dot{y}_1^2} \tag{3.15}$$

The equations for a point on arm 2 are

$$x_2=L_1\cos\theta_1-w_1\sin\theta_1+u_2\cos(\theta_1+\theta_2+\alpha_{1e})-w_2\sin(\theta_1+\theta_2+\alpha_{1e}) \tag{3.16a}$$

$$y_2=L_1\sin\theta_1+w_1\cos\theta_1+u_2\sin(\theta_1+\theta_2+\alpha_{1e})-w_2\cos(\theta_1+\theta_2+\alpha_{1e}) \tag{3.16b}$$

and

$$v_2(L_1,u_2,\theta_1,\theta_2,\alpha_{1e},t)=\sqrt{\dot{x}_2^2+\dot{y}_2^2} \tag{3.17}$$

where α_{1e} is the bending slope angle at the far end of the first arm, which is defined as

$$\alpha_{1e}=\arctan\left(\frac{\partial w_1(u_1,t)}{\partial u_1}\right)\Big|_{u_1=L_1}=\arctan\left(\sum_{i=1}^{M}\psi'_{1i}(u_1)\varphi_{1i}(t)\right)\Big|_{u_1=L_1} \tag{3.18}$$

The prime (') stands for the first derivative with respect to the variable u. The total kinetic energy of the system can be expressed as

$$\begin{aligned}T=&\frac{1}{2}I_{h1}(\dot{\theta}_1+\dot{\alpha}_{1h})^2+\frac{1}{2}\rho_1A_1\int_0^{L_1}v_1^2du_1+\frac{1}{2}m_{r2}v_1^2|_{u_1=L_1}+\\&\frac{1}{2}I_{r2}(\dot{\theta}_1+\dot{\alpha}_{1e})^2+\frac{1}{2}I_{h2}(\dot{\theta}_1+\dot{\theta}_2+\dot{\alpha}_{1e}+\dot{\alpha}_{2h})^2+\frac{1}{2}m_{h2}v_2^2|_{u_2=0}+\\&\frac{1}{2}\rho_2A_2\int_0^{L_2}v_2^2du_2+\frac{1}{2}m_pv_2^2|_{u_2=L_2}+\frac{1}{2}I_p(\dot{\theta}_1+\dot{\theta}_2+\dot{\alpha}_{1e}+\dot{\alpha}_{2e})^2+\\&\frac{1}{2}I_{j1}\dot{\theta}_3^2+\frac{1}{2}I_{j2}(\dot{\theta}_1+\dot{\alpha}_{1e}+\dot{\theta}_4)^2\end{aligned} \tag{3.19}$$

where the dot ($\cdot$) represents the first derivative with respect to time. Subscript *h1* is used for hub 1, *h2* for hub 2, *r2* for motor 2, *j1* for rotor 1, *j2* for rotor 2, and *p* for the payload. The letter I denotes the mass momentum of inertia, ρ the density of a link, and A the cross-section area of the arm; α_{1h} and α_{2h} are the orientations of the first arm and the second arm at the hub, respectively; α_{2e} is the slope of the second arm at the far end - its definition is very similar to the one for α_{1e}; θ_3 and θ_4 are rotating angles of rotor 1 and rotor 2 respectively with respect to their local coordinate systems.

The total potential energy of the system, resulting from the elastic deformation of the arms and the joints, can be expressed as

$$U=\frac{1}{2}E_1I_1\int_0^{L_1}\frac{\partial^2 w_1(u_1,t)}{\partial u_1^2}du_1+\frac{1}{2}E_2I_2\int_0^{L_2}\frac{\partial^2 w_2(u_2,t)}{\partial u_2^2}du_2+ \tag{3.20}$$

$$\frac{1}{2}K_1(\theta_3-\theta_1)^2+\frac{1}{2}K_2(\theta_4-\theta_2)^2$$

Using the Lagrangian equation [106]

$$\frac{d}{dt}(\frac{\partial L}{\partial \dot{q}_i})-\frac{\partial L}{\partial q_i}+\frac{\partial(V_D+V_B)}{\partial \dot{q}_i}=Q_i \quad \text{with} \quad L=T-U \tag{3.21}$$

the dynamic equations of the system can be derived. For the flexible manipulator, L in equation (3.21) is defined by equations (3.19) and (3.20); V_D is the dissipation function resulting from the internal structural damping of the arms, which is given by equation (3.8), and V_B is caused by the backlash phenomenon at the second joint, which is defined by equations (3.10) and (3.11). The generalized coordinates, q, which consist of the joint variables and the links bending modal coordinates, are given as:

$$q=\left[\ \theta_1\ \theta_2\ \theta_3\ \theta_4\ \varphi_{11}\ \ldots\ \varphi_{1M}\ \varphi_{21}\ \ldots\ \varphi_{2M}\ \right]^T$$

and the corresponding generalized forces, Q, are given by

$$Q=\left[\ T_{f1}\ T_{f2}\ \tau_1\ \tau_2\ 0\ \ldots\ 0\ 0\ \ldots\ 0\ \right]^T$$

where τ_1 and τ_2 are the driving torques of motor 1 and motor 2, respectively. The joint dry friction torques, T_{f1} and T_{f2}, are defined by equation (3.12). Therefore

$$\frac{d}{dt}(\frac{\partial(T-U)}{\partial \dot{\theta}_1})-\frac{\partial(T-U)}{\partial \theta_1}+\frac{\partial(V_D+V_B)}{\partial \dot{\theta}_1}=T_{f1} \tag{3.22a}$$

$$\frac{d}{dt}(\frac{\partial(T-U)}{\partial \dot{\theta}_2})-\frac{\partial(T-U)}{\partial \dot{\theta}_2}+\frac{\partial(V_D+V_B)}{\partial \dot{\theta}_2}=T_{f2} \tag{3.22b}$$

$$\frac{d}{dt}(\frac{\partial(T-U)}{\partial \dot{\theta}_3})-\frac{\partial(T-U)}{\partial \dot{\theta}_3}+\frac{\partial(V_D+V_B)}{\partial \dot{\theta}_3}=\tau_1 \tag{3.22c}$$

$$\frac{d}{dt}(\frac{\partial(T-U)}{\partial \dot{\theta}_4})-\frac{\partial(T-U)}{\partial \dot{\theta}_4}+\frac{\partial(V_D+V_B)}{\partial \dot{\theta}_4}=\tau_2 \tag{3.22d}$$

$$\frac{d}{dt}\left(\frac{\partial(T-U)}{\partial \dot{\varphi}_{1i}}\right)-\frac{\partial(T-U)}{\partial \varphi_{1i}}+\frac{\partial(V_D+V_B)}{\partial \dot{\varphi}_{1i}}=0.0 \quad i=1,2,\ldots,M \qquad (3.22e)$$

$$\frac{d}{dt}\left(\frac{\partial(T-U)}{\partial \dot{\varphi}_{2i}}\right)-\frac{\partial(T-U)}{\partial \varphi_{2i}}+\frac{\partial(V_D+V_B)}{\partial \dot{\varphi}_{2i}}=0.0 \quad i=1,2,\ldots,M \qquad (3.22f)$$

After mathematical manipulations, the final form of the equations can be concisely given as:

$$\begin{bmatrix} m_{11} & m_{12} & m_{13} & m_{14} & \ldots & m_{1N} \\ m_{21} & m_{22} & m_{23} & m_{24} & \ldots & m_{2N} \\ m_{31} & m_{32} & m_{33} & m_{34} & \ldots & m_{3N} \\ m_{41} & m_{42} & m_{43} & m_{44} & \ldots & m_{4N} \\ \cdot & & & & & \cdot \\ \cdot & & & & & \cdot \\ \cdot & & & & & \cdot \\ \cdot & & & & & \cdot \\ \cdot & & & & & \cdot \\ m_{N1} & m_{N2} & m_{N3} & m_{N4} & \ldots & m_{NN} \end{bmatrix} \begin{bmatrix} \ddot{\theta}_1 \\ \ddot{\theta}_2 \\ \ddot{\theta}_3 \\ \ddot{\theta}_4 \\ \ddot{\varphi}_{11} \\ \vdots \\ \ddot{\varphi}_{1M} \\ \ddot{\varphi}_{21} \\ \vdots \\ \ddot{\varphi}_{2M} \end{bmatrix} = \begin{bmatrix} f_1 \\ f_2 \\ f_3 \\ f_4 \\ f_5 \\ \cdot \\ \cdot \\ \cdot \\ \cdot \\ f_N \end{bmatrix} \qquad (3.23)$$

where $N=2M+4$ and ($\ddot{}$) denotes the second derivative with respect to time. Each element of m_{ij} is dependent on the position and configuration of the manipulator and is a function of the system variables. The right side of the equation depends on system variables, their first derivatives, the friction torques, and the input torques. Equation (3.23) represents a highly nonlinear, multi-degree of freedom dynamic system. The complete expressions of the equation are given in Appendix A.

3.7 Numerical Simulations

In the numerical simulations, the dynamic characteristics of the excitation DC motors are considered. A DC motor's output torque can be approximately given as

$$\tau = C_\tau i \times (1 - e^{-\frac{t}{\omega_m \cdot \tau_e}}) \qquad (3.24)$$

where τ is the motor's output torque, i is its input current, C_τ is the motor's torque constant, and ε_m and ε_e are the mechanical and electrical time constants of the motor, respectively. Usually the mechanical time constant is much smaller than the electrical time constant and can be neglected.

A computer program has been written to simulate the dynamics of the manipulator. The numerical integration of equation (3.23) is implemented through a fourth order Runge-Kutta algorithm and a Gaussian elimination scheme. The program code consists of a number of function routines and subroutines. Three major subroutines are the dynamic equation, the Gaussian elimination, and the Runge-Kutta integration, as shown by the flow chart of the program (Figure 3.4). The simulations are implemented on a SUN SPARC 330 workstation, and the simulation results will be presented in Chapter 4 together with experimental verifications.

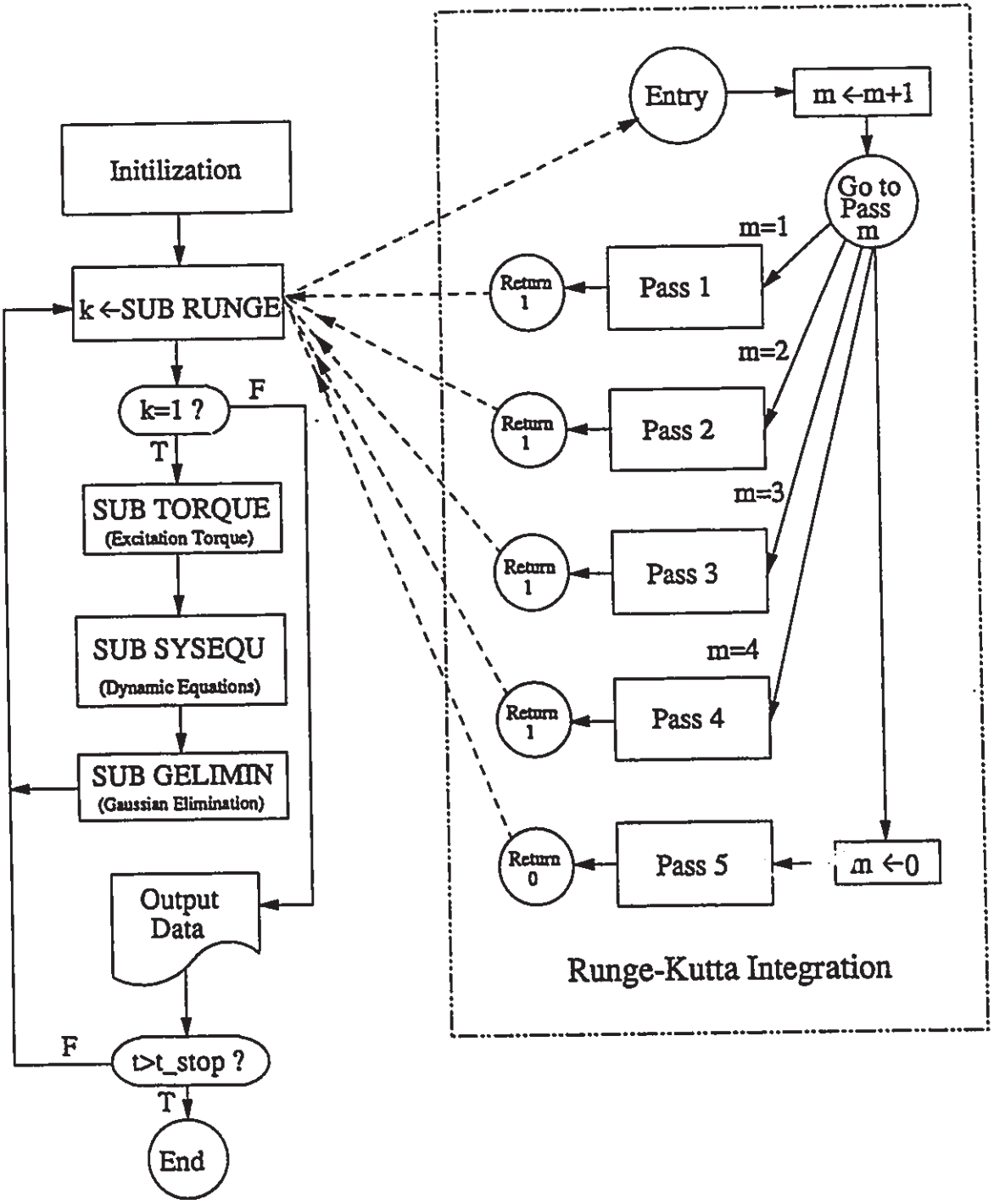

Figure 3.4 Flow Chart of Simulation Program

MODEL VERIFICATION

4.1 Introduction

An experimental manipulator is developed to verify the simulation results. Generally, the theoretical analysis is performed based on certain assumptions. The validity of the theoretical assumption is best evaluated through experimental studies. The theoretical analysis itself also needs experimental validation. This chapter presents the development of the experimental facility and the experimental verification of the dynamic equations derived in the previous chapter.

4.2 Development Of Experimental Facility

The experimental facility consists of a two degrees of freedom robotic manipulator, an electrical sensory system, and a monitoring personal computer. The manipulator is designed to suit its theoretical pattern discussed in Chapter 3. The dynamic performance of the manipulator is measured through the sensory

system and read in by the computer. The actuation torques of the manipulator are completely controlled through the written program code.

4.2.1 Design Of The Experimental Manipulator

There are three major considerations for the design of the experimental manipulator. The first one is to make the experimental structure fit the assumed theoretical pattern as closely as possible. Since the torsional deformation of the links is theoretically assumed as being zero, the actual manipulator arms should be designed with a large polar momentum of inertia for the cross-section area and a large area momentum of inertia along vertical direction so that the arm's bending deflection caused by the gravity force in the vertical direction and the torsional deformation resulting from twisting disturbance are small and negligible.

The second consideration is the desired natural frequencies of the system. The performance control of the manipulator will be implemented in real time through a 386 IBM personal computer. The vibration frequencies of the system must be low enough to satisfy the computer speed limitation. Theoretically increasing the length of the manipulator arm lowers its natural frequencies, but it also reduces the rigidity of the arm along the vertical direction and decreases its torsional deformation resistance. Reducing the arm's thickness results in a similar effect.

The third consideration is the determination of the joint stiffness. In the theoretical pattern, the two flexible joints are simplified as two linear torsional springs. The oscillation effect of the joint angle, caused by the elasticity of the

joint on the endpoint position of the manipulator, is magnified through the length of the link. In order to examine the effect of both the link flexibility and the joint elasticity on the manipulator's performance at the same time, the torsional springs should possess reasonably large stiffness and hence the two kinds of flexibilities have approximately the same effect on the endpoint of the manipulator.

The final dimensions of the facility are determined as:

The first link:	0.9 (m) x 0.035 (m) x 0.0045 (m)
The second link:	0.8 (m) x 0.030 (m) x 0.0030 (m)
The first joint:	761.59 (Nm/rad.) (custom-made)
The second joint:	497.96 (Nm/rad.) (custom-made)

A structural sketch of the experimental manipulator is shown in Figure 4.1 and its components are listed on Table 1. The whole mechanism operates on a horizontal plane. The second link is mounted on the free end of the first arm and is totally carried by the first arm. Both arms are driven by DC Servo motors. In order to enhance the output torque of the first motor, a pair of gears with a transmission ratio of 5:1 is used. The motor for the second arm has a built-in harmonic drive system with a transmission ratio of 48.96:1.

The two torsional springs are inserted between the motors and the arm hubs. Two optical incremental encoders, one connected with the motor shaft and one attached to the hub shaft, are used at each joint to monitor the joint angle position and the torsional spring's elastic deformation. In order to eliminate the backlash between the pair of gears at the first joint, the axial distance between the gears is adjustable. The second motor is located vertically very close to the first arm to reduce the twisting disturbance.

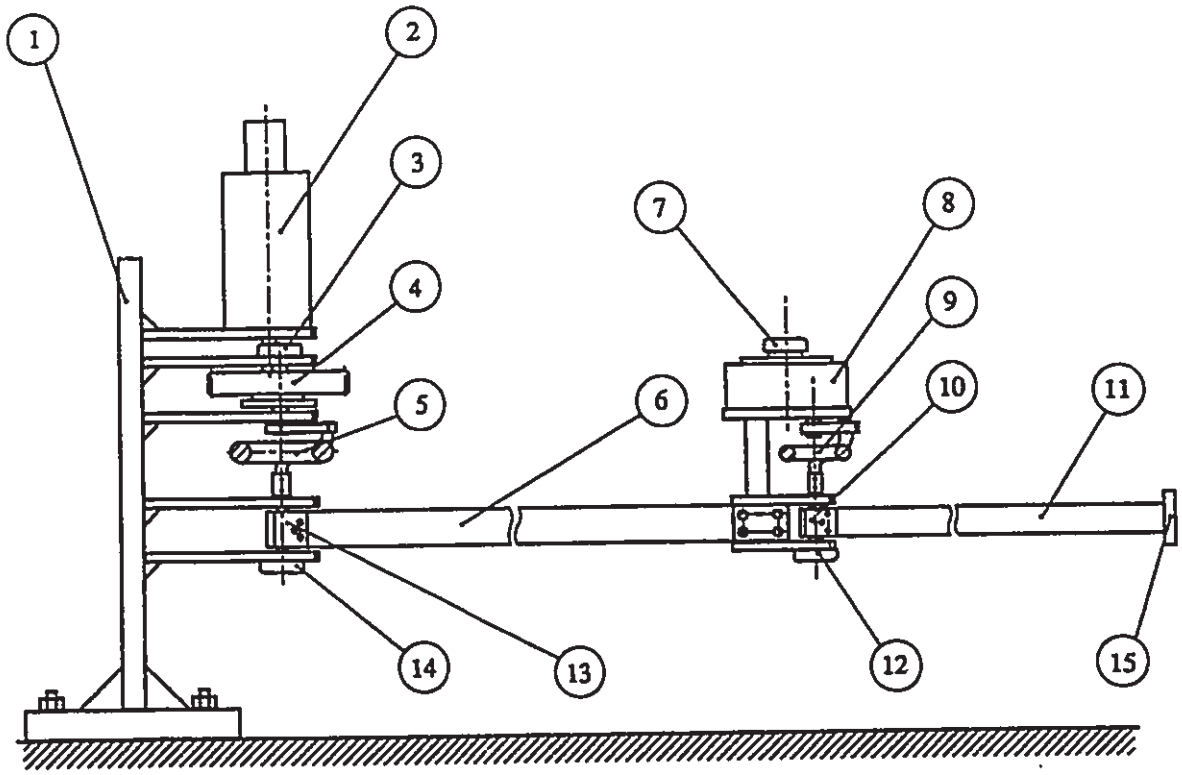

Figure 4.1 Structure Of The Experimental Manipulator

Ref. No (Fig. 4.1)	Part Description	Ref. No (Fig. 4.1)	Part Description
1	Support	9	Flexible Joint 2
2	DC Motor 1	10	Hub 2
3	Optical Encoder 1	11	Link 2
4	Driving Gear Pair	12	Optical Encoder 4
5	Flexible Joint 1	13	Hub 1
6	Link 1	14	Optical Encoder 2
7	Optical Encoder 3	15	Payload
8	DC Motor 2		

Table 1. Components Of The Experimental Manipulator

The manipulator is mounted to a reverse "T" shape support, which is a one inch thick steel plate that is bolted to a large, thick steel block. Compared to the manipulator, the supporting base is much stiffer and the effects of the base's elastic deformation on the dynamic performance of the robot are negligible.

4.2.2 Sensory System

For a closed-loop dynamic process, the control input is calculated based on the system's response and the dynamic response of the system is monitored through detecting sensors. A successfully controlled process is usually associated with an accurate and reliable sensory system. In the flexible manipulator area, several different kinds of sensing techniques have been applied. One of the popular approaches is using a video camera with a vision algorithm to monitor the manipulator's endpoint position. The major drawbacks of using a video camera as a sensor include the requirement of intensive computation and the limitation of the sensing range.

A strain gage is a simple but effective electrical sensing device. It translates the strain variation of a measurant into an electrical signal, which can be easily monitored. The strain gages are used here to sense the bending vibrations of the flexible arm. Ten strain gages are used on each arm and their locations are optimized through strain distribution analysis. The joint angle positions and the joint elastic deformations of the manipulator are detected by a set of optical encoders. The encoders are interfaced to the control computer using a custom-design counting circuit. Combining the information provided by these two

types of sensors, the endpoint position of the manipulator can be determined with little computation.

The detailed sensory system setups are given in Appendix B.

4.2.3 Computer Interfacing

The data communication among the computer, the motor amplifiers, the encoder counting circuit, and the strain gage amplifiers is implemented through a Data Translation's Analog and Digital I/O boards (DT2831). The board provides a A/D converting subsystem with up to 16 input channels with 12-bit resolution, a D/A subsystem featuring 2 independent D/A converters with 12-bit resolution, and eight digital I/O channels. The first 10 A/D input channels are used here for the sampling of the strain gage's signals. The eight digital I/O lines are connected with the counting circuit output bits to read in the joint angle position. The two D/A converter channels provide the command signals for the motor amplifiers. The data translations are monitored by a written program.

The complete experimental setup is outlined in Figure 4.2, and Figure 4.3 is a photograph of the actual experimental hardware.

4.3 Model Verification

The dynamic response of the manipulator to certain excitations was predicted using numerical simulations. The excitation input is a square wave with a period of 1.0 second and the excitation torques last for a full second. With the same excitation, the experiments are conducted and the actual vibration data of the

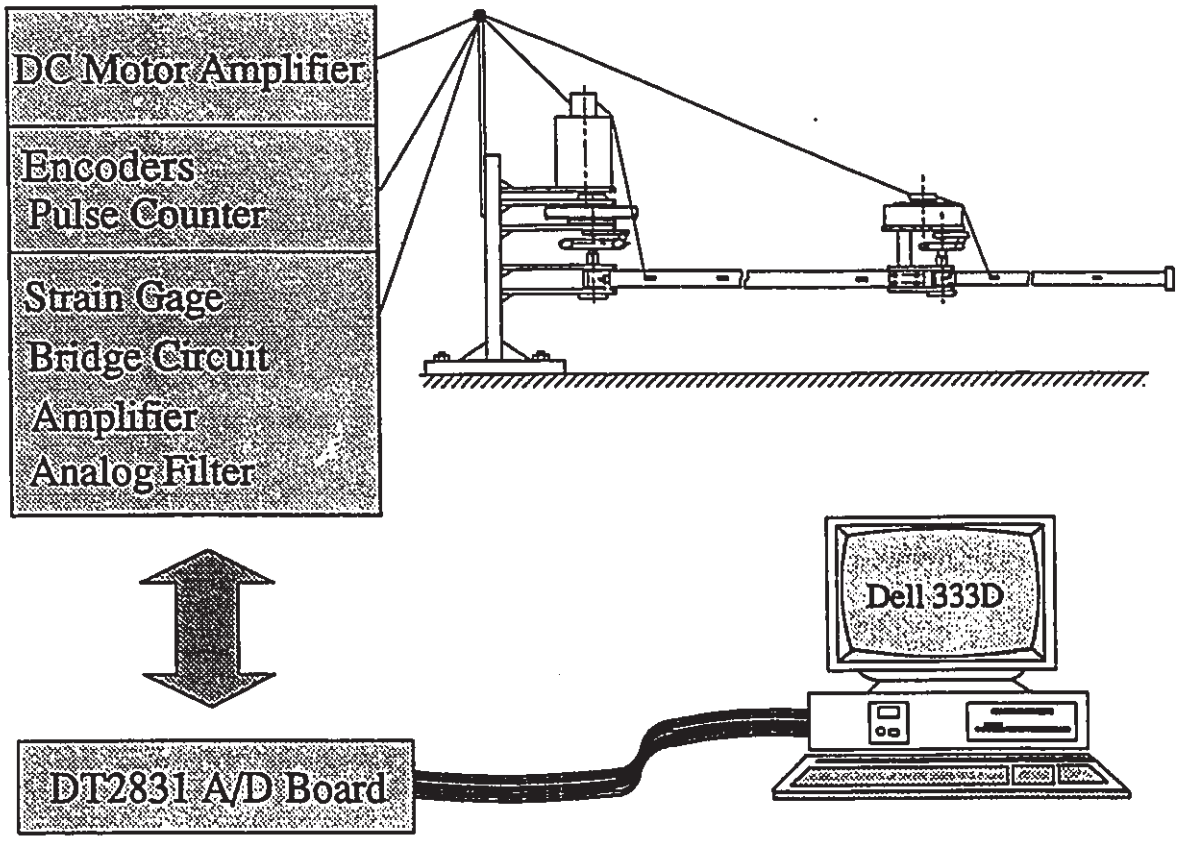

Figure 4.2 Experimental Setup

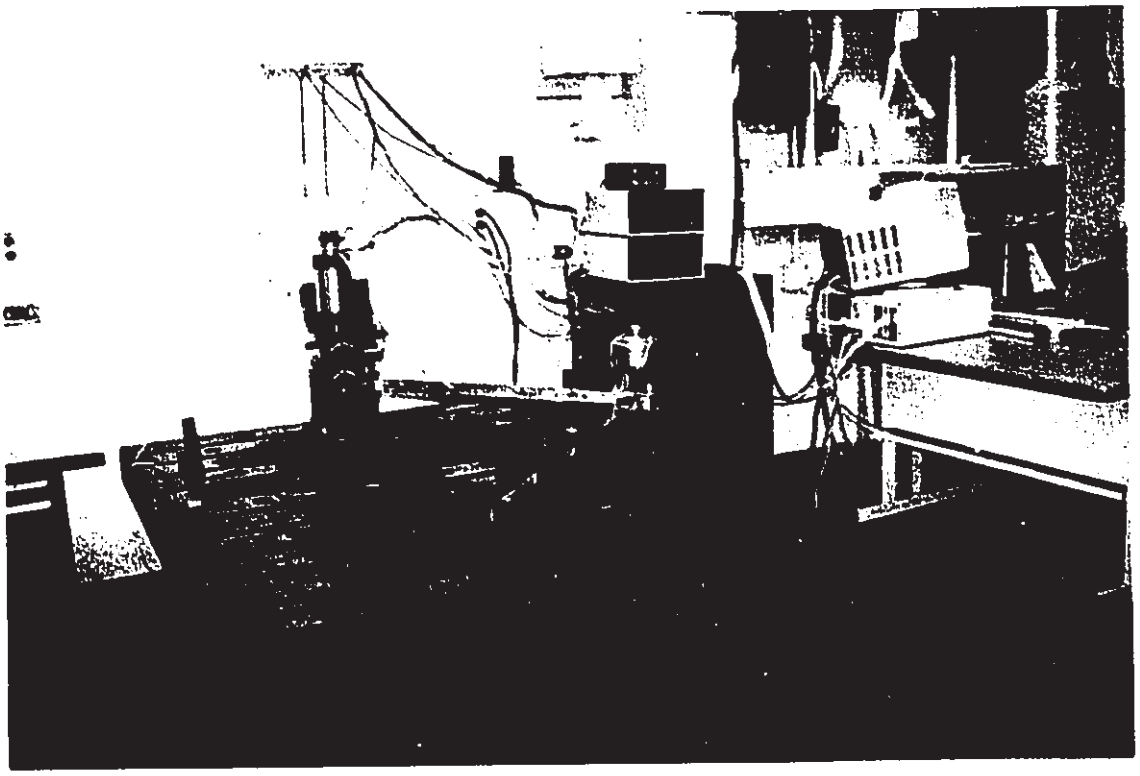

Figure 4.3 Photograph of Experimental Facility

manipulator are collected. Table 2 lists the system parameter values used in the simulation. Figure 4.4 and 4.5 shows the comparison of the simulation results with experimental data. The bending deflection of the arms are given in Figure 4.4, and the variations of the joint angles in Figure 4.5.

The First Link				
A_1 (m^2)	D_1(kg/m^3)	E_1(N/m^2)	I_1(m^4)	L_1(m)
1.575×10^{-4}	2.707×10^{4}	6.890×10^{11}	2.657×10^{-10}	0.8
The Second Link				
A_2 (m^2)	D_2(kg/m^3)	E_2(N/m^2)	I_2(m^4)	L_2(m)
9.525×10^{-5}	2.707×10^{4}	6.890×10^{11}	8.001×10^{-11}	0.9
Joints					
K_1(Nm/rad)	K_2(Nm/rad)	J_1(kgm^2)	J_2(kgm^2)	K_{F1}(Nm)	K_{F2}(Nm)
761.59	497.96	1.07×10^{-2}	9.25×10^{-3}	0.16	0.01
Hubs			Actuators	
I_{h1}(kgm^2)	I_{h2}(kgm^2)	M_{h2}(kg)	I_{r2}(kgm^2)	M_{r2}(kg)
1.43×10^{-7}	1.05×10^{-7}	0.24	1.15×10^{-2}	3.03
Internal Damping		Payload	
Ratio 1	Ratio 2	I_p(kgm^2)	M_p(kg)
0.03	0.03	1.078×10^{-7}	0.1

Table 2 System Parameters

Both Figures 4.4 and 4.5 clearly show that the theoretical model is in good agreement with the experiments. There is some small disagreement between the two sets of data, particularly at high frequencies. These differences could be due to minor differences between the theoretical assumptions and the experiments, and non-perfect alignment of the experimental apparatus.

The theoretical model is derived based on the assumption that there are no gravity effects or torsional vibrations for both of the arms. This assumption is not completely satisfied by the experimental facility. Gravity and non-perfect alignment cause some twisting motions of the arms and bending deflections along the vertical direction. These motions definitely affect the strain gages' outputs. Also the actual torsional springs are not perfectly linear and the modelling of the gear backlash and the dry friction at the joints is just a mathematical approximation. However, it is felt that the results of the simulations are reasonably close to the experimental data and the derived theoretical model is reasonably adequate for studying the effects of link and joint flexibilities on the manipulator dynamics and for control purposes.

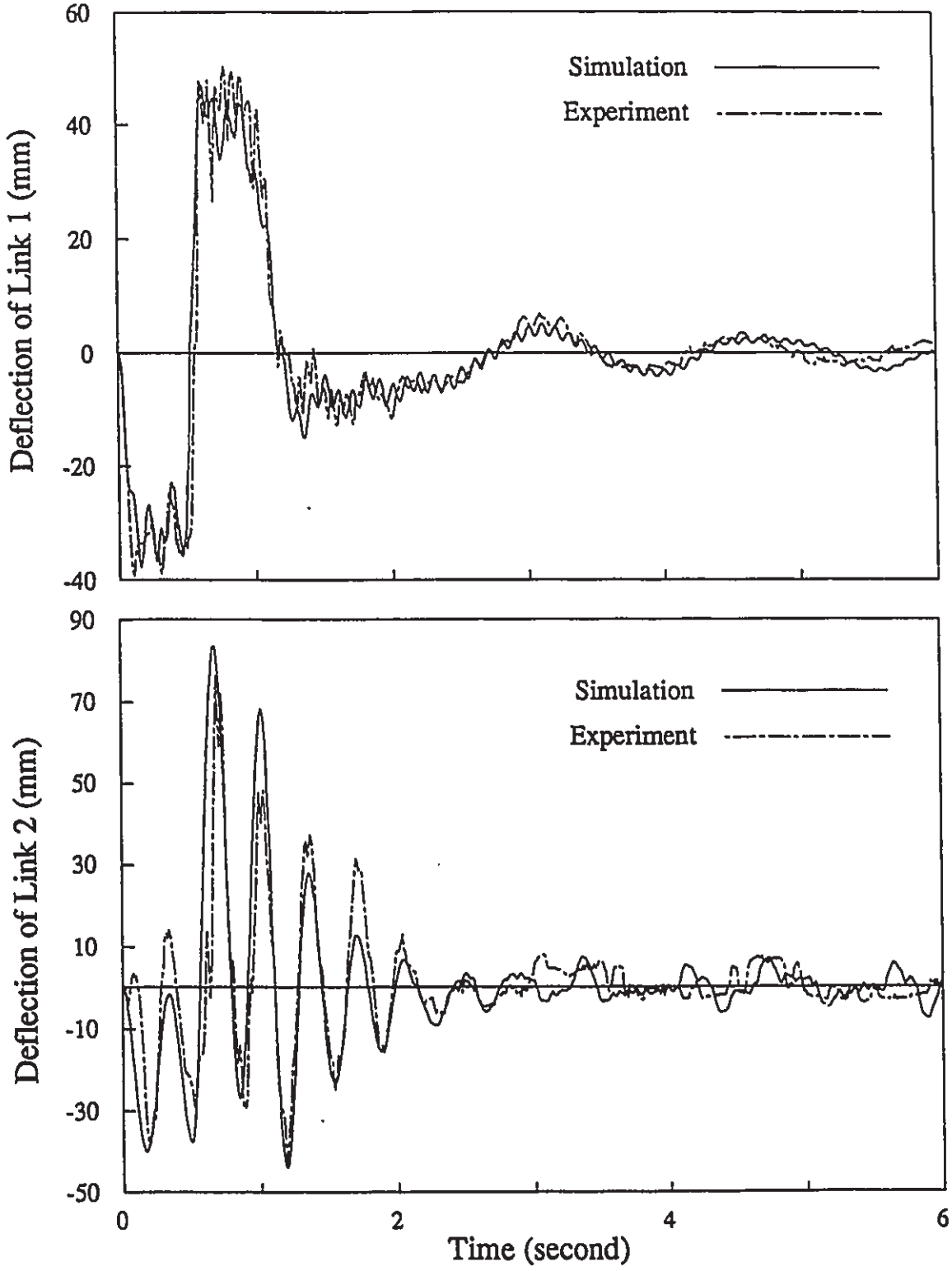

Figure 4.4 Bending Deflections Of The Arms

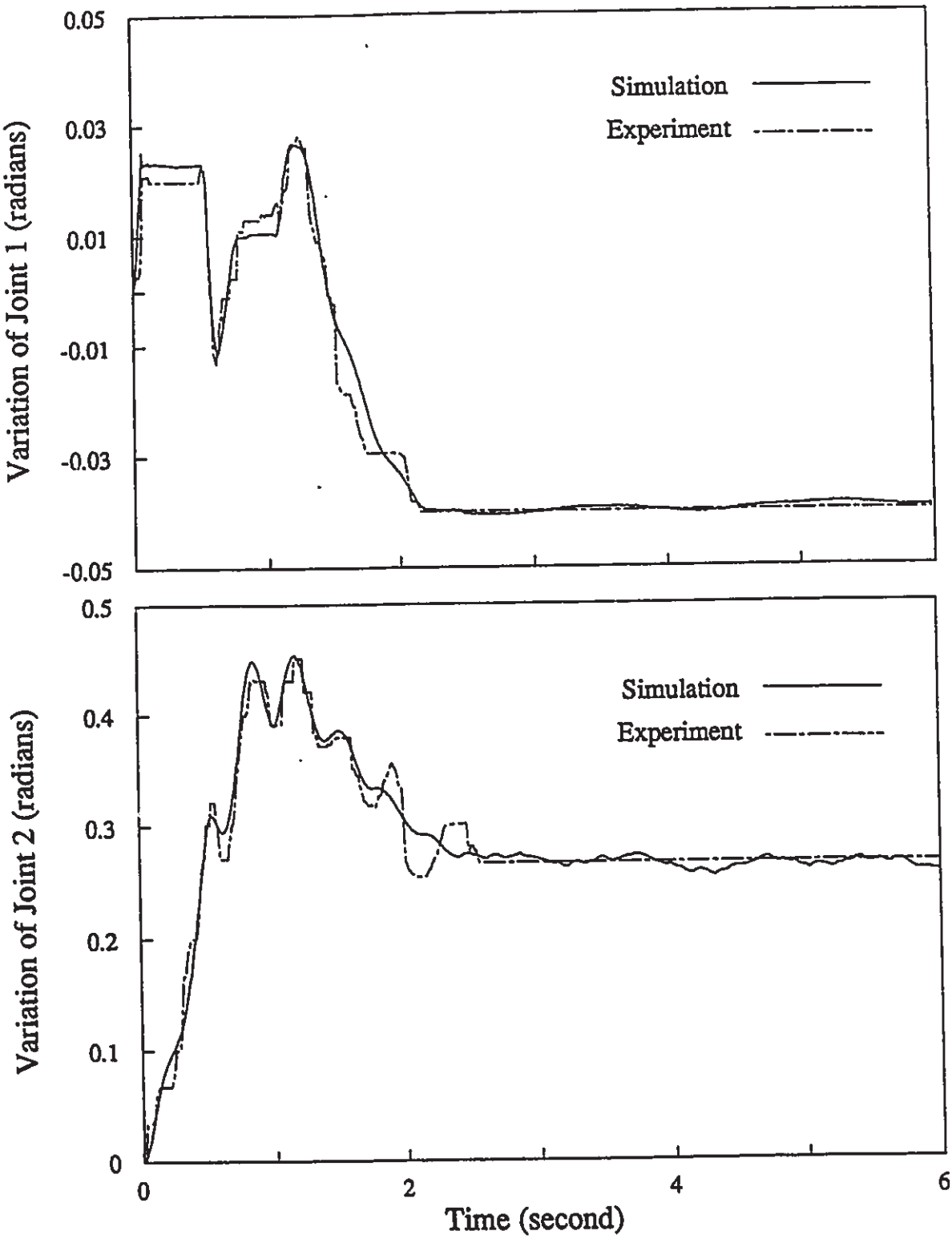

Figure 4.5 Angle Oscillations Of The Joints

PARAMETRIC ANALYSIS

5.1 Introduction

The manipulator in the current study is a rather complex dynamic system with many system parameters. Every system parameter has certain influence on the system dynamics, but their effects are not equal. The objective of the parametric analysis is to examine the effects of each of the system parameters on the dynamic performance of the manipulator and sequentially find out the dynamic interactions among its members.

Using the experimentally verified dynamic equations as a "baseline model", numerical simulations were performed by varying each parameter one at a time. The results were examined in the frequency domain. The parameters considered included the payload, the stiffnesses of the joints, the lengths of the links, the backlash clearance, and the friction torques. The system response was evaluated by examining the bending motions for both links and the angle variations of the two joints.

5.2 Effects Of System Parameters

As expected, the variation of the payload magnitude affects both the vibration amplitude and the frequency of the links. Increasing the payload lowers the link's natural frequency. Figure 5.1 shows that the vibration magnitude of the first link increases with the increment of the payload value. For the second link, the vibration magnitude reaches its maximum around the payload of 0.8 kg and has its minimum around the payload of 0.3 kg. The payload's effects on the joints are similar to those on the corresponding links. The dynamic interaction between the two links is quite significant.

The joint stiffness (see Figure 5.2) determines the joint angle's variation magnitude and its oscillation frequencies. Although increasing the stiffness dramatically reduces the joint oscillation magnitude and lowers the frequency content, its effect on the link's performance is not significant since the links are much more flexible than the joints. This statement holds for both joints. The dynamic interaction between the two joints is not as strong as that between the links.

The dry friction at the joint results in a damping effect and change in the link's boundary conditions. The boundary conditions directly affect the link's natural frequencies, and hence influence the vibration magnitude. Except for the condition where the friction is close to zero, increasing the friction value at the joints results in the reduction of the bending magnitude and the increase of the vibration frequencies for both links (see Figure 5.3). The results for both links are very similar and hence plots for link 1 are omitted here. Further increase of the

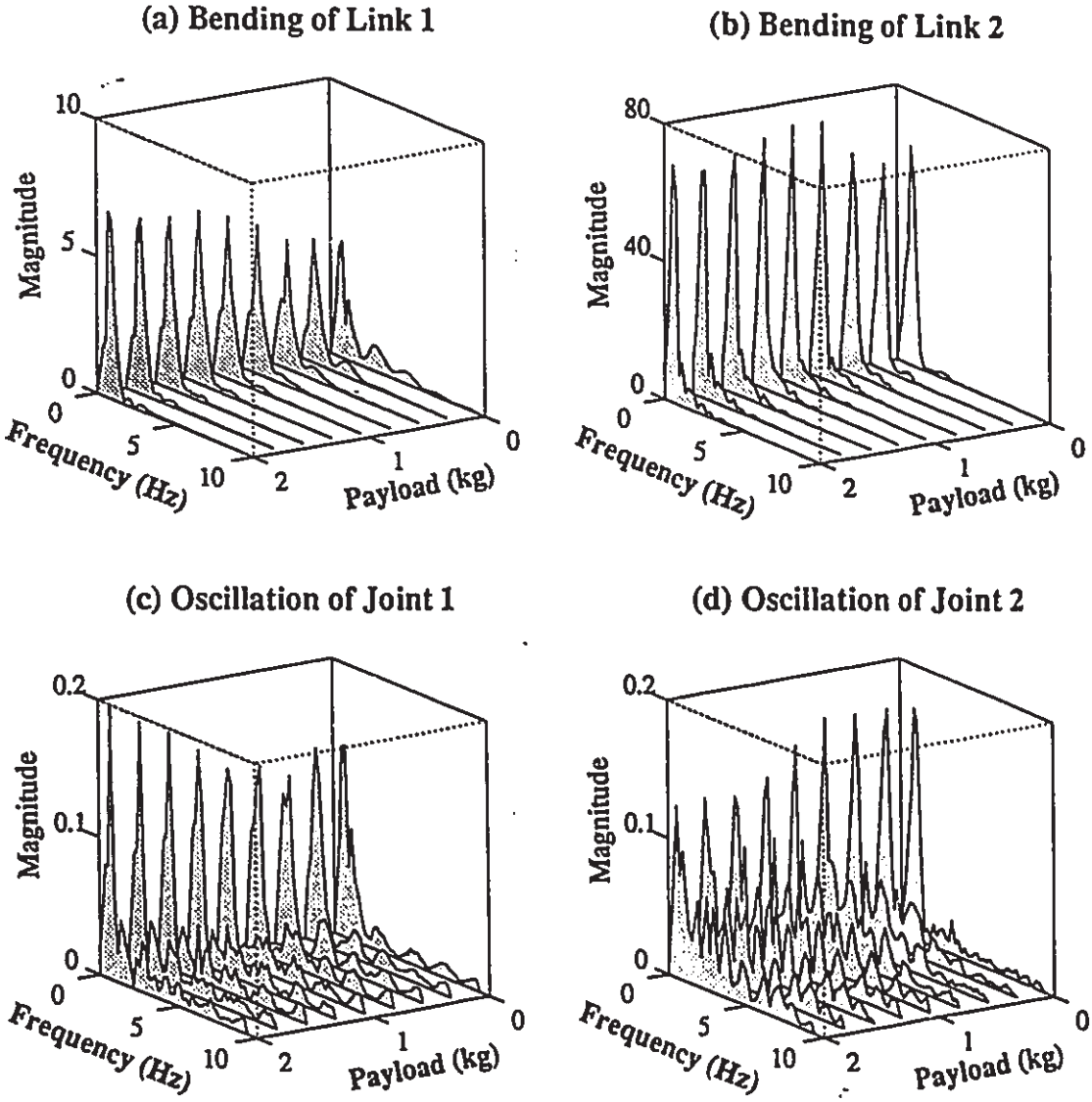

Figure 5.1 Effects Of Payload

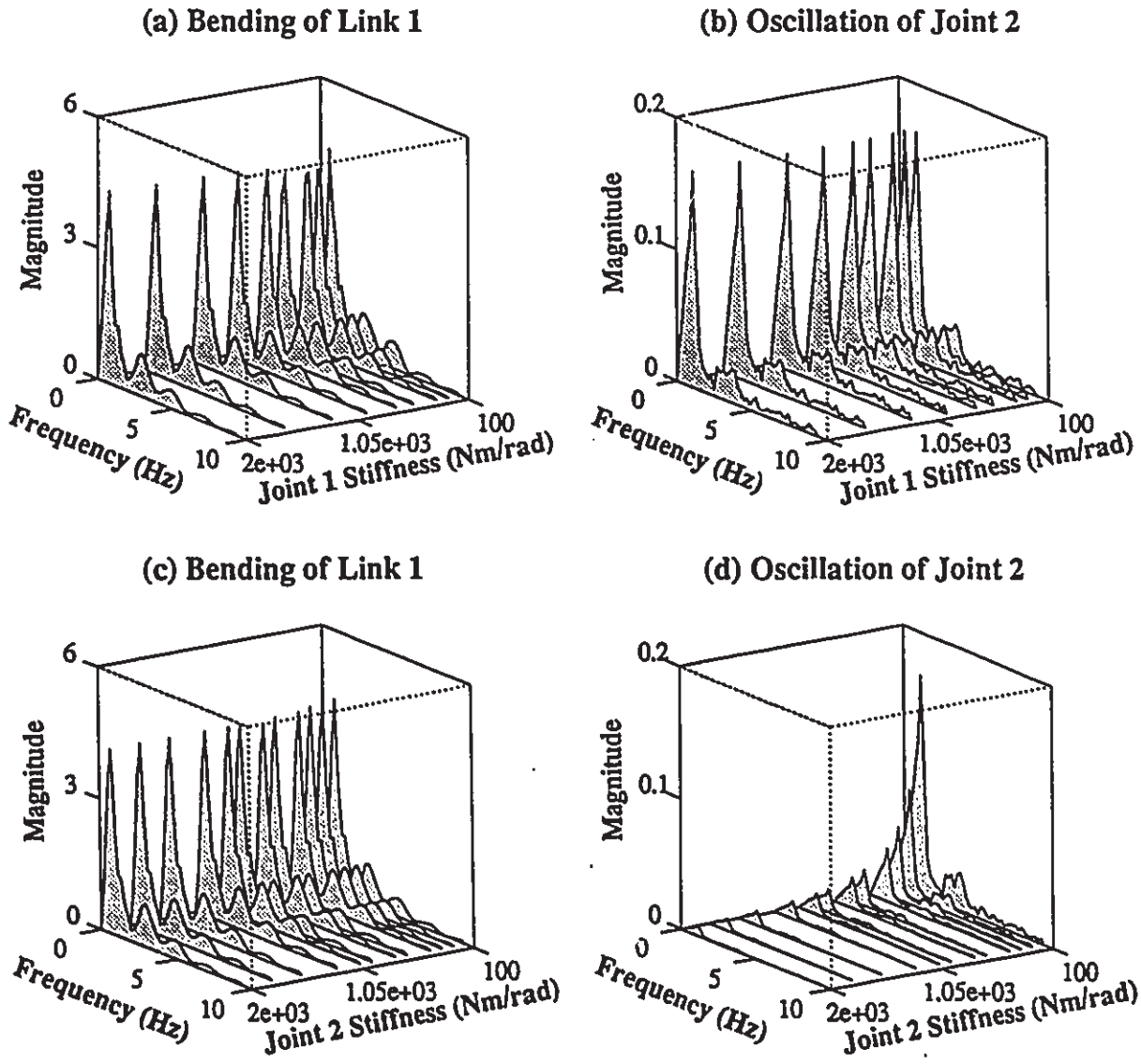

Figure 5.2 Effects Of Joint Stiffness

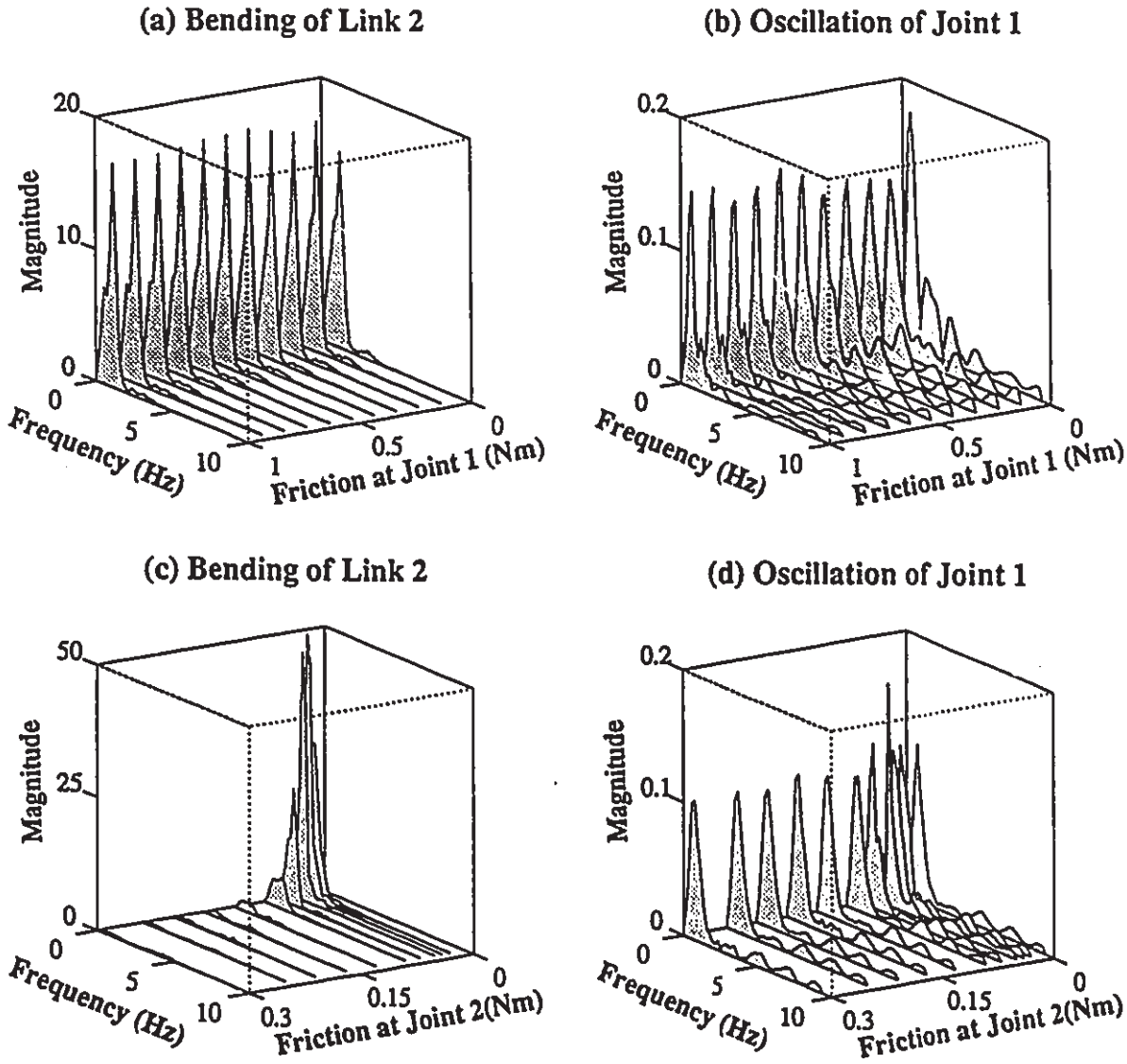

Figure 5.3 Effects Of Joint Friction

friction value does not enhance the damping effect linearly. The damping effects on the joint oscillations are not as significant as those on the links.

The backlash phenomenon between gears is modelled as an impact damper. The damping effect is dependent on the clearance of backlash and the coefficient of restitution. Figure 5.4 shows that the most effective damping occurs at the gear backlash magnitude of 0.2 degree. Further increasing the backlash reduces its damping effect. When the magnitude exceeds 2 degrees, the damping is nearly constant. This conclusion can be reached both for the links and the joints performance. The damping effects on the second link and the second joint oscillations are much more significant than those on the first link and joint. Backlash exists only at the second joint and the backlash between the gears at the first joint is considered to be zero.

Generally, the link with longer dimension has lower natural frequencies and a larger vibration magnitude, as shown in Figure 5.5. The minimum occurs around a length of 0.6 meter, due to the changing of the link natural frequency and the closeness of the natural frequency to the excitation. The length of the link has little effect on the performance of both joints. The dynamic coupling between the two links with respect to the length variation is not very significant. Increasing the length of the first link slightly decreases the magnitude of the second link's vibration. A longer second link causes lower vibration frequency for the first link.

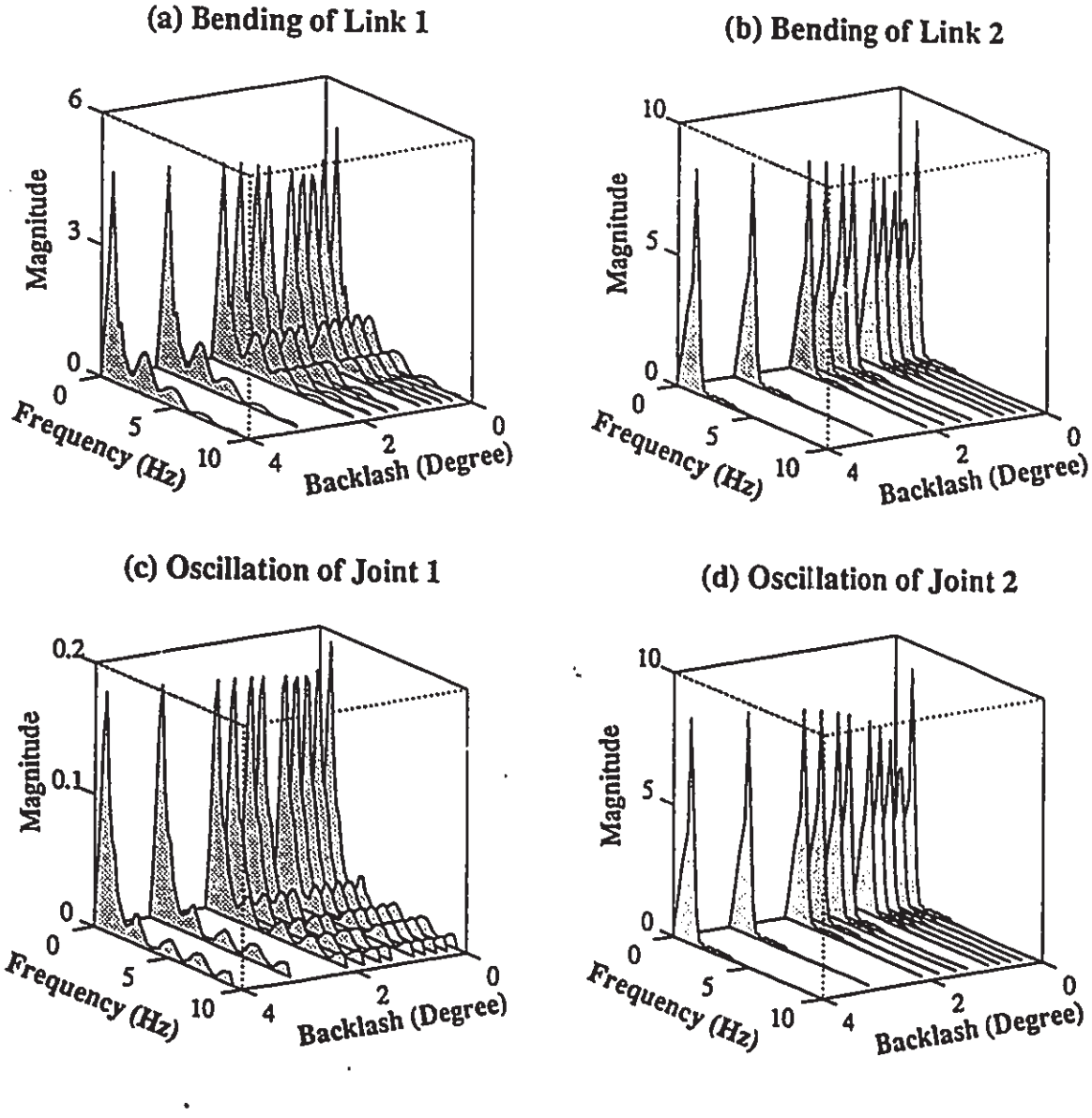

Figure 5.4 Effects of Gear Backlash

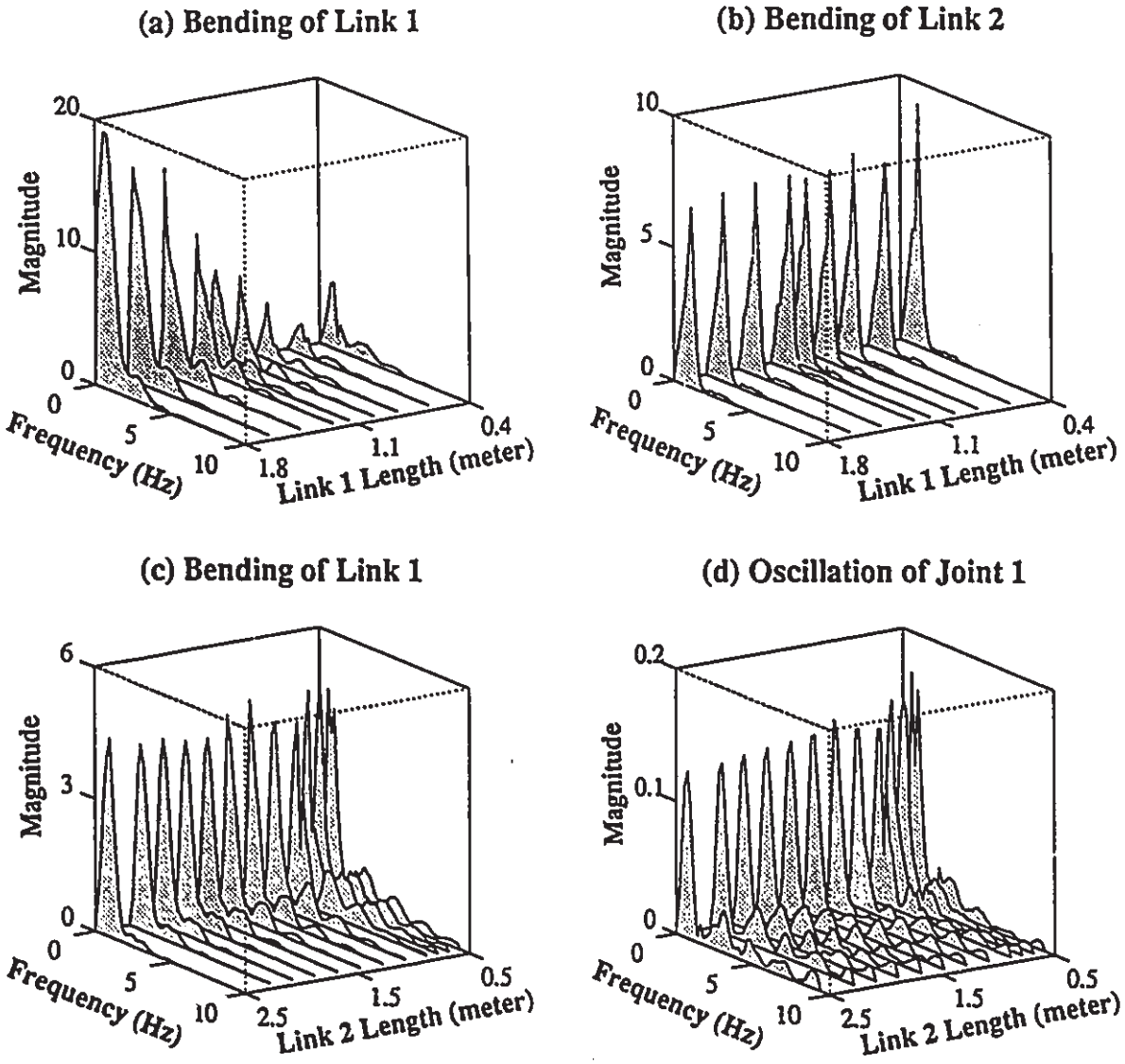

Figure 5.5 Effects Of Arm Length

5.3 Dynamic Interactions Among Manipulator's Members

The parametric studies have revealed some important dynamic relations between the system parameters and the manipulator dynamics, as well as the dynamic interactions between the members of the manipulator. It is clear that the dynamic interaction between the joints is not as strong as that between the links. In fact, the dynamics of one joint are almost completely independent of the parameter values of another joint within the examined range of parameter values. The performance of one link is definitely affected by the values of the parameter of another link, but not as strongly as it is affected by its own parameters. The dynamic coupling relation between one link and its driving joint is very significant and varies with the system parameters. The values of the parameters of the second joint affect both links, however their effect on the second link is stronger.

Model Linearization And Order Reduction

6.1 Introduction

The dynamic modelling of the manipulator is implemented with the Lagrangian assumed-modes method. With this approach, the bending deformation of the arm is considered as the superposition of its natural modes. The obtained model relies on the truncation of the infinite modal series, which not only directly determines the model's order and accuracy, but also affects the corresponding control algorithm's design and performance. Generally, a higher order model improves the controller's robustness and performance, yet requires larger bandwidth sensors and faster computation. The idea of model order reduction is to obtain a lower order model such that the dominant features of the whole system are retained.

Although the dynamic model of the manipulator is verified experimentally, it is too complicated to be used directly for control purposes. In this chapter, the

derived nonlinear model of the manipulator is linearized and the proper truncation of the infinite modal series is determined. Using the power contribution of the system states as the criterion, a new approach for model order reduction of nonlinear dynamic systems is developed and is applied to the two link flexible manipulator.

6.2 Model Linearization

The state space representation of equation (3.23) can be given as

$$M[x(t)]\,\dot{x} = F[x(t), u(t)] \tag{6.1}$$

with the state vector $x(t) = [\, q \;\; \dot{q} \,]^T$ and the system input vector $u(t)$. $M(x)$ and $F(x,u)$ are vector valued functions.

The linearization of equation (6.1) is performed around a nominal trajectory $\bar{x}(t)$, which is obtained by the application of the nominal input $\bar{u}(t)$ to the system. The variables of the nominal path satisfy the system's dynamic equations:

$$M[\bar{x}(t)]\,\dot{\bar{x}} = F[\bar{x}(t), \bar{u}(t)] \qquad \bar{x}(t_0) = x(t_0) \tag{6.2}$$

Suppose that the motion of the manipulator evolving along the nominal trajectory $(\bar{x}(t), \bar{u}(t))$ is perturbed, which results in deviations $(\delta x(t), \delta u(t))$ from the nominal trajectory. The perturbed variables also satisfy the motion equations of the manipulator:

$$M[\bar{x}(t) + \delta x(t)]\frac{d}{dt}(\bar{x}(t) + \delta x(t)) = F[\bar{x}(t) + \delta x(t), \bar{u}(t) + \delta u(t)] \tag{6.3}$$

Performing Taylor's series expansion on M and F in equation (6.3), using equation (6.2), and disregarding the terms higher than the first order, we obtain the following equation:

$$M[\bar{x}(t)]\delta\dot{x} = \left(\left.\frac{\partial F}{\partial x}\right|_{(\bar{x},\bar{u})} - \left.\frac{\partial M}{\partial x}\right|_{(\bar{x})} \dot{\bar{x}} \right)\delta x + \left.\frac{\partial F}{\partial x}\right|_{(\bar{x},\bar{u})} \delta u \tag{6.4}$$

where the derivatives $\partial F/\partial x, (\partial M/\partial x)\,\dot{\bar{x}}$, and $\partial F/\partial u$ are the Jacobian matrices evaluated at the nominal path $(\bar{x}, \bar{u})$. With the given nominal trajectory, equation (6.4) stands for a linear dynamic system with the state variable δx and the system input δu.

The nonlinear dynamic model of the manipulator (6.1) includes the effects of the friction force at the joints and the backlash clearance between the driving gears, which are characterized by equations (3.12) and (3.11). These two equations do not possess a continuous first derivative with respect to the system variables. In order to calculate $\partial F/\partial x$ for model linearization, a hyperbolic tangent function $\tanh(kx)$ is used to approximate the switching function features in equation (3.14) and the equation for the coefficient of restitution e; k is a gain constant. Increasing the magnitude of k improves the approximation accuracy and also increases the value of the function's first derivative.

The derived linear model (6.4) is validated through numerical simulations. The simulation results are presented in Figure 6.1 and 6.2. With a small perturbation ∂u, the dynamic performance of the linearized system is very close to the performance of the original nonlinear system.

6.3 Power Balancing Method

The power balancing technique is proposed by Han et al. [108] for the model reduction of undamped linear time-invariant dynamic systems. Assuming the damping effects being negligible for lightly damped systems, the power balancing technique can be applied for the systems which the balanced realization method fails to deal with due to the numerical difficulties. The power balancing method is extended here in order to be applicable to distributed parameter systems.

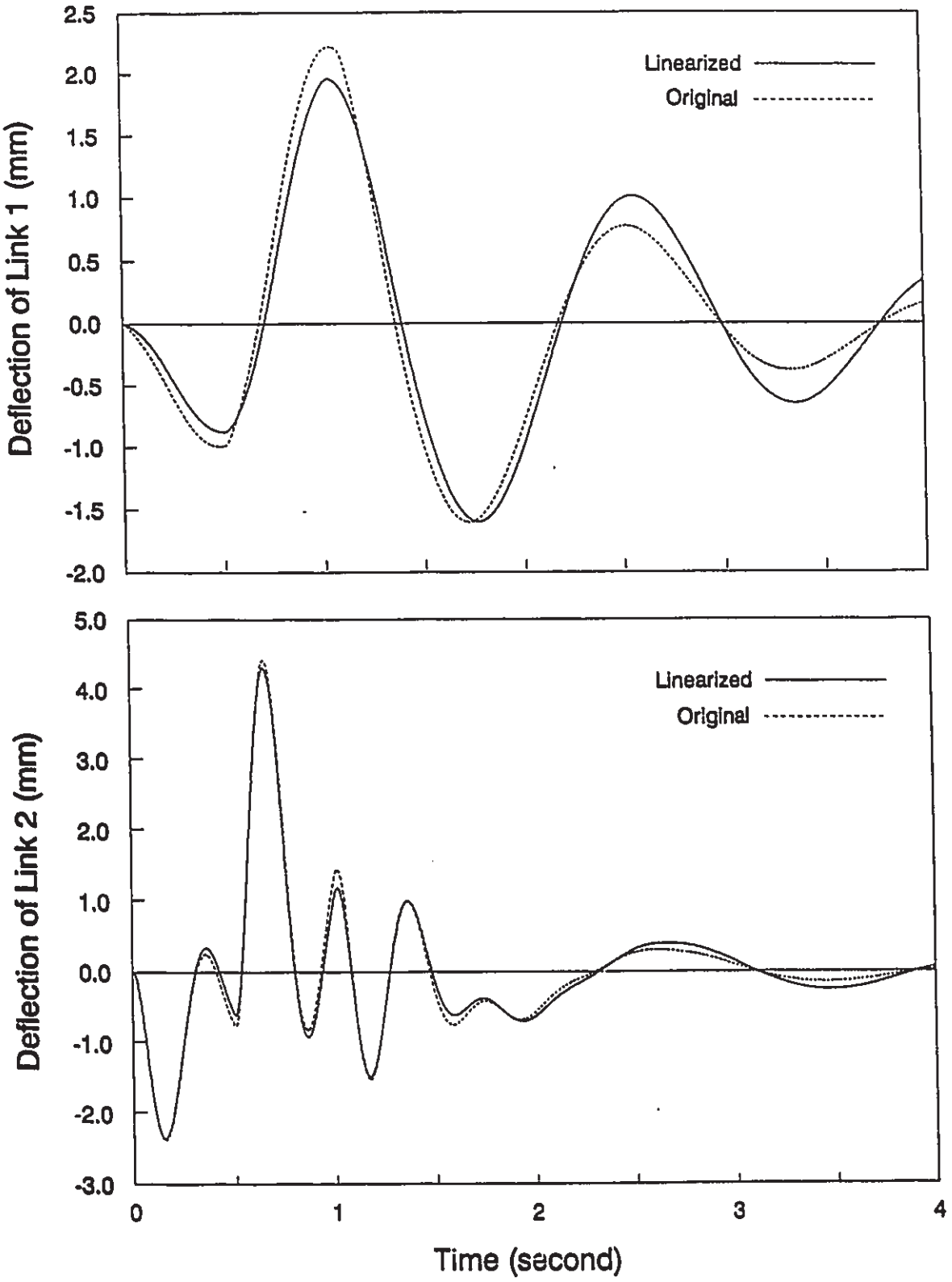

Figure 6.1 Verification of Linearized Model - Bending Deflection

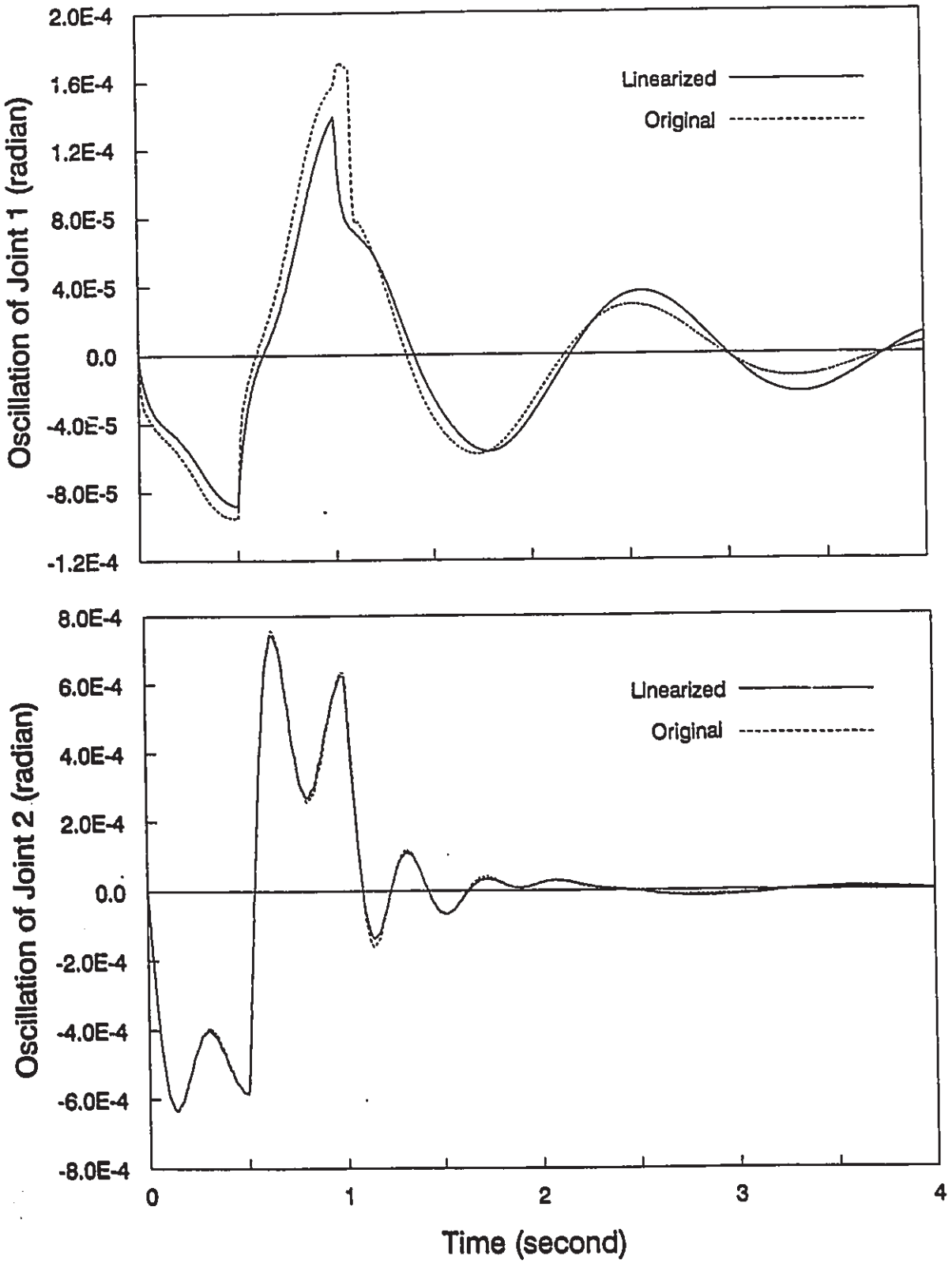

Figure 6.2 Verification of Linearized Model - Angle Oscillation

For an undamped linear time-invariant system

$$\dot{z} = Az + Bu \tag{6.5a}$$

$$y = Cz \tag{6.5b}$$

with

$$A=\begin{bmatrix} 0 & Q_1 \\ -Q_2 & 0 \end{bmatrix}, B=\begin{bmatrix} 0 \\ B_0 \end{bmatrix}, C=\begin{bmatrix} C_0 & 0 \end{bmatrix}$$

and

$$Q_1 = Q_1^T > 0, \quad Q_2 = Q_2^T > 0, \tag{6.6}$$

we define the system power matrix P_s as

$$P_s = \lim_{t\to\infty} \frac{2}{t} \int_0^t e^{A\tau} BB^T e^{A^T\tau} d\tau \tag{6.7}$$

and the output power matrix P_o as

$$P_o = \lim_{t\to\infty} \frac{2}{t} \int_0^t e^{A^T\tau} C^T C e^{A\tau} d\tau. \tag{6.8}$$

Using condition (6.6), a non-singular matrix S_1 can be found such that

$$Q_1 = S_1 S_1^T \quad \text{and} \quad \det S_1 \neq 0.$$

Letting

$$Q_3 = S_1^T Q_2 S_1$$

and performing a spectral decomposition on Q_3,

$$Q_3 = S_2 D^2 S_2^T$$

where S_2 is an orthogonal matrix, we obtain a diagonal matrix D,

$$D = \text{diag}(\omega_1, \omega_2, ..., \omega_n).$$

The non-zero diagonal elements ω_i ($i=1, 2, ..., n$) are the eigen-frequencies of the system. Now, through the state space coordinate transformation of

$$\xi = R_1 z \tag{6.9}$$

with

$$R_1 = \begin{bmatrix} S_2^T S_1^{-1} & 0 \\ 0 & S_2^{-1} S_1^T \end{bmatrix},$$

system (6.5) becomes

$$\dot{\xi}=\begin{bmatrix} 0 & I \\ -D^2 & 0 \end{bmatrix}\xi+\begin{bmatrix} 0 \\ \overline{B} \end{bmatrix}u \tag{6.10a}$$

$$y=\begin{bmatrix} \overline{C} & 0 \end{bmatrix}\xi \tag{6.10b}$$

with

$$\overline{B}=S_2^{-1}S_1^TB_0=[b_1^T,...,b_n^T]^T$$

and

$$\overline{C}=C_0S_1S_2^{-T}=[c_1,...,c_n].$$

By defining another state transformation

$$\eta=R_3R_2\xi \tag{6.11}$$

with

$$R_2=[\,e_1\ e_3\ \dots\ e_{2n-1}\ \vdots\ e_2\ e_4\ \dots\ e_{2n}\,]$$

$$R_3=\text{diag}\left(\sqrt{\frac{\|b_1\|}{\|c_1\|\omega_1}},\sqrt{\frac{\|b_1\|\omega_1}{\|c_1\|}},\dots,\sqrt{\frac{\|b_n\|}{\|c_n\|\omega_n}},\sqrt{\frac{\|b_n\|\omega_n}{\|c_n\|}}\right)$$

where e_k is the kth unit vector, we have the internally power balanced system

$$\dot{\eta}=\hat{A}\eta+\hat{B}u \tag{6.12a}$$

$$y=\hat{C}\eta \tag{6.12b}$$

with

$$\hat{P}_s=\text{diag}\left(\frac{\|b_1\|\|c_1\|}{\omega_1},\frac{\|b_1\|\|c_1\|}{\omega_1},\dots,\frac{\|b_n\|\|c_n\|}{\omega_n},\frac{\|b_n\|\|c_n\|}{\omega_n}\right)=\hat{P}_o$$

The contribution of each pair of states to the system power and the output power is represented uniquely by the power element ρ_i, which is defined as

$$\rho_i=\frac{\|b_i\|\|c_i\|}{\omega_i},\ i=1,2,..,n. \tag{6.13}$$

Using the power element's value as the model reduction criterion, a reduced order model can be obtained.

The above discussion outlines the power balancing technique proposed by Han et al.. The detailed derivation of the method is given in [108].

For many distributed parameter mechanical systems, such as flexible manipulators, with the assumption of damping being zero, their linearized state space models are in the form of equations (1) with Q_1 being the identity matrix and Q_2 being non-symmetric, which conflicts with the condition of $Q_2=Q_2^T$. This condition needs to be relaxed before the power balancing technique can be applied for distributed parameter systems. It is found that if Q_1 is the identity matrix and Q_2 is diagonalizable and has distinct positive eigenvalues, a system in the form of equations (6.5) can still be made internally power balanced by modifying the proposed state transformation matrices. Let

$$Q_3 = Q_2$$

and perform the decomposition

$$Q_3 = S_2 \Lambda S_2^{-1}.$$

Since Λ is a diagonal matrix and all its elements are non-negative, we can assign

$$D^2 = \Lambda.$$

Re-defining

$$R_1 = \begin{bmatrix} S_2^{-1} & 0 \\ 0 & S_2^{-1} \end{bmatrix}$$

and using the R_2 and R_3 defined earlier, an internally power balanced state transformation for the system (6.5) with the relaxed conditions can be given as

$$\eta = R_3 R_2 R_1 z.$$

The proof is similar to the one for proposition 3.2 in [108] and is given in Appendix D.

6.4 Power Elements Of Original System States

The power balancing technique discussed above provides the power elements of the internally power balanced system states, η, which represent the power contributions of the states η and reflect their relative importance with respect to the system power and the output power. This section presents the derivation of the power elements for the original system states, z, based on the determined power elements of η.

For system (6.5) with zero initial conditions and unit impulse inputs, the system states at time τ can be expressed as

$$z(\tau) = e^{A\tau}B. \tag{6.14}$$

The system power matrix can be written as

$$P_s = \lim_{t\to\infty} \frac{2}{t}\int_0^t e^{A\tau}BB^T e^{A^T\tau}d\tau = \lim_{t\to\infty}\int_0^t zz^T d\tau. \tag{6.15}$$

With the internally power balanced state transformation, we have

$$\lim_{t\to\infty} \frac{2}{t}\int_0^t \eta_i\eta_j d\tau = \begin{cases} \rho_i & i=j \\ 0 & i\neq j \end{cases} \tag{6.16}$$

where η_i is the ith internally power balanced state variable and ρ represents the power contribution of η_i to the system power. The transformed state variables, η, are completely decoupled from each other, and their cross power contributions are equal to zero.

Accordingly, the power element of the state z_i is defined as:

$$\mu_i = \lim_{t\to\infty} \frac{2}{t}\int_0^t z_i^2 d\tau, \tag{6.17}$$

which represents the power contribution of the ith original system state, z_i. It is known that the states z are related to the states η by a transformation matrix L:

$$z = L\eta \quad \text{with} \quad L = (R_3R_2R_1)^{-1}$$

It follows that

$$z_i = l_{i1}\eta_1 + l_{i2}\eta_2 + \ldots + l_{ij}\eta_j + \ldots + l_{in}\eta_n \tag{6.18}$$

where l_{ij} is an element of the matrix L and n is the dimension of the vector η. Substituting equation (6.18) into equation (6.17), we get

$$\mu_i = \lim_{T\to\infty} \frac{2}{T}\int_0^T (l_{i1}\eta_1 + l_{i2}\eta_2 + \ldots + l_{in}\eta_n)^2 dt. \tag{6.19}$$

Using equation (6.16) and defining

$$\Phi_x = \left[\ \rho_1\ \ \rho_2\ \ \ldots\ \ \rho_n\ \right]^T, \tag{6.20}$$

we have

$$\begin{aligned}\mu_i &= l_{i1}^2\rho_1 + l_{i2}^2\rho_2 + \ldots + l_{in}^2\rho_n \\ &= h_i\Phi_x\end{aligned} \tag{6.20}$$

where

$$h_i = \left[\ l_{i1}^2\ \ l_{i2}^2\ \ \ldots\ \ l_{in}^2\ \right].$$

By defining

$$\Phi_z = \left[\ \mu_1\ \ \mu_2\ \ \ldots\ \ \mu_n\ \right]^T, \tag{6.21}$$

it follows that

$$\Phi_z = H\Phi_x. \tag{6.22}$$

H is formed by squaring every element of the matrix L:

$$H = \begin{bmatrix} l_{11}^2 & l_{12}^2 & \cdots & l_{1n}^2 \\ l_{21}^2 & l_{22}^2 & \cdots & l_{2n}^2 \\ \vdots & \vdots & & \vdots \\ l_{n1}^2 & l_{n2}^2 & \cdots & l_{nn}^2 \end{bmatrix}.$$

The vector Φ_z has a very definite physical meaning. The magnitude of each element in Φ_z represents the corresponding system state's contribution to the system power. It reflects the internal property of the system. Using the power element's values of the original system states as a criterion, the dominant original state variables can be determined and a lower order model in the original state variables can be directly derived from the original model. It should be pointed out

that in case the original state variables, z_i, are not completely independent of each other, and their cross power contributions are not equal to zero, the vector Φ_z still reflects the relative importance of the states z_i in the sense of the system power contribution.

The technique presented here for determining the power elements of the original state variables based on the power elements of the internally power balanced state variables can be easily extended for some other model reduction methods. Rozsa et al. [109] have shown that with the balanced realization, the reachability Grammian and the observability Grammian are equivalent to the system's energy and the output energy, respectively. Each diagonal element of the internally balanced Grammians represents the contribution of the corresponding transformed state to the system energy or the output energy. Following the approach discussed above, we can determine the contribution of the original system states to the system energy and hence find the relative importance of the original state variables.

Tracing the relative importance of the original (or physical) state variables from that of the internally balanced state variables does not always make some original states negligible, i.e. the model's order is not always reducible via the original state variables. It may happen that the internally balanced states have very obvious order reduction features: one group of power elements is far larger than the rest, while the traced power elements of the original states are very close and none of them seem to be significantly dominant. This situation does not imply that the derived relation (6.22) is not valid, rather it indicates that the original state variables are not properly selected and they are significantly dependent on each

other. By properly selecting the state variables during model derivation, the above difficulty may be avoided.

6.5 Model Reduction For The Flexible Manipulator

As discussed earlier, the dynamic model of the manipulator is dependent on the approximate modal series expansions. The truncation of the infinite modal series directly defines the obtained model's order. The method presented above provides a systematic way of determining the adequate truncation of the modal series from the power contribution point of view. This new approach is applied to the manipulator in this section.

6.5.1 Dynamic Model Of The Manipulator

The linearized version of the system model (6.4) can also be given as:

$$\delta \dot{x} = A(\bar{x})\delta x + B\,\delta u \tag{6.21a}$$

$$\partial y = C\,\delta x \tag{6.21b}$$

with

$$A = \begin{bmatrix} 0 & I \\ A_1 & A_2 \end{bmatrix}, \quad B = \begin{bmatrix} 0 \\ B_1 \end{bmatrix} \quad \text{and} \quad C = \begin{bmatrix} C_1 & 0 \end{bmatrix}$$

and

$$\|A_1\| >> \|A_2\|.$$

where δx is the system state variable, consisting of the joint angle variables and the link's vibration modal coordinates, δu is the system input, and δy is the system output describing the position variations of the manipulator's end point.

The manipulator considered here is a lightly damped mechanical system. Its damping is considered from two sources: the internal structural damping of the

arms and the dry friction and backlash phenomena at the joints. Their total damping effect is very limited. In order to apply the power balancing technique, the system's damping is assumed to be negligible. So that A_2=0 and equations (6.21) are in the form of equations (6.5).

6.5.2 Model Reduction

For a given constant nominal trajectory $\bar{x}$, equations (6.21) represent a linear time-invariant system, which describes the manipulator's dynamics for a small variation around the given $\bar{x}$. The power elements of δx, obtained by the internal power balancing transformation on equations (6.21), are directly dependent on the given $\bar{x}$. The derived reduced order model is only valid for that small region. A lower order model which is adequate for the entire workspace of the manipulator should be derived with a varying nominal trajectory $\bar{x}$ which covers the whole workspace.

Using a piece-wise approximation, the entire variation space of $\bar{x}$ is divided into a finite number of small subspaces. Within each subspace, $\bar{x}$ is assumed be a constant. Hence equations (6.21) are linear time-invariant and the power balancing technique can be applied. If the subspaces are small enough and the nominal trajectory is continuous, this piece-wise approximation will adequately represent the original system and provide reasonably accurate results, since the power elements of the system states are also continuous.

Within each subspace, we perform the internal power balancing transformation and calculate the power elements of the state variables. Comparing the power element's values, the dominant system states can be determined. If the first k states are dominant for each subspace, it is concluded that the first k states

are dominant for the entire workspace. Therefore, we can disregard the rest of the state variables and obtain a lower order model

The dominance of the first k system states is described by the power contribution coefficient, which is defined as,

$$\varepsilon_k = \frac{\sum_{i=1}^{k} \mu_i}{\sum_{i=1}^{M} \mu_i} \times 100 \quad (\%) \tag{6.22}$$

where M is the highest vibration mode included in the original model for each link.

The vector $\bar{x}$ consists of the joint angle variables and the link's bending modal co-ordinates. Since the equilibrium position of the vibration modal coordinates is zero and the bending deformations of the links are relatively small, the assumption

$$\varphi_{1i0} = \dot{\varphi}_{1i0} = \varphi_{2i0} = \dot{\varphi}_{2i0} = 0$$

is reasonable in order to reduce the dimensions of the nominal trajectory's variation space. Then, the variation of q_0 consists of the changes of the joint angle variables. The variation ranges of the joint variables are directly determined by the physical configuration of the manipulator. According to the experimental set-up, it is known that the maximum rotating speed of joint 1 is 4 rad./sec. and the angular velocity of joint 2 cannot exceed 6 rad./sec.. With respect to the first link, the second link can only sweep from -90 degree position to +90 degree position. Due to the symmetry of the structure, it is only necessary to cover a moving range of 0 degree to 90 degree for joint angle 2. The angle position of link 1 does not affect the system's performance and hence its variation is disregarded. Therefore, the variation space of $\bar{x}$ is three dimensional, which consists of the angular velocity of joint 1, angle position of joint 2, and the angular velocity of joint 2.

6.5.3 Results And Discussions

The variation space of the nominal trajectory is spanned by three variables: the angular velocity of joint 1, the angle position of joint 2, and the angular velocity of joint 2. Dividing each variable's varying region into 20 small intervals, the entire space of q_0 is divided into 8000 small cubes. At the centre of each small cube, the internal power balancing transformation is performed and the power contribution coefficient is calculated. Some typical results are presented below.

Figures 6.3 to 6.5 show the power contributions of the first k states with k changing from 0 to 10 with the specified $\bar{x}$ values. It is observed that the value of ε_k increases with the increment of k, while the curve's slope decreases. The power contribution of the first vibration mode is stronger than that of any other vibration modes. This statement holds for both links. The power distribution among the vibration modes for each link is affected by the given nominal trajectory. The effect of $\bar{x}$ on the second link is more significant than that on the first link. It is interesting to note that when the two links are perpendicular to each other, that is $\theta_2=90^0$, the first modal co-ordinate dominance is more significant than with any other configuration. This observation is further confirmed by Figures 6.6 to 6.9.

The power contributions of the first two vibration modes for each link with various $\bar{x}$ are given by Figures 6.6 through 6.9. Each of those figures consists of two subplots. The upper subplot is a 3-dimensional view of the data with the elevation angle of 0 degree, which is intended to show the minimum value of the power contribution. The normal 3-dimensional lower subplot illustrates the variation of the power contribution with respect to the nominal trajectory.

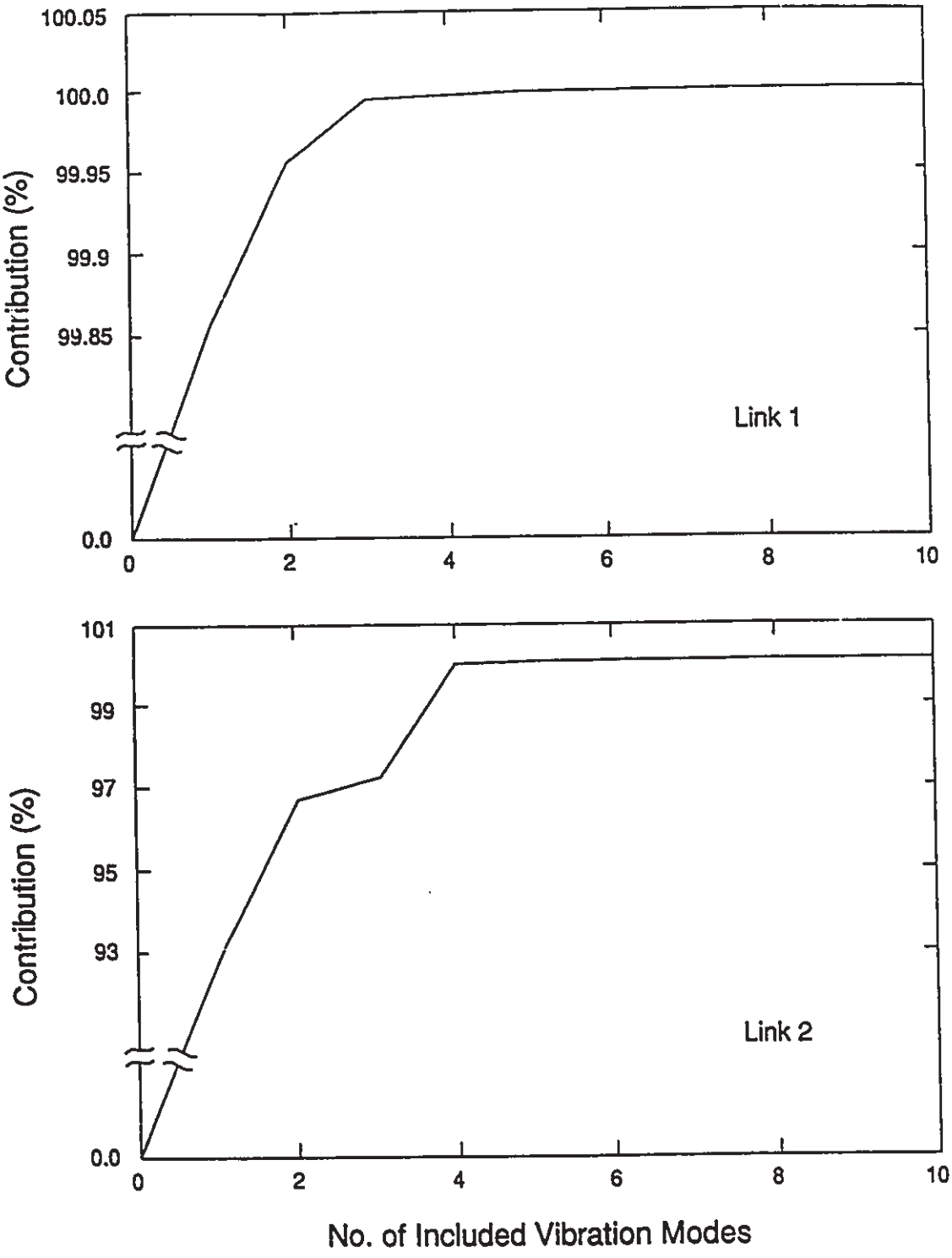

Figure 6.3 Effect of Number of Vibration Modes on Power Contribution
($\theta_2 = 0, \dot{\theta}_1 = 0$, and $\dot{\theta}_2 = 0$)

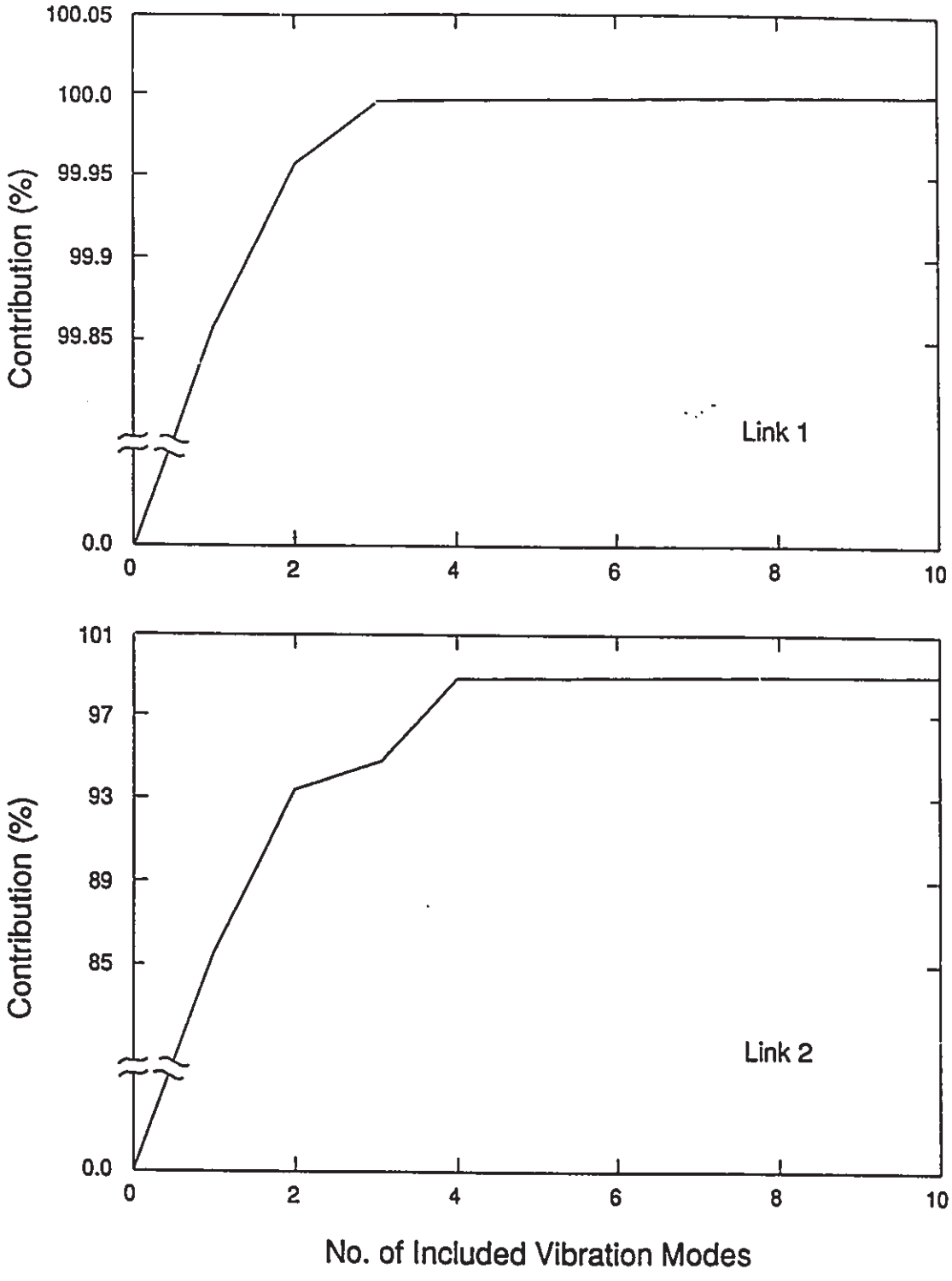

Figure 6.4 Effect of Number of Vibration Modes on Power Contribution
($\theta_1 = 45^0, \dot{\theta}_1 = -1.0$ (rad/sec) and $\dot{\theta}_2 = 3.0$ (rad/sec))

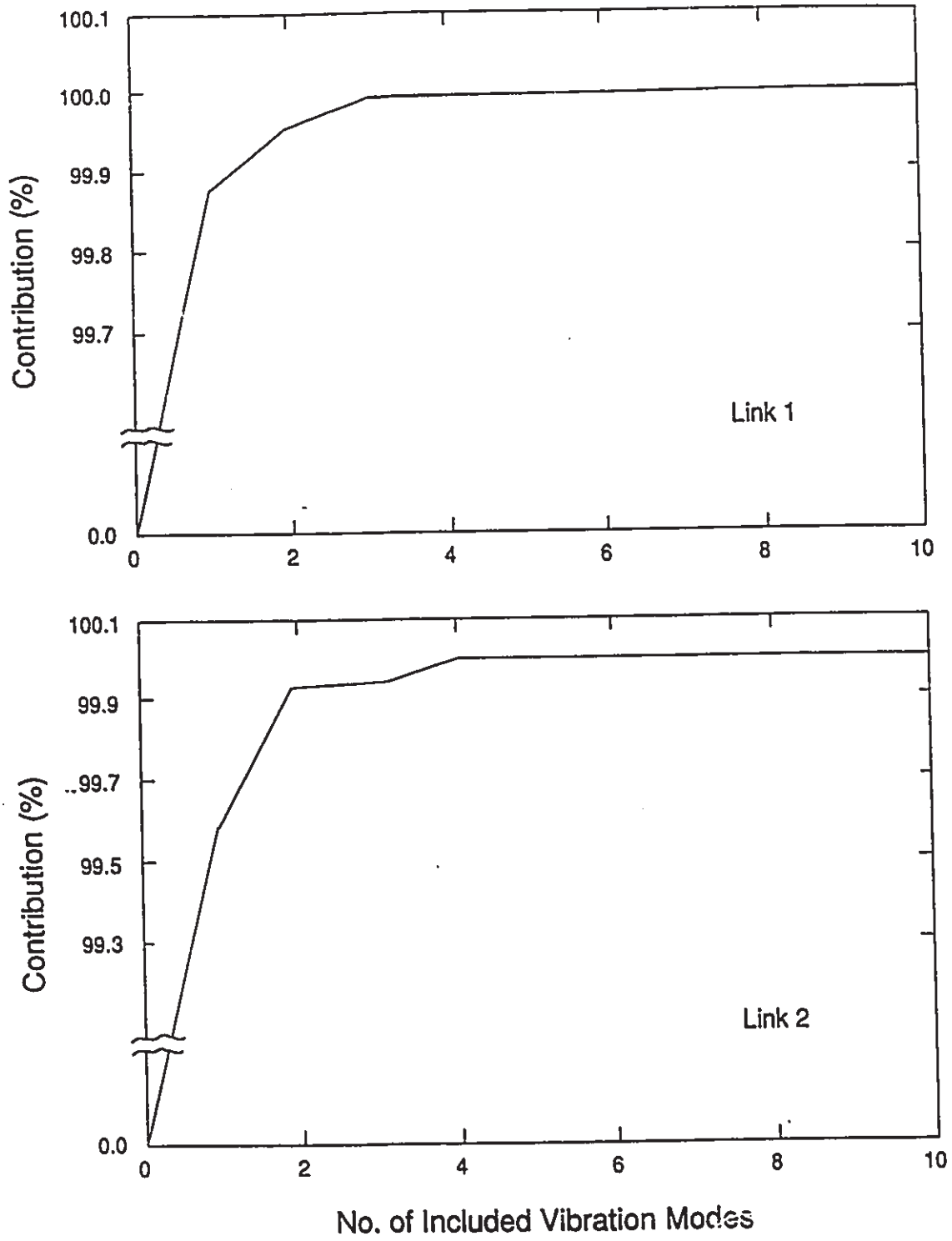

Figure 6.5 Effect of Number of Vibration Modes on Power Contribution
($\theta_2 = 90^0$, $\dot{\theta}_2 = -4.0$ (rad/sec), and $\dot{\theta}_2 = -6.0$(rad/sec))

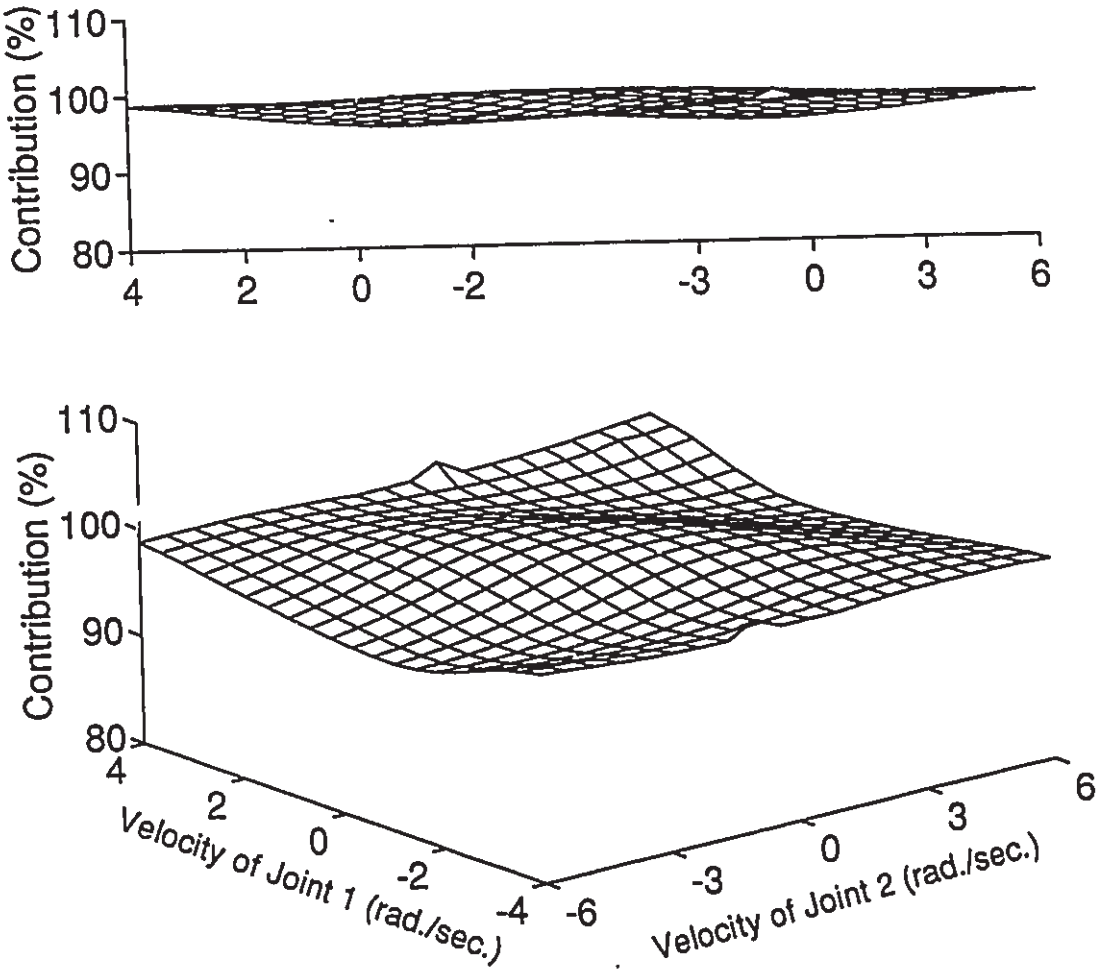

Figure 6.6 Power Contribution of First Two Vibration Modes For Each Link ($\theta_2 = 0^0$)

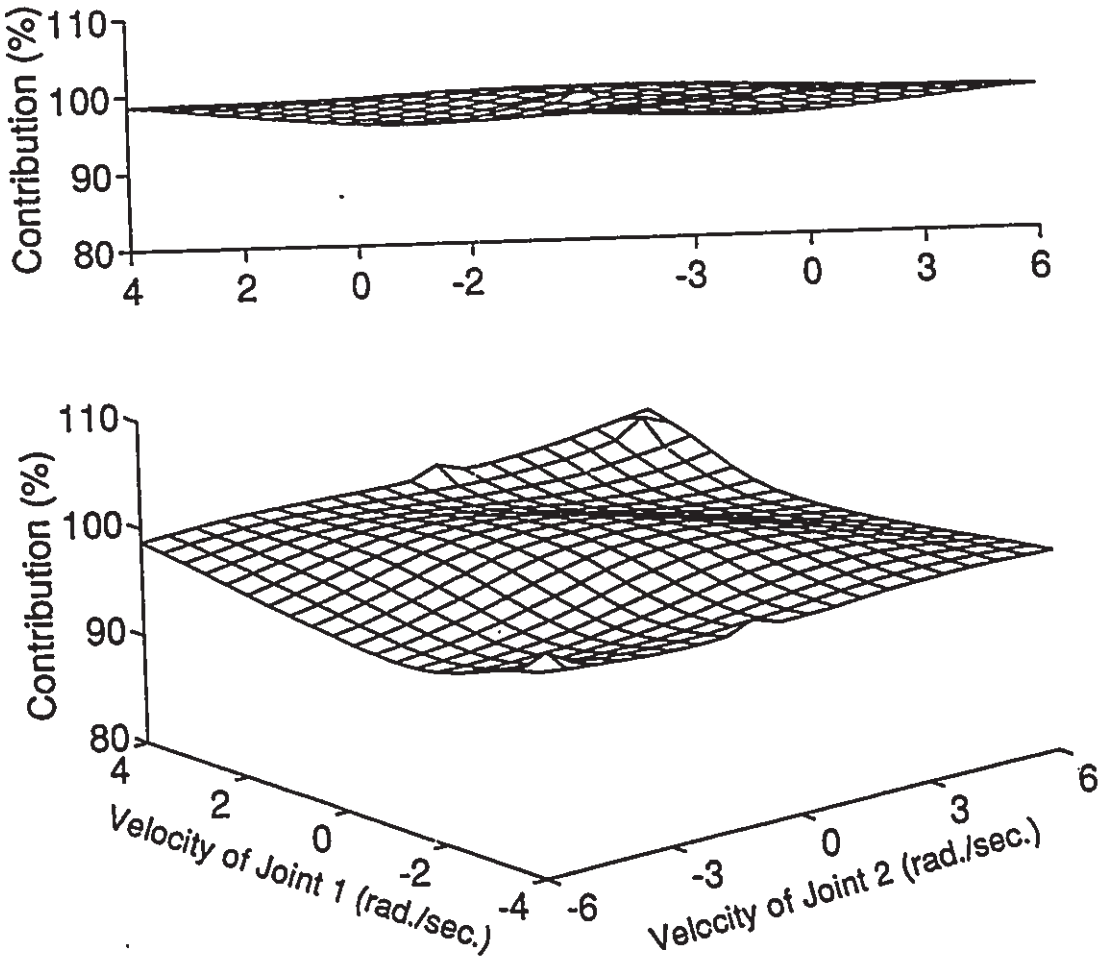

Figure 6.7 Power Contribution of First Two Vibration Modes For Each Link

($\theta_2 = 28.4^0$)

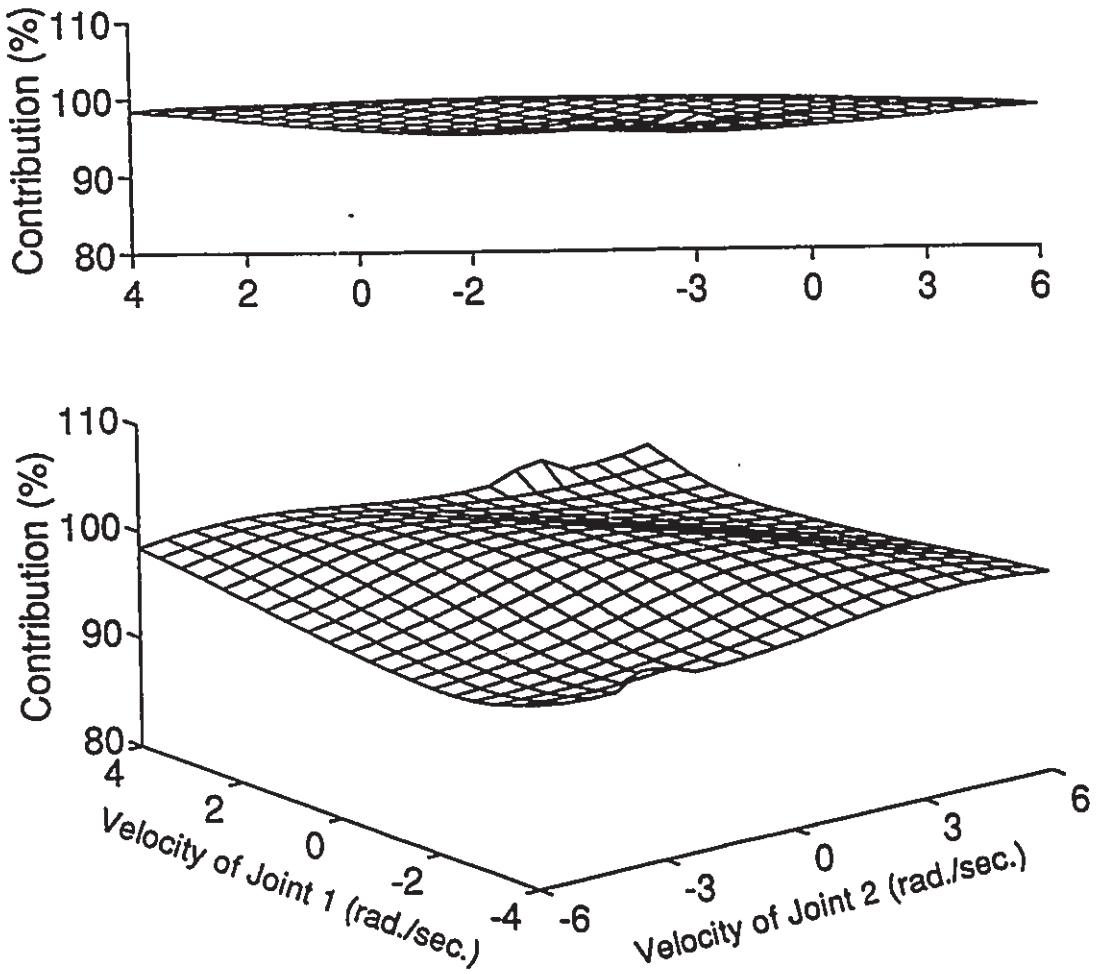

Figure 6.8 Power Contribution of First Two Vibration Modes For Each Link ($\theta_2 = 61.6^0$)

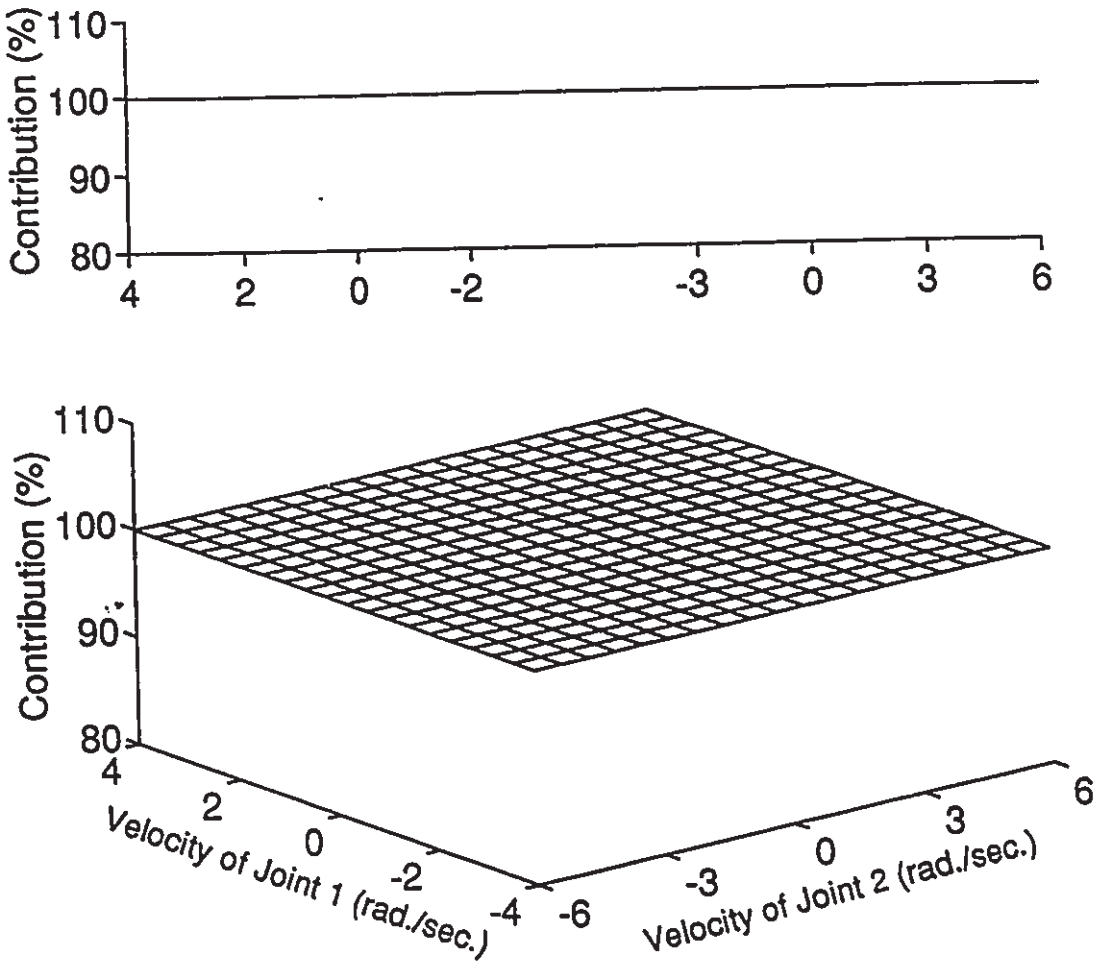

Figure 6.9 Power Contribution of First Two Vibration Modes For Each Link

($\theta_2 = 90.0^0$)

The results clearly indicate that the dominance of the first two bending vibration modes for each link varies with the joint variables and depends on the manipulator's configurations. However, the variation is limited and the first two vibration mode's dominance is very obvious. Using the power contribution coefficient as the model reduction criterion, the infinite modal series of each link can be truncated at the second mode and the contributions of the higher modes are considered to be negligible.

DEVELOPMENT OF CONTROL STRATEGY

7.1 Introduction

The last four chapters have been devoted to the understanding of the manipulator dynamics. In this chapter, some fundamental characteristics of the manipulator are examined from the control point of view and the major difficulties in the control design are discussed. A model reference adaptive control algorithm, proposed by Sobel [111], is then summarized, modified, and applied to the manipulator. Computer simulations are performed to evaluate the algorithm's properties and to select adequate values for the control matrices. Real time testing is implemented to validate the theoretical study.

7.2 Control Features Of The Manipulator

The manipulator in the current study possesses the following undesirable control features, which complicate the control design process:

a. Nonlinearity and time-variance. The dynamic model of the manipulator is represented by a set of nonlinear differential equations, which is too complicated to be used directly for control design. The linearized version of the dynamic model is derived around a nominal trajectory. The system matrix of the linear model depends on the nominal trajectory and varies with the manipulator's configuration.

b. Non-minimum phase. For the manipulator, the system input consists of the motor's actuating torques at the joints and the output is its end-point position. Due to the structural flexibility, the system input cannot change the system output instantaneously. There always exists a non-zero time gap between the input's action and the output's response to that action. In the control field, the system with this delay feature is considered to be a non-minimum phase. The non-minimum phase system does not possess stable inverse dynamics and needs some special attention during control algorithm development. From the location of the actuator and the response sensor point of view, this type of system is also called a non-colocated system.

c. Non-asymptolic stability. In order to effectively control the structural vibrations of the manipulator, the actuating DC motors at the joints are set in torque mode, which results in one joint dynamics pole resting at the origin of the s-plane. Moving this pole to the left side of the s-plane means that the manipulator arm will always rotate back to its zero joint angle position when the command input torque is set to zero, which is the case when the end-effector reaches the predefined location. In order to be able to

place the end-effector of the manipulator to a desired location other than the zero position, this pole has to be retained at the origin so that the system is always marginally stable. This feature excludes the applicability of some well known control algorithms.

d. Not satisfying the perfect model-following condition. The perfect model-following condition is defined for linear model-following control systems. Many model reference adaptive control algorithms are based on the satisfaction of this condition. For a linear system with the nominal model of

$$\dot{x}_p = A_p x_p + B_p u_p \tag{7.1a}$$

$$y_p = C_p x_p, \tag{7.1b}$$

the reference model is selected as

$$\dot{x}_m = A_m x_m + B_m u_m \tag{7.2a}$$

$$y_m = C_m x_m. \tag{7.2b}$$

If the following relation stands

$$\text{rank } B_p = \text{rank } [B_p, A_p\text{-}A_m] \tag{7.3}$$

the system is considered satisfying the perfect model following condition [110]. For the manipulator, the number of control inputs is far less than the number of system states, and condition (7.3) can in general not be satisfied.

Also, the manipulator is a distributed parameter mechanical system with multiple flexible members. Each flexible member itself is a continuous system and possesses an infinite number of natural vibration modes. Only a finite number of the modes can be included in the dynamic model. A controller based on a model with a finite number of equation variables may encounter spillover problems which can lead to instability of the closed-loop system. The state space representation of the dynamic model for the manipulator is at least of order 12

(counting one natural mode for each link). The design of a controller for such a high order system is usually complex, and the associated computation often involves numerical difficulties.

7.3 Control Strategy

Based on the Command Generator Trackor (CGT) control, Sobel [111] developed a model reference adaptive control (MRAC) algorithm that ensures Lyapunov stability. The algorithm has the following desirable features:

a. The perfect model following condition is not required. This is suitable for the current application.

b. The order of the nominal model and the reference model can be lower than the order of the actual plant. As pointed out in the previous section, the manipulator is a distributed parameter mechanical system and has an infinite number of natural frequencies. Although the model order reduction study concluded that the first two vibration modes dominate the link's bending motions, the dynamic model with a finite number of state variables is just an approximation of the original system. The order of the theoretical model is always lower than that of the plant.

c. The plant parameters can be unknown but constrained to a set with known bounds. This is necessary since the system parameters cannot be known perfectly.

d. Explicit parameter identification is not needed. This saves some computation and makes the real-time testing feasible.

In order to make Sobel's algorithm easier to understand, a brief discussion of CGT control, which was originally developed by O'Brien and Broussard [112], is given first.

7.3.1 Command Generator Tracker Control

For a plant, defined by the following discrete linear equations:

$$x_p(k+1) = A_p x_p(k) + B_p u_p(k) \tag{7.4a}$$

$$y_p(k) = C_p x_p(k) \tag{7.4b}$$

where x_p is the $(n\text{x}1)$ system state vector, u_p is the $(m\text{x}1)$ control vector, y_p is the $(q\text{x}1)$ system output vector, and A_p and B_p are matrices with the appropriate dimensions, with the reference model which defines the desired plant performance being expressed as:

$$x_m(k+1) = A_m x_m(k) + B_m u_m(k) \tag{7.5a}$$

$$y_m(k) = C_m x_m(k) \tag{7.5b}$$

where x_m is the $(n\text{x}1)$ system state vector, u_m is the $(m\text{x}1)$ control vector, y_m is the $(q\text{x}1)$ system output vector, and A_m and B_m are matrices with the appropriate dimensions, the CGT control method assumes the existence of an ideal plant trajectory in the form given by:

$$x_p^*(k+1) = A_p x_p^*(k) + B_p u_p^*(k) \tag{7.6a}$$

$$C_p x_p^*(k) = C_m x_m(k). \tag{7.6b}$$

When perfect tracking occurs, the real plant trajectories become the ideal plant trajectories and the real plant outputs become the ideal plant outputs which are the reference model's outputs. The ideal control input, which generates perfect output tracking, and the ideal state trajectory are assumed to be a linear combination of the reference model's state and input, that is:

$$\begin{bmatrix} x_p^*(k) \\ u_p^*(k) \end{bmatrix} = \begin{bmatrix} S_{11} & S_{12} \\ S_{21} & S_{22} \end{bmatrix} \begin{bmatrix} x_m(k) \\ u_m(k) \end{bmatrix} \tag{7.7}$$

with S_{ij} matrices satisfying

$$S_{11} = \Omega_{11} S_{11} (A_m - I) + \Omega_{12} C_m \tag{7.8a}$$

$$S_{12} = \Omega_{11} S_{11} B_m \tag{7.8b}$$

$$S_{21} = \Omega_{21} S_{11} (A_m - I) + \Omega_{22} C_m \tag{7.8c}$$

$$S_{22} = \Omega_{21} S_{11} B_m \tag{7.8d}$$

where

$$\Omega = \begin{bmatrix} \Omega_{11} & \Omega_{12} \\ \Omega_{21} & \Omega_{22} \end{bmatrix} = \begin{bmatrix} A_p - I & B_p \\ C_p & 0 \end{bmatrix}^{-1} \tag{7.9}$$

The conditions for the existence of the S_{ij} matrices include: (1) u_m is a step function, (2) the number of controls, m, *is* not less than the number of outputs q, and (3) the product of the ith eigenvalue of Ω_{11} and the jth eigenvalue of A_m is not equal to unity for all i, j.

7.3.2 Sobel's Algorithm

With a plant whose nominal model is given by equation (7.4), whose reference model is defined by equation (7.5), and whose ideal plant trajectory is expressed by equation (7.6), we define the error function as:

$$e(k) = x_p^*(k) - x_p(k) \tag{7.10}$$

and the Lyapunov function candidate as:

$$V[e(k), K_I(k)] = e^T(k) P e(k) + tr\{S(K_I(k) - \tilde{K}) T^{-1} (K_I(k) - \tilde{K})^T S^T\}. \tag{7.11}$$

The control algorithm is derived to insure that the difference

$$\Delta V = V[e(k+1), K_I(k+1)] - V[e(k), K_I(k)] \tag{7.12}$$

is negative definite. The obtained control law can be summarized as:

$$u_p(k) = K_r(k) r(k) \tag{7.13}$$

with

$$r(k)=\begin{bmatrix} y_m(k)-y_p(k) \\ x_m(k) \\ u_m(k) \end{bmatrix}.$$

The gain matrix $K_r(k)$ consists of two parts: a proportional part $K_p(k)$ and a integral part $K_I(k)$. They are adapted according to the following scheme:

$$K_r(k)=K_p(k)+K_I(k) \tag{7.14a}$$

$$K_p(k)=v(k)r^T(k)\bar{T} \tag{7.14b}$$

$$K_I(k+1)=K_I(k)+v(k)r^T(k)T \tag{7.14c}$$

$$K_I(0)=K_{I0} \tag{7.14d}$$

$$v(k)=Fe(k)+Gz(k) \tag{7.14e}$$

$$z(k)=u_p^*(k)-u_p(k)+\bar{K}_eC_pe(k) \tag{7.14f}$$

where T, $\bar{T}$ are n_fxn_r time invariant weighting matrices, K_{I0} is the initial integral gain, F and G are matrices of appropriate dimensions, and $u_p^*(k)$ is the desired control input. The selection of F, G, and the weighting matrices T and $\bar{T}$ is limited by the sufficient conditions for stability.

The asymptotically stable error for the closed loop system with the above control algorithm is shown provided that $u_p^*(k)$ is precisely known and

$$S(z)=J+C_p(zI-A_p+B_p\bar{K}_eC_p)^{-1}B_p \tag{7.15}$$

is strictly positive real for some gain J and $\bar{K}_e$. According to the discrete positive real lemma, the transfer matrix (7.15) is discrete positive real if and only if there exists a real symmetric positive definite matrix P and real matrices L and W such that

$$(A_P-B_P\bar{K}_eC_P)^TP(A_P-B_P\bar{K}_eC_P)-P=-LL^T \tag{7.16a}$$

$$(A_P-B_P\bar{K}_eC_P)^TPB_P=C_P^T-LW \tag{7.16b}$$

$$W^TW=J+J^T-B_P^TPB_P. \tag{7.16c}$$

If in addition to satisfying equation (7.16), the matrix $-LL^T$ is negative definite, then $S(z)$ is strictly positive real. The procedure of choosing the matrix J such that $S(z)$ is strictly positive real includes the selection of the matrix $\bar{K}_e$ which output stabilizes the plant and the determination of the matrix J by solving equation (7.16). Since the priori knowledge of $u_p^*(k)$ is not possible, the approximation of

$$u_p^*(k) = S_{11}x_m(k) + S_{22}u_m(k) \tag{7.17}$$

is used. It is shown that using this nominal value of $u_p^*(k)$ will at worst results in system stability with bounded error. The complete stability analysis of the algorithm is given in Appendix E.

7.3.3 Modification Of Sobel's Algorithm

The selection of the output matrix C_p directly affects the stability of the closed-loop system. In the event that the original system description does not yield a strictly positive real transfer matrix, the output configuration of the system needs to be reselected to ensure strict positive realness of $S(z)$. Sobel proposed to use the solution to the linear quadratic regulator problem as the output matrix C_p with $\bar{K}_e$ an identity matrix. It is found that the modified quadratic regulator proposed by Anderson and Moore [113] provides a better solution, specially for a nominal model with uncertainties.

With the conventional optimal design, the stability of the closed-loop system with the given nominal model is ensured. There is no guarantee for stability of the system with the tolerance of model uncertainties, time delays, and nonlinearities. By pushing the closed-loop poles to the left side of a line $\mathrm{Re}(s)=-\alpha$ $(\alpha \geq 0)$ on the s-plane, the resulting closed-loop system becomes less sensitive to the plant parameter variations and has a greater margin for tolerance of time delays and

nonlinearities. The method of minimizing a quadratic performance index and, at the same time, ensuring that the closed-loop poles lie to the left of a line Re(s)=-α, for a prescribed $\alpha \geq 0$, is presented below [113].

For a linear time-invariant system with complete controllability

$$\dot{x} = Fx + Gu \qquad x(t_0) = x_0 \tag{7.18}$$

with a linear control law

$$u = -K^T x, \tag{7.19}$$

define the performance index

$$P = \int_{t_0}^{\infty} (u^T R u + x^T Q x) e^{2\alpha t} dt \tag{7.20}$$

with F being constant and nxn, G and K constant and nxp, the state vector x being an n vector, and the system input u being a p vector, R being positive definite symmetric and constant, and Q being non-negative definite symmetric and constant.

To minimize P subject to the conditions of equation (7.18), set

$$\hat{x} = xe^{\alpha t} \qquad \hat{u} = ue^{\alpha t}. \tag{7.21}$$

Then, equation (7.18) is equivalent to

$$\dot{\hat{x}} = (F + \alpha I)\hat{x} + G\hat{u} \qquad \hat{x}(t_0) = x_0 e^{\alpha t} \tag{7.22}$$

while

$$(u^T R u + x^T Q x) e^{2\alpha t} = \hat{u}^T R \hat{u} + \hat{x}^T Q \hat{x}$$

and thus the minimization of the performance index (7.20) with respect to equation (7.18) is equivalent to the minimization with respect to equation (7.22) of

$$P = \int_{t_0}^{\infty} (\hat{u}^T R \hat{u} + \hat{x} Q \hat{x}) dt. \tag{7.23}$$

The construction of the desired control law is essentially no more difficult than for the conventional case with α=0. With this modified optimal regulator, the system with certain model uncertainties and nonlinearities can be output stabilized by a

properly selected α. Computer simulations show that the adequate α value not only ensures the system's stability, but also significantly improves the control performance of the closed-loop system, see Figures 7.1 to 7.3. When α=0, which is equivalent to conventional optimal control, the resulting closed-loop system is unstable. As α increases, the system becomes stable and the control errors become smaller. With α being around 3.0, the system performance reaches it at peak. Further increasing the value of α (say α>3.2) degrades the control performance. The value of α also affects the vibration frequencies of the system. A larger α leads to a closed-loop system with higher vibration frequencies.

As discussed before, imperfect priori knowledge of $u_p^*(k)$ results in a stable system with bounded errors. Improving the approximation of $u_p^*(k)$ certainly improves the system performance and reduces control errors. But how to give a better estimate of $u_p^*(k)$ is an unanswered question.

The model-following control was developed for linear systems with quite accurate nominal models. If a system satisfies the perfect model-following condition and its model is exactly known, the system can be controlled by a control law with fixed gains to follow the predefined trajectories without any error. So that in the case of the plant nominal model satisfying the perfect model-following condition, the control law from the model-following algorithm should be used as the estimate of $u_p^*(k)$. However, the nominal model of the manipulator does not satisfy the perfect model-following condition, as discussed before. This non-satifaction is primarily caused by the dry friction at the joints and the gear backlash within the actuation. The dynamic effect of the dry friction and the gear backlash on the whole system is limited. Considering the part of the nominal

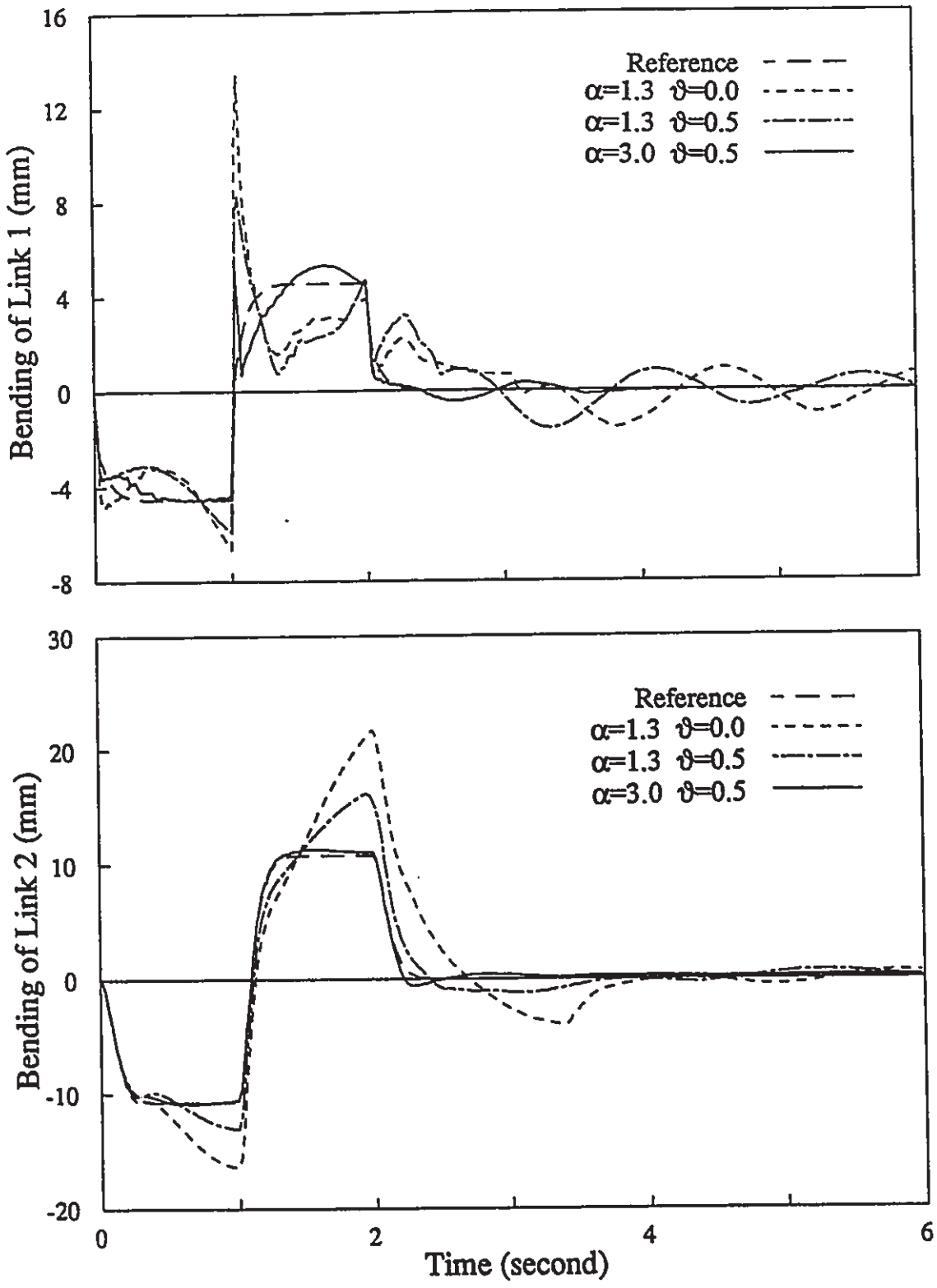

Figure 7.1 Effect of α and ϑ on Bending Motion

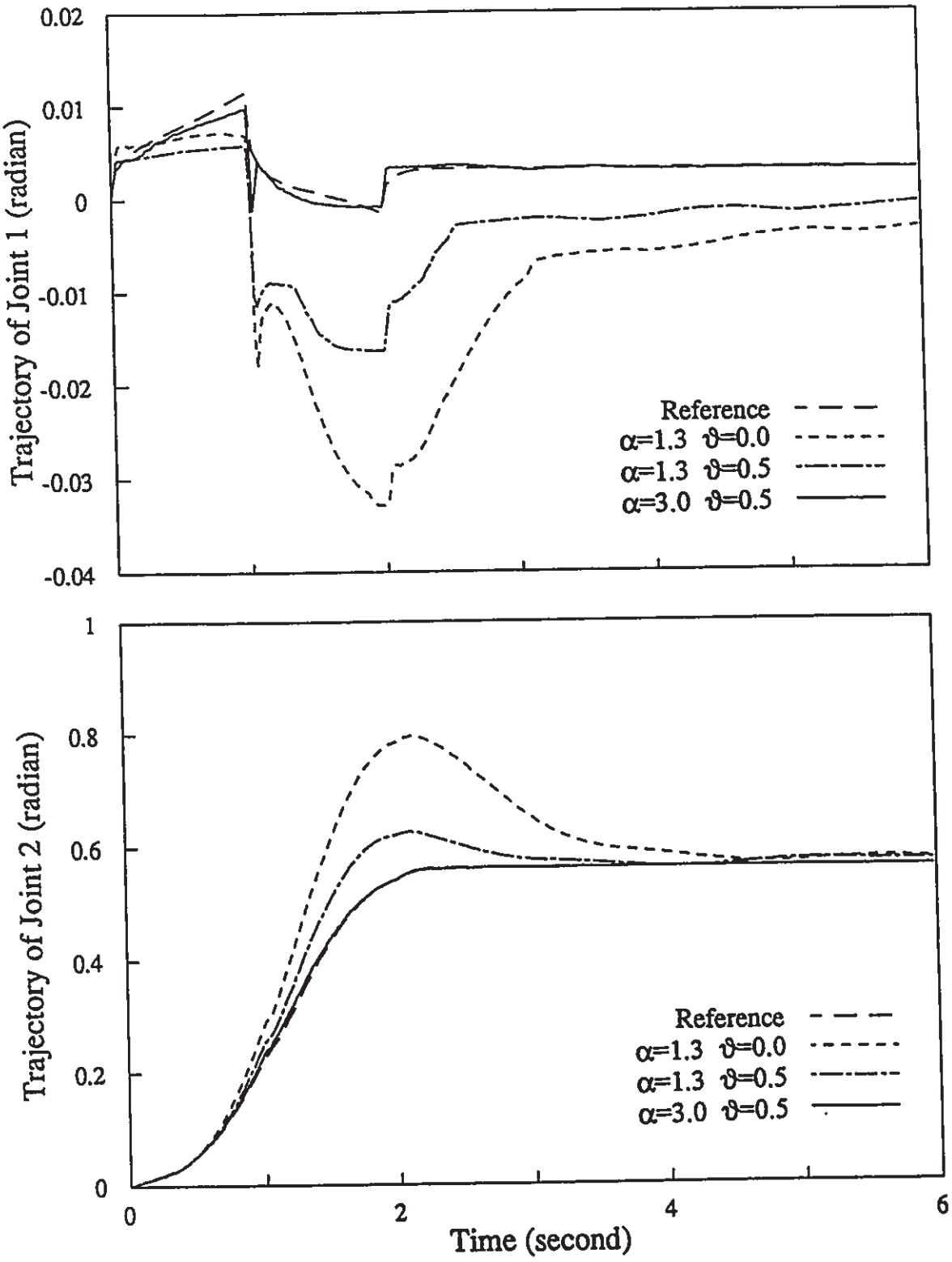

Figure 7.2 Effect of α and ϑ on Joint Trajectory

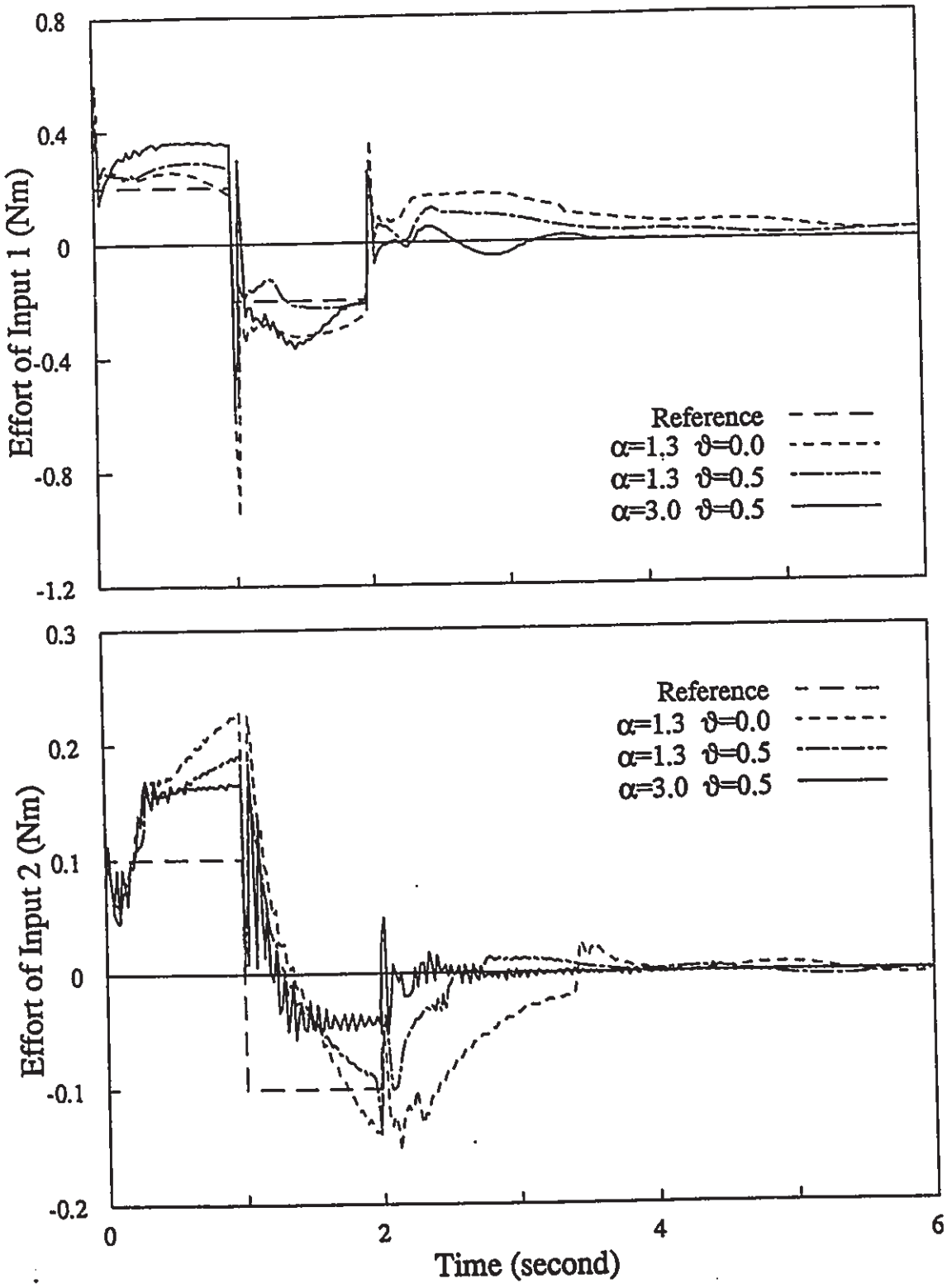

Figure 7.3 Effect of α and ϑ on Control Effort

model which violates the perfect model-following condition as the uncertainty and taking it out of the nominal model, the plant matrix A_p becomes A_p' and the perfect model-following control law is calculated based on A_p'. The modified nominal value of $u_p^*(k)$ is then selected as a combination of the two control efforts:

$$u_p^*(k) = \vartheta u_f(k) + (1-\vartheta)u_c(k) \tag{7.24}$$

with u_f being the perfect model-following control input based on A_p'[110]:

$$u_f(k) = (B_p^T B_p)^{-1} B_p^T [-(A_m - A_p')x_m + B_m^T u_m] \tag{7.25}$$

and u_c being the CGT control input calculated from A_p:

$$u_c(k) = S_{21}x_m(k) + S_{22}u_m(k). \tag{7.26}$$

ϑ in equation (7.24) is a weighting constant, valued between 0 and 1. An adequate value of the weighting constant is determined through numerical simulations. With ϑ=0.5, the improvement of the system performance with the use of (7.24) is shown by Figures 7.1 to 7.3.

7.4 Computer Simulations

Numerical simulations are designed to study the properties of the control algorithm, examine the closed-loop system's stability, and select proper values for the control gain matrices. The manner of α and ϑ affecting the system output is also investigated through the simulations.

With the model reference adaptive control, the desired performance of a system is specified by its reference model. The reference model defined for the manipulator is derived from the linearized dynamic equations of the manipulator around the zero nominal trajectory so that the reference model and the nominal model have the same model structure and similar dynamic properties. The dynamic effects of dry friction and gear backlash are neglected in the defined reference

model and the link's internal structural damping ratio is intentionally increased to the critical level to damp out the bending vibrations completely. Due to its structural flexibility, the manipulator arm always experiences bending deformation when it rotates with acceleration. This deformation is opposite to the acceleration direction and cannot be completely eliminated by any control techniques. The selected reference model retains the dynamic features of the system and shares the same system parameters such as joint stiffness and link dimensions with the nominal model.

For the manipulator with an infinite number of vibration frequencies, the order of the nominal model definitely affects its controlled performance. The model order reduction analysis showed that the first two natural modes dominate each link's bending vibration, and the first vibration mode contributes the most. Here two nominal models with different order are used for simulations: one counts the first two natural modes for each link (order of 16) and one only counts each link's first mode (order of 12). The plant dynamics include the first four vibration modes for each link. It is observed that the 16th order model requires much more computation and causes numerical difficulties in solving the Lyapunov equation. Its improvement on the system performance over the 12th order nominal model is not significant. Hence, the nominal model with the order of 12 is retained for further studies. The spillover problem, which often occurs in similar situations, is examined by varying the order of the plant model. It is found that even when the order of the plant model is much higher than that of the nominal model, instability does not occur and the system performance remains similar.

Computer simulations are implemented with the computation software, MATLAB, on a SPARC 330 SUN workstation. The linearized dynamic model obtained around the zero trajectory is used as the nominal model. The plant dynamics are simulated by the original nonlinear dynamic equations. The nominal value of the payload is assumed to be 0.1 kg and the actual payload varies from 0.01kg to 0.2kg. Simulation results are presented in Figures 7.4 to 7.12.

Figures 7.4 to 7.6 show the simulated closed-loop system performance with the actual payload of 0.01 kg. The simulation data for the system with the payload of 0.1 kg are illustrated in Figures 7.7 to 7.9 and the results for the manipulator with 0.2 kg payload are presented in Figures 7.10 to 7.12. It is clear that for the examined payload variation range, the proposed controller results in a stable closed-loop system with zero steady state errors and damps out the structural vibrations of the manipulator within 2 seconds after command excitation, although the system performance varies with the payload values and the best one is obtained for the case of the actual payload equal to its nominal value. For all three cases, the performance of the second link is much better than that of the first link. This is because the dynamic response of the second link is more precisely described by the nominal model. With the selected nominal model, the model uncertainties for the first link are much larger than those with the second link. Figures 7.4 to 7.12 also reveal that a heavier payload requires more control effort and results in the links vibrating with larger magnitude and lower frequencies.

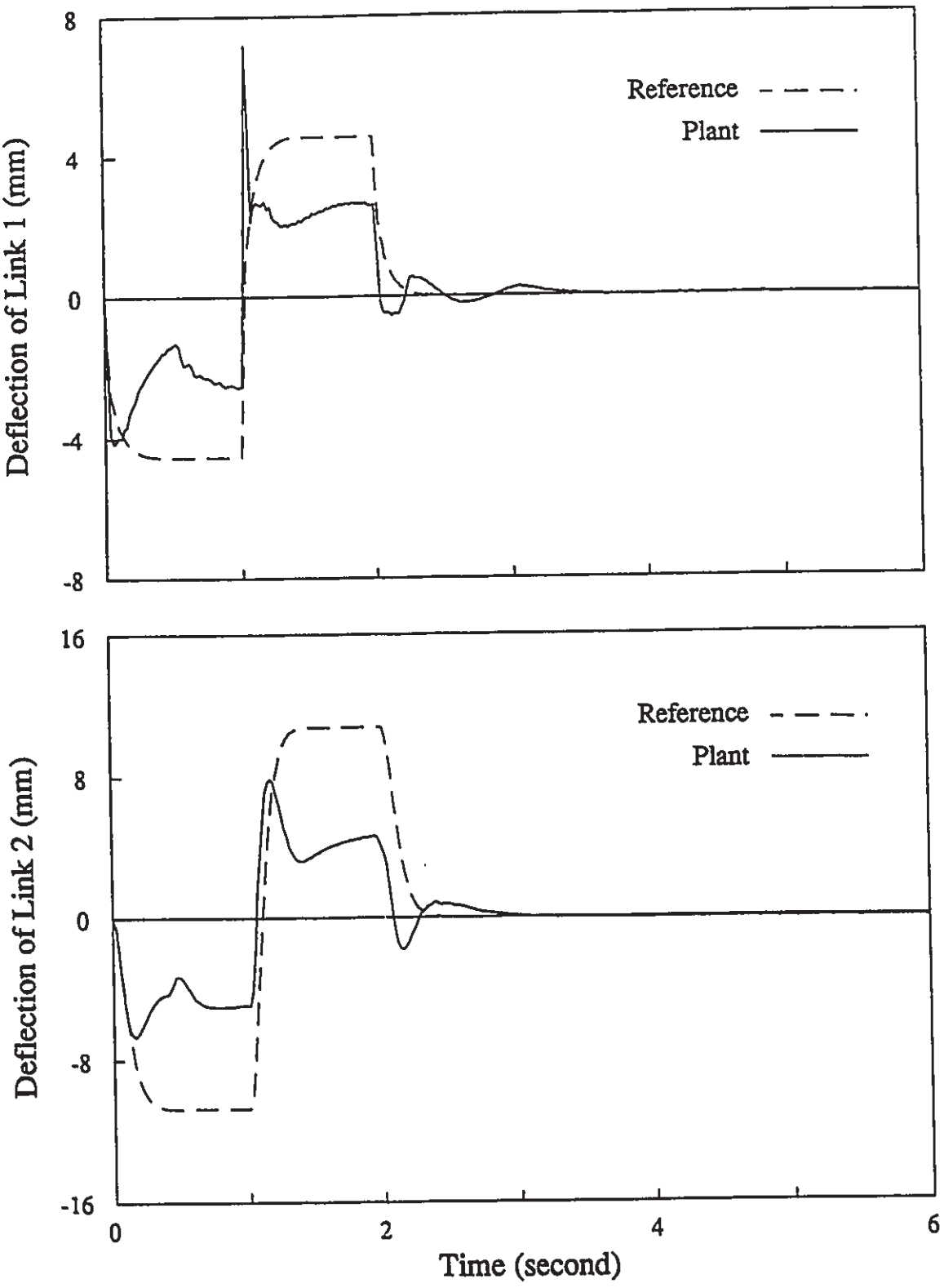

Figure 7.4 Control Simulation with Payload of 0.01 kg - Bending Motion

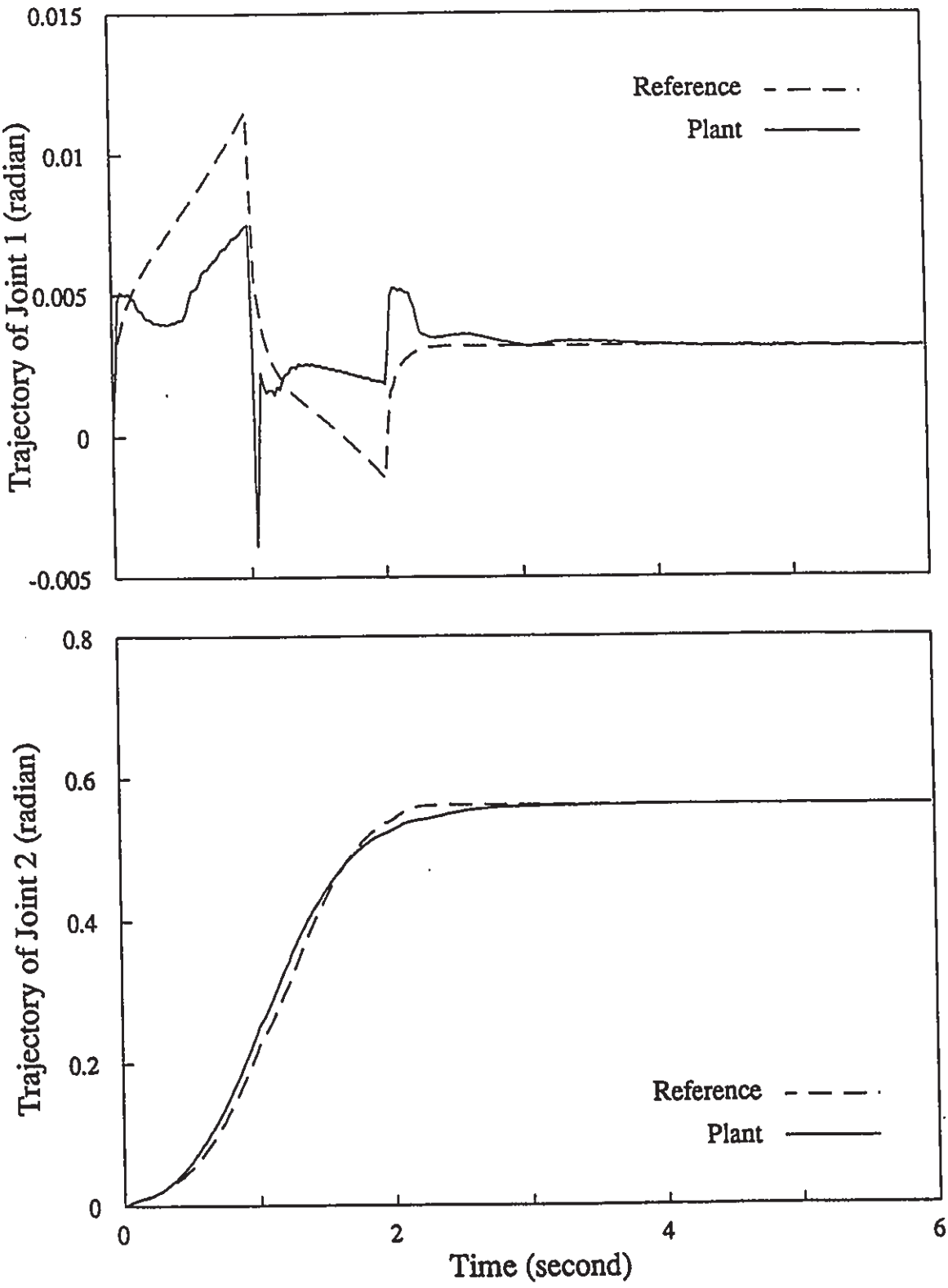

Figure 7.5 Control Simulation with Payload of 0.01kg - Joint Trajectory

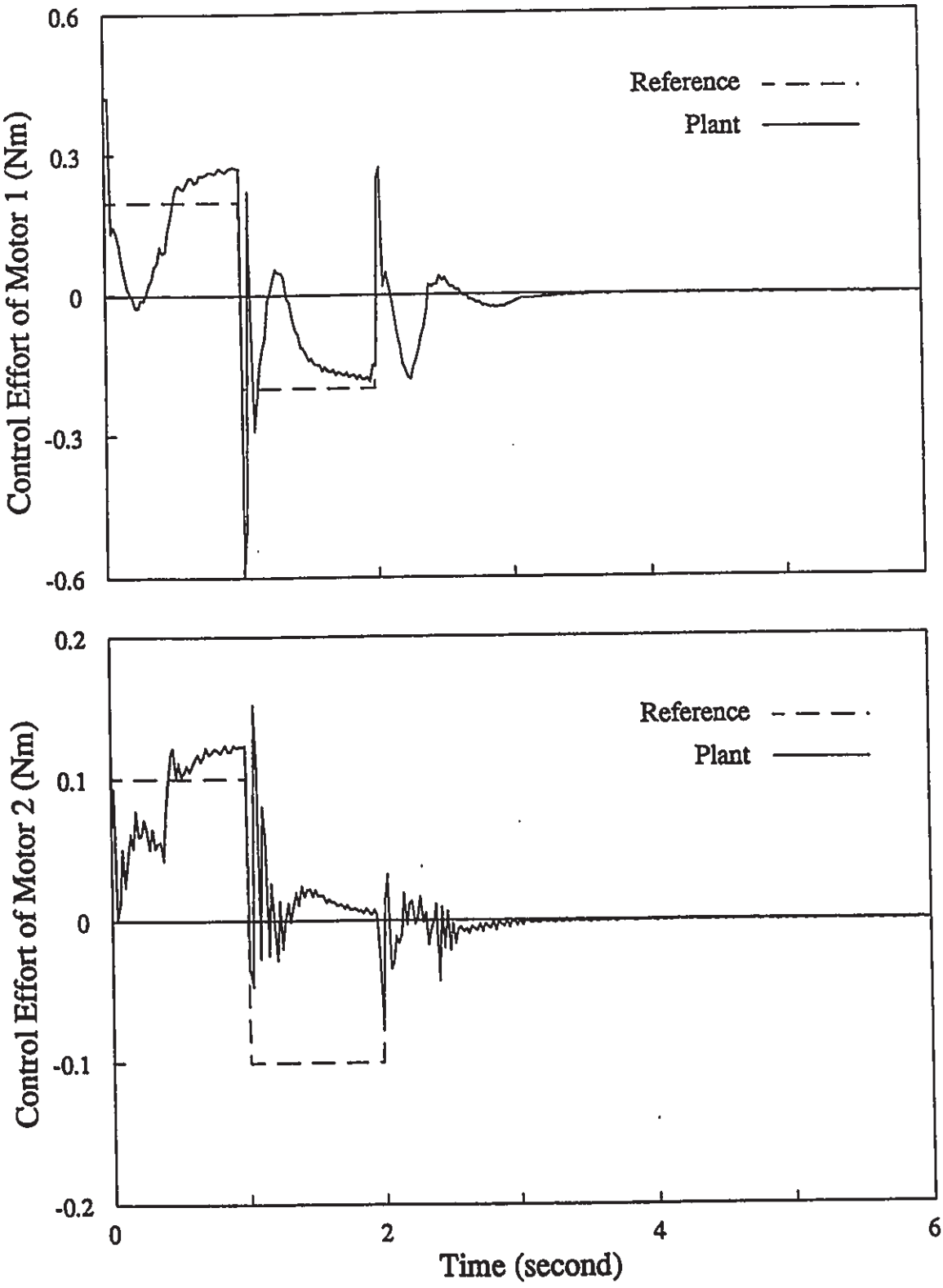

Figure 7.6 Control Simulation with Payload of 0.01kg - Control Effort

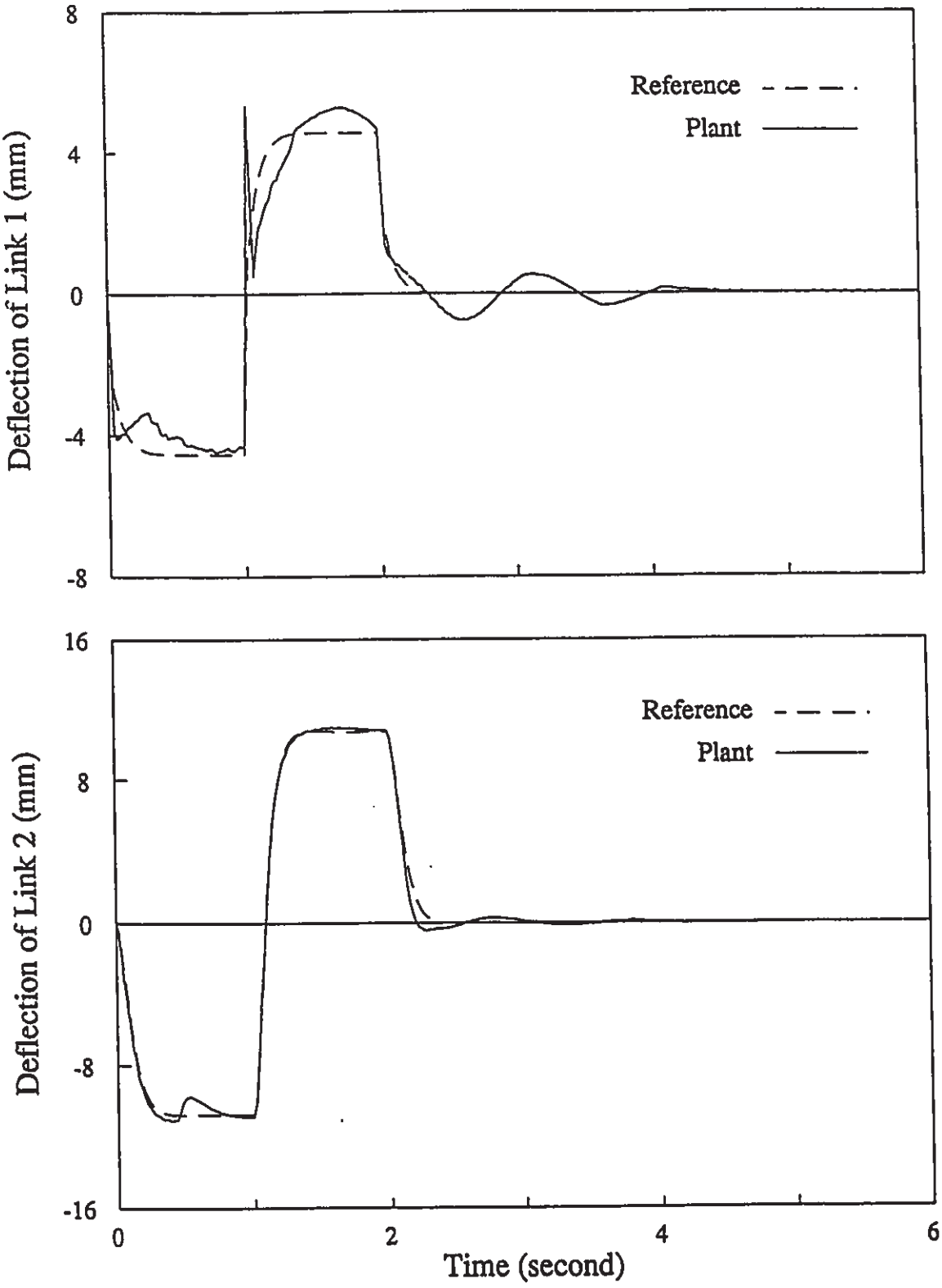

Figure 7.7 Control Simulation with Payload of 0.1kg - Bending Motion

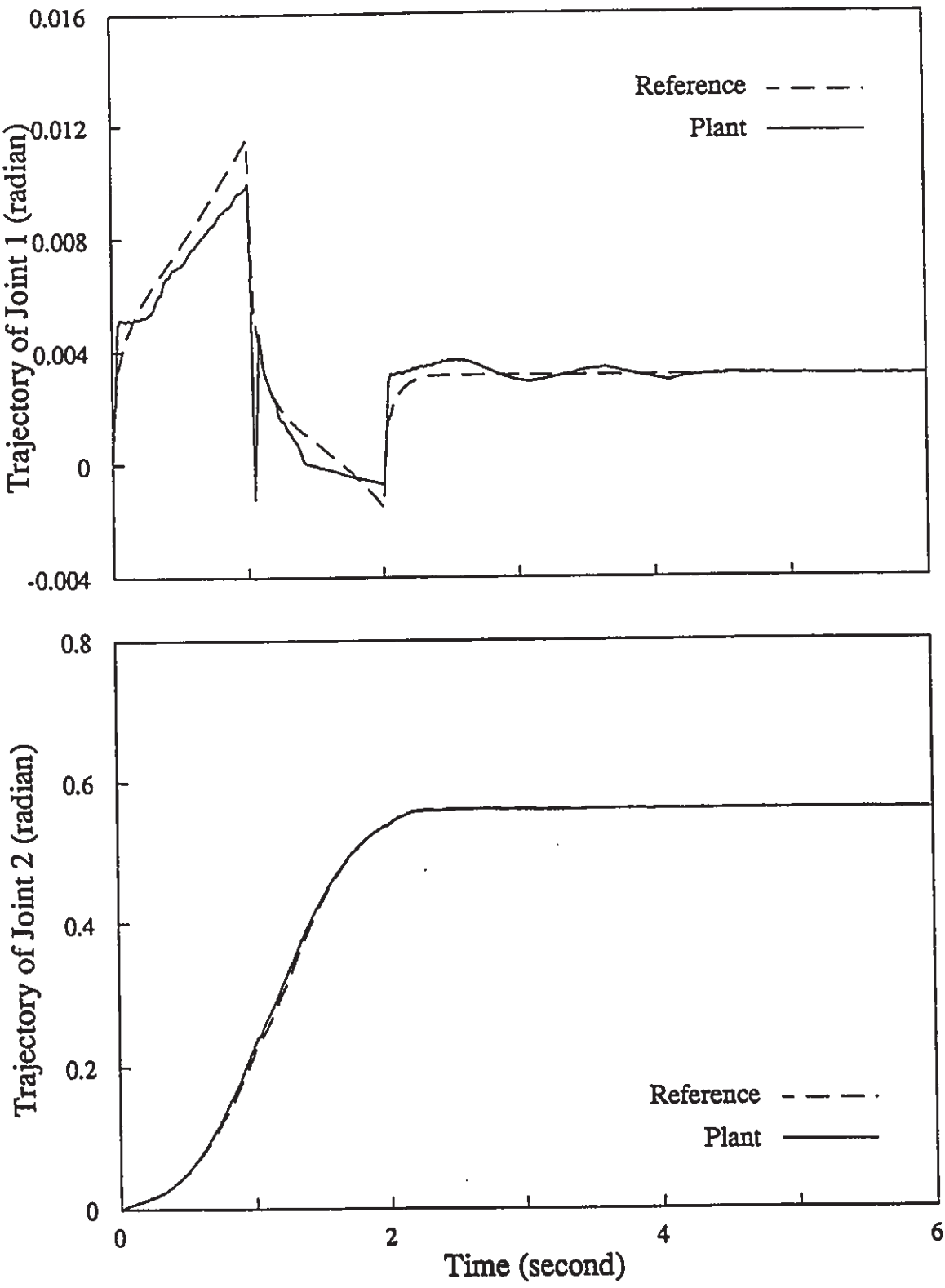

Figure 7.8 Control Simulation with Payload of 0.1kg - Joint Trajectory

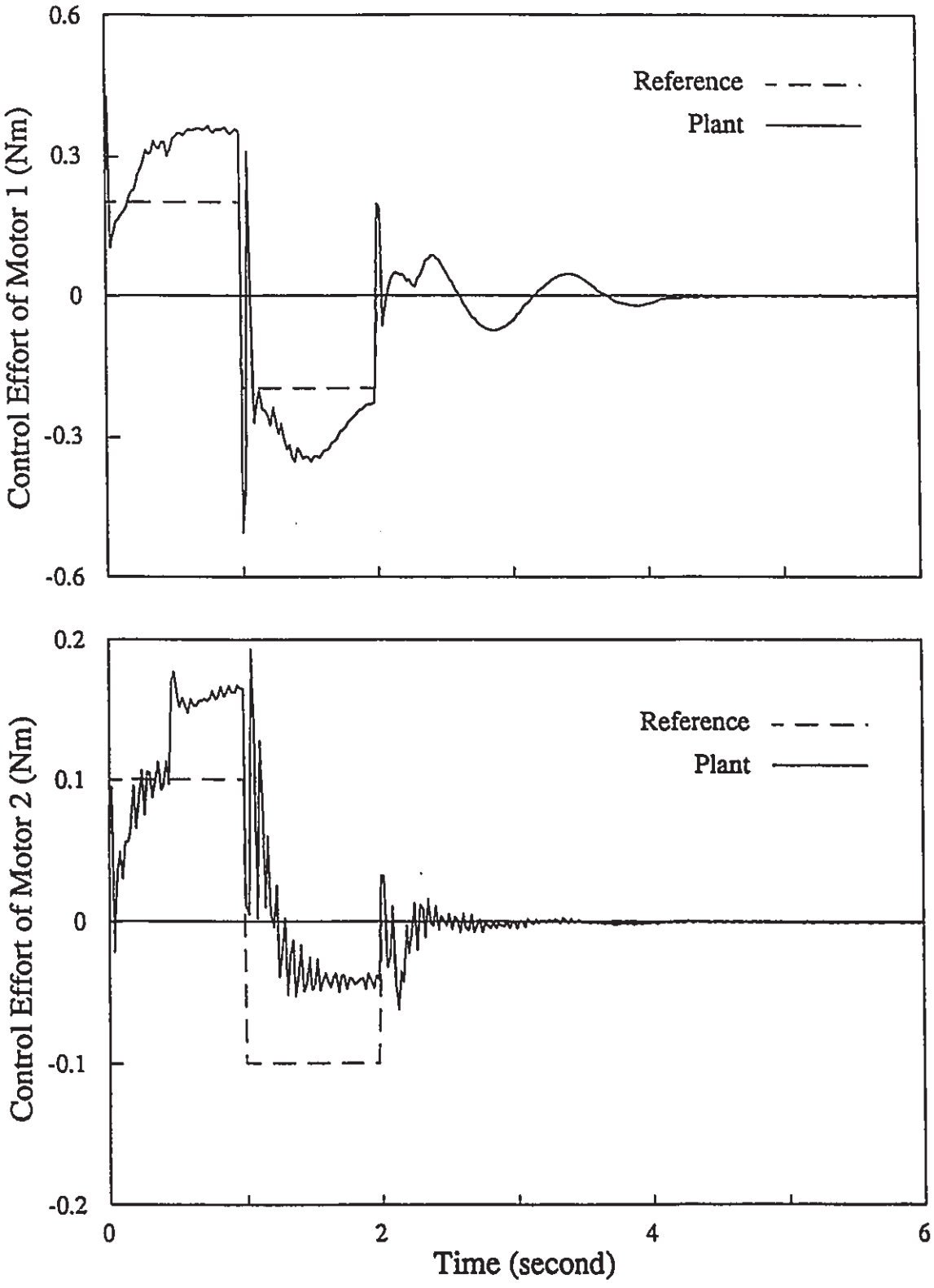

Figure 7.9 Control Simulation with Payload of 0.1kg - Control Effort

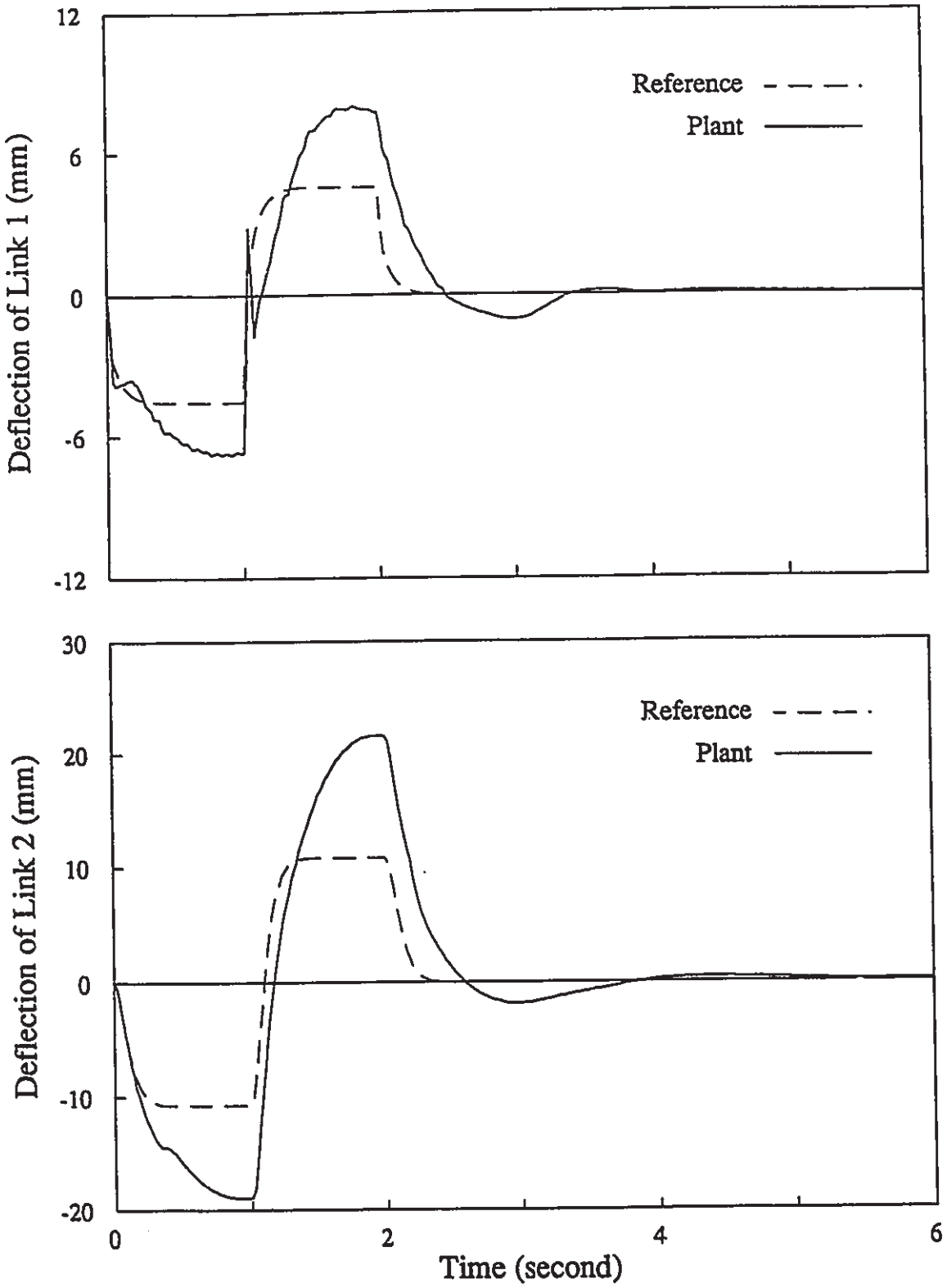

Figure 7.10 Control Simulation with Payload of 0.2kg - Bending Motion

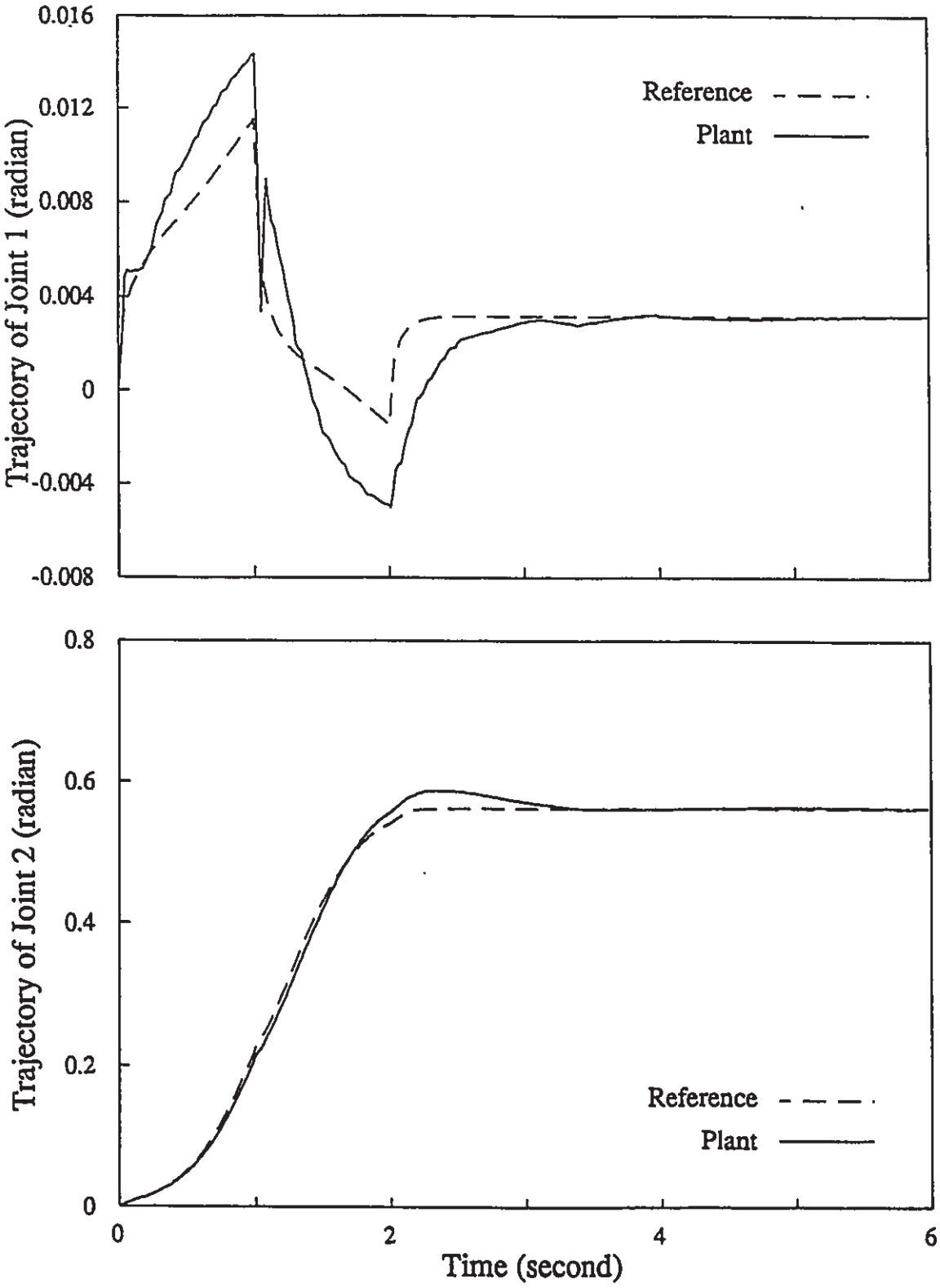

Figure 7.11 Control Simulation with Payload of 0.2kg - Joint Trajectory

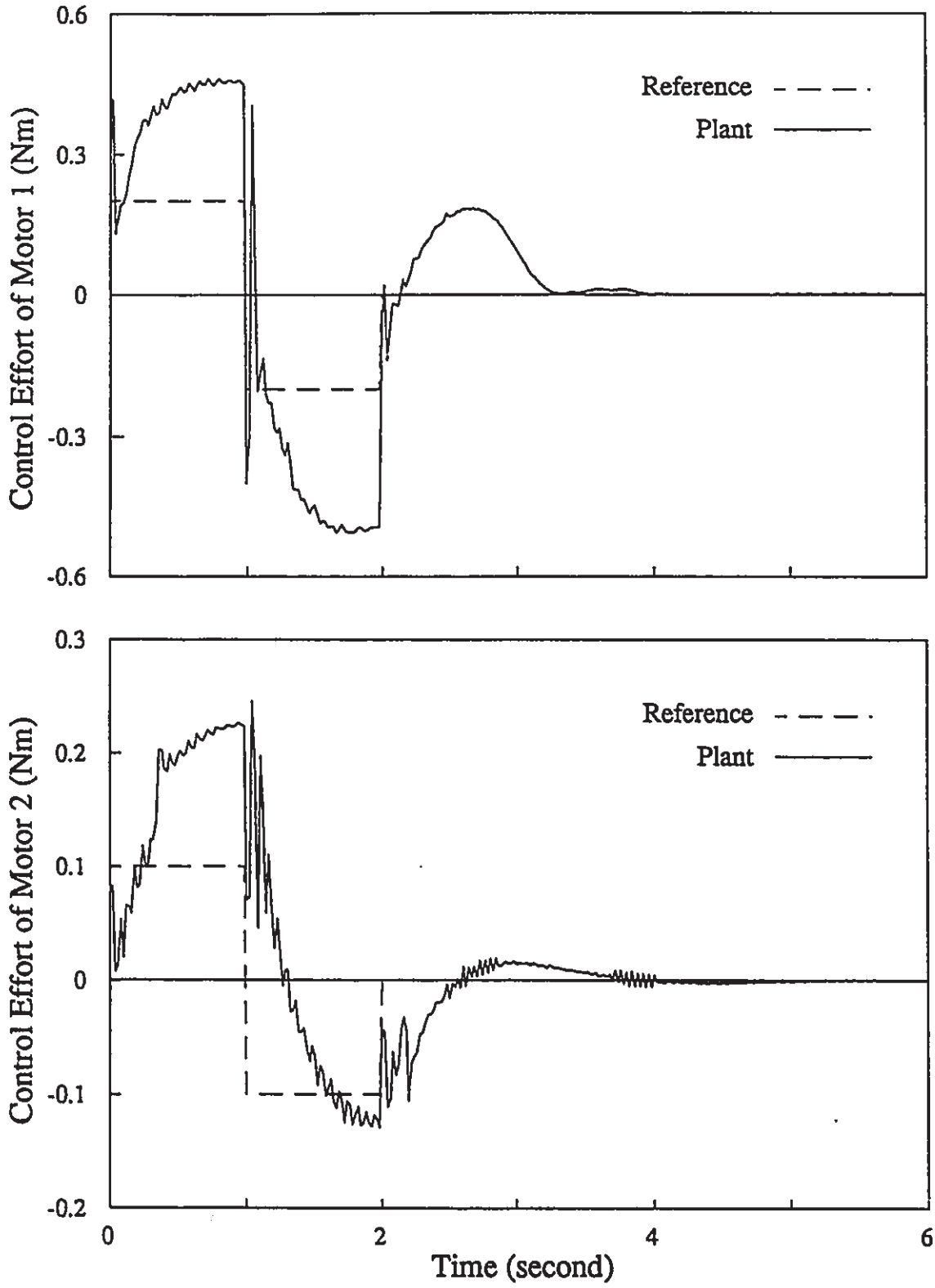

Figure 7.12 Control Simulation with Payload of 0.2kg - Control Effort

7.5 Real Time Testing

Real time testing is different from computer simulations. In the numerical simulation, the system states are known precisely. The plant dynamics are represented by a set of the derived dynamic equations. The model uncertainties result from the differences between the linear nominal model and the nonlinear plant dynamics. The computation time delay can be neglected. For real time testing, the system states have to be measured directly or indirectly by measurement sensors. Sensor signals are often contaminated by noise and disturbances and the measurement accuracy is limited. The model uncertainties are not only from model simplification, but are also caused by the unmodelled dynamics, violation of the theoretical assumptions, and environmental disturbances. The time delay caused by the calculation of the proper control action cannot be neglected in the real time implementation and its effect has to be considered.

The major unmodelled dynamics for the manipulator are the torsional vibrations of the links. Theoretically the gravity effect is assumed to be zero so that the manipulator is operating on a horizontal plane without any twisting motions. In reality, when the relative joint angle between the two links becomes non-zero or the first link rotates with a certain acceleration, the off-balanced force at the far end of the first link causes the links to vibrate torsionally. The vibration amplitude is proportional to the magnitude of the off-balanced force. The twisting motions of the links are sensed by the strain gages and accordingly the controller takes action to eliminate them, which is impossible since the torsional vibration of

the link is perpendicular to the motor's driving direction. Ultimately, system instability occurs. In order to reduce the first link's twisting motion, a "V" shaped support, made of a coated steel wire, is mounted to the underside of the second joint and a plastic plate is used as the guiding surface, as shown in Figure 7.13. When the twisting motion of the link is zero, the support does not make contact with the plate. The clearance between them is adjusted to a very small magnitude. The twisting motions of the link are constrained by the contact force generated between the support and plate. The contact friction along the support direction of movement is reduced by a lubrication oil film on the plate. The dynamic effect of this contact friction is considered as insignificant and is neglected in the model.

The computation time delay can be neglected for the numerical simulations since the plant process can be easily held after each sampling action and resumed when the required control effort is determined. In real time implementation, the dynamics of the plant process cannot be interrupted and the computation of the desired control action consumes computer time. There always exists a time delay between the moment of sensing the plant's response and that of outputting the calculated control effort based on the plant's sensed response, although the delay is not necessarily a full sampling period. The non-zero time delay degrades the algorithm's performance and sometimes results in unstability of the controlled system. The negative effects of the time delay can be partially compensated for by using a prediction algorithm such as a Kalman filter to predict the system response one or several steps ahead. Due to the limitation of computer speed, the nominal model is used here as the system response predictor. With this simple and open

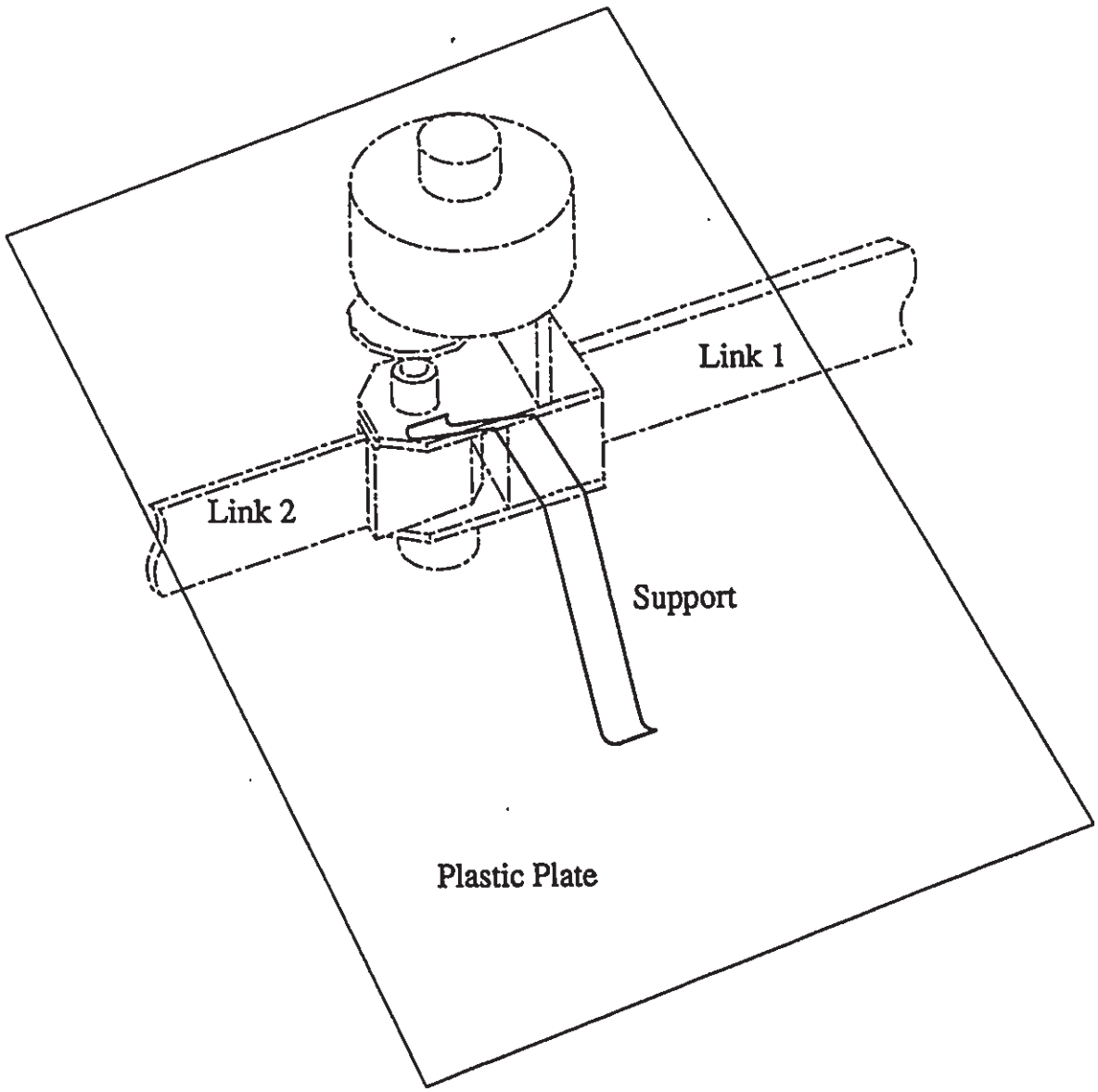

Figure 7.13 Twisting Motion Constraint Mechanism

-loop prediction, the closed-loop system's stability is ensured and the control performance is improved.

The system states of the manipulator consist of the link's bending vibration coordinates and the joint angle variables. The joint angle positions are measured with optical encoders. Since the output signal of the encoder is essentially digital and its noise level is virtually zero, the joint angle velocities can be quite accurately obtained by differentiating the measured joint angle positions.

The determination of the link's vibration coordinates requires a little more computation. The bending deformation of a link is the superposition of the contributions from all its natural modes. The contribution of the first few modes is much more significant than that from the rest of the modes. Based on the model order reduction study, it is assumed that the actual bending of the link results from its first two vibration modes and the contribution of higher modes is negligible. Therefore

$$w(u_i) = \varphi_1\psi_1(u_i)+\varphi_2\psi(u_i) \tag{7.26}$$

with u_i being the ith strain gage location, $w(u_i)$ being the bending deflection of the link at the point u_p which is determined by using the strain gage signals in the method described in Chapter 4, ψ being the mode shape function given in Chapter 3, and φ being the mode coordinates. The first two vibration mode coordinates are determined by solving the above set of equations. Using the strain gage signals at five different locations along the link, the two coordinate coefficients are obtained with a least squares fit. The reason for using all the strain gage signals other than the required two is to take advantage of the low-pass filtering feature of the least squares scheme and reduce the influence of high frequency noise on the estimated

coefficients. The vibration velocity coordinates are then determined by differentiating the estimated vibration displacement coordinates. With the additional filtering of the strain gage signals by an analog low-pass filter, the proposed approach provides satisfactory results. One of the drawbacks of the proposed approach is the introduction of an extra half sampling period time delay for the velocity states.

Real time testing is implemented through a 386 personal computer. The control algorithm is programmed in C. All involved non-adaptive control gains and the reference model performance are calculated off-line. The sampling frequency is set at 50 Hz and the experimental period for each test lasts 6 seconds. Four different payloads, 0.0, 0.01 kg, 0.1 kg, and 0.2 kg, and two types of input excitation, square wave and sinusoidal, are used. The test results are presented below.

Figures 7.14 to 7.25 show the results for the square wave excitation and the data for the sinusoidal excitation are presented by Figures 7.26 to 7.34. Within the examined payload variation range, the closed-loop system is stable with zero steady state errors and the structural vibrations of the manipulator are effectively controlled. Comparing with the simulation results, the performance of the closed-loop system in the real time implementation is slightly worse and the joint angle trajectory is less smooth, which may be caused by the inaccuracy of the model for the dynamics of the joint friction and the gear backlash. The time during which the vibrations last in the real time test is quite close to that predicted by the simulations. With the same reference input amplitude, the sinusoidal input results

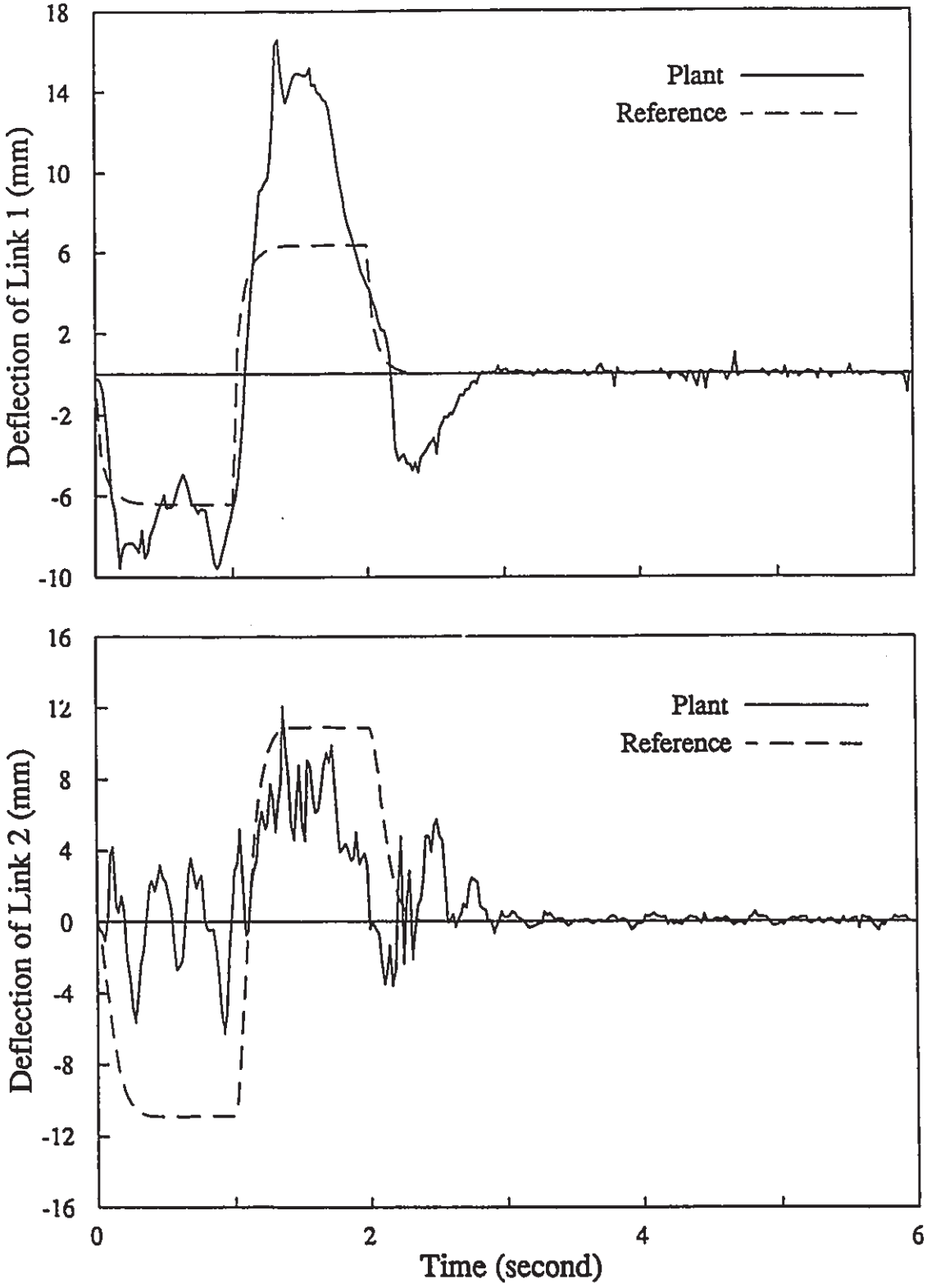

Figure 7.14 Control Experiment with Square Wave Excitation
Payload of 0.0kg - Bending Motion

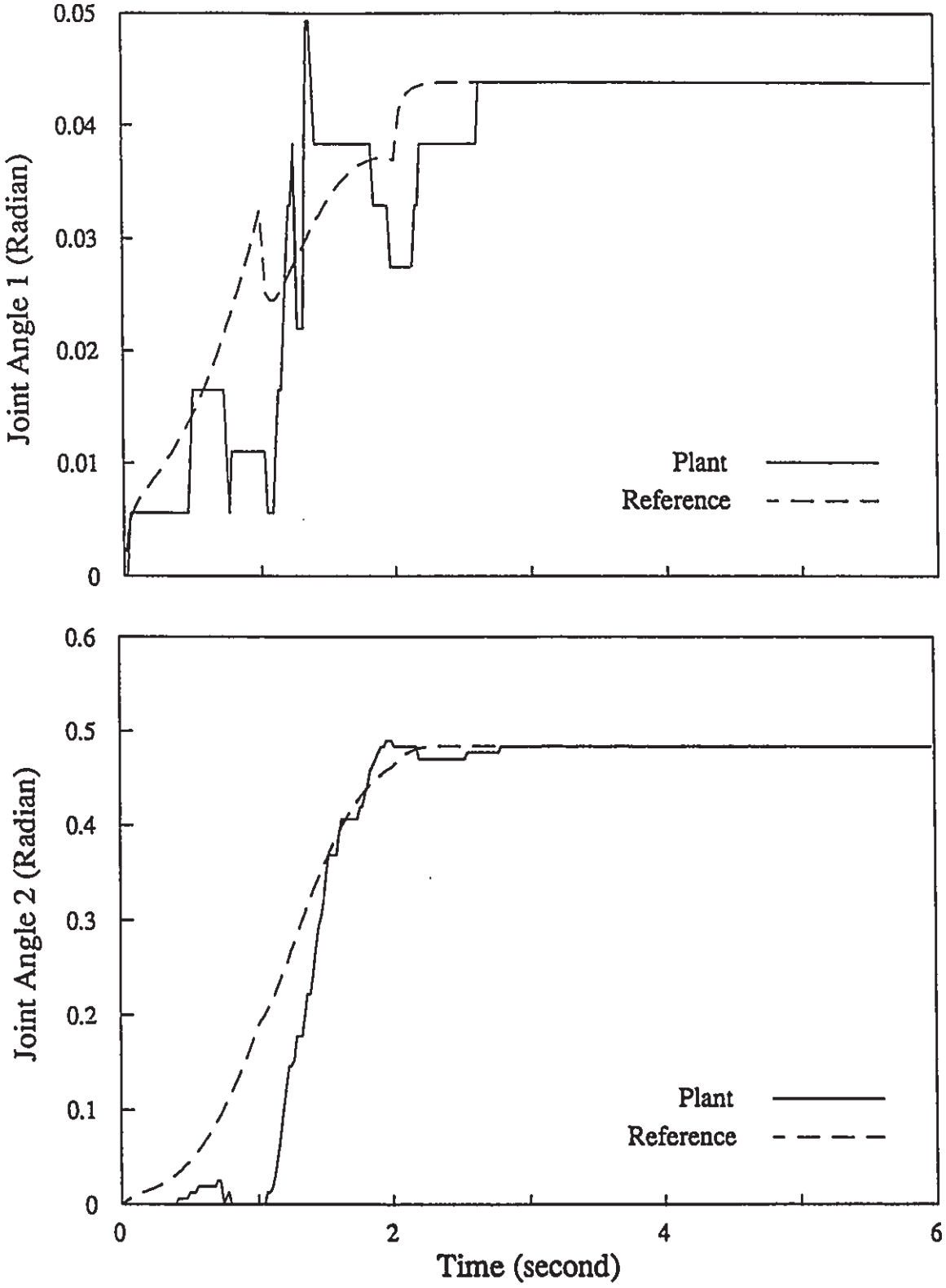

Figure 7.15 Control Experiment with Square Wave Excitation
Payload of 0.0kg - Joint Trajectory

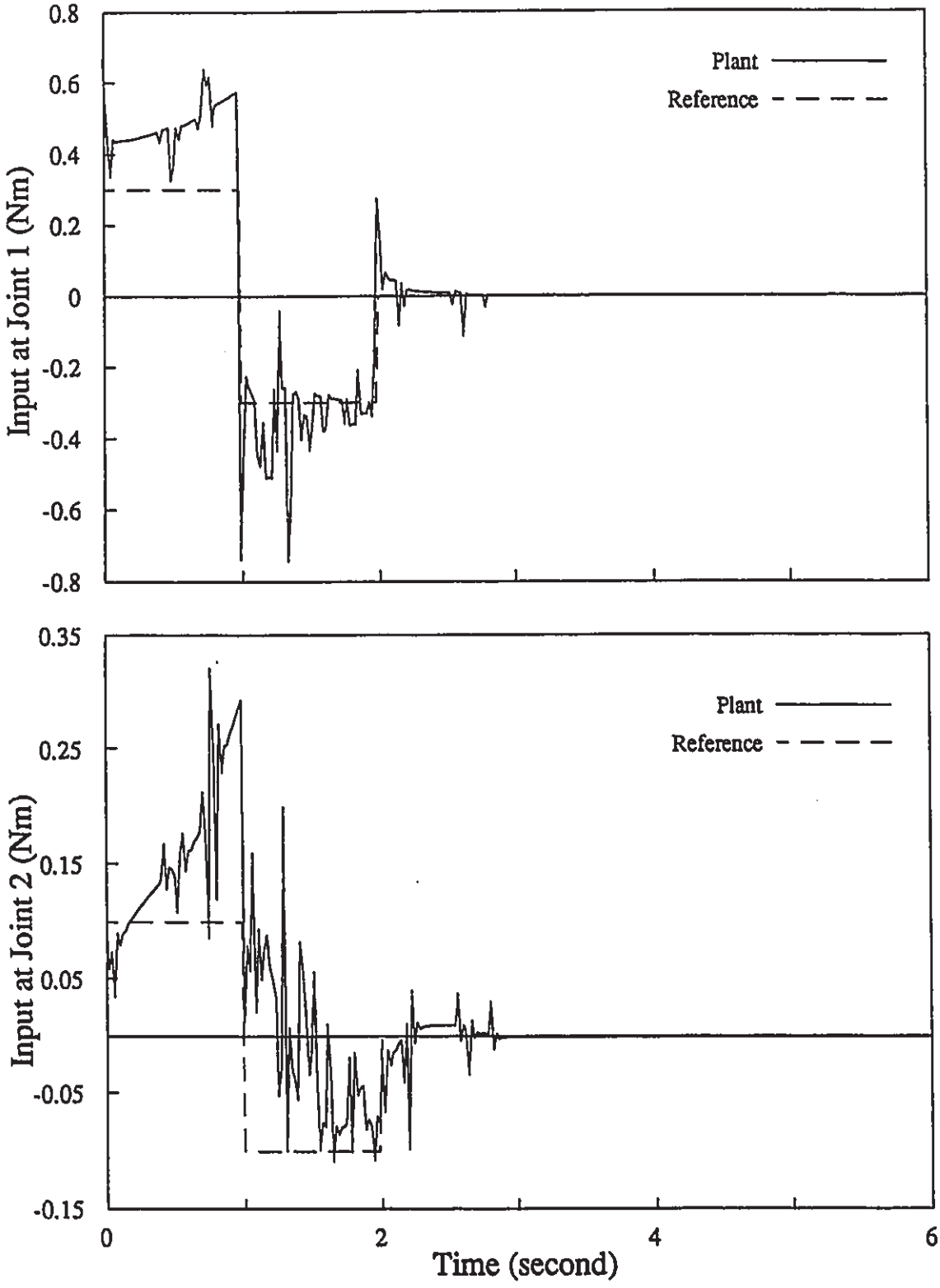

Figure 7.16 Control Experiment with Square Wave Excitation
Payload of 0.0kg - Control Effort

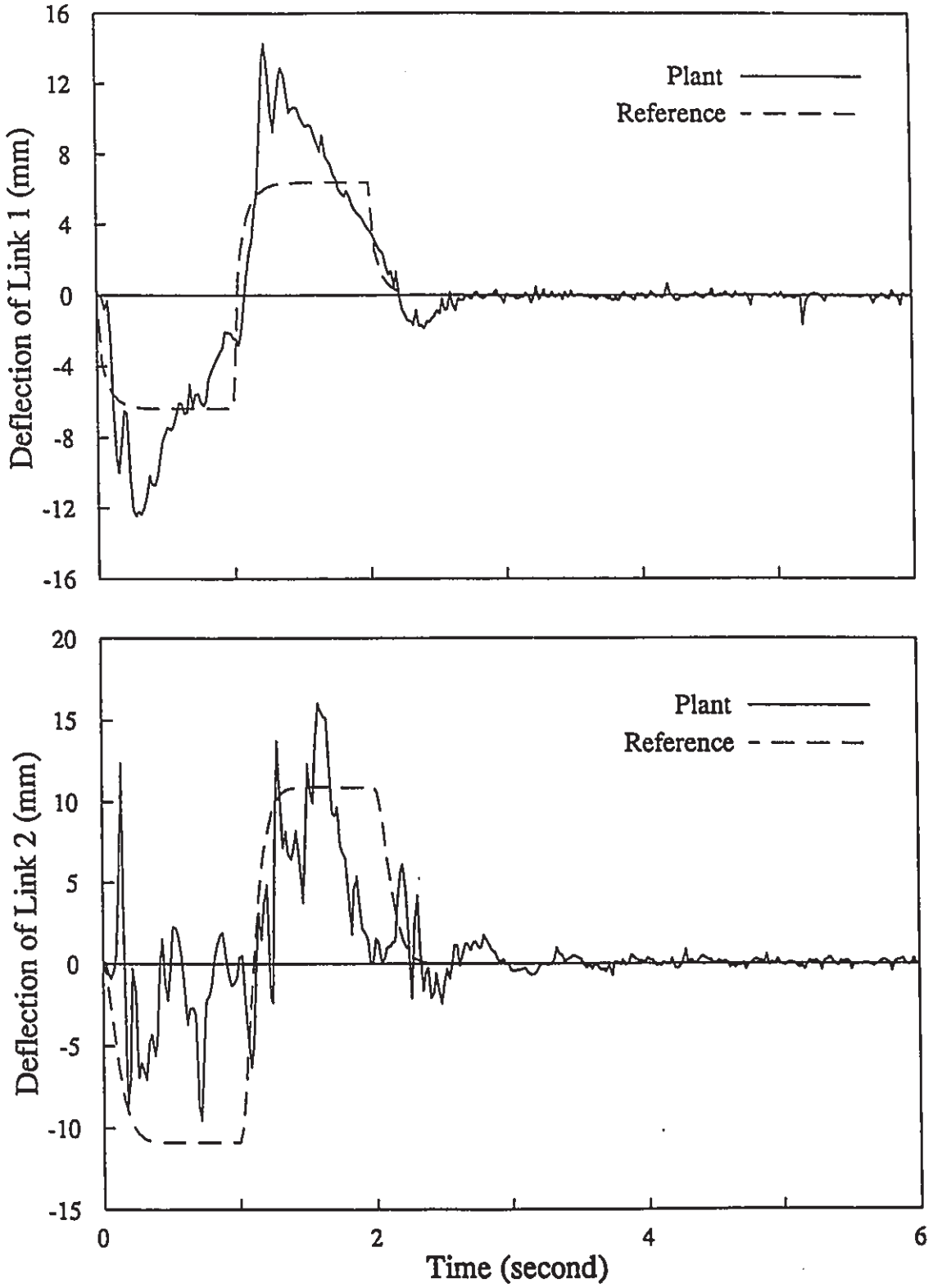

Figure 7.17 Control Experiment with Square Wave Excitation
Payload of 0.01kg - Bending Motion

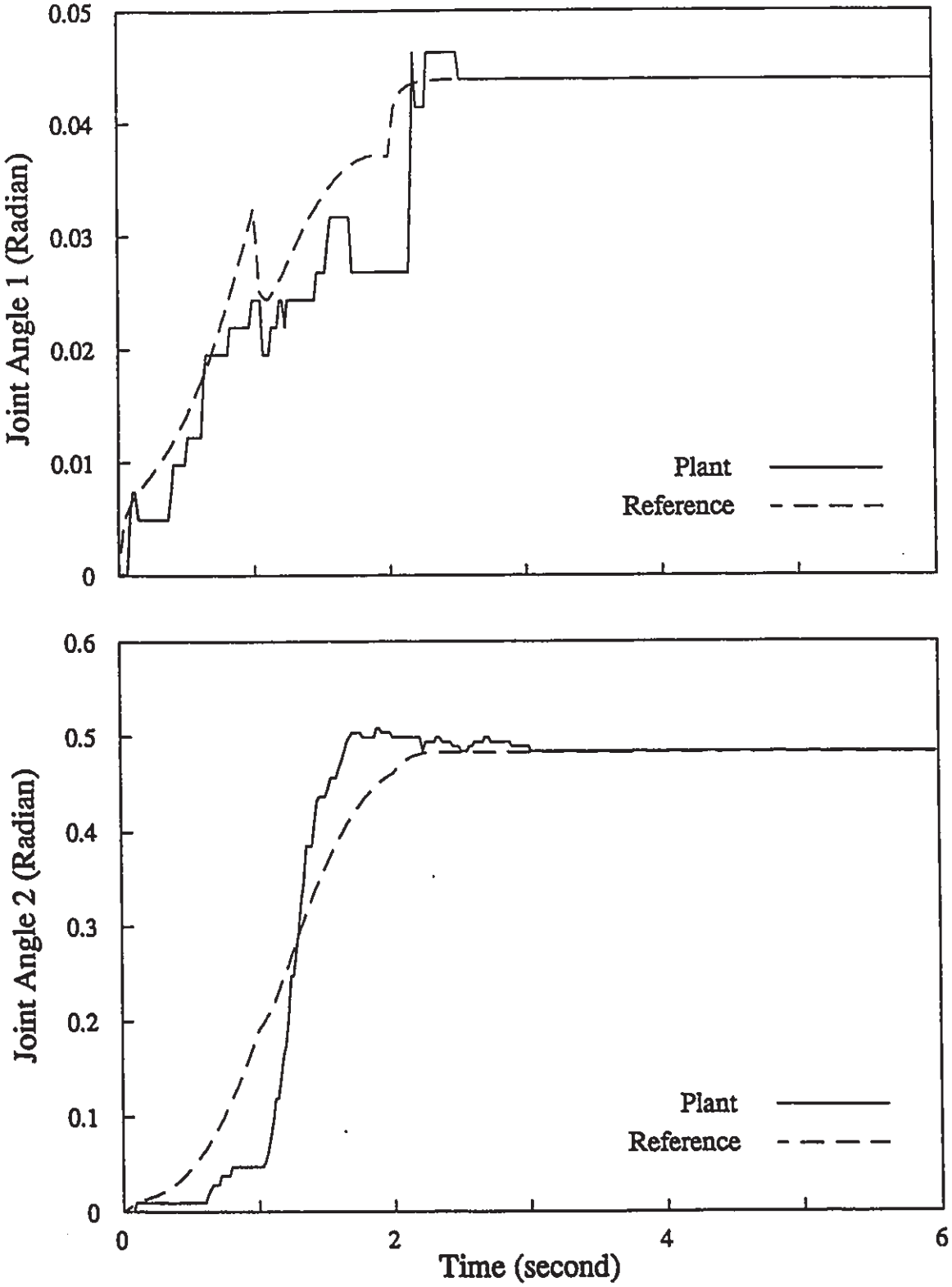

Figure 7.18 Control Experiment with Square Wave Excitation
Payload of 0.01kg - Joint Trajectory

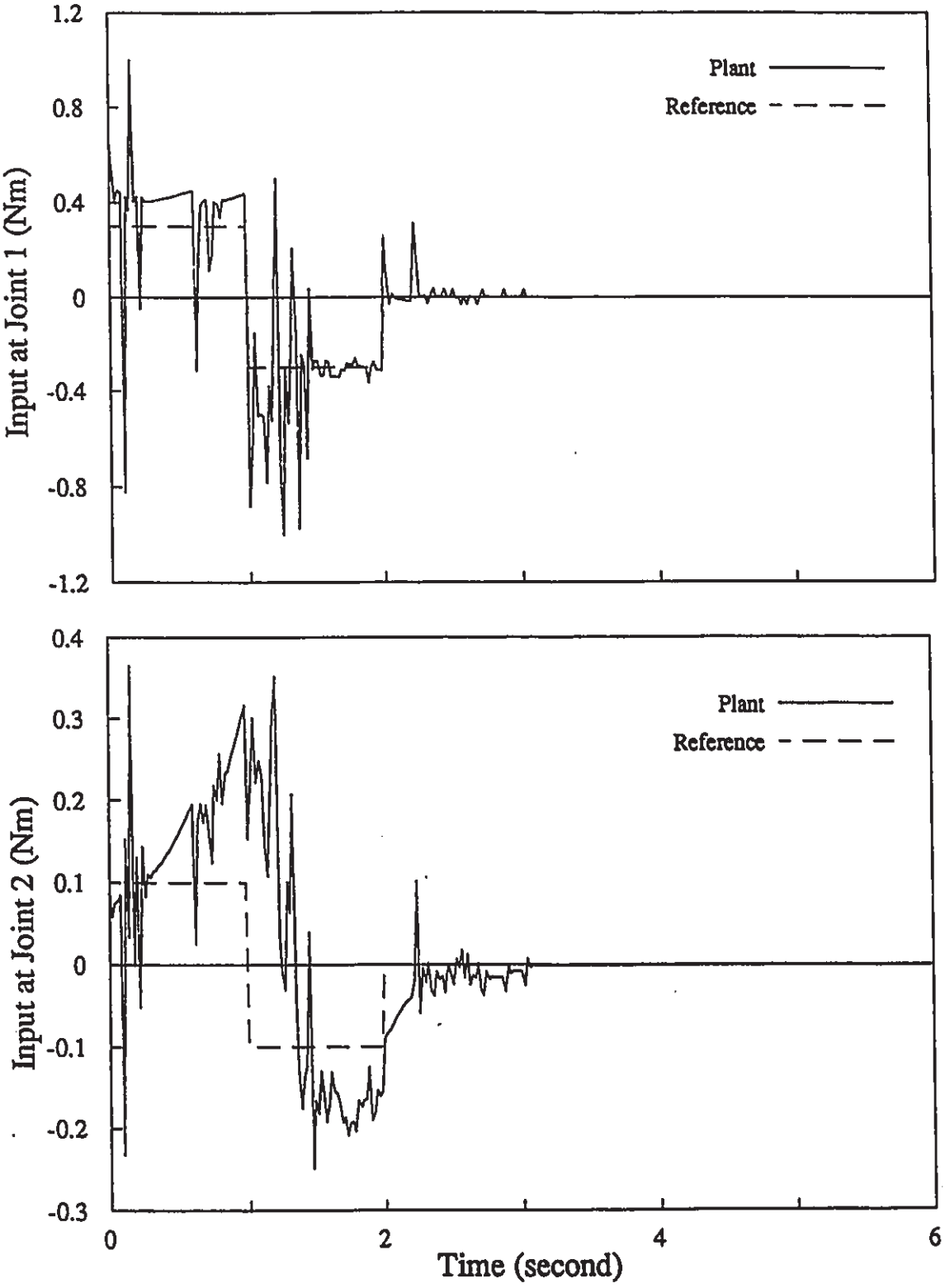

Figure 7.19 Control Experiment with Square Wave Excitation
Payload of 0.01kg - Control Effort

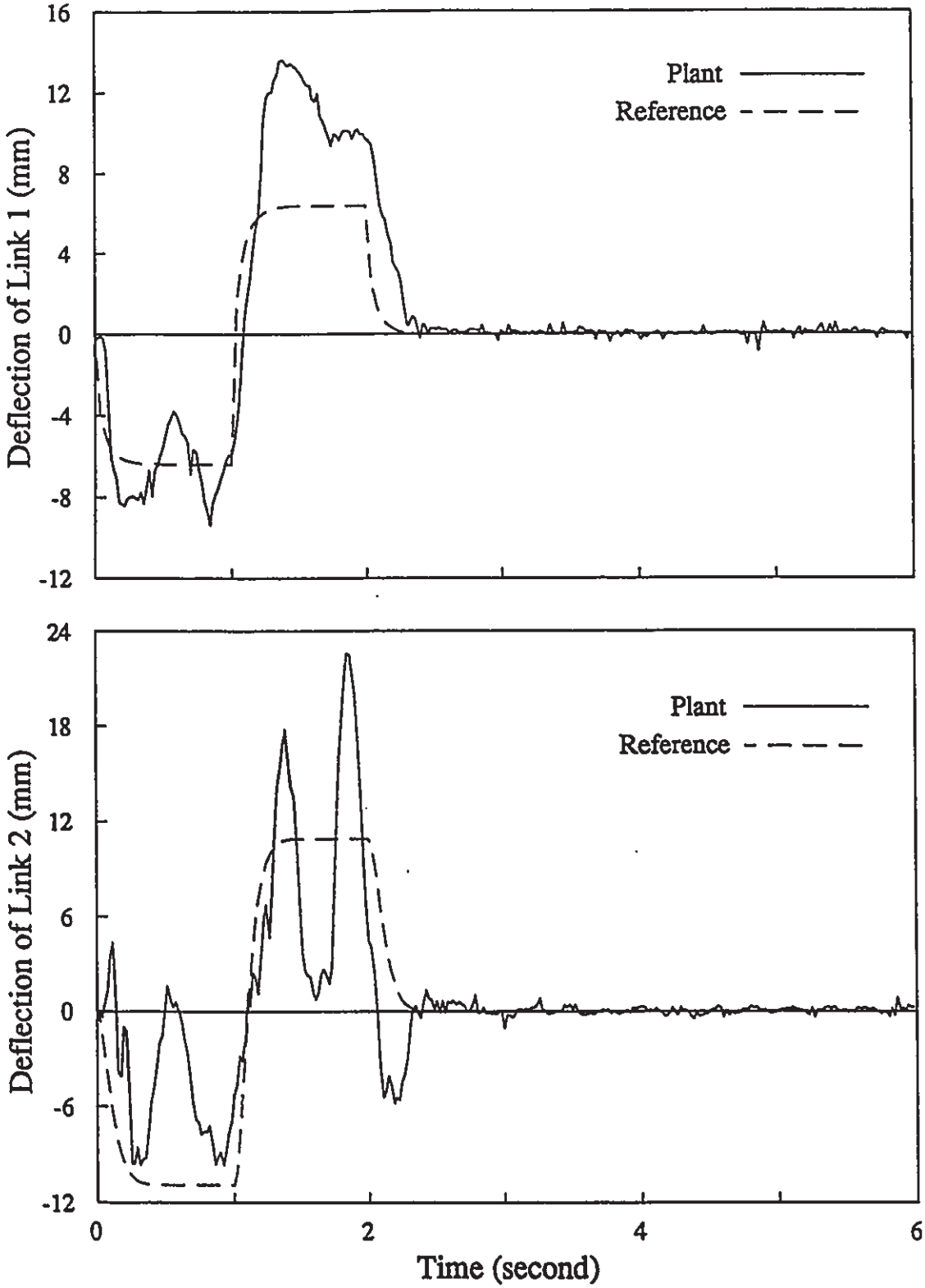

Figure 7.20 Control Experiment with Square Wave Excitation
Payload of 0.1kg - Bending Motion

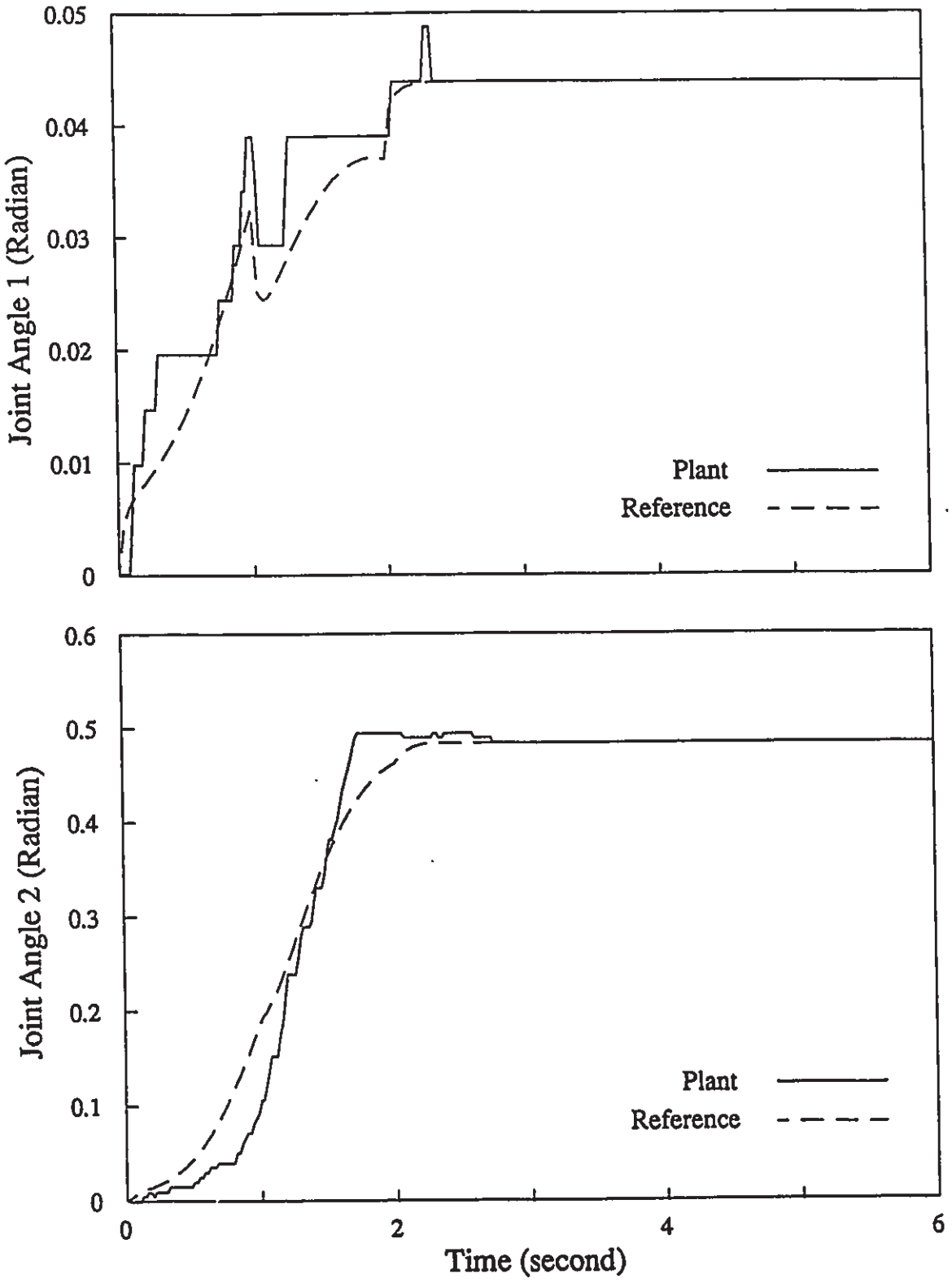

Figure 7.21 Control Experiment with Square Wave Excitation
Payload of 0.1kg - Joint Trajectory

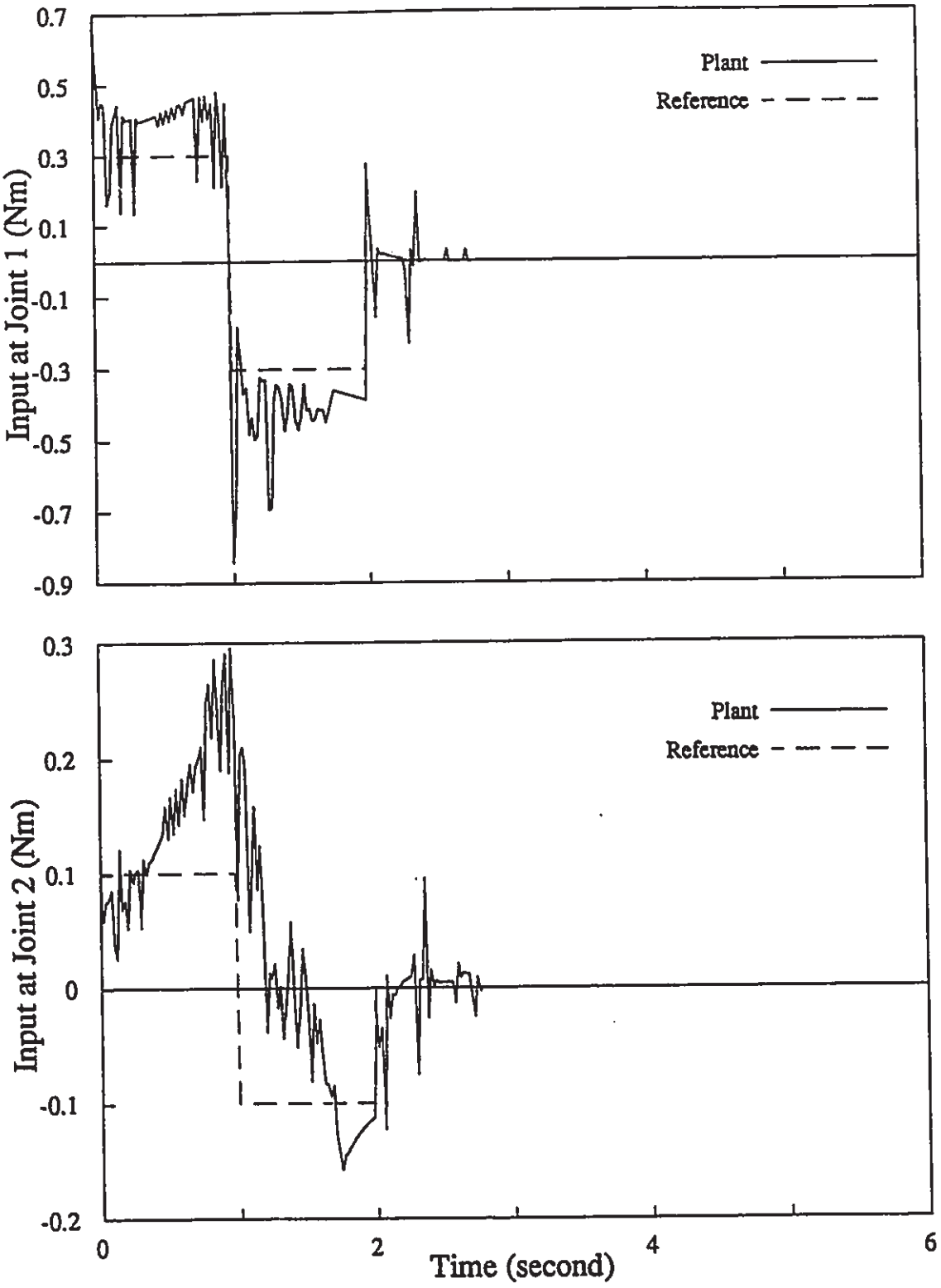

Figure 7.22 Control Experiment with Square Wave Excitation
Payload of 0.1kg - Control Effort

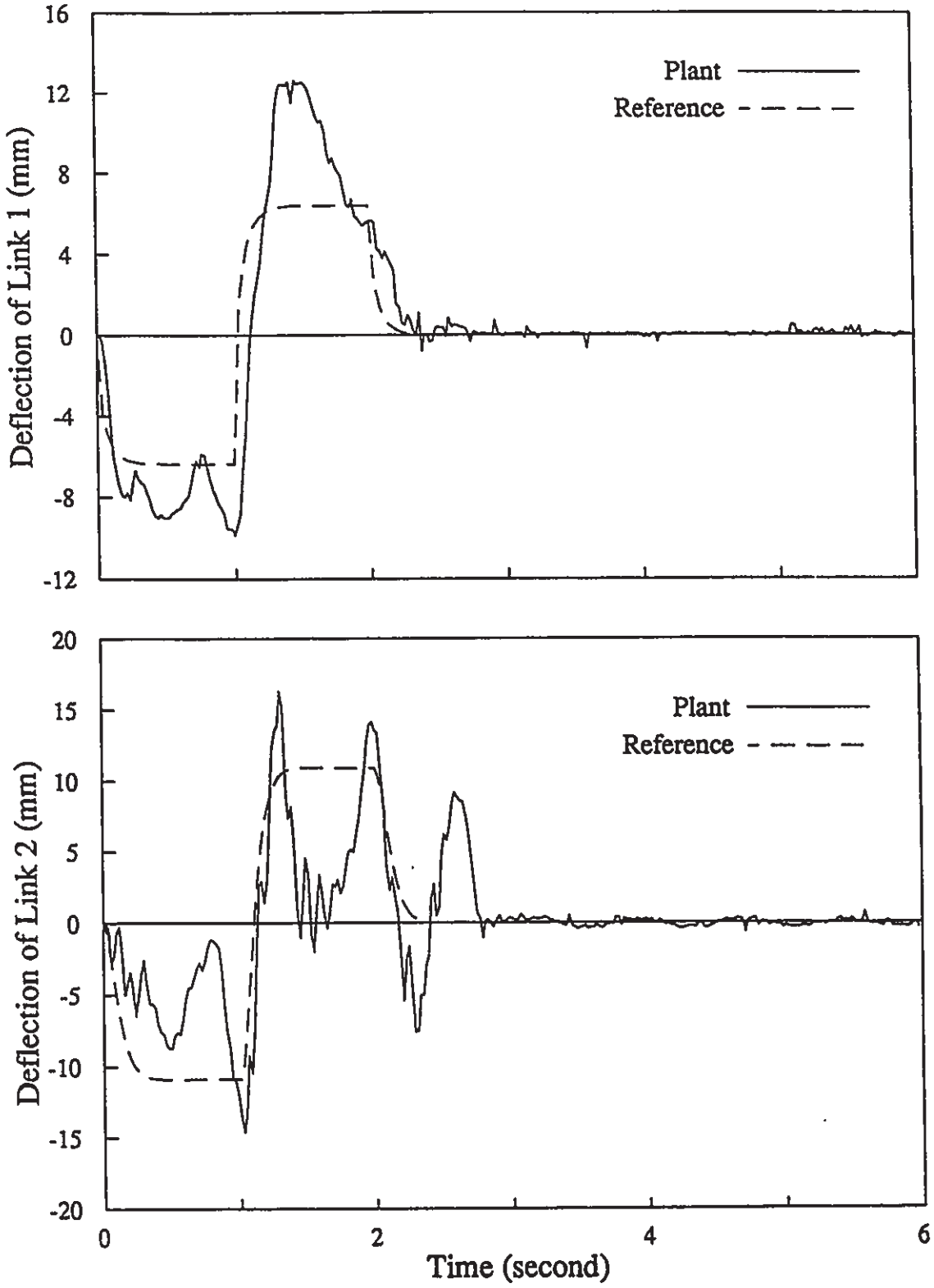

Figure 7.23 Control Experiment with Square Wave Excitation
Payload of 0.2kg - Bending Motion

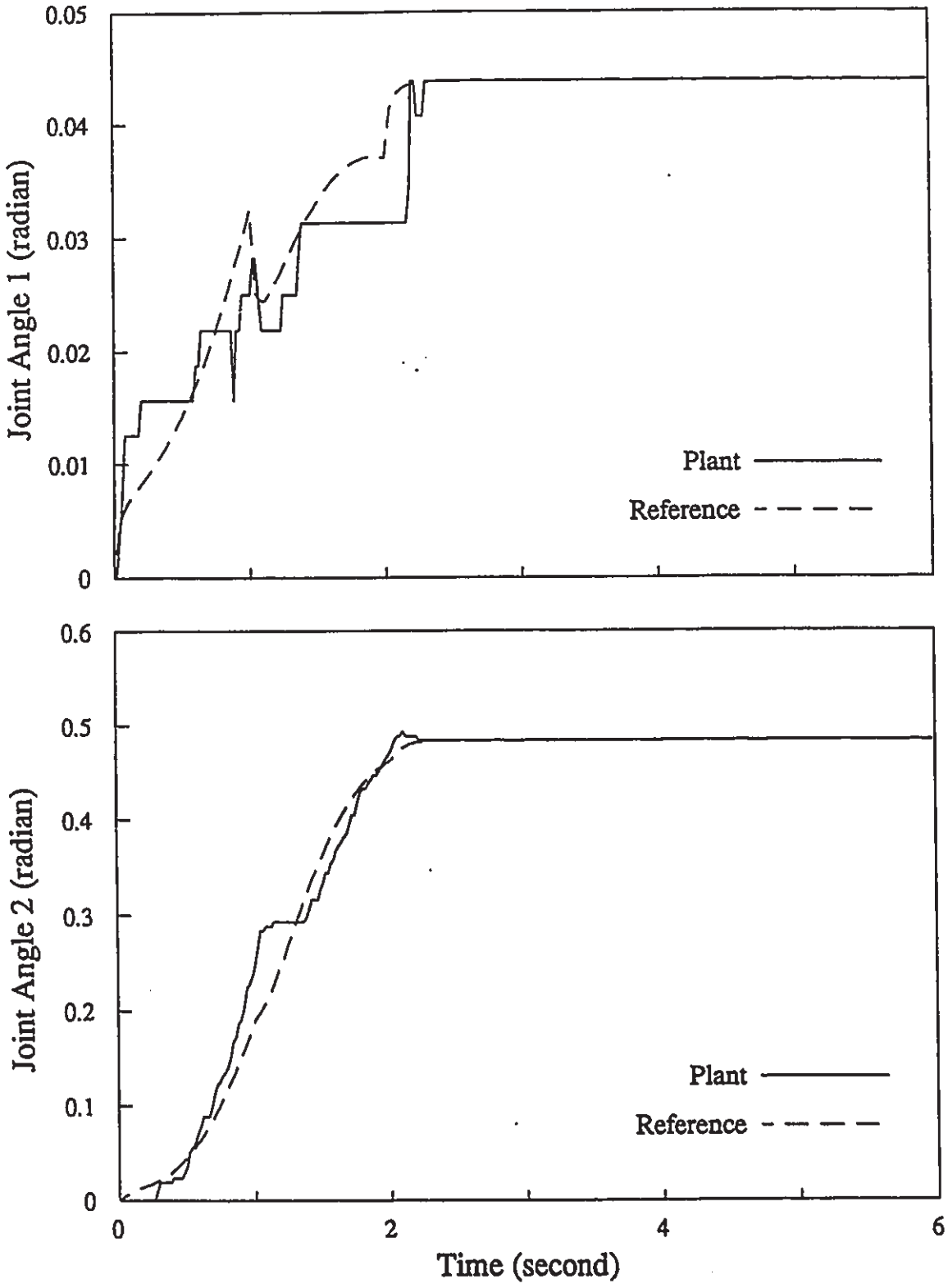

Figure 7.24 Control Experiment with Square Wave Excitation
Payload of 0.2kg - Joint Trajectory

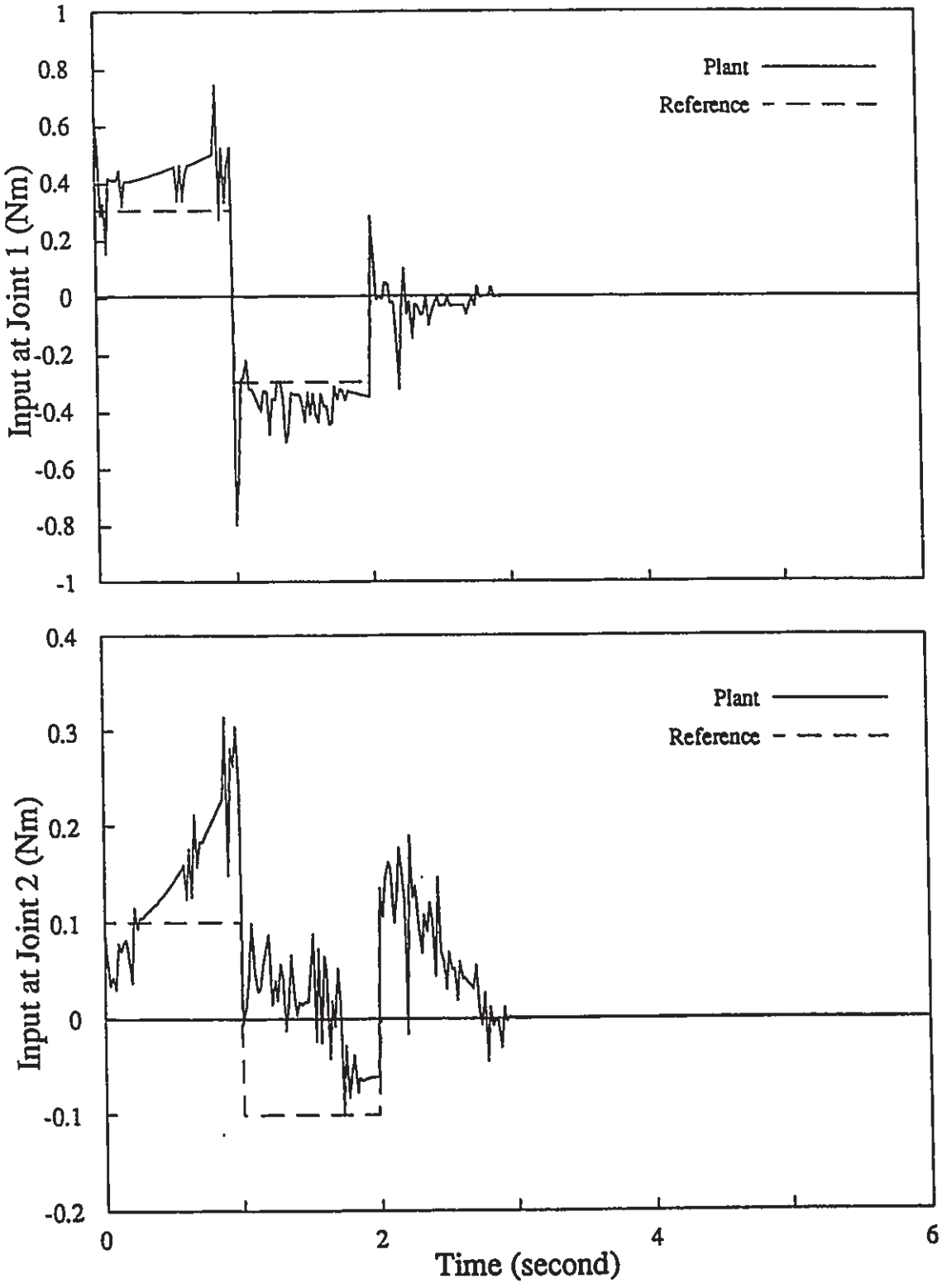

Figure 7.25 Control Experiment with Square Wave Excitation
Payload of 0.2kg - Control Effort

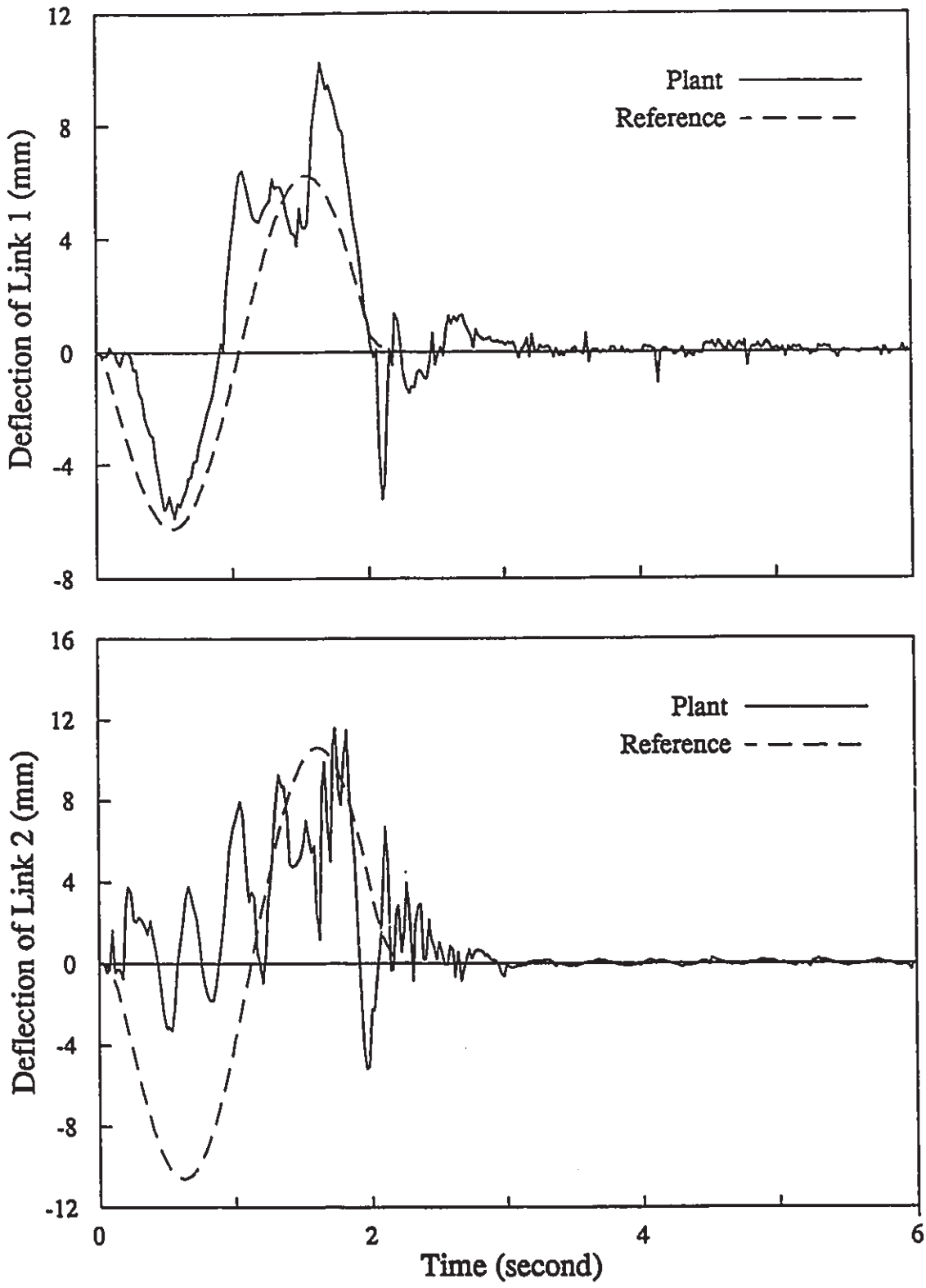

Figure 7.26 Control Experiment with Sinusoidal Excitation
Payload of 0.01kg - Bending Motion

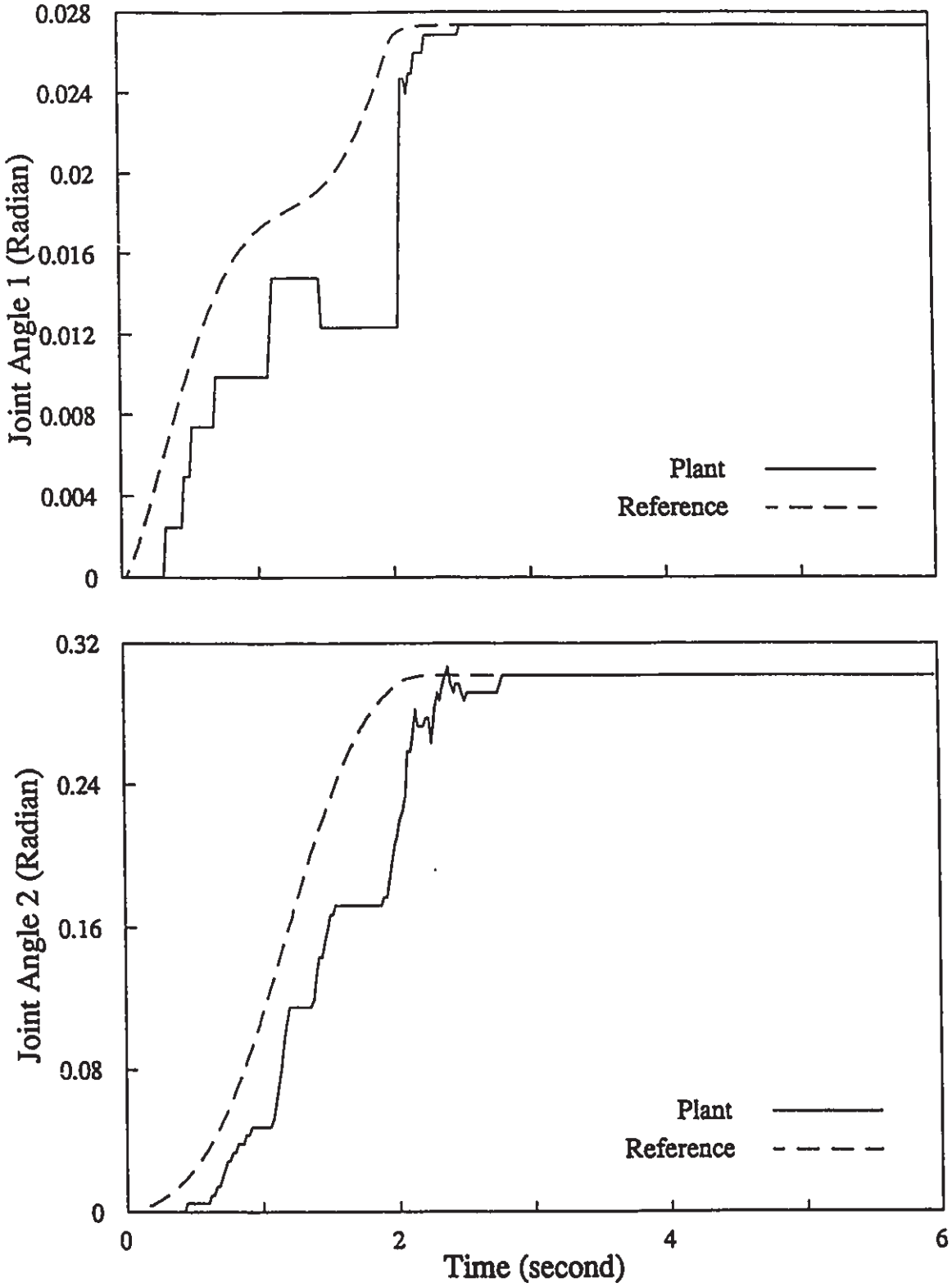

Figure 7.27 Control Experiment with Sinusoidal Excitation
Payload of 0.01kg - Joint Trajectory

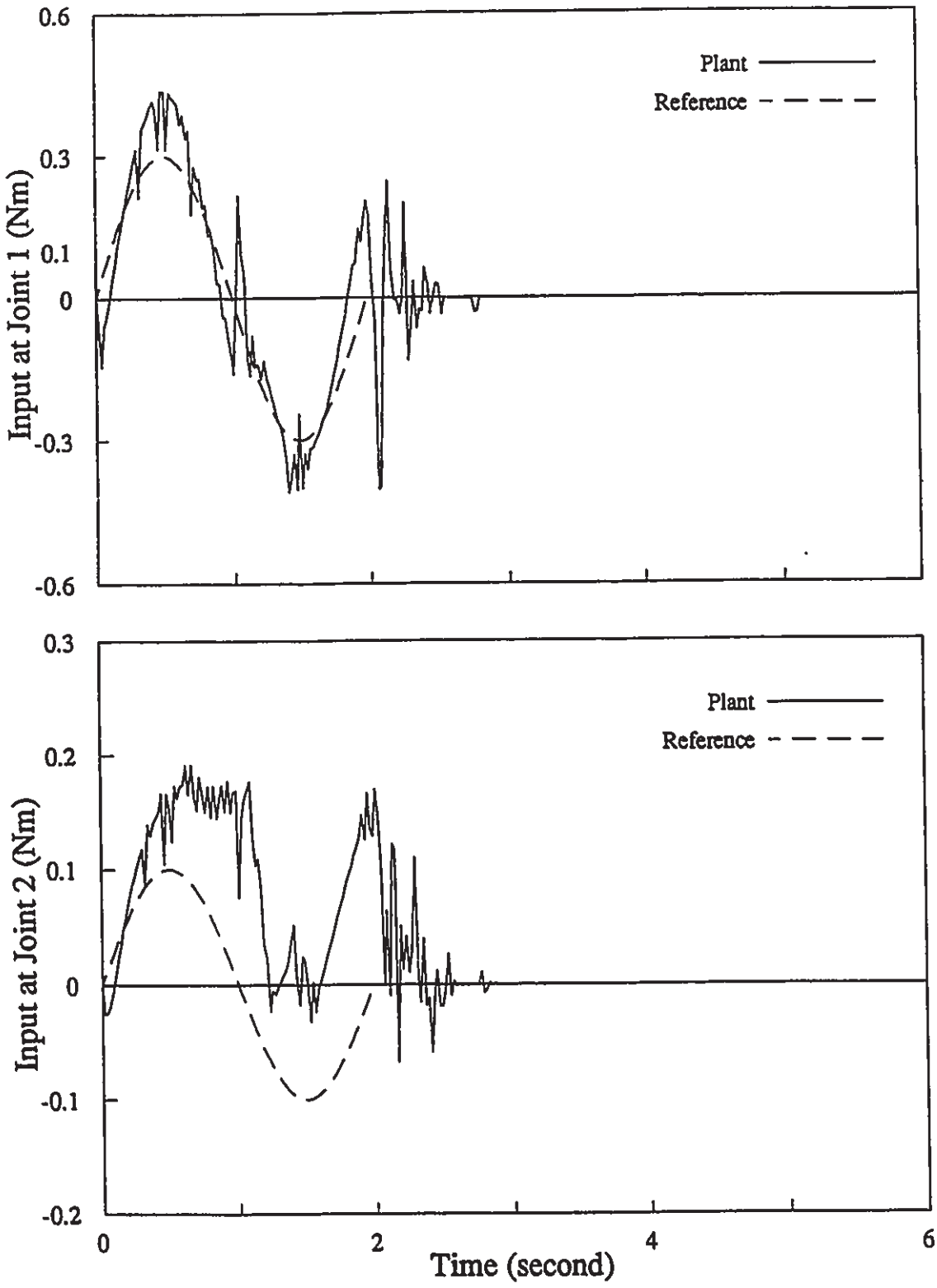

Figure 7.28 Control Experiment with Sinusoidal Excitation
Payload of 0.01kg - Control Effort

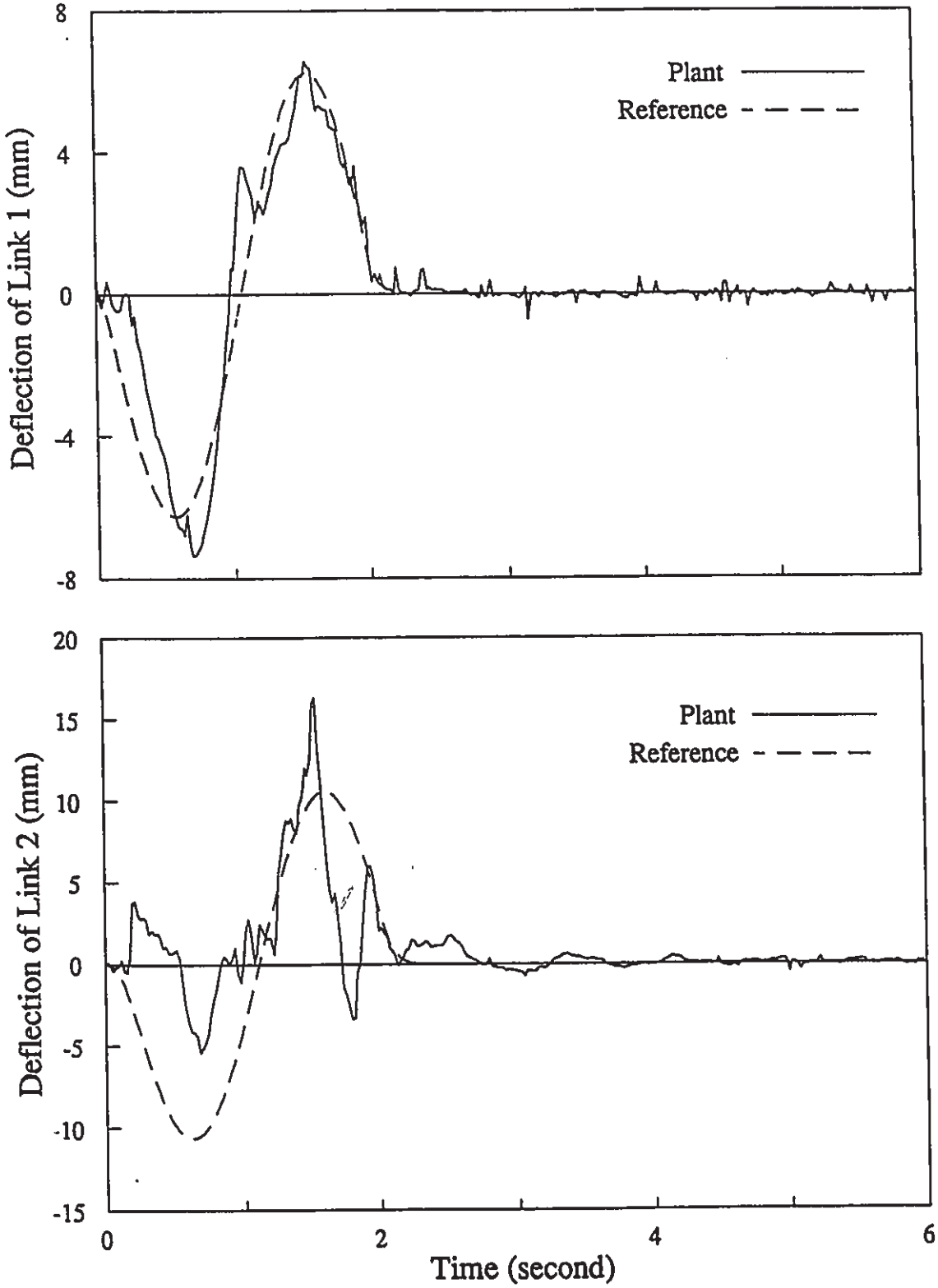

Figure 7.29 Control Experiment with Sinusoidal Excitation
Payload of 0.1kg - Bending Motion

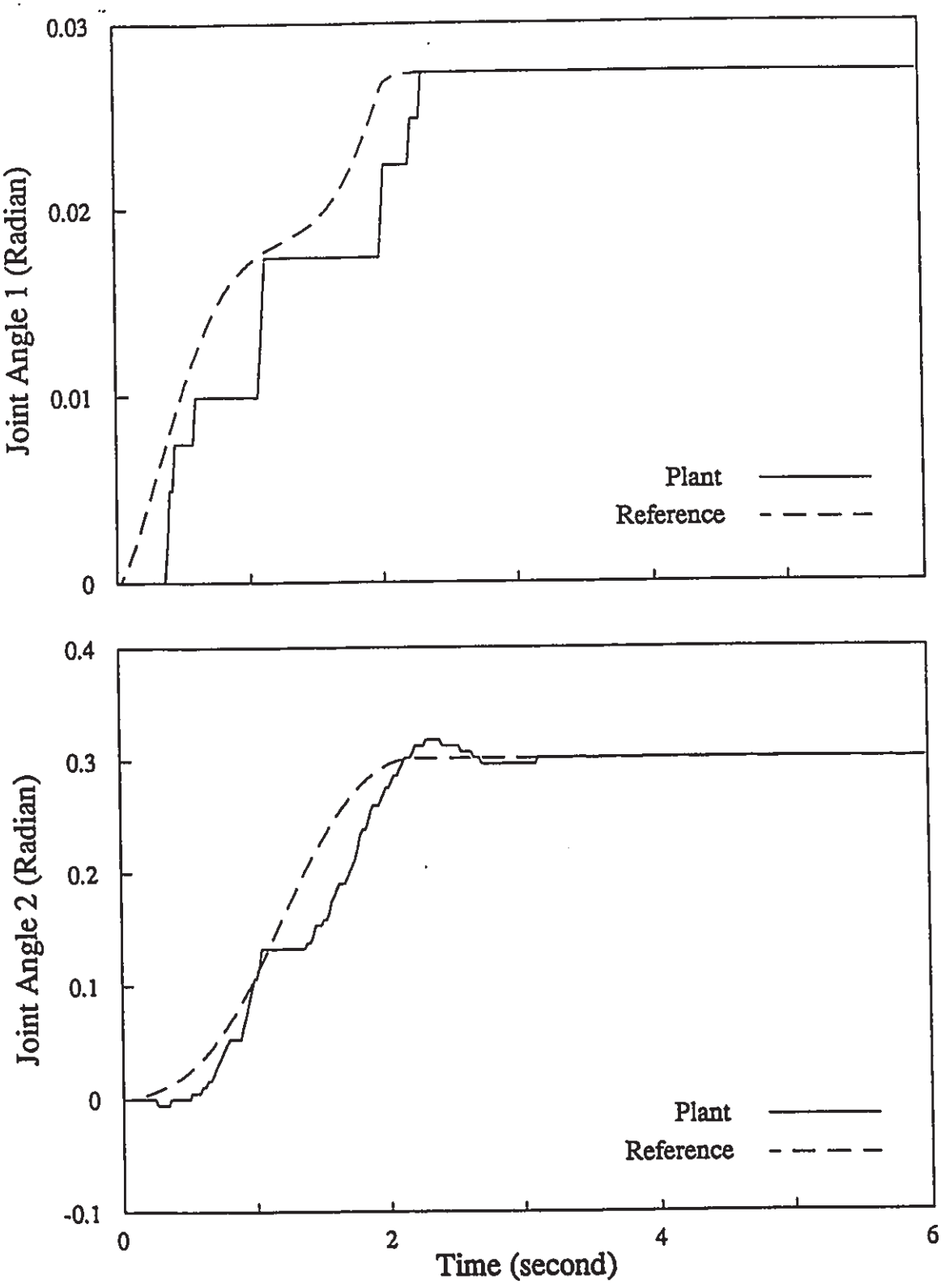

Figure 7.30 Control Experiment with Sinusoidal Excitation
Payload of 0.1kg - Joint Trajectory

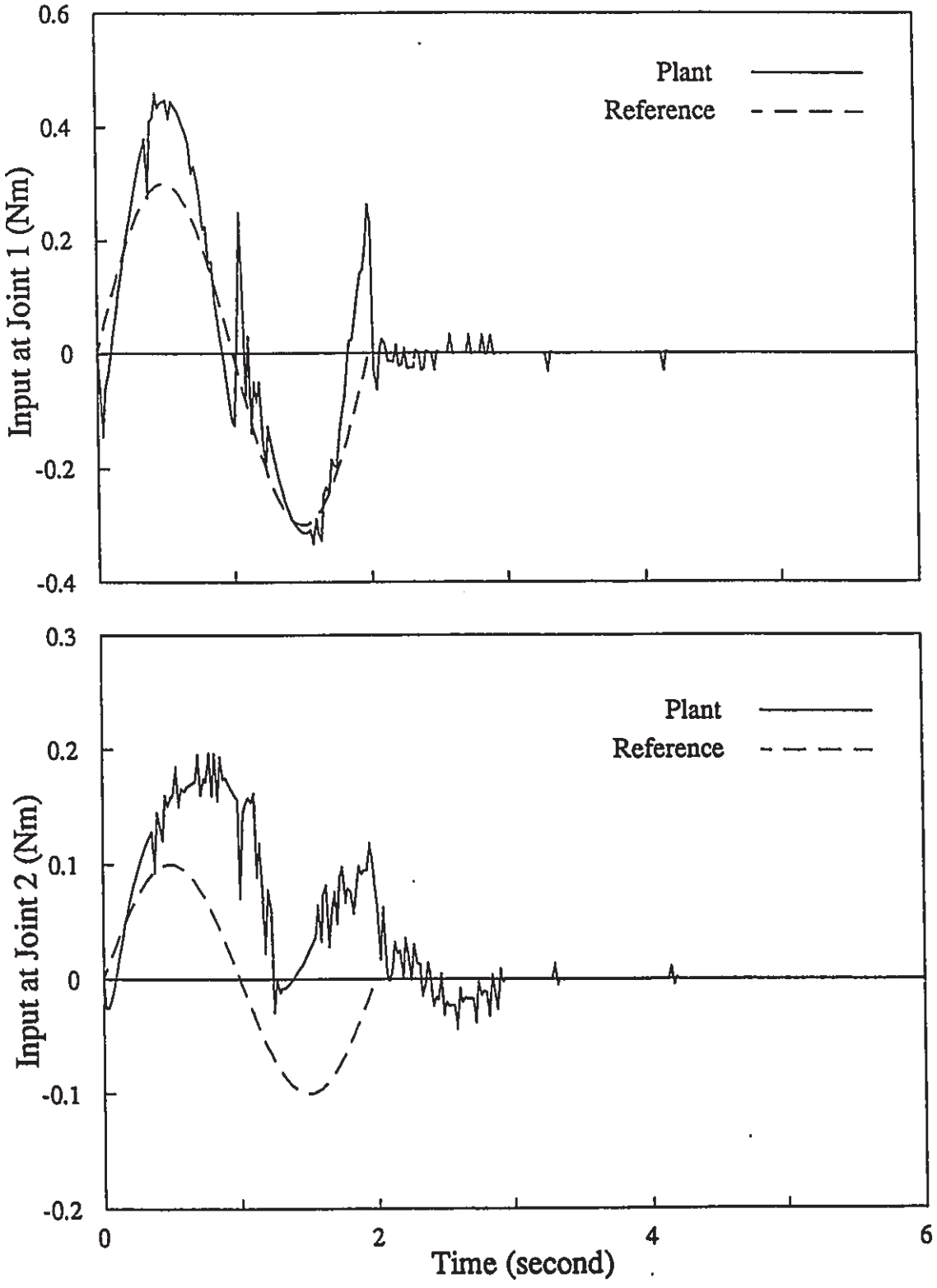

Figure 7.31 Control Experiment with Sinusoidal Excitation
Payload of 0.1kg - Control Effort

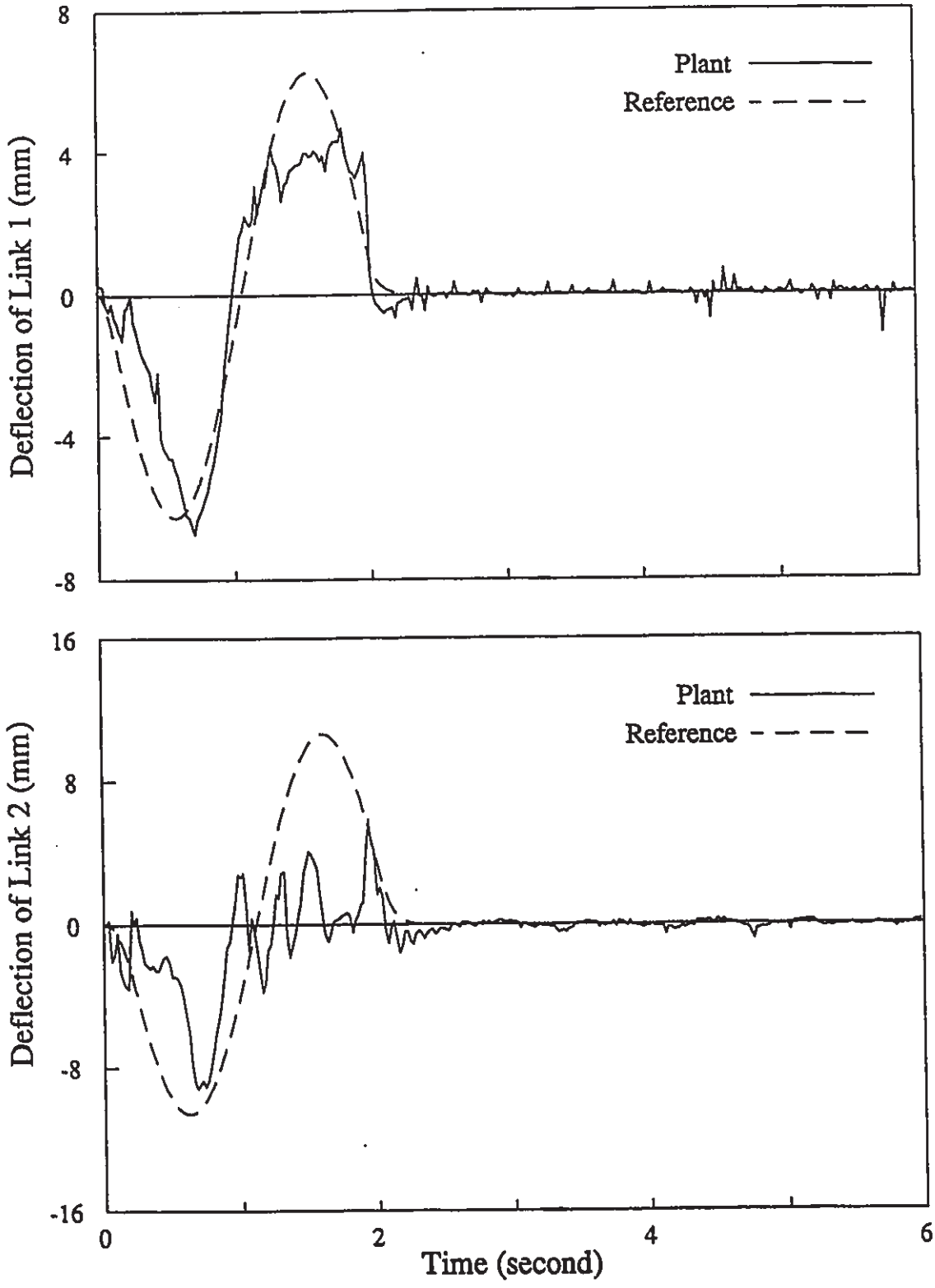

Figure 7.32 Control Experiment with Sinusoidal Excitation
Payload of 0.2kg - Bending Motion

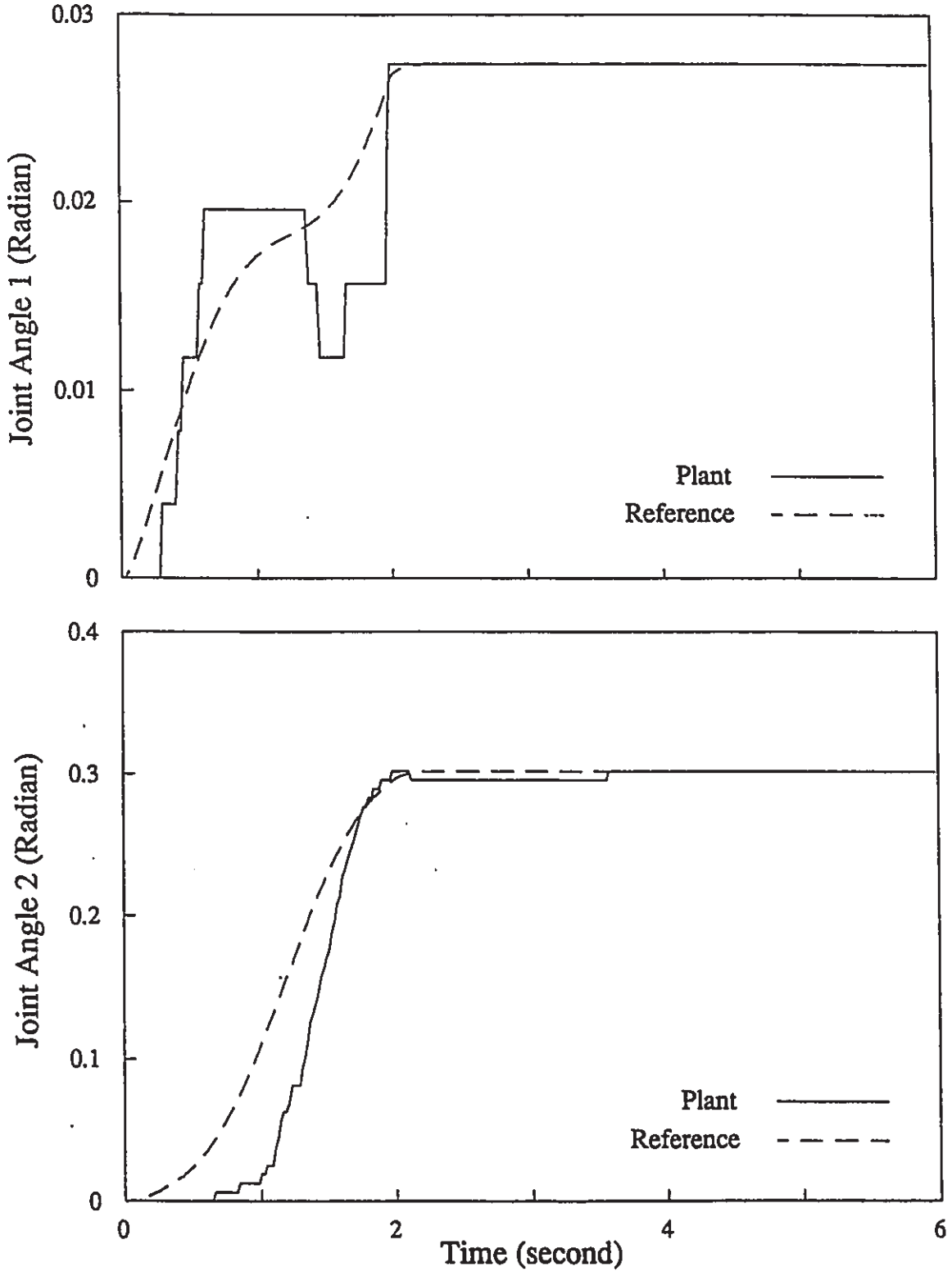

Figure 7.33 Control Experiment with Sinusoidal Excitation
Payload of 0.2kg - Joint Trajectory

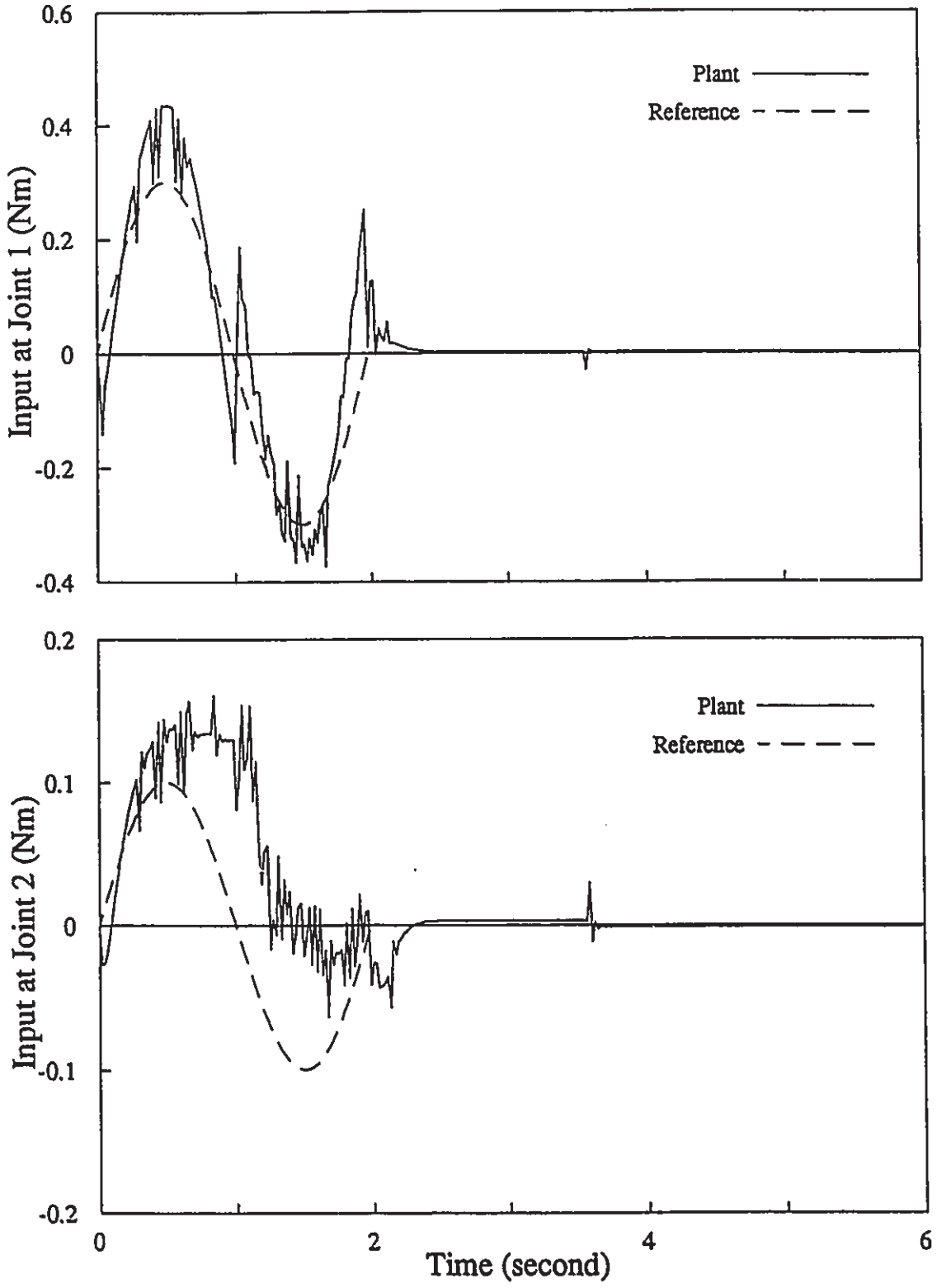

Figure 7.34 Control Experiment with Sinusoidal Excitation
Payload of 0.2kg - Control Effort

in smaller joint angle rotations and link deflections. The lag of the joint trajectory with respect to the reference one is slightly greater.

The payload's effect on the system performance is not as significant as the simulation predicted, but its effect on the vibration frequencies of the system is further confirmed by the experimental data. A larger payload results in lower vibration frequencies for the system. The lower vibration frequencies of the system provide better estimates for the system states and make the negative effects of the computation time delay smaller. This may explain why the closed-loop performance with the payload of 0.2 kg is better than that with the payload of 0.01 kg. In the simulations, the control errors for these two cases are within the same level.

SUMMARY AND CONCLUSIONS

8.1 Introduction

This chapter provides a brief summary of the dissertation content. The main conclusions are outlined and some prospective research topics, from unsolved issues encounted in the present research, are stated.

8.2 Summary

An overview of the research done in flexible manipulator modelling, dynamics, and control is presented and the major difficulties in the field are summarized. In this work, the dynamics of a two degree of freedom planar manipulator with elastic joints and very flexible arms is studied for control purposes. The joints are approximated by linear torsional springs. The assumed mode approach is employed to represent the bending vibrations of the arms. The eigenvalues and eigenfunctions of the arms are determined with the transfer matrix

method. The motion equations of the manipulator are derived using the Lagrangian formulation. The dynamic effects of dry friction at the joints and gear backlash within the actuation are taken into account. The internal structural damping of the arms is considered.

An experimental two degree of freedom robot is designed and developed to verify the theoretical studies. The robot is driven by DC servo motors and its performance is sensed with strain gages and optical encoders. A personal computer is interfaced for control purposes. By comparing the experimental data with the simulation results, the derived theoretical model is validated.

The effects of the main system parameters on the dynamic performance of the manipulator are investigated by means of a parametric analysis. Some significant interactions between the members of the manipulator are observed.

The power balancing technique is extended and applied to the model order reduction of the manipulator. The relation between the power elements of the original system states and the ones of the balanced system states are derived. Using the power elements of the original system states as the criterion, the model order reduction is carried out with the original state variables. It is found that the first two vibration modes dominate the bending motions of each arm. The contributions of the higher modes are negligible.

A discussion of the manipulator's basic control features is presented. A model reference adaptive control algorithm proposed by Sobel is summarized and modified. The modified algorithm is then used to control the manipulator with an unknown payload. The algorithm's properties are examined through computer

simulations and the proper control gains are accordingly determined. Real time testing is implemented to verify the simulation results. It is concluded that with a 12th order nominal model, the proposed algorithm provides satisfactory performance of the closed-loop system.

8.3 Main Contributions

The main contributions of the current study include:

a. An analytic model of a two degree of freedom manipulator with elastic joints and very flexible arms is derived and experimentally verified. The dynamic effects of dry friction at the joints, gear backlash within the actuators, and the internal structural damping of the arms are all considered.

b. The dynamic effects of the major system parameters on the manipulator's performance are investigated. The interactions between the members of the manipulator are examined. It is found that the dynamic interrelation between the two links is much stronger than that between the joints and the parameter value of each joint significantly affects the dynamics of its driven link.

c. The power balancing technique developed by Han et al. [108] is extended and a new approach for model order reduction of nonlinear dynamic systems is proposed. Based on the power elements of the balanced system states, an analytic expression for the power elements of the original system states is derived. Using the power elements as the criterion for model order reduction, a lower order model with the original physical state variables is

obtained. The model order reduction of the manipulator shows that the first two vibration modes dominate the bending vibrations of each link. The contributions of higher modes are negligible.

d. The Sobel's model reference adaptive control algorithm is modified and applied to the manipulator. The modification improves the controller's performance significantly. Both computer simulations and the real time testing show that the proposed control strategy damps the structural vibrations effectively and provides satisfactory system performance.

8.4 Recommendations For Future Work

Although the derived model is experimentally verified and the resulting closed-loop system has satisfactory performance, it is felt that more accurate models for the dynamics of friction, gear backlash, and internal structural damping are required.

This work is based on the assumption that the effect of gravity is negligible and the torsional vibrations of the arms are zero. This is suitable for space applications. Without the satisfaction of this assumption, the dynamics of the torsional vibrations have to be considered. The issues of controlling a manipulator with links vibrating both laterally and torsionally need to be explored.

The power balancing technique is an effective tool for model order reduction. The use of this technique for model order reduction of a nonlinear dynamic system is based on piece-wise linearization of the nonlinear model and on neglecting the system's light damping. A technique for performing model order

reduction on nonlinear systems without these approximations needs to be developed.

The control work done in the current study is just a first step. There are many related issues waiting to be explored, such as designing a controller directly based on a nonlinear model rather on a simplified linear model, performing real time sensing of system states with better accuracy, and improving the priori knowledge of u_p^* for the Sobel's algorithm. The limitations of the proposed algorithm also need to be explored.

Finally, the manipulator considered in the current study is just a two degree of freedom planar robot without any torsional motions. Taking into account other vibration motions such as twisting motion or increasing the manipulator's degrees of freedom are natural continuations of this research.

DYNAMIC EQUATIONS

The complete listing of the manipulator's dynamic equations derived in Chapter 3 is given here. The equations are presented in state space form:

$$\left[\begin{array}{c|c} I & 0 \\ \hline 0 & M'(x) \end{array}\right] \begin{bmatrix} \dot{x}_1 \\ \dot{x}_2 \\ \dot{x}_3 \\ \dot{x}_4 \\ \dot{x}_{21} \\ \vdots \\ \dot{x}_{2M} \\ \dot{x}_{41} \\ \vdots \\ \dot{x}_{4M} \\ \dot{x}_7 \\ \dot{x}_8 \\ \dot{x}_9 \\ \dot{x}_{10} \\ \dot{x}_{111} \\ \vdots \\ \dot{x}_{11M} \\ \dot{x}_{121} \\ \vdots \\ \dot{x}_{12M} \end{bmatrix} = \begin{bmatrix} x_7 \\ x_8 \\ x_9 \\ x_{10} \\ x_{111} \\ \vdots \\ x_{11M} \\ x_{121} \\ \vdots \\ x_{12M} \\ B_1(x) \\ B_2(x) \\ B_3(x) \\ B_4(x) \\ B_{21}(x) \\ \vdots \\ B_{2M}(x) \\ B_{41}(x) \\ \vdots \\ B_{4M}(x) \end{bmatrix} + \begin{bmatrix} 0 & 0 \\ & \\ & \\ & \\ \cdot & \cdot \\ \cdot & \cdot \\ \cdot & \cdot \\ & \\ & \\ & \\ 0 & 0 \\ 1 & 0 \\ 0 & 1 \\ 0 & 0 \\ \cdot & \cdot \\ \cdot & \cdot \\ \cdot & \cdot \\ 0 & 0 \end{bmatrix} \begin{bmatrix} u_1 & u_2 \end{bmatrix}^T$$

where I represents the identity matrix of dimension $(2M+4)$x$(2M+4)$. $M'(x)$ is the mass matrix with the same dimensions. The integer M is the highest vibration mode of the link considered in the model. The elements of the matrix M' are denoted by m_{ij}.

$$m_{11} = I_{h1} + I_{h2} + I_{r2} + I_p + J_2 + \frac{1}{3}\lambda_1 L_1^3 + \frac{1}{3}\lambda_2 L_2^3 + (m_{r2} + m_{h2} + \lambda_2 L_2 + m_p) L_1^2 + m_p L_2^2 +$$
$$\cos(\theta_2 + \alpha_{1e})[(\lambda_2 L_2 + 2m_p) L_1 L_2 + 2\lambda_2 \sum_{i=1}^{M} \psi_{1i}\varphi_{1i} \sum_{i=1}^{M} \varphi_{2i} K_i)] +$$
$$\lambda_2 \sin(\theta_2 + \alpha_{1e})(L_2^2 \sum_{i=1}^{M} \psi_{1i}\varphi_{1i} - 2L_1 \sum_{i=1}^{M} \varphi_{2i} K_{2i})$$

$$m_{12} = I_{h2} + I_p + \frac{1}{3}\lambda_2 L_2^3 + m_p[L_2^2 + L_1 L_2 \cos(\theta_2 + \alpha_{1e})] + \lambda_2 \cos(\theta_2 + \alpha_{1e})[\frac{1}{2} L_1 L_2^2 +$$
$$\sum_{i=1}^{M} \psi_{1i}\varphi_{1i} \sum_{i=1}^{M} \varphi_{2i} K_{2i}) + \lambda_2 (\frac{1}{2} L_2^2 \sum_{i=1}^{M} \psi_{1i}\varphi_{1i} - L_1 \sum_{i=1}^{M} \varphi_{2i} K_{2i}) \sin(\theta_2 + \alpha_{1e}) +$$
$$\lambda_2 \sum_{i=1}^{M}\sum_{j=1}^{M} \varphi_{2i}\varphi_{2j} N_{2ij}$$

$$m_{13} = 0.0$$

$$m_{14} = J_2$$

$$m_{15i} = \lambda_1 M_{1i} + \psi_{1i}[(m_{r2} + m_{h2} + \lambda_2 L_2 + m_p) L_1 + (\frac{1}{2}\lambda_2 L_2 + m_p) L_2 \cos(\theta_2 + \alpha_{1e}) -$$
$$\lambda_2 \sin(\theta_2 + \alpha_{1e}) \sum_{j=1}^{M} \varphi_{2j} K_{2j}] + \frac{1}{\eta_1} \dot{\psi}_{1i} \{I_{h2} + \frac{1}{3}\lambda_2 L_2^3 + m_p L_2^2 + [(\frac{1}{2}\lambda_2 L_2 + m_p) L_1 L_2 +$$
$$\lambda_2 \sum_{j=1}^{M} \psi_{1j}\varphi_{1j} \sum_{j=1}^{M} \psi_{2i} K_{2i}] \cos(\theta_2 + \alpha_{1e}) - (\lambda_2 \sum_{j=1}^{M} \psi_{2j} K_{2j} + m_p \sum_{j=1}^{M} \psi_{2j}\varphi_{2j}) L_1$$
$$\sin(\theta_2 + \alpha_{1e}) + I_{r2} + I_p + J_2\} \qquad (i=1, \ldots, M)$$

$$m_{16i} = \lambda_2 K_{2i}[L_1 \cos(\theta_2 + \alpha_{1e}) + \sum_{j=1}^{M} \psi_{1i}\varphi_{1i} \sin(\theta_2 + \alpha_{1e})] + \lambda_2 M_{2i} +$$
$$\psi_{2i}[m_p L_1 \cos(\theta_2 + \alpha_{1e}) + m_p L_2] + \frac{1}{\eta_2} I_p \dot{\psi}_{2i} \qquad (i=1, \ldots, M)$$

$$B_1 = K_1(\theta_3 - \theta_1) + T_{f1} - 2\lambda_1 \dot{\theta}_1 \sum_{i=1}^{M}\sum_{j=1}^{M} \varphi_{1i} \dot{\varphi}_{1j} N_{1ij} - 2(m_{r2} + m_{h2} + \lambda_2 L_2 + m_p) \dot{\theta}_1$$
$$\sum_{i=1}^{M} \psi_{1i}\varphi_{1i} \sum_{j=1}^{M} \psi_{1j} \dot{\varphi}_{1j} + \{[(\frac{1}{2}\lambda_2 L_2 + m_p) L_1 L_2 + \lambda_2 \sum_{i=1}^{M} \psi_{1j}\varphi_{1j} \sum_{j=1}^{M} \psi_{2j} K_{2j}] \sin(\theta_2 + \alpha_{1e}) +$$
$$[(\lambda_2 \sum_{i=1}^{M} \psi_{2i} K_{2i} + m_p \sum_{i=1}^{M} \psi_{2i}\varphi_{2i}) L_1 - (\frac{1}{2}\lambda_2 L_2 + m_p) L_2 \sum_{i=1}^{M} \psi_{1i}\varphi_{1i}] \cos(\theta_2 + \alpha_{1e})\}$$
$$(2\dot{\theta}_1 + \dot{\theta}_2 + \dot{\alpha}_{1e})(\dot{\theta}_2 + \dot{\alpha}_{1e}) + 2(\lambda_2 \sum_{i=1}^{M} \dot{\varphi}_{2i} K_{2i} + m_p \sum_{i=1}^{M} \psi_{2i} \dot{\varphi}_{2i})(\dot{\theta}_1 + \dot{\theta}_2 + \dot{\alpha}_{1e})$$
$$[L_1 \sin(\theta_2 + \alpha_{1e}) - \cos(\theta_2 + \alpha_{1e}) \sum_{i=1}^{M} \psi_{1i}\varphi_{1i}] - (\lambda_2 L_2 + 2m_p) L_2 \dot{\theta} \sin(\theta_2 + \alpha_{1e})$$

$$\sum_{i=1}^{M}\psi_{1i}\,\dot{\varphi}_{1i}-2(\lambda_2\sum_{i=1}^{M}\varphi_{2i}K_{2i}+m_p\sum_{i=1}^{M}\psi_{2i}\varphi_{2i})\,\dot{\theta}_1\sum_{i=1}^{M}\psi_{1i}\,\dot{\varphi}_{1i}\cos(\theta_2+\alpha_{1e})$$

$$-2(\lambda_2\sum_{i=1}^{M}\sum_{j=1}^{M}\varphi_{2i}\,\dot{\varphi}_{2j}N_{2ij}+m_p\sum_{j=1}^{M}\psi_{2i}\varphi_{2j}\sum_{j=1}^{M}\psi_{2i}\,\dot{\varphi}_{2j})(\dot{\theta}_1+\dot{\theta}_2+\dot{\alpha}_{1e})+$$

$$\frac{2}{\eta_1^2}(\sum_{i=1}^{M}\psi'_{1i}\,\dot{\varphi}_{1i})^2(\sum_{i=1}^{M}\psi'_{1i}\varphi_{1i})\{I_{h2}+[(\frac{1}{2}\lambda_2L_2+m_p)L_1L_2+\lambda_2\sum_{i=1}^{M}\psi_{1i}\varphi_{1i}$$

$$\sum_{i=1}^{M}\varphi_{2i}K_{2i}]\cos(\theta_2+\alpha_{1e})-\lambda_2L_1\sin(\theta_2+\alpha_{1e})\sum_{i=1}^{M}\varphi_{2i}K_{2i}+\frac{1}{3}\lambda_2L_2^3+$$

$$+m_pL_2^2+I_{r2}+I_p+J_2]+\frac{2}{\eta_2^2}I_p(\sum_{i=1}^{M}\psi'_{2i}\,\dot{\varphi}_{2i})^2(\sum_{i=1}^{M}\psi'_{2i}\varphi_{2i})$$

$$m_{21}=I_{h2}+I_p+[(\frac{1}{2}\lambda_2L_2+m_p)L_1L_2+\lambda_2\sum_{i=1}^{M}\psi_{1i}\varphi_{1i}\sum_{i=1}^{M}\varphi_{2i}K_{2i}]\cos(\theta_2+\alpha_{1e})$$

$$-\lambda_2L_1\sin(\theta_2+\alpha_{1e})\sum_{i=1}^{M}\varphi_{2i}K_{2i}+(\frac{1}{3}\lambda_2L_2+m_p)L_2^2$$

$$m_{22}=I_{h2}+(\frac{1}{3}\lambda_2L_2+m_p)L_2^2+\lambda_2\sum_{i=1}^{M}\sum_{j=1}^{M}\varphi_{2i}\varphi_{2j}N_{2ij}+m_p\sum_{i=1}^{M}\psi_{2i}\varphi_{2i}\sum_{j=1}^{M}\psi_{2j}\varphi_{2j}+I_p$$

$$m_{23}=0.0$$

$$m_{24}=0.0$$

$$m_{25i}=\psi_{1i}[(\frac{1}{2}\lambda_2L_2+m_p)L_2\cos(\theta_2+\alpha_{1e})-(\lambda_2\sum_{i=1}^{M}\varphi_{2i}K_{2i}+m_p\sum_{i=1}^{M}\psi_{2i}\varphi_{2i})\sin(\theta_2+\alpha_{1e})]$$

$$+\frac{1}{\eta_1}\psi'_{1i}[I_{h2}+(\frac{1}{3}\lambda_2L_2+m_p)L_2^2+\lambda_2\sum_{j=1}^{M}\sum_{i=1}^{M}\varphi_{2j}\varphi_{2i}N_{2ji}+I_p]\quad(i=1,\ \ldots,\ M)$$

$$m_{26i}=\lambda_2M_{2i}+m_pL_2\psi_{2i}+\frac{1}{\eta_2}\psi'_{2i}I_p\qquad(i=1,\ \ldots,\ M)$$

$$B_2=K_2(\theta_4-\theta_2)+T_{f2}-[(\frac{1}{2}\lambda_2L_2+m_p)(L_1L_2\,\dot{\theta}_1+2L_2\sum_{i=1}^{M}\psi_{1i}\,\dot{\varphi}_{1i})+$$

$$\lambda_2\,\dot{\theta}_1\sum_{i=1}^{M}\psi_{1i}\varphi_{1i}\sum_{i=1}^{M}\varphi_{2i}K_{2i}]\,\dot{\theta}_1\sin(\theta_2+\alpha_{1e})-[(\lambda_2\sum_{i=1}^{M}\varphi_{2i}K_{2i}+m_p\sum_{i=1}^{M}\psi_{2i}\varphi_{2i})$$

$$(\dot{\theta}_1L_1+2\sum_{i=1}^{M}\psi_{1i}\,\dot{\varphi}_{1i})-(\frac{1}{2}\lambda_2L_2+m_p)\,\dot{\theta}_1L_2\sum_{i=1}^{M}\psi_{1i}\varphi_{1i}]\,\dot{\theta}_1\cos(\theta_2+\alpha_{1e})-$$

$$2(\lambda_2\sum_{i=1}^{M}\sum_{j=1}^{M}\varphi_{2i}\,\dot{\varphi}_{2j}N_{2ij}+m_p\sum_{i=1}^{M}\sum_{j=1}^{M}\psi_{2i}\psi_{2j}\varphi_{2i}\,\dot{\varphi}_{2j})(\dot{\theta}_1+\dot{\theta}_2+\dot{\alpha}_{1e})+$$

$$\frac{2}{\eta_1^2}(\sum_{i=1}^{M}\psi'_{1i}\,\dot{\varphi}_{1i})^2(\sum_{i=1}^{M}\psi'_{1i}\varphi_{1i})[I_{h2}+I_p+(\frac{1}{3}\lambda_2L_2+m_p)L_2^2+\lambda_2\sum_{i=1}^{M}\sum_{j=1}^{M}\psi_{2i}\psi_{2j}N_{2ij})+$$

$$\frac{2}{\eta_2^2}(\sum_{i=1}^{M}\psi'_{1i}\,\dot{\varphi}_{1i})^2(\sum_{i=1}^{M}\psi'_{1i}\varphi_{1i})I_p$$

$$m_{31}=0.0$$

$$m_{32}=0.0$$

$$m_{33}=J_1$$

$$m_{34}=0.0$$

$$m_{35i}=0.0\qquad(i=1,\ \ldots,\ M)$$

$$m_{36i} = 0.0 \qquad (i=1, \ldots, M)$$

$$B_3 = \tau_1 + T_{f2} - K_1(\theta_3 - \theta_1)$$

$$m_{41} = J_2$$

$$m_{42} = 0.0$$

$$m_{43} = 0.0$$

$$m_{44} = J_2$$

$$m_{45i} = \frac{1}{\eta_1} J_2 \psi'_{1i} \qquad (i=1, \ldots, M)$$

$$m_{46i} = 0.0 \qquad (i=1, \ldots, M)$$

$$B_4 = \tau_2 - K_2(\theta_4 - \theta_2) + \frac{2}{\eta_1^2}(\sum_{i=1}^{M} \psi'_{1i}\,\dot{\varphi}_{1i})^2(\sum_{i=1}^{M} \psi'_{1i}\varphi_{1i})J_2 + B_K$$

$$m_{51n} = \lambda_1 M_{1n} + \psi_{1n}[(m_{r2} + m_{h2} + \lambda_2 L_2 + m_p)L_1 + (\frac{1}{2}\lambda_2 L_2 + m_p)L_2\cos(\theta_2 + \alpha_{1e}) -$$
$$(\lambda_2 \sum_{i=1}^{M} \psi_{2i}K_{2i} + m_p \sum_{i=1}^{M} \psi_{2i}\varphi_{2i})\sin(\theta_2 + \alpha_{1e})] + \frac{1}{\eta_1}\psi'_{1n}\{I_{h2} + I_{r2} + I_p + J_2 +$$
$$(\frac{1}{3}\lambda_2 L_2 + m_p)L_2^2 + [(\frac{1}{2}\lambda_2 L_2 + m_p)L_1 L_2 + \lambda_2 \sum_{i=1}^{M} \psi_{1i}\varphi_{1i} \sum_{i=1}^{M} \varphi_{2i}K_{2i}]$$
$$\cos(\theta_2 + \alpha_{1e}) - \lambda_2(L_1 \sum_{i=1}^{M} \varphi_{2i}K_{2i} - \frac{1}{2}L_2^2 \sum_{i=1}^{M} \psi_{1i}\varphi_{1i})\sin(\theta_2 + \alpha_{1e}) +$$
$$\lambda_2 \sum_{i=1}^{M}\sum_{j=1}^{M} \varphi_{2i}\varphi_{2j}N_{2ij}\} \qquad (n=1, \ldots, M)$$

$$m_{52n} = \psi_{1n}[(\frac{1}{2}\lambda_2 L_2 + m_p)L_2\cos(\theta_2 + \alpha_{1e}) - (\lambda_2 \sum_{i=1}^{M} \varphi_{2i}K_{2i} + m_p \sum_{i=1}^{M} \psi_{2i}\varphi_{2i})\sin(\theta_2 + \alpha_{1e})] +$$
$$\frac{1}{\eta_1}\psi'_{1i}[I_{h2} + I_p + (\frac{1}{3}\lambda_2 L_2 + m_p)L_2^2 + m_p \sum_{i=1}^{M} \psi_{2i}\varphi_{2i} \sum_{j=1}^{M} \psi_{2j}\varphi_{2j}] (n=1, \ldots, M)$$

$$m_{53n} = 0.0 \qquad (n=1, \ldots, M)$$

$$m_{54n} = \frac{1}{\eta_1} J_2 \psi'_{1n} \qquad (n=1, \ldots, M)$$

$$m_{55ni} = \lambda_1 N_{1ni} + (m_{r2} + m_{h2} + m_p + \lambda_2 L_2)\psi_{1n}\psi_{1i} + \frac{1}{\eta_1^2}\psi'_{1n}\psi'_{1i}(I_{h2} + I_{r2} + I_p$$
$$+ J_2 + \frac{1}{3}\lambda_2 L_2^3 + m_p L_2^2 + \lambda_2 \sum_{j=1}^{M}\sum_{i=1}^{M} \psi_{2j}\psi_{2i}N_{2ji} + m_p \sum_{j=1}^{M} \psi_{2j}\varphi_{2j} \sum_{i=1}^{M} \psi_{2i}\varphi_{2i}) +$$
$$\frac{1}{\eta_1}(\psi'_{1n}\psi_{1i} + \psi_{1n}\psi'_{1i})[(\frac{1}{2}\lambda_2 L_2 + m_p)L_2\cos(\theta_2 + \alpha_{1e}) -$$
$$(\lambda_2 \sum_{j=1}^{M} \varphi_{2i}K_{2j} + m_p \sum_{j=1}^{M} \psi_{2i}\varphi_{2j})\sin(\theta_2 + \alpha_{1e})] \qquad (n=1,\ldots,M;\ i=1,\ldots,M)$$

$$m_{56ni} = (\lambda_2 K_{2i} + m_p\psi_{2i})\psi_{1n}\cos(\theta_2 + \alpha_{1e}) + \frac{1}{\eta_1}(\lambda_2 M_{2i} + m_p L_2\psi_{2i})\psi'_{1n} +$$
$$\frac{1}{\eta_1\eta_2}\psi'_{1n}\psi'_{2i}I_p \qquad (n=1,\ldots,M;\ i=1,\ldots,M)$$

$$B_{5n} = -\frac{1}{\eta_1}\psi'_{1n}[(\frac{1}{2}\lambda_2 L_2 + m_p)L_2(\dot{\theta}_1 L_1 + 2\sum_{i=1}^{M} \psi_{1i}\,\dot{\varphi}_{1i}) + \lambda_2\,\dot{\theta}_1 \sum_{i=1}^{M} \psi_{1i}\varphi_{1i}$$
$$\sum_{j=1}^{M} \varphi_{2j}K_{2j}]\,\dot{\theta}_1 \sin(\theta_2 + \alpha_{1e}) + 2(\lambda_2 \sum_{i=1}^{M} \dot{\varphi}_{2i}K_{2i} + m_p \sum_{i=1}^{M} \psi_{2i}\,\dot{\varphi}_{2i})\psi_{1n}(\dot{\theta}_1 + \dot{\theta}_2 + \dot{\alpha}_{1e})$$

$$\sin(\theta_2+\alpha_{1e})+[(\frac{1}{2}\lambda_2 L_2+m_p)L_2\sin(\theta_2+\alpha_{1e})+(\lambda_2\sum_{i=1}^{M}\varphi_{2i}K_{2i}+m_p\sum_{i=1}^{M}\psi_{2i}\varphi_{2i})$$

$$\cos(\theta_2+\alpha_{1e})]\psi_{1n}(\dot\theta_1+\dot\theta_2+\dot\alpha_{1e})^2-\frac{1}{\eta_1}\psi'_{1n}[(\lambda_2\sum_{i=1}^{M}\varphi_{2i}K_{2i}+m_p\sum_{i=1}^{M}\psi_{2i}\varphi_{2i})$$

$$(\dot\theta_1 L_1+2\sum_{i=1}^{M}\psi_{1i}\dot\varphi_{1i})-(\frac{1}{2}\lambda_2 L_2+m_p)\dot\theta_1 L_2\sum_{i=1}^{M}\psi_{1i}\varphi_{1i}]\dot\theta_1\cos(\theta_2+\alpha_{1e})$$

$$\frac{2}{\eta_1}\psi_{1n}(\lambda_2\sum_{i=1}^{M}\sum_{j=1}^{M}\varphi_{2i}\dot\varphi_{2j}N_{2ij}+m_p\sum_{i=1}^{M}\psi_{2i}\varphi_{2i}\sum_{j=1}^{M}\psi_{2j}\dot\varphi_{2i})(\dot\theta_1+\dot\theta_2+\dot\alpha_{1e})+$$

$$\frac{2}{\eta_1^2}(\sum_{i=1}^{M}\psi'_{1i}\dot\varphi_{1i})^2(\sum_{i=1}^{M}\psi'_{1i}\varphi_{1i})\{\frac{1}{\eta_1}\psi'_{1n}(I_{h2}+I_{r2}+I_p+J_2+\frac{1}{3}\lambda_2 L_2^3+m_p L_2^2+$$

$$m_p\sum_{i=1}^{M}\psi_{2i}\varphi_{2i}\sum_{j=1}^{M}\psi_{2j}\varphi_{2j}+\lambda_2\sum_{i=1}^{M}\sum_{j=1}^{M}\varphi_{2i}\varphi_{2j}N_{2ij})+\psi_{1n}[(\frac{1}{2}\lambda_2 L_2+m_p)L_2$$

$$\cos(\theta_2+\alpha_{1e})-(\lambda_2\sum_{i=1}^{M}\varphi_{2i}K_{2i}+m_p\sum_{i=1}^{M}\psi_{2i}\varphi_{2i})\sin(\theta_2+\alpha_{1e})]\}+\lambda_1\dot\theta_1^2\sum_{i=1}^{M}\varphi_{1i}N_{1ni}$$

$$+(m_{r2}+m_{h2}+\lambda_2 L_2+m_p)\psi_{1n}\dot\theta_1^2\sum_{i=1}^{M}\psi_{1i}\varphi_{1i}-E_1 I_1\sum_{i=1}^{M}\varphi_{1i}G_{1ni}+$$

$$+\frac{1}{\eta_1}\psi'_{1n}\frac{2}{\eta_2^2}(\sum_{i=1}^{M}\psi'_{1i}\dot\varphi)^2(\sum_{i=1}^{M}\psi'_{1i}\varphi)I_P-\beta_1 I_1\sum_{i=1}^{M}\dot\varphi G_{1ni} \qquad (n=1,...,M;\ i=1,...,M)$$

$$m_{61n}=(\lambda_2 K_{2n}+m_p\psi_{2n})L_1\cos(\theta_2+\alpha_{1e})+\lambda_2 K_{2n}\sin(\theta_2+\alpha_{1e})\sum_{i=1}^{M}\psi_{1i}\varphi_{1i}+\lambda_2 M_{2n}+$$

$$+m_p L_2\psi_{2n}+\frac{1}{\eta_2}I_p\psi'_{2n} \qquad (n=1,\ ...,\ M)$$

$$m_{62n}=\lambda_2 M_{2n}+m_p L_2\psi_{2n}+\frac{1}{\eta_2}I_p\psi'_{2n} \qquad (n=1,\ ...,\ M)$$

$$m_{63n}=0.0 \qquad (n=1,\ ...,\ M)$$

$$m_{64n}=0.0 \qquad (n=1,\ ...,\ M)$$

$$m_{65ni}=(\lambda_2 K_{2n}+m_p\psi_{2n})\psi_{1i}\cos(\theta_2+\alpha_{1e})+\frac{1}{\eta_1}\psi'_{1i}(\lambda_2 M_{2n}+m_p L_2\psi_{2n})+$$

$$\frac{1}{\eta_1\eta_2}I_p\psi'_{1i}\psi'_{2n} \qquad (n=1,...,M;\ i=1,...,M)$$

$$m_{66ni}=\lambda_2 N_{2ni}+m_p\psi_{2n}\psi_{2i}+\frac{1}{\eta_2^2}I_p\psi'_{2i}\psi'_{2n} \qquad (n=1,...,M;\ i=1,...,M)$$

$$B_{6n}=(\lambda_2 K_{2n}+m_p\psi_{2n})\dot\theta_1[\dot\theta_1\cos(\theta_2+\alpha_{1e})\sum_{i=1}^{M}\psi_{1i}\varphi_{1i}-(L_1\dot\theta_1+2\sum_{i=1}^{M}\psi_{1i}\dot\varphi_{1i})$$

$$\sin(\theta_2+\alpha_{1e})]+(\lambda_2\sum_{i=1}^{M}\varphi_{2i}N_{2ni}+m_p\psi_{2n}\sum_{i=1}^{M}\psi_{2i}\varphi_{2i})(\dot\theta_1+\dot\theta_2+\dot\alpha_{1e})^2$$

$$-E_2 I_2\sum_{i=1}^{M}\varphi_{2i}G_{2ni}+\frac{2}{\eta_1^2}(\sum_{i=1}^{M}\psi'_{1i}\dot\varphi_{1i})^2(\sum_{j=1}^{M}\psi'_{1j}\varphi_{1j})(\lambda_2 M_{2n}+m_p L_2\psi_{2n}+$$

$$\frac{1}{\eta_2}I_p\psi'_{2n})+\frac{2}{\eta_2^3}I_p\psi'_{2n}(\sum_{i=1}^{M}\psi'_{2i}\dot\varphi_{2i})^2(\sum_{j=1}^{M}\psi'_{2j}\varphi_{2j})-$$

$$\beta_2 I_2\sum_{i=1}^{M}\dot\varphi_{2i}G_{2ni} \qquad (n=1,...,M;\ i=1,...,M)$$

with

$$N_{1ij} = \int_0^{L_1} \psi_{1i}(u_1)\psi_{1j}(u_1)du_1$$

$$M_{1i} = \int_0^{L_1} \psi_{1i}(u_1)u_1 du_1$$

$$G_{1ij} = \int_0^{L_1} \left(\frac{\partial^2 \psi_{1i}(u_1)}{\partial u_1^2}\right)\left(\frac{\partial^2 \psi_{1j}(u_1)}{\partial u_1^2}\right)du_1$$

$$N_{2ij} = \int_0^{L_2} \psi_{2i}(u_2)\psi_{2j}(u_2)du_2$$

$$\eta_1 = 1 + (\sum_{i=1}^{M} \psi_{1i}\varphi_{1i})^2$$

$$M_{2i} = \int_0^{L_2} \psi_{2i}(u_2)u_2 du_2$$

$$G_{2ij} = \int_0^{L_2} \left(\frac{\partial^2 \psi_{2i}(u_2)}{\partial u_2^2}\right)\left(\frac{\partial^2 \psi_{2j}(u_2)}{\partial u_2^2}\right)du_2$$

$$K_{2i} = \int_0^{L_2} \psi_{2i}(u_2)du_2$$

$$\eta_2 = 1 + (\sum_{i=1}^{M} \psi_{2i}\varphi_{2i})^2$$

$$B_K = \frac{I_{m1}I_{m2}}{d_b(I_{m1}+I_{m2})}\dot{\theta}_4^3\zeta(4-5\zeta|\dot{\theta}_4|)$$

SENSORY SYSTEM

B1. Strain Gages

Strain gages are simple but effective electrical sensors. They are used here to detect the bending deflections of flexible arms. At each selected point on the arms, a pair of strain gages are used and one is mounted on each side of the arm to eliminate thermal effects. A half bridge circuit is applied and two precision metal film resistors with tolerance of 1% and a potentiometer are utilized for circuit balancing. The output signal of the circuit is enhanced by an AC amplifier with the gain of 1000. Its high frequency noise is attenuated by a low-pass analogue filter with the cut-off frequency of 20 Hz, which is cascaded after the amplifier, as shown in Figure B.1.

Ten strain gages are used for each arm. The locations of the selected measurement points are determined by the strain distribution analysis and the points with a local maximum strain value are selected. Assuming that the actual bending shape of the arm is described by the following polynomial:

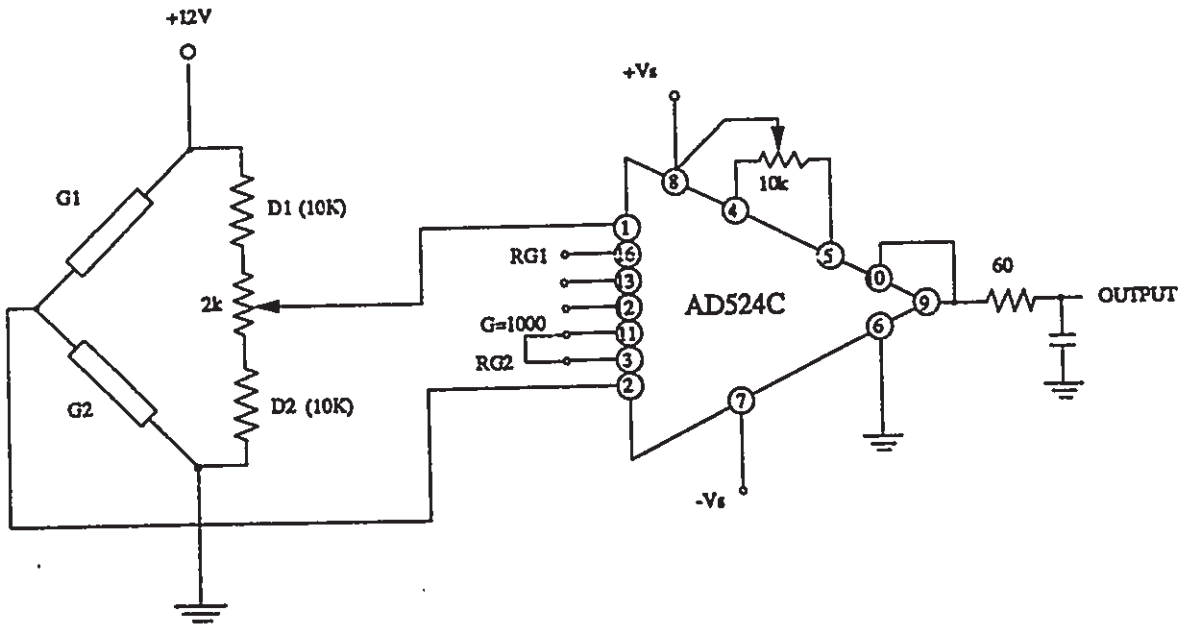

Figure B.1 Strain Gage Circuit

$$w(u,t) = a_1(t)u^2 + a_2(t)u^3 + a_3(t)u^4 + a_4(t)u^5 + a_5(t)u^6, \qquad \text{(B.1)}$$

the strain equation can be given as

$$\delta\frac{\partial^2 w}{\partial u^2} = \delta(2a_1 + 6a_2u + 12a_3u^2 + 20a_4u^3 + 30a_5u^4) \qquad \text{(B.2)}$$

where δ is half of the beam's thickness and a_1, a_2, a_3, and a_4 are equation coefficients, which need to be determined. At each sampling instance, the computer reads in the bending strains of the arm along five pre-selected locations and solves for the equation coefficients a_i(i=1, ..., 5). Then equation (B.1) is used to determine the bending deflection. The algorithm is verified by comparing the strain gage measurement results with the results of a displacement sensor. The displacement sensor used here consists of a sliding central rod and a fixed outer cylinder. The central rod slides freely within the fixed cylinder and the whole unit acts as an adjustable inductor. Through measuring the inductance change caused

by the relative movement of the rod with respect to the cylinder, the move distance is detected. The measurement data are shown in Figure B.2. It is clear that the strain gage sensing system is very accurate. The offset from zero at the end of oscillation is caused by the non-zero friction between the central rod and the outer cylinder of the displacement sensor.

B2. Optical Encoders

An optical encoder is an electrical unit with an output consisting of a sequence of 5V amplitude pulses. Each pulse represents one resolution of the encoder. The shaft rotating angle can be determined by counting the number of generated pulses. The continuous counting process is performed by an encoder counting circuit, which is connected with the computer. The counting process is monitored by a written computer program.

The circuit consists of a 8 bit up/down counter, a tri-state octal D-type transparent latch, a decoder, a dual retriggerable monostable multivibrator, a AND gate, and two Schmitt triggers, as shown in Figure B.3. Before entering the counter, the signals from the encoders are filtered by the triggers to make sure that they have a standard TTL level and are jitter-free. The multivibrator is used to reset and trigger the counter. At the sampling instance, the latch freezes the output of the counter and lets the computer read in the latched state. There are altogether five 8 bit counters in the circuit, one for each optical encoder except encoder 3, which needs two 8-bit counters. The computer reads in one counter at a time. The decoder is used to control the reading order.

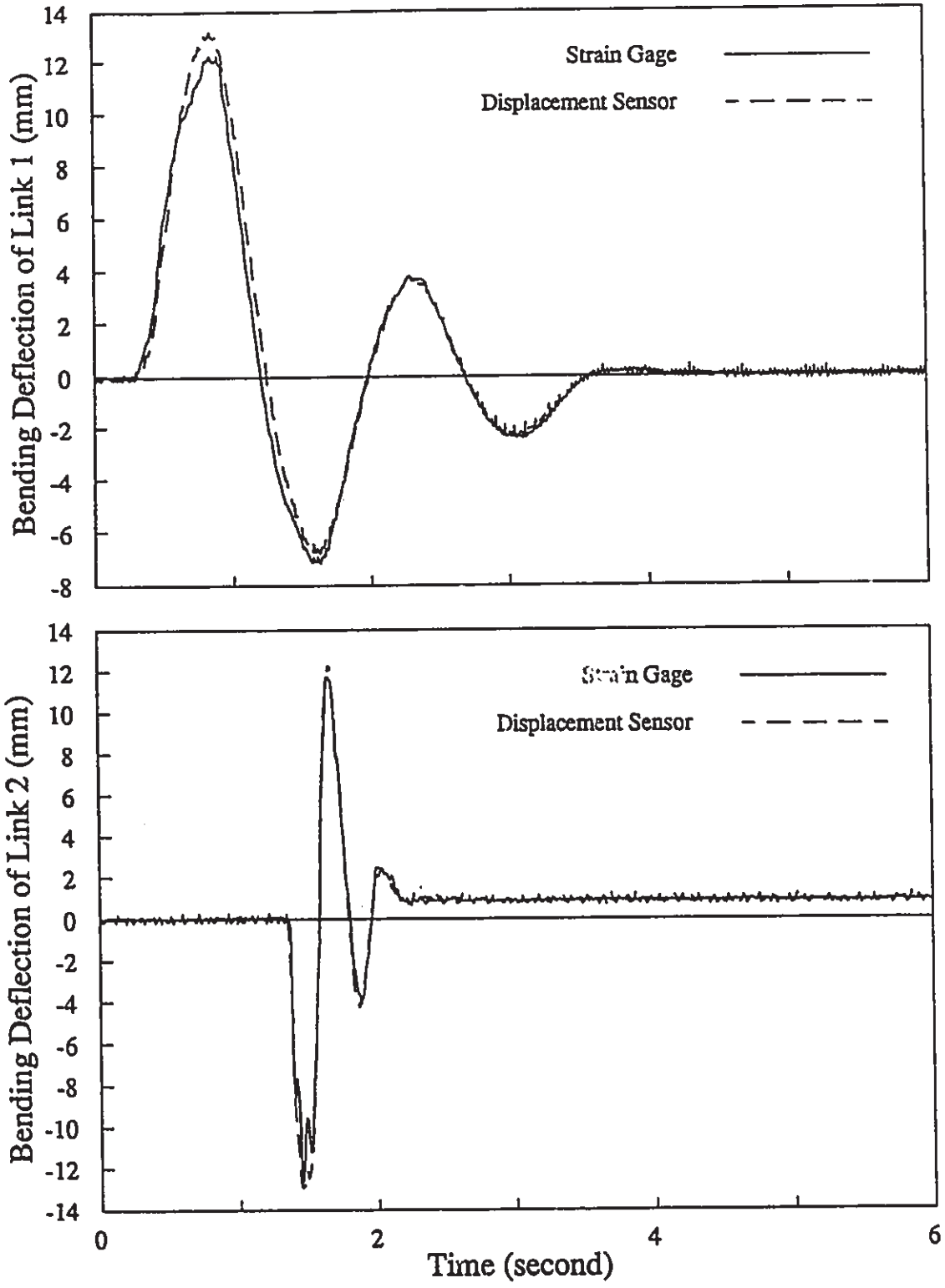

Figure B.2 Strain Gage Calibration

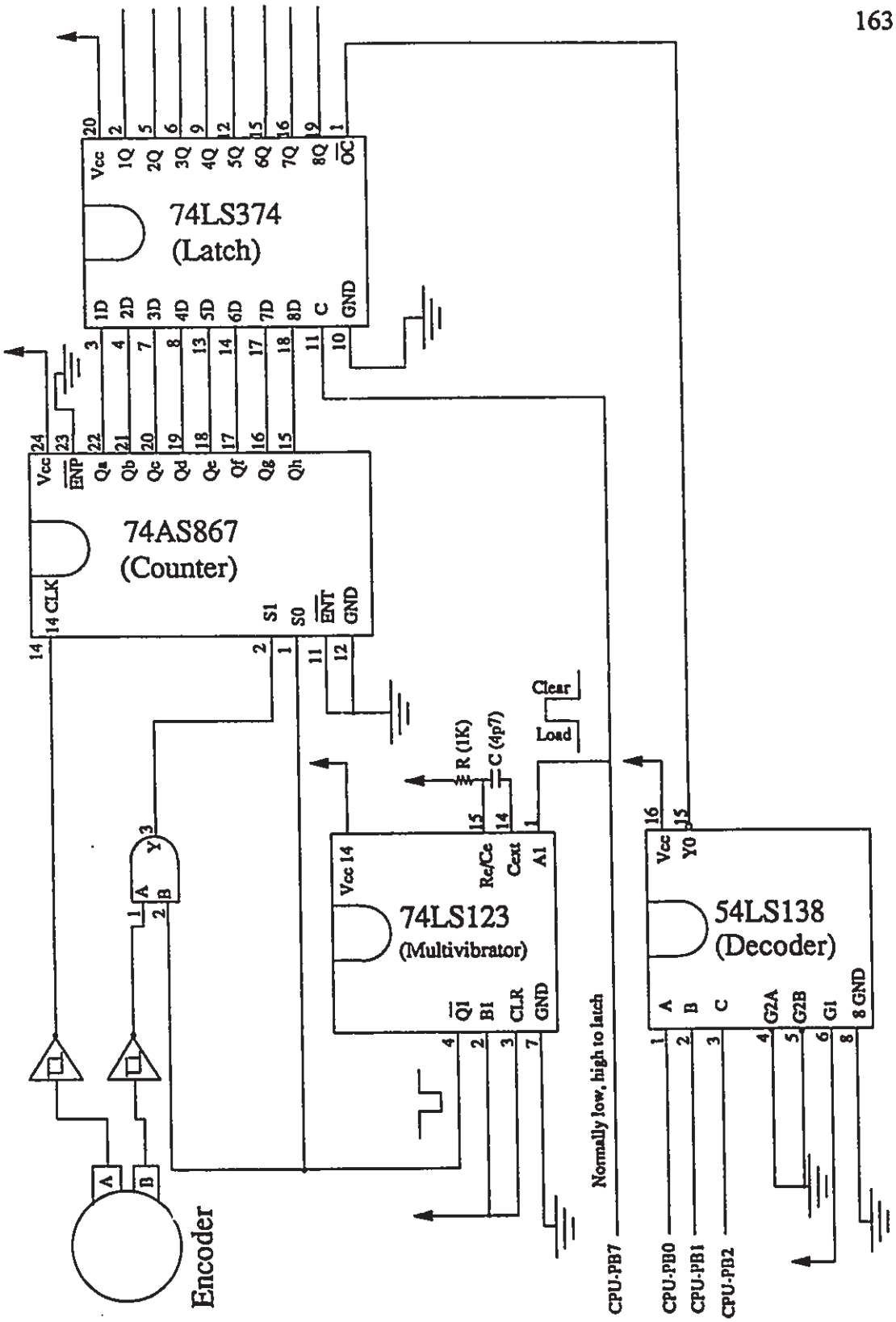

Figure B.3 Encoder Counting Circuit

The counter's bit number is selected to satisfy the need of the system's performance. Each optical encoder has a resolution of 2540. With the assumption that the maximum joint speed is 60 rpm, the output pulse rate of an encoder will be 2540 per second. By considering the computer sampling frequency as 100 Hz, the number of pulses generated by a encoder during each sampling interval is less than 25. With some extra bits for flexibility, the 8 bit counter is considered to be satisfactory. The encoder connected to the shaft of the second DC motor is built-in. Its resolution is 500 pulses per revolution. Including the harmonic driver ratio of 48.96:1, the number of pulses during each sampling period is less than 250, which requires a 9 bit counter. Instead, two 8 bit counters are cascaded.

The counting circuit is controlled by the computer through the parallel port and the data communication is achieved by the digital I/O channels of a Data Translation I/O board. Pin 7 of the computer's parallel port is used to control the counter and the latch, and pins 0, 1, 2 are connected to the decoder to monitor the sampling order.

B3. Limit Switches

The safety mechanism here is a set of limit switches, which turns the motor's power off once the manipulator's motion exceeds the pre-defined range. The circuit consists of a relay, a reset switch, four limit switches, and one emergency switch, as shown in Figure B.4. The relay is used to ensure that once a limit switch is hit or the emergency switch is turned off, the power amplifiers of both motors will be disabled until the start button is pressed. The unit uses 24 VDC power.

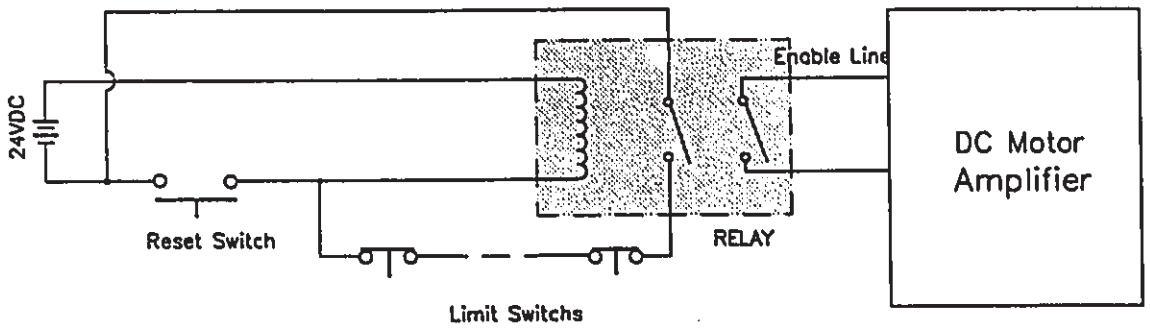

Figure B.4 Limit Switch Circuit

LINEARIZED DYNAMIC EQUATIONS

The linearized version of the manipulator's dynamic equations is listed here. The equations are presented in state space form, which is shown on the next page. I represents the identity matrix of dimension $(2M+4)$x$(2M+4)$. M', A', A'', and $\tilde{A}$ are the matrices with same dimensions. The integer M is the highest vibration mode of the link considered in the model. The matrix M' here.is exactly same as that defined in Appendix A except that the equation variables of M' in Appendix A are replaced by the nominal trajectory variables here. Therefore, the listing of M' is omitted here.

$$
\begin{bmatrix} I & 0 \\ 0 & M'(\bar{x}) \end{bmatrix}
\begin{bmatrix} \Delta x_1 \\ \Delta x_2 \\ \Delta x_3 \\ \Delta x_4 \\ \Delta x_{21} \\ \Delta x_{22} \\ \Delta x_{23} \\ \Delta x_{24} \\ \Delta x_{31} \\ \Delta x_{32} \\ \Delta x_{33} \\ \Delta x_{34} \end{bmatrix}
=
\begin{bmatrix} I & 0 \\ 0 & A'(\bar{x})-\bar{A}(\bar{x}) \end{bmatrix}
\begin{bmatrix} \Delta x_1 \\ \Delta x_2 \\ \Delta x_3 \\ \Delta x_4 \\ \Delta x_{21} \\ \Delta x_{22} \\ \Delta x_{23} \\ \Delta x_{24} \\ \Delta x_{31} \\ \Delta x_{32} \\ \Delta x_{33} \\ \Delta x_{34} \end{bmatrix}
+
\begin{bmatrix} 0 & \cdots & 0 \\ 0 & \cdots & 0 \end{bmatrix}
\begin{bmatrix} \Delta x_1 \\ \Delta x_2 \\ \Delta x_3 \\ \Delta x_4 \\ \Delta x_{21} \\ \Delta x_{22} \\ \Delta x_{23} \\ \Delta x_{24} \\ \Delta x_{31} \\ \Delta x_{32} \\ \Delta x_{33} \\ \Delta x_{34} \end{bmatrix}
\begin{bmatrix} I & 0 \\ 0 & A''(\bar{x}) \end{bmatrix}
\begin{bmatrix} \Delta x_1 \\ \Delta x_2 \\ \Delta x_3 \\ \Delta x_4 \\ \Delta x_{21} \\ \Delta x_{22} \\ \Delta x_{23} \\ \Delta x_{24} \\ \Delta x_{31} \\ \Delta x_{32} \\ \Delta x_{33} \\ \Delta x_{34} \end{bmatrix}
+
\begin{bmatrix} 0 & \cdots & 0 \\ 0 & \cdots & 0 \end{bmatrix}
[a_1 \quad a_2]^T
$$

Elements for Matrix A_1 :

$$a'_{11} = \left.\frac{\partial B_1}{\partial \theta_1}\right|_{\bar{x}} = -k_1$$

$$a'_{12} = \left.\frac{\partial B_1}{\partial \theta_2}\right|_{\bar{x}} = \{[(\frac{1}{2}\lambda_2 L_2 + m_p)L_1 L_2 + \lambda_2 \sum_{i=1}^{M} \psi_{1i}\bar{\varphi}_{1i} \sum_{i=1}^{M} \bar{\varphi}_{2i}K_{2i})]\cos(\bar{\theta}_2 + \bar{\alpha}_{1e}) -$$
$$[(\lambda_2 \sum_{i=1}^{M} \bar{\varphi}_{2i}K_{2i} + m_p \sum_{i=1}^{M} \psi_{2i}\bar{\varphi}_{2i})L_1 - (\frac{1}{2}\lambda_2 L_2 + m_p)L_2 \sum_{i=1}^{M} \psi_{1i}\bar{\varphi}_{1i}]\sin(\bar{\theta}_2 + \bar{\alpha}_{1e})\}$$
$$(2\dot{\bar{\theta}}_1 + \dot{\bar{\theta}}_2 + \dot{\bar{\alpha}}_{1e})(\dot{\bar{\theta}}_2 + \dot{\bar{\alpha}}_{1e}) + 2(\lambda_2 \sum_{i=1}^{M} \dot{\bar{\varphi}}_{2i}K_{2i} + m_p \sum_{i=1}^{M} \psi_{2i}\dot{\bar{\varphi}}_{2i})(\dot{\bar{\theta}}_1 + \dot{\bar{\theta}}_2 + \dot{\bar{\alpha}}_{1e})$$
$$[L_1\cos(\bar{\theta}_2 + \bar{\alpha}_{1e}) + \sum_{i=1}^{M} \psi_{1i}\bar{\varphi}_{1i}\sin(\bar{\theta}_2 + \bar{\alpha}_{1e})] - \dot{\bar{\theta}}_1 \sum_{i=1}^{M} \psi_{1i}\dot{\bar{\varphi}}_{1i}[(\lambda_2 L_2 + 2m_p)$$
$$L_2\cos(\bar{\theta}_2 + \bar{\alpha}_{1e}) - 2(\lambda_2 \sum_{i=1}^{M} \bar{\varphi}_{2i}K_{2i} + m_p \sum_{i=1}^{M} \psi_{2i}\bar{\varphi}_{2i})\sin(\bar{\theta}_2 + \bar{\alpha}_{1e})] - \frac{2}{\eta_1^2}(\sum_{i=1}^{M} \psi'_{1i}\dot{\bar{\varphi}}_{1i})^2$$
$$(\sum_{i=1}^{M} \psi'_{1i}\bar{\varphi}_{1i})\{(\frac{1}{2}\lambda_2 L_2 + m_p)L_1 L_2\sin(\bar{\theta}_2 + \bar{\alpha}_{1e}) - \lambda_2[L_1\cos(\bar{\theta}_2 + \bar{\alpha}_{1e})$$
$$+\sin(\bar{\theta}_2 + \bar{\alpha}_{1e}) \sum_{i=1}^{M} \psi_{1i}\bar{\varphi}_{1i}] \sum_{i=1}^{M} \bar{\varphi}_{2i}K_{2i}\}$$

$$a'_{13} = \left.\frac{\partial B_1}{\partial \theta_3}\right|_{\bar{x}} = k_1$$

$$a'_{14} = \left.\frac{\partial B_1}{\partial \theta_4}\right|_{\bar{x}} = 0.0$$

$$a'_{15i} = \left.\frac{\partial B_1}{\partial \varphi_{1i}}\right|_{\bar{x}} = -2\lambda_1 \dot{\bar{\theta}}_1 \sum_{j=1}^{M} \dot{\bar{\varphi}}_{1j}N_{1ij} - 2(m_{r2} + m_{h2} + m_p + \lambda_2 L_2)\dot{\bar{\theta}}_1 \psi_{1i} \sum_{j=1}^{M} \psi_{1j}\dot{\bar{\varphi}}_{1j} +$$
$$\lambda_2 \psi_{1i} \sum_{j=1}^{M} \bar{\varphi}_{2j}K_{2j}(2\dot{\bar{\theta}}_1 + \dot{\bar{\theta}}_2 + \dot{\bar{\alpha}}_{1e})(\dot{\bar{\theta}}_2 + \dot{\bar{\alpha}}_{1e})\sin(\bar{\theta}_2 + \bar{\alpha}_{1e}) + [(\frac{1}{2}\lambda L_2 + m_p)L_1 L_2 +$$
$$\lambda_2 \sum_{j=1}^{M} \psi_{1j}\bar{\varphi}_{1j} \sum_{j=1}^{M} \bar{\varphi}_{2j}K_{2j}][(2(\dot{\bar{\theta}}_1 + \dot{\bar{\theta}}_2 + \dot{\bar{\alpha}}_{1e})\sin(\bar{\theta}_2 + \bar{\alpha}_{1e}) \left.\frac{\partial \dot{\alpha}_{1e}}{\partial \varphi_{1i}}\right|_{\bar{x}} + (2\dot{\bar{\theta}}_1 + \dot{\bar{\theta}}_2 + \dot{\bar{\alpha}}_{1e})$$
$$(\dot{\bar{\theta}}_2 + \dot{\bar{\alpha}}_{1e})\cos(\bar{\theta}_2 + \bar{\alpha}_{1e}) \left.\frac{\partial \alpha_{1e}}{\partial \varphi_{1i}}\right|_{\bar{x}}] + 2(\lambda_2 \sum_{j=1}^{M} \dot{\bar{\varphi}}_{2j}K_{2j} + m_p \sum_{j=1}^{M} \psi_{2j}\dot{\bar{\varphi}}_{2j})\{L_1[\sin(\bar{\theta}_2 + \bar{\alpha}_{1e})$$
$$\left.\frac{\partial \dot{\alpha}}{\partial \varphi_{1i}}\right|_{\bar{x}} + (\dot{\bar{\theta}}_1 + \dot{\bar{\theta}}_2 + \dot{\bar{\alpha}}_{1e})\cos(\bar{\theta}_2 + \bar{\alpha}_{1e}) \left.\frac{\partial \alpha}{\partial \varphi_{1i}}\right|_{\bar{x}}] - [\varphi_{1i}(\dot{\bar{\theta}}_1 + \dot{\bar{\theta}}_2 + \dot{\bar{\alpha}}_{1e})\cos(\bar{\theta}_2 + \bar{\alpha}_{1e}) +$$
$$\sum_{j=1}^{M} \psi_{1j}\bar{\varphi}_{1j}\cos(\bar{\theta}_2 + \bar{\alpha}_{1e}) \left.\frac{\partial \dot{\alpha}}{\partial \varphi_{1i}}\right|_{\bar{x}} - \sum_{j=1}^{M} \psi_{1j}\bar{\varphi}_{1j}(\dot{\bar{\theta}}_1 + \dot{\bar{\theta}}_2 + \dot{\bar{\alpha}}_{1e})\sin(\bar{\theta}_2 + \bar{\alpha}_{1e}) \left.\frac{\partial \alpha}{\partial \varphi_{1i}}\right|_{\bar{x}}]$$
$$-(\frac{1}{2}\lambda_2 L_2 + m_p)L_2\cos(\bar{\theta}_2 + \bar{\alpha}_{1e})[2\dot{\bar{\theta}}_1 \sum_{j=1}^{M} \psi_{1j}\dot{\bar{\varphi}}_{1j} \left.\frac{\partial \dot{\alpha}_{1e}}{\partial \varphi_{1i}}\right|_{\bar{x}} + \psi_{1i}(2\dot{\bar{\theta}}_1 + \dot{\bar{\theta}}_2 + \dot{\bar{\alpha}}_{1e})$$
$$(\dot{\bar{\theta}}_2 + \dot{\bar{\alpha}}_{1e})] + [\lambda_2 L_1 \sum_{j=1}^{M} \bar{\varphi}_{2j}K_{2j} + m_p L_1 \sum_{j=1}^{M} \psi_{2j}\bar{\varphi}_{2j} - (\frac{1}{2}\lambda_2 L_2 + m_p)L_2 \sum_{j=1}^{M} \psi_{1j}\bar{\varphi}_{1j}]$$
$$[(2(\dot{\bar{\theta}}_1 + \dot{\bar{\theta}}_2 + \dot{\bar{\alpha}}_{1e})\cos(\bar{\theta}_2 + \bar{\alpha}_{1e}) \left.\frac{\partial \dot{\alpha}_{1e}}{\partial \varphi_{1i}}\right|_{\bar{x}} - (2\dot{\bar{\theta}}_1 + \dot{\bar{\theta}}_2 + \dot{\bar{\alpha}}_{1e})(\dot{\bar{\theta}}_2 + \dot{\bar{\alpha}}_{1e})$$

$$\sin(\bar{\theta}_2+\bar{\alpha}_{1e})\left.\frac{\partial\alpha_{1e}}{\partial\varphi_{1i}}\right|_{\bar{x}}]+2(\lambda_2\sum_{j=1}^{M}\bar{\varphi}_{2j}K_{2j}+m_p\sum_{j=1}^{M}\psi_{2j}\bar{\varphi}_{2j})\,\dot{\bar{\theta}}_1\sum_{j=1}^{M}\psi_{1j}\,\dot{\bar{\varphi}}_{1j}$$

$$\sin(\bar{\theta}_2+\bar{\alpha}_{1e})\left.\frac{\partial\alpha_{1e}}{\partial\varphi_{1i}}\right|_{\bar{x}}-2(\sum_{j=1}^{M}\sum_{l=1}^{M}\bar{\varphi}_{2j}\,\dot{\bar{\varphi}}_{2l}\,N_{2jl}+m_p\sum_{j=1}^{M}\psi_{2j}\bar{\varphi}_{2j}\sum_{l=1}^{M}\psi_{2l}\,\dot{\bar{\varphi}}_{2l})\left.\frac{\partial\,\dot{\alpha}_{1e}}{\partial\varphi_{1i}}\right|_{\bar{x}}$$

$$+[\frac{\partial}{\partial\varphi_{1i}}(\frac{2}{\eta_1^2})(\sum_{j=1}^{M}\psi'_{1j}\bar{\varphi}_{1j})+\frac{2}{\eta_1^2}\psi'_{1i}](\sum_{j=1}^{M}\psi'_{1j}\,\dot{\bar{\varphi}}_{1j})^2\{I_{h2}+(\frac{1}{2}\lambda_2L_2+m_p)L_1L_2$$

$$\cos(\bar{\theta}_2+\bar{\alpha}_{1e})-\lambda_2\sum_{j=1}^{M}\bar{\varphi}_{2j}K_{2j}[L_1\sin(\bar{\theta}_2+\bar{\alpha}_{1e})-\cos(\bar{\theta}_2+\bar{\alpha}_{1e})\sum_{j=1}^{M}\psi_{1j}\bar{\varphi}_{1j}]$$

$$+\frac{1}{3}\lambda_2L_2^3+m_pL_2^2+I_{r2}+I_p+J_2\}-\frac{2}{\eta_1^2}(\sum_{j=1}^{M}\psi'_{1j}\,\dot{\bar{\varphi}}_{1j})^2(\sum_{j=1}^{M}\psi'_{1j}\bar{\varphi}_{1j})$$

$$\Big\{\{(\frac{1}{2}\lambda_2L_2+m_p)L_1L_2\,\sin(\bar{\theta}_2+\bar{\alpha}_{1e})+\lambda_2\sum_{j=1}^{M}\bar{\varphi}_{2j}K_{2j}[L_1\cos(\bar{\theta}_2+\bar{\alpha}_{1e})$$

$$+\sin(\bar{\theta}_2+\bar{\alpha}_{1e})\sum_{j=1}^{M}\psi'_{1j}\bar{\varphi}_{1j}]\}\left.\frac{\partial\alpha_{1e}}{\partial\varphi_{1i}}\right|_{\bar{x}}-\lambda_2\cos(\bar{\theta}_2+\bar{\alpha}_{1e})\psi_{1i}\sum_{j=1}^{M}\bar{\varphi}_{2j}K_{2j}\Big\}$$

$$(i=1,\ \ldots,\ M)$$

$$a'_{16i}=\left.\frac{\partial B_1}{\partial\varphi_{2i}}\right|_{\bar{x}}=(2\,\dot{\bar{\theta}}_1+\dot{\bar{\theta}}_2+\dot{\bar{\alpha}}_{1e})(\dot{\bar{\theta}}_2+\dot{\bar{\alpha}}_{1e})[\lambda_2K_{2i}\sin(\bar{\theta}_2+\bar{\alpha}_{1e})\sum_{j=1}^{M}\psi_{1j}\bar{\varphi}_{1j}+$$

$$(\lambda_2K_{2i}+m_p\psi_{2i})L_1\cos(\bar{\theta}_2+\bar{\alpha}_{1e})]-2(\lambda_2K_{2i}+m_p\psi_{2i})\,\dot{\bar{\theta}}_1\cos(\bar{\theta}_2+\bar{\alpha}_{1e})$$

$$\sum_{j=1}^{M}\psi_{1j}\,\dot{\bar{\varphi}}_{1j}-2(\lambda_2\sum_{j=1}^{M}\dot{\bar{\varphi}}_{2j}N_{2ij}+m_p\psi_{2i}\sum_{j=1}^{M}\psi_{2j}\,\dot{\bar{\varphi}}_{2j})(\dot{\bar{\theta}}_1+\dot{\bar{\theta}}_2+\dot{\bar{\alpha}}_{1e})$$

$$-\frac{2}{\eta_1^2}(\sum_{j=1}^{M}\psi'_{1j}\,\dot{\bar{\varphi}}_{1j})^2(\sum_{j=1}^{M}\psi'_{1j}\bar{\varphi}_{1j})\lambda_2K_{2i}[L_1\sin(\bar{\theta}_2+\bar{\alpha}_{1e})-\cos(\bar{\theta}_2+\bar{\alpha}_{1e})\sum_{j=1}^{M}\psi_{1j}\bar{\varphi}_{1j}]$$

$$+[\left.\frac{\partial}{\partial\varphi_{2i}}(\frac{2}{\eta_2^2})\right|_{\bar{x}}(\sum_{j=1}^{M}\psi'_{2j}\bar{\varphi}_{2j})+\frac{2}{\eta_2^2}\psi'_{2i}](\sum_{j=1}^{M}\psi'_{2j}\,\dot{\bar{\varphi}}_{2j})^2I_p\qquad(i=1,\ \ldots,\ M)$$

$$a'_{21}=\left.\frac{\partial B_2}{\partial\theta_1}\right|_{\bar{x}}=0.0$$

$$a'_{22}=\left.\frac{\partial B_2}{\partial\theta_2}\right|_{\bar{x}}=-k_2-[(\frac{1}{2}\lambda_2L_2+m_p)L_2(L_1\,\dot{\bar{\theta}}_1+2\sum_{i=1}^{M}\psi_{1i}\,\dot{\bar{\varphi}}_{1i})+\lambda_2\,\dot{\bar{\theta}}_1$$

$$\sum_{i=1}^{M}\psi_{1i}\bar{\varphi}_{1i}\sum_{i=1}^{M}\bar{\varphi}_{2i}K_{2i}]\,\dot{\bar{\theta}}_1\cos(\bar{\theta}_2+\bar{\alpha}_{1e})+[(\lambda_2\sum_{i=1}^{M}\bar{\varphi}_{2i}K_{2i}+m_p\sum_{i=1}^{M}\psi_{2i}\bar{\varphi}_{2i})(L_1\,\dot{\bar{\theta}}_1+$$

$$2\sum_{i=1}^{M}\psi_{1i}\,\dot{\bar{\varphi}}_{1i})-(\frac{1}{2}\lambda_2L_2+m_p)L_2\,\dot{\bar{\theta}}_1\sum_{i=1}^{M}\psi_{1i}\bar{\varphi}_{1i}]\,\dot{\bar{\theta}}_1\sin(\bar{\theta}_2+\bar{\alpha}_{1e})$$

$$a'_{23}=\left.\frac{\partial B_2}{\partial\theta_3}\right|_{\bar{x}}=0.0$$

$$a'_{24}=\left.\frac{\partial B_2}{\partial\theta_4}\right|_{\bar{x}}=k_2$$

$$a'_{25i}=\left.\frac{\partial B_2}{\partial\varphi_{1i}}\right|_{\bar{x}}=-\lambda_2\psi_{1i}\,\dot{\bar{\theta}}_1^2\sin(\bar{\theta}_2+\bar{\alpha}_{1e})\sum_{j=1}^{M}\bar{\varphi}_{2j}K_{2j}-\{[(\frac{1}{2}\lambda_2L_2+m_p)L_2(L_1\,\dot{\bar{\theta}}_1$$

$$+2\sum_{j=1}^{M}\psi_{1j}\,\dot{\bar{\varphi}}_{1j})+\lambda_2\,\dot{\bar{\theta}}_1\sum_{j=1}^{M}\psi_{1j}\bar{\varphi}_{1j}\sum_{j=1}^{M}\bar{\varphi}_{2j}K_{2j}]\left.\frac{\partial\alpha_{1e}}{\partial\varphi_{1i}}\right|_{\bar{x}}+(\frac{1}{2}\lambda_2L_2+m_p)L_2\,\dot{\bar{\theta}}_1\,\psi_{1i}\}$$

$$\dot{\bar{\theta}}_1 \cos(\bar{\theta}_2+\bar{\alpha}_{1e})+[(\lambda_2\sum_{j=1}^{M}\bar{\varphi}_{2j}K_{2j}+m_p\sum_{j=1}^{M}\psi_{2j}\bar{\varphi}_{2j})(L_1\dot{\bar{\theta}}_1+2\sum_{j=1}^{M}\psi_{1j}\dot{\bar{\varphi}}_{1j})$$

$$-(\frac{1}{2}\lambda_2L_2+m_p)L_2\dot{\bar{\theta}}_1\sum_{j=1}^{M}\psi_{1j}\bar{\varphi}_{1j}]\dot{\bar{\theta}}_1\sin(\bar{\theta}_2+\bar{\alpha}_{1e})\left.\frac{\partial\alpha_{1e}}{\partial\varphi_{1i}}\right|_{\bar{x}}-2(\lambda_2\sum_{j=1}^{M}\sum_{k=1}^{M}\bar{\varphi}_{2j}\dot{\bar{\varphi}}_{2k}N_{2jk}$$

$$+m_p\sum_{j=1}^{M}\psi_{2j}\bar{\varphi}_{2j}\sum_{j=1}^{M}\psi_{2j}\dot{\bar{\varphi}}_{2j})\left.\frac{\partial\dot{\alpha}_{1e}}{\partial\varphi_{1i}}\right|_{\bar{x}}+[\left.\frac{\partial}{\partial\varphi_{1i}}(\frac{2}{\eta_1^2})\right|_{\bar{x}}(\sum_{j=1}^{M}\psi'_{1j}\bar{\varphi}_{1j})+\frac{2}{\eta_1^2}\psi'_{1i}]$$

$$(\sum_{j=1}^{M}\psi'_{1j}\dot{\bar{\varphi}}_{1j})^2(I_{h2}+I_p+\frac{1}{3}\lambda_2L_2^3+m_pL_2^2+\lambda_2\sum_{j=1}^{M}\sum_{k=1}^{M}\bar{\varphi}_{2j}\dot{\bar{\varphi}}_{2k}N_{2jk})\quad(i=1,\ldots,M)$$

$$a'_{26i}=\left.\frac{\partial B_2}{\partial\varphi_{2i}}\right|_{\bar{x}}=-\lambda_2K_{2i}\dot{\bar{\theta}}_1^2\sin(\bar{\theta}_2+\bar{\alpha}_{1e})\sum_{j=1}^{M}\psi_{1j}\bar{\varphi}_{1j}-(\lambda_2K_{2i}+m_p\psi_{2i})(L_1\dot{\bar{\theta}}_1+$$

$$2\sum_{j=1}^{M}\psi_{1j}\dot{\bar{\varphi}}_{1j})\dot{\bar{\theta}}_1\cos(\bar{\theta}_2+\bar{\alpha}_{1e})-2(\lambda_2\sum_{j=1}^{M}\dot{\bar{\varphi}}_{2j}N_{2ij}+m_p\psi_{2i}\sum_{j=1}^{M}\psi_{2j}\dot{\bar{\varphi}}_{2j})$$

$$(\dot{\bar{\theta}}_1+\dot{\bar{\theta}}_2+\dot{\bar{\alpha}}_{1e})+\frac{4}{\eta_1^2}(\sum_{j=1}^{M}\psi'_{1j}\dot{\bar{\varphi}}_{1j})^2(\sum_{j=1}^{M}\psi'_{1j}\bar{\varphi}_{1j})\lambda_2(\sum_{j=1}^{M}\bar{\varphi}_{2j}N_{2ij})+[\left.\frac{\partial}{\partial\varphi_{2i}}(\frac{2}{\eta_2^2})\right|_{\bar{x}}$$

$$\sum_{j=1}^{M}\psi'_{2j}\bar{\varphi}_{2j}+\frac{2}{\eta_2^2}\psi_{2i}](\sum_{j=1}^{M}\psi'_{2j}\dot{\bar{\varphi}}_{2j})^2I_p\qquad(i=1,\ldots,M)$$

$$a'_{31}=\left.\frac{\partial B_3}{\partial\theta_1}\right|_{\bar{x}}=k_1$$

$$a'_{32}=\left.\frac{\partial B_3}{\partial\theta_2}\right|_{\bar{x}}=0.0$$

$$a'_{33}=\left.\frac{\partial B_3}{\partial\theta_3}\right|_{\bar{x}}=-k_1$$

$$a'_{34}=\left.\frac{\partial B_3}{\partial\theta_4}\right|_{\bar{x}}=0.0$$

$$a'_{35i}=\left.\frac{\partial B_3}{\partial\varphi_{1i}}\right|_{\bar{x}}=0.0\qquad(i=1,\ldots,M)$$

$$a'_{36i}=\left.\frac{\partial B_3}{\partial\varphi_{2i}}\right|_{\bar{x}}=0.0\qquad(i=1,\ldots,M)$$

$$a'_{41}=\left.\frac{\partial B_4}{\partial\theta_1}\right|_{\bar{x}}=0.0$$

$$a'_{42}=\left.\frac{\partial B_4}{\partial\theta_2}\right|_{\bar{x}}=k_2$$

$$a'_{43}=\left.\frac{\partial B_4}{\partial\theta_3}\right|_{\bar{x}}=0.0$$

$$a'_{44}=\left.\frac{\partial B_4}{\partial\theta_4}\right|_{\bar{x}}=-k_2$$

$$a'_{45i}=\left.\frac{\partial B_4}{\partial\varphi_{1i}}\right|_{\bar{x}}=J_2[\left.\frac{\partial}{\partial\varphi_{1i}}(\frac{2}{\eta_1^2})\right|_{\bar{x}}(\sum_{j=1}^{M}\psi'_{1j}\bar{\varphi}_{1j})+\frac{2}{\eta_1^2}\psi'_{1i}](\sum_{j=1}^{M}\psi'_{1j}\dot{\bar{\varphi}}_{1j})^2\quad(i=1,\ldots,M)$$

$$a'_{46i}=\left.\frac{\partial B_4}{\partial\varphi_{2i}}\right|_{\bar{x}}=0.0\qquad(i=1,\ldots,M)$$

$$a'_{51n} = \left.\frac{\partial B_{5n}}{\partial \theta_1}\right|_{\bar{x}} = 0.0 \qquad (n=1, \ldots, M)$$

$$a'_{52n} = \left.\frac{\partial B_{5n}}{\partial \theta_2}\right|_{\bar{x}} = -\frac{1}{\eta_1}\psi'_{1n}\ddot{\theta}_1\{[(\frac{1}{2}\lambda_2 L_2 + m_p)(L_1 L_2\ddot{\theta}_1 + 2L_2\sum_{i=1}^{M}\psi_{1i}\ddot{\varphi}_{1i}) +$$
$$\lambda_2\ddot{\theta}_1\sum_{i=1}^{M}\psi_{1i}\bar{\varphi}_{1i}\sum_{i=1}^{M}\bar{\varphi}_{2i}K_{2i}]\ddot{\theta}\cos(\bar{\theta}_2+\bar{\alpha}_{1e}) + [(\lambda_2\sum_{i=1}^{M}\bar{\varphi}_{2i}K_{2i} + m_p\sum_{i=1}^{M}\psi_{2i}\bar{\varphi}_{2i})$$
$$(L_1\ddot{\theta}_1 + 2\sum_{i=1}^{M}\psi_{1i}\ddot{\varphi}_{1i}) - (\frac{1}{2}\lambda_2 L_2 + m_p)L_2\ddot{\theta}_1\sum_{i=1}^{M}\psi_{1i}\bar{\varphi}_{1i}]\sin(\bar{\theta}_2+\bar{\alpha}_{1e})\} +$$
$$\{[2(\lambda_2\sum_{i=1}^{M}\dot{\bar{\varphi}}_{2i}K_{2i} + m_p\sum_{i=1}^{M}\psi_{2i}\dot{\varphi}_{2i}) + (\frac{1}{2}\lambda_2 L_2 + m_p)L_2(\dot{\ddot{\theta}}_1 + \dot{\ddot{\theta}}_2 + \dot{\ddot{\alpha}}_{1e})]\cos(\bar{\theta}_2+\bar{\alpha}_{1e})$$
$$-(\lambda_2\sum_{i=1}^{M}\bar{\varphi}_{2i}K_{2i} + m_p\sum_{i=1}^{M}\psi_{2i}\bar{\varphi}_{2i})(\ddot{\theta}_1 + \ddot{\theta}_2 + \ddot{\alpha}_{1e})\sin(\bar{\theta}_2+\bar{\alpha}_{1e})\}\psi_{1n}(\ddot{\theta}_1 + \ddot{\theta}_2 + \ddot{\alpha}_{1e})$$
$$-\frac{2}{\eta_1^2}(\sum_{i=1}^{M}\psi'_{1i}\ddot{\varphi}_{1i})^2(\sum_{i=1}^{M}\psi'_{1i}\bar{\varphi}_{1i})\psi_{1n}[(\frac{1}{2}\lambda_2 L_2 + m_p)L_2\sin(\bar{\theta}_2+\bar{\alpha}_{1e}) + (\lambda_2\sum_{i=1}^{M}\bar{\varphi}_{2i}K_{2i}$$
$$+m_p\sum_{i=1}^{M}\psi_{2i}\bar{\varphi}_{2i})\cos(\bar{\theta}_2+\bar{\alpha}_{1e})] \qquad (n=1, \ldots, M)$$

$$a'_{53n} = \left.\frac{\partial B_{5n}}{\partial \theta_3}\right|_{\bar{x}} = 0.0 \qquad (n=1, \ldots, M)$$

$$a'_{54n} = \left.\frac{\partial B_{5n}}{\partial \theta_4}\right|_{\bar{x}} = 0.0 \qquad (n=1, \ldots, M)$$

$$a'_{55ni} = \left.\frac{\partial B_{5n}}{\partial \varphi_{1i}}\right|_{\bar{x}} = -[\left.\frac{\partial}{\partial \varphi_{1i}}(\frac{1}{\eta_1})\right|_{\bar{x}}\sin(\bar{\theta}_2+\bar{\alpha}_{1e}) + \frac{1}{\eta_1}\cos(\bar{\theta}_2+\bar{\alpha}_{1e})\left.\frac{\partial \alpha_{1e}}{\partial \varphi_{1i}}\right|_{\bar{x}}]\psi'_{1n}$$
$$\ddot{\theta}_1[(\frac{1}{2}\lambda_2 L_2 + m_p)L_2(L_1\ddot{\theta}_1 + 2\sum_{j=1}^{M}\psi_{1j}\ddot{\varphi}_{1j}) + \lambda_2\ddot{\theta}_1\sum_{j=1}^{M}\psi_{1j}\bar{\varphi}_{1j}\sum_{j=1}^{M}\bar{\varphi}_{2j}K_{2j}] -$$
$$\frac{1}{\eta_1}\psi'_{1n}\psi_{1i}\lambda_2\dot{\ddot{\theta}}_1^2\sum_{j=1}^{M}\bar{\varphi}_{2j}K_{2j}\sin(\bar{\theta}_2+\bar{\alpha}_{1e}) + 2(\lambda_2\sum_{j=1}^{M}\dot{\bar{\varphi}}_{2j}K_{2j} + m_p\sum_{j=1}^{M}\psi_{2j}\dot{\varphi}_{2j})\psi_{1n}$$
$$[\left.\frac{\partial \dot{\alpha}_{1e}}{\partial \varphi_{1i}}\right|_{\bar{x}}\sin(\bar{\theta}_2+\bar{\alpha}_{1e}) + (\ddot{\theta}_1 + \ddot{\theta}_2 + \ddot{\alpha}_{1e})\cos(\bar{\theta}_2+\bar{\alpha}_{1e})\left.\frac{\partial \alpha_{1e}}{\partial \varphi_{1i}}\right|_{\bar{x}}] -$$
$$[\left.\frac{\partial}{\partial \varphi_{1i}}(\frac{1}{\eta_1})\right|_{\bar{x}}\cos(\bar{\theta}_2+\bar{\alpha}_{1e}) - \frac{1}{\eta_1}\sin(\bar{\theta}_2+\bar{\alpha}_{1e})\left.\frac{\partial \alpha_{1e}}{\partial \varphi_{1i}}\right|_{\bar{x}}]\psi'_{1n}\ddot{\theta}_1[(\lambda_2\sum_{j=1}^{M}\bar{\varphi}_{2j}K_{2j} +$$
$$m_p\sum_{j=1}^{M}\psi_{2j}\bar{\varphi}_{2j})(\ddot{\theta}_1 L_1 + 2\sum_{j=1}^{M}\psi_{1j}\ddot{\varphi}_{1j}) - (\frac{1}{2}\lambda_2 L_2 + m_p)L_2\ddot{\theta}_1\sum_{j=1}^{M}\psi_{1j}\bar{\varphi}_{1j}] + \frac{1}{\eta_1}\psi'_{1n}$$
$$(\frac{1}{2}\lambda_2 L_2 + m_p)L_2\dot{\ddot{\theta}}_1^2\psi_{1i}\cos(\bar{\theta}_2+\bar{\alpha}_{1e}) + +(\lambda_2\sum_{j=1}^{M}\bar{\varphi}_{2j}K_{2j} + m_p\sum_{j=1}^{M}\psi_{2j}\bar{\varphi}_{2j})\psi_{1n}$$
$$[2(\ddot{\theta}_1 + \ddot{\theta}_2 + \ddot{\alpha}_{1e})\cos(\bar{\theta}_2+\bar{\alpha}_{1e})\left.\frac{\partial \dot{\alpha}_{1e}}{\partial \varphi_{1i}}\right|_{\bar{x}} - (\ddot{\theta}_1 + \ddot{\theta}_2 + \ddot{\alpha}_{1e})^2\sin(\bar{\theta}_2+\bar{\alpha}_{1e})\left.\frac{\partial \alpha_{1e}}{\partial \varphi_{1i}}\right|_{\bar{x}}] -$$
$$[(\ddot{\theta}_1 + \ddot{\theta}_2 + \ddot{\alpha}_{1e})\left.\frac{\partial}{\partial \varphi_{1i}}(\frac{2}{\eta_1})\right|_{\bar{x}} + \frac{2}{\eta_1}\left.\frac{\partial \dot{\alpha}_{1e}}{\partial \varphi_{1i}}\right|_{\bar{x}}]\psi'_{1n}(\lambda_2\sum_{j=1}^{M}\sum_{k=1}^{M}\bar{\varphi}_{2j}\ddot{\varphi}_{2k}N_{2jk} +$$
$$m_p\sum_{j=1}^{M}\psi_{2j}\bar{\varphi}_{2j}\sum_{j=1}^{M}\psi_{2j}\ddot{\varphi}_{2j}) + [\left.\frac{\partial}{\partial \varphi_{1i}}(\frac{2}{\eta_1^2})\right|_{\bar{x}}\sum_{j=1}^{M}\psi_{1j}\ddot{\varphi}_{1j} + \frac{2}{\eta_1^2}\psi'_{1i}](\sum_{j=1}^{M}\psi'_{1j}\ddot{\varphi}_{1j})^2$$

$$\{\frac{1}{\eta_1}\psi'_{1n}[I_{h2}+(\frac{1}{3}\lambda_2 L_2+m_p)L_2^2]+\psi_{1n}[(\frac{1}{2}\lambda_2 L_2+m_p)L_2\cos(\bar{\theta}_2+\bar{\alpha}_{1e})$$

$$-(\lambda_2\sum_{j=1}^{M}\bar{\varphi}_{2j}K_{2j}+m_p\sum_{j=1}^{M}\psi_{2j}\bar{\varphi}_{2j})\sin(\bar{\theta}_2+\bar{\alpha}_{1e})]\}+\frac{2}{\eta_1^2}(\sum_{j=1}^{M}\psi'_{1j}\dot{\bar{\varphi}}_{1j})^2(\sum_{j=1}^{M}\psi'_{1j}\bar{\varphi}_{1j})$$

$$\{\psi'_{1n}\frac{\partial}{\partial\varphi_{1i}}(\frac{1}{\eta_1})\Big|_{\bar{x}}[I_{h2}+(\frac{1}{3}\lambda_2 L_2+m_p)L_2^2]-\psi_{1n}[(\frac{1}{2}\lambda_2 L_2+m_p)L_2\sin(\bar{\theta}_2+\bar{\alpha}_{1e})$$

$$+(\lambda_2\sum_{j=1}^{M}\bar{\varphi}_{2j}K_{2j}+m_p\sum_{j=1}^{M}\psi_{2j}\bar{\varphi}_{2j})\cos(\bar{\theta}_2+\bar{\alpha}_{1e})]\frac{\partial\alpha_{1e}}{\partial\varphi_{1i}}\Big|_{\bar{x}}+\lambda_2\dot{\bar{\theta}}_1^2 N_{2ni}+\dot{\bar{\theta}}_1^2\psi_{1n}\psi_{1i}(m_{r2}$$

$$+\lambda_2 L_2+m_{h2}+m_p)-E_1I_1G_{1ni}+[\frac{\partial}{\partial\varphi_{1i}}(\frac{2}{\eta_1^3})\Big|_{\bar{x}}\sum_{j=1}^{M}\psi'_{1j}\bar{\varphi}_{1j}+\frac{2}{\eta_1^3}\psi'_{1i}]$$

$$(\sum_{j=1}^{M}\psi'_{1j}\dot{\bar{\varphi}}_{1j})^2\psi'_{1n}(I_{r2}+I_p+J_2)+\frac{2}{\eta_2^2}(\sum_{j=1}^{M}\psi'_{2j}\dot{\bar{\varphi}}_{2j})^2(\sum_{j=1}^{M}\psi'_{2j}\bar{\varphi}_{2j})\psi'_{1n}$$

$$I_p\frac{\partial}{\partial\varphi_{1i}}(\frac{1}{\eta_1})\Big|_{\bar{x}} \qquad (i=1,...,M;n=1,...,M)$$

$$a'_{56ni}=\frac{\partial B_{5n}}{\partial\varphi_{2i}}\Big|_{\bar{x}}=-\frac{1}{\eta_1}\psi'_{1n}\dot{\bar{\theta}}_1\{\lambda_2\dot{\bar{\theta}}_1K_{2i}\sum_{j=1}^{M}\psi_{1j}\bar{\varphi}_{1j}\sin(\bar{\theta}_2+\bar{\alpha}_{1e})-[\lambda_2K_{2i}(\dot{\bar{\theta}}_1L_1+$$

$$2\sum_{j=1}^{M}\psi_{1j}\dot{\bar{\varphi}}_{1j})+m_p\psi_{2i}(L_1\dot{\bar{\theta}}_1+2\sum_{j=1}^{M}\psi_{1j}\dot{\bar{\varphi}}_{1j})]\cos(\bar{\theta}_2+\bar{\alpha}_{1e})\}+(\lambda_2K_{2i}+m_p\psi_{2i})\psi_{1n}$$

$$[(\dot{\bar{\theta}}_1+\dot{\bar{\theta}}_2+\dot{\bar{\alpha}}_{1e})^2\cos(\bar{\theta}_2+\bar{\alpha}_{1e})-\frac{2}{\eta_1^2}(\sum_{j=1}^{M}\psi'_{1j}\dot{\bar{\varphi}}_{1j})^2(\sum_{j=1}^{M}\psi'_{1j}\bar{\varphi}_{1j})\sin(\bar{\theta}_2+\bar{\alpha}_{1e})]$$

$$\frac{2}{\eta_1}\psi'_{1n}(\lambda_2\sum_{j=1}^{M}\dot{\bar{\varphi}}_{2j}N_{2ij}+m_p\psi_{2i}\sum_{j=1}^{M}\psi_{2j}\dot{\bar{\varphi}}_{2j})(\dot{\bar{\theta}}_1+\dot{\bar{\theta}}_2+\dot{\bar{\alpha}}_{1e})+[\frac{\partial}{\partial\varphi_{2i}}(\frac{2}{\eta_2^2})\Big|_{\bar{x}}\sum_{j=1}^{M}\psi'_{2j}\bar{\varphi}_{2j}$$

$$+\frac{2}{\eta_2^2}\psi'_{2i}](\sum_{j=1}^{M}\psi'_{2j}\dot{\bar{\varphi}}_{2j})^2(\frac{1}{\eta_1})\psi'_{1n}I_p \qquad (i=1,...,M;n=1,...,M)$$

$$a'_{61n}=\frac{\partial B_{6n}}{\partial\theta_1}\Big|_{\bar{x}}=0.0 \qquad (n=1,\ ...,\ M)$$

$$a'_{62n}=\frac{\partial B_{6n}}{\partial\theta_2}\Big|_{\bar{x}}=-[\lambda_2K_{2n}+m_p\psi_{2n}]\dot{\bar{\theta}}_1[\dot{\bar{\theta}}_1\sum_{i=1}^{M}\psi_{1i}\bar{\varphi}_{1i}\sin(\bar{\theta}_2+\bar{\alpha}_{1e})+(L_1\dot{\bar{\theta}}_1+$$

$$2\sum_{i=1}^{M}\psi_{1i}\dot{\bar{\varphi}}_{1i})\cos(\bar{\theta}_2+\bar{\alpha}_{1e})] \qquad (n=1,\ ...,\ M)$$

$$a'_{63n}=\frac{\partial B_{6n}}{\partial\theta_3}\Big|_{\bar{x}}=0.0 \qquad (n=1,\ ...,\ M)$$

$$a'_{64n}=\frac{\partial B_{6n}}{\partial\theta_4}\Big|_{\bar{x}}=0.0 \qquad (n=1,\ ...,\ M)$$

$$a'_{65ni}=\frac{\partial B_{6n}}{\partial\varphi_{1i}}\Big|_{\bar{x}}=(\lambda_2K_{2n}+m_p\psi_{2n})\dot{\bar{\theta}}_1\{\dot{\bar{\theta}}_1\psi_{1i}\cos(\bar{\theta}_2+\bar{\alpha}_{1e})-[\dot{\bar{\theta}}_1\sum_{j=1}^{M}\psi_{1j}\bar{\varphi}_{1j}\sin(\bar{\theta}_2+\bar{\alpha}_{1e})$$

$$+(L_1\dot{\bar{\theta}}_1+2\sum_{j=1}^{M}\psi_{1j}\dot{\bar{\varphi}}_{1j})\cos(\bar{\theta}_2+\bar{\alpha}_{1e})]\frac{\partial\alpha_{1e}}{\partial\varphi_{1i}}\Big|_{\bar{x}}\}+2(\lambda_2\sum_{j=1}^{M}\dot{\bar{\varphi}}_{2j}N_{2nj}+$$

$$m_p\psi_{2n}\sum_{j=1}^{M}\psi_{2j}\dot{\bar{\varphi}}_{2j})(\dot{\bar{\theta}}_1+\dot{\bar{\theta}}_2+\dot{\bar{\alpha}}_{1e})\frac{\partial\dot{\alpha}_{1e}}{\partial\varphi_{1i}}\Big|_{\bar{x}}+[\frac{\partial}{\partial\varphi_{1i}}(\frac{2}{\eta_1^2})\Big|_{\bar{x}}\sum_{j=1}^{M}\psi'_{1j}\dot{\bar{\varphi}}_{1j}+\frac{2}{\eta_1^2}\psi'_{1i}]$$

$$(\sum_{j=1}^{M}\psi'_{1j}\dot{\bar{\varphi}}_{1j})^2(\lambda_2 M_{2n}+m_p L_2\psi_{2n}+\frac{1}{\eta_2}I_p\psi'_{2n}) \qquad (i=1,\ldots,M;n=1,\ldots,M)$$

$$a'_{66nl}=\left.\frac{\partial B_{6n}}{\partial\varphi_{2l}}\right|_{\bar{x}}=(\lambda_2 N_{2nl}+m_p\psi_{2n}\psi_{2l})(\dot{\bar{\theta}}_1+\dot{\bar{\theta}}_2+\dot{\bar{\alpha}}_{1e})^2-E_2I_2G_{2nl}+\frac{2}{\eta_1^2}(\sum_{j=1}^{M}\psi'_{1j}\dot{\bar{\varphi}}_{1j})^2$$

$$(\sum_{j=1}^{M}\psi'_{1j}\bar{\varphi}_{1j})I_p\psi'_{2n}\left.\frac{\partial}{\partial\varphi_{2l}}(\frac{1}{\eta_2})\right|_{\bar{x}}+[\left.\frac{\partial}{\partial\varphi_{2l}}(\frac{2}{\eta_2^2})\right|_{\bar{x}}\sum_{j=1}^{M}\psi'_{2j}\bar{\varphi}_{2j}+\frac{2}{\eta_2^2}\psi'_{2n}]$$

$$I_p\psi'_{2n}(\sum_{j=1}^{M}\psi'_{2j}\dot{\bar{\varphi}}_{2j})^2 \qquad (i=1,\ldots,M;n=1,\ldots,M)$$

Elements of Matrix A'':

$$a''_{11} = \left.\frac{\partial B_1}{\partial \dot{\theta}_1}\right|_{\bar{x}} = -2\lambda_1 \sum_{i=1}^{M}\sum_{j=1}^{M} \bar{\varphi}_{1i}\,\dot{\bar{\varphi}}_{1j} N_{1ij} - 2(m_p + m_{h2} + \lambda_2 L_2 + m_p) \sum_{i=1}^{M} \psi_{1i}\bar{\varphi}_{1i} \sum_{i=1}^{M} \psi_{1i}\,\dot{\bar{\varphi}}_{1i}$$
$$+2(\frac{1}{2}\lambda_2 L_1 L_2^2 + \lambda_2 \sum_{i=1}^{M} \psi_{1i}\bar{\varphi}_{1i} \sum_{i=1}^{M} \bar{\varphi}_{2i} K_{2i} + m_p L_1 L_2)(\dot{\bar{\theta}}_2 + \dot{\bar{\alpha}}_{1e})\sin(\bar{\theta}_2 + \bar{\alpha}_{1e}) +$$
$$2(\lambda_2 \sum_{i=1}^{M} \dot{\bar{\varphi}}_{2i} K_{2i} + m_p \sum_{i=1}^{M} \psi_{2i}\,\dot{\bar{\varphi}}_{2i})L_1 \sin(\bar{\theta}_2 + \bar{\alpha}_{1e}) - (\lambda_2 L_2 + 2m_p)L_2 \sin(\bar{\theta}_2 + \bar{\alpha}_{1e})$$
$$\sum_{i=1}^{M} \psi_{1i}\,\dot{\bar{\varphi}}_{1i} + 2[\lambda_2 L_1 \sum_{i=1}^{M} \bar{\varphi}_{2i} K_{2i} + m_p L_2 \sum_{i=1}^{M} \psi_{2i}\bar{\varphi}_{2i} - (\frac{1}{2}\lambda_2 L_2 + m_p)L_2 \sum_{i=1}^{M} \psi_{1i}\bar{\varphi}_{1i}]$$
$$(\dot{\bar{\theta}}_2 + \dot{\bar{\alpha}}_{1e})\cos(\bar{\theta}_2 + \bar{\alpha}_{1e}) - 2(\lambda_2 \sum_{i=1}^{M} \bar{\varphi}_{2i} K_{2i} + m_p \sum_{i=1}^{M} \psi_{2i}\bar{\varphi}_{2i})\cos(\bar{\theta}_2 + \bar{\alpha}_{1e}) \sum_{i=1}^{M} \psi_{1i}\,\dot{\bar{\varphi}}_{1i} -$$
$$2(\lambda_2 \sum_{i=1}^{M} \dot{\bar{\varphi}}_{2i} K_{2i} + m_p \sum_{i=1}^{M} \psi_{2i}\,\dot{\bar{\varphi}}_{2i})\cos(\bar{\theta}_2 + \bar{\alpha}_{1e}) \sum_{i=1}^{M} \psi_{1i}\bar{\varphi}_{1i} - 2(\lambda_2 \sum_{i=1}^{M}\sum_{j=1}^{M} \bar{\varphi}_{2i}\,\dot{\bar{\varphi}}_{2j} N_{2ij}$$
$$+m_p \sum_{i=1}^{M} \psi_{2i}\bar{\varphi}_{2i} \sum_{j=1}^{M} \psi_{2j}\,\dot{\bar{\varphi}}_{2j})$$

$$a''_{12} = \left.\frac{\partial B_1}{\partial \dot{\theta}_2}\right|_{\bar{x}} = 2[(\frac{1}{2}\lambda_2 L_2 + m_p)L_1 L_2 + \lambda_2 \sum_{i=1}^{M} \psi_{1i}\bar{\varphi}_i \sum_{i=1}^{M} \bar{\varphi}_{2i} K_{2i}](\dot{\bar{\theta}}_1 + \dot{\bar{\theta}}_2 + \dot{\bar{\alpha}}_{1e})$$
$$\sin(\bar{\theta}_2 + \bar{\alpha}_{1e}) + 2(\lambda_2 \sum_{i=1}^{M} \dot{\bar{\varphi}}_{2i} K_{2i} + m_p \sum_{i=1}^{M} \psi_{2i}\,\dot{\bar{\varphi}}_{2i})[L_1 \sin(\bar{\theta}_2 + \bar{\alpha}_{1e}) - \sum_{i=1}^{M} \psi_{1i}\bar{\varphi}_{1i}$$
$$\cos(\bar{\theta}_2 + \bar{\alpha}_{1e})] + 2[\lambda_2 L_1 \sum_{i=1}^{M} \bar{\varphi}_{2i} K_{2i} + m_p L_1 \sum_{i=1}^{M} \psi_{2i}\bar{\varphi}_{2i} - (\frac{1}{2}\lambda_2 L_2 + m_p)L_2 \sum_{i=1}^{M} \psi_{1i}\bar{\varphi}_{1i}]$$
$$(\dot{\bar{\theta}}_1 + \dot{\bar{\theta}}_2 + \dot{\bar{\alpha}}_{1e})\cos(\bar{\theta}_2 + \bar{\alpha}_{1e}) - 2(\lambda_2 \sum_{i=1}^{M}\sum_{j=1}^{M} \bar{\varphi}_{2i}\,\dot{\bar{\varphi}}_{2j} N_{2ij} + m_p \sum_{i=1}^{M} \psi_{2i}\bar{\varphi}_{2i} \sum_{j=1}^{M} \psi_{2j}\,\dot{\bar{\varphi}}_{2j})$$

$$a''_{33} = \left.\frac{\partial B_1}{\partial \dot{\theta}_3}\right|_{\bar{x}} = 0.0$$

$$a''_{43} = \left.\frac{\partial B_1}{\partial \dot{\theta}_2}\right|_{\bar{x}} = 0.0$$

$$a''_{15l} = \left.\frac{\partial B_1}{\partial \dot{\varphi}_{1l}}\right|_{\bar{x}} = -2\lambda_1\,\dot{\bar{\theta}}_1 \sum_{j=1}^{M} \bar{\varphi}_{1j} N_{1lj} - 2(m_{r2} + m_{h2} + \lambda_2 L_2 + m_p)\,\dot{\bar{\theta}}_1\,\psi_{1l} \sum_{j=1}^{M} \psi_{1j}\bar{\varphi}_{1j} +$$
$$\{[(\lambda_2 L_2 + 2m_p)L_1 L_2 + 2\lambda_2 \sum_{j=1}^{M} \psi_{1j}\bar{\varphi}_{1j} \sum_{j=1}^{M} \bar{\varphi}_{2j} K_{2j}](\dot{\bar{\theta}}_1 + \dot{\bar{\theta}}_2 + \dot{\bar{\alpha}}_{1e})\sin(\bar{\theta}_2 + \bar{\alpha}_{1e})$$
$$+2(\lambda_2 \sum_{j=1}^{M} \dot{\bar{\varphi}}_{2j} K_{2j} + m_p \sum_{j=1}^{M} \psi_{2j}\,\dot{\bar{\varphi}}_{2j})L_1 \sin(\bar{\theta}_2 + \bar{\alpha}_{1e})\} \left.\frac{\partial \dot{\alpha}_{1e}}{\partial \dot{\varphi}_{1l}}\right|_{\bar{x}} - 2(\frac{1}{2}\lambda_2 L_2 + m_p)$$
$$L_2\,\dot{\bar{\theta}}_1\,\psi_{1l}\sin(\bar{\theta}_2 + \bar{\alpha}_{1e}) + 2[(\lambda_2 \sum_{j=1}^{M} \bar{\varphi}_{2j} K_{2j} + m_p \sum_{j=1}^{M} \psi_{2j}\bar{\varphi}_{2j})L_1 - (\frac{1}{2}\lambda_2 L_2 + m_p)L_2$$
$$\sum_{j=1}^{M} \psi_{1j}\bar{\varphi}_{1j}](\dot{\bar{\theta}}_1 + \dot{\bar{\theta}}_2 + \dot{\bar{\alpha}}_{1e})\cos(\bar{\theta}_2 + \bar{\alpha}_{1e}) \left.\frac{\partial \dot{\alpha}_{1e}}{\partial \dot{\varphi}_{1l}}\right|_{\bar{x}} - 2(\lambda_2 \sum_{j=1}^{M} \bar{\varphi}_{2j} K_{2j} + m_p \sum_{j=1}^{M} \psi_{2j}\bar{\varphi}_{2j})$$
$$\dot{\bar{\theta}}_1\,\psi_{1l}\cos(\bar{\theta}_2 + \bar{\alpha}_{1e}) - 2[(\lambda_2 \sum_{j=1}^{M} \dot{\bar{\varphi}}_{2j} K_{2j} + m_p \sum_{j=1}^{M} \psi_{2j}\,\dot{\bar{\varphi}}_{2j}) \sum_{j=1}^{M} \psi_{1j}\bar{\varphi}_{1j}\cos(\bar{\theta}_2 + \bar{\alpha}_{1e}) +$$

$$\lambda_2 \sum_{j=1}^{M}\sum_{k=1}^{M} \bar{\varphi}_{2j}\,\dot{\bar{\varphi}}_{2k} N_{2jk} + + m_p \sum_{j=1}^{M} \psi_{2j}\bar{\varphi}_{2j} \sum_{j=1}^{M} \psi_{2j}\,\dot{\bar{\varphi}}_{2j}\,]\,\frac{\partial\,\dot{\alpha}_{1e}}{\partial\,\dot{\varphi}_{1i}}\bigg|_{\bar{x}} + \frac{4}{\eta_1^2}(\sum_{j=1}^{M} \psi'_{1j}\,\dot{\bar{\varphi}}_{1j})$$

$$(\sum_{j=1}^{M} \psi'_{1j}\bar{\varphi}_{1j})\psi'_{1i}\{I_{h2} + (\frac{1}{2}\lambda_2 L_2 + m_p)L_1 L_2 \cos(\bar{\theta}_2 + \bar{\alpha}_{1e}) - \lambda_2[L_1 \sin(\bar{\theta}_2 + \bar{\alpha}_{1e}) -$$

$$\sum_{j=1}^{M} \psi_{1j}\bar{\varphi}_{1j}\cos(\bar{\theta}_2 + \bar{\alpha}_{1e})]\sum_{j=1}^{M} \bar{\varphi}_{2j}K_{2j} + (\frac{1}{3}\lambda_2 L_2 + m_p)L_2^2 + I_{r2} + I_p + J_2\} \quad (i=1, \ldots, M)$$

$$a''_{16i} = \frac{\partial B_1}{\partial\,\dot{\varphi}_{2i}}\bigg|_{\bar{x}} = 2(\lambda_2 K_{2i} + m_p\psi_{2i})(\dot{\bar{\theta}}_1 + \dot{\bar{\theta}}_2 + \dot{\bar{\alpha}}_{1e})[L_1 \sin(\bar{\theta}_2 + \bar{\alpha}_{1e}) - \sum_{j=1}^{M} \psi_{1j}\bar{\varphi}_{1j}$$

$$\cos(\bar{\theta}_2 + \bar{\alpha}_{1e})] - 2(\lambda_2 \sum_{j=1}^{M} \bar{\varphi}_{2j}N_{2ij} + m_p\psi_{2i}\sum_{j=1}^{M} \psi_{2j}\bar{\varphi}_{2j})(\dot{\bar{\theta}}_1 + \dot{\bar{\theta}}_2 + \dot{\bar{\alpha}}_{1e}) +$$

$$\frac{4}{\eta_2^2} I_p(\sum_{j=1}^{M} \psi'_{2j}\,\dot{\bar{\varphi}}_{2j})\psi'_{2i}(\sum_{j=1}^{M} \psi'_{2j}\bar{\varphi}_{2j}) \qquad (i=1, \ldots, M)$$

$$a''_{21} = \frac{\partial B_2}{\partial\,\dot{\theta}_1}\bigg|_{\bar{x}} = -[(\frac{1}{2}\lambda_2 L_2 + m_p)L_1 L_2 + \lambda_2 \sum_{i=1}^{M} \psi_{1i}\bar{\varphi}_{1i} \sum_{i=1}^{M} \bar{\varphi}_{2i}K_{2i}]\,\dot{\bar{\theta}}_1 \sin(\bar{\theta}_2 + \bar{\alpha}_{1e}) -$$

$$[(\frac{1}{2}\lambda_2 L_2 + m_p)L_2(L_1\,\dot{\bar{\theta}}_1 + 2\sum_{i=1}^{M} \psi_{1i}\,\dot{\bar{\varphi}}_{1i}) + \lambda_2\,\dot{\bar{\theta}}_1 \sum_{i=1}^{M} \psi_{1i}\bar{\varphi}_{1i}\sum_{i=1}^{M} \bar{\varphi}_{2i}K_{2i}]$$

$$\sin(\bar{\theta}_2 + \bar{\alpha}_{1e}) - [(\lambda_2 \sum_{i=1}^{M} \bar{\varphi}_{2i}K_{2i} + m_p \sum_{i=1}^{M} \psi_{2i}\bar{\varphi}_{2i})L_1 - (\frac{1}{2}\lambda_2 L_2 + m_p)L_2 \sum_{i=1}^{M} \psi_{1i}\bar{\varphi}_{1i}]\,\dot{\bar{\theta}}_1$$

$$\cos(\bar{\theta}_2 + \bar{\alpha}_{1e}) - [(\lambda_2 \sum_{i=1}^{M} \bar{\varphi}_{2i}K_{2i} + + m_p \sum_{i=1}^{M} \psi_{2i}\bar{\varphi}_{2i})(L_1\,\dot{\bar{\theta}}_1 + 2\sum_{i=1}^{M} \psi_{1i}\,\dot{\bar{\varphi}}_{1i}) -$$

$$(\frac{1}{2}\lambda_2 L_2 + m_p)L_2\,\dot{\bar{\theta}}_1 \sum_{i=1}^{M} \psi_{1i}\bar{\varphi}_{1i}]\cos(\bar{\theta}_2 + \bar{\alpha}_{1e}) - 2(\lambda_2 \sum_{i=1}^{M}\sum_{j=1}^{M} \bar{\varphi}_{1i}\,\dot{\bar{\varphi}}_{1j}N_{2ij} +$$

$$m_p \sum_{i=1}^{M} \psi_{2i}\bar{\varphi}_{2i}\sum_{j=1}^{M} \psi_{2j}\,\dot{\bar{\varphi}}_{2j})$$

$$a''_{22} = \frac{\partial B_2}{\partial\,\dot{\theta}_2}\bigg|_{\bar{x}} = -2(\lambda_2 \sum_{i=1}^{M}\sum_{j=1}^{M} \bar{\varphi}_{2i}\,\dot{\bar{\varphi}}_{2j}N_{2ij} + m_p \sum_{i=1}^{M} \psi_{2i}\bar{\varphi}_{2i}\sum_{j=1}^{M} \psi_{2j}\,\dot{\bar{\varphi}}_{2j})$$

$$a''_{23} = \frac{\partial B_2}{\partial\,\dot{\theta}_3}\bigg|_{\bar{x}}$$

$$a''_{24} = \frac{\partial B_2}{\partial\,\dot{\theta}_4}\bigg|_{\bar{x}}$$

$$a''_{25i} = \frac{\partial B_2}{\partial\,\dot{\varphi}_{1i}}\bigg|_{\bar{x}} = -(\lambda_2 L_2 + 2m_p)L_2\psi_{1i}\,\dot{\bar{\theta}}_1 \sin(\bar{\theta}_2 + \bar{\alpha}_{1e}) - 2(\lambda_2 \sum_{j=1}^{M} \bar{\varphi}_{2j}K_{2j} +$$

$$m_p \sum_{j=1}^{M} \psi_{2j}\bar{\varphi}_{2j})\psi_{1i}\,\dot{\bar{\theta}}_1 \cos(\bar{\theta}_2 + \bar{\alpha}_{1e}) - 2(\lambda_2 \sum_{j=1}^{M}\sum_{k=1}^{M} \bar{\varphi}_{2j}\,\dot{\bar{\varphi}}_{2k}N_{2jk} + m_p \sum_{i=1}^{M} \psi_{2j}\bar{\varphi}_{2j}$$

$$\sum_{j=1}^{M} \psi_{2j}\,\dot{\bar{\varphi}}_{2j})\,\frac{\partial\,\dot{\alpha}_{1e}}{\partial\,\dot{\varphi}_{1i}}\bigg|_{\bar{x}} + \frac{4}{\eta_1^2}(\sum_{j=1}^{M} \psi'_{1j}\,\dot{\bar{\varphi}}_{1j})\psi'_{1i}(\sum_{j=1}^{M} \psi'_{1j}\bar{\varphi}_{1j})(I_{h2} + I_p + \frac{1}{3}\lambda_2 L_2^3$$

$$+\lambda_2 \sum_{j=1}^{M}\sum_{k=1}^{M} \bar{\varphi}_{2j}\bar{\varphi}_{2k}N_{2jk} + m_p L_2^2) \qquad (i=1, \ldots, M)$$

$$a''_{26i} = \left.\frac{\partial B_2}{\partial \dot{\varphi}_{2i}}\right|_{\bar{x}} = -2(\lambda_2 \sum_{j=1}^{M} \bar{\varphi}_{2j} N_{2ij} + m_p \psi_{2i} \sum_{j=1}^{M} \psi_{2j} \bar{\varphi}_{2j})(\dot{\theta}_1 + \dot{\bar{\theta}}_2 + \dot{\bar{\alpha}}_{1e}) +$$
$$\frac{4}{\eta_2^2}(\sum_{j=1}^{M} \psi'_{2j} \dot{\bar{\varphi}}_{2j})\psi'_{2i}(\sum_{j=1}^{M} \psi'_{2j} \bar{\varphi}_{2j}) I_p \qquad (i=1, \ldots, M)$$

$$a''_{31} = \left.\frac{\partial B_3}{\partial \dot{\theta}_3}\right|_{\bar{x}} = 0.0$$

$$a''_{32} = \left.\frac{\partial B_3}{\partial \dot{\theta}_2}\right|_{\bar{x}} = 0.0$$

$$a''_{33} = \left.\frac{\partial B_3}{\partial \dot{\theta}_3}\right|_{\bar{x}} = 0.0$$

$$a''_{34} = \left.\frac{\partial B_3}{\partial \dot{\theta}_4}\right|_{\bar{x}} = 0.0$$

$$a''_{35i} = \left.\frac{\partial B_3}{\partial \dot{\varphi}_{1i}}\right|_{\bar{x}} = 0.0 \qquad (i=1, \ldots, M)$$

$$a''_{36i} = \left.\frac{\partial B_3}{\partial \dot{\varphi}_{2i}}\right|_{\bar{x}} = 0.0 \qquad (i=1, \ldots, M)$$

$$a''_{41} = \left.\frac{\partial B_4}{\partial \dot{\theta}_1}\right|_{\bar{x}} = 0.0$$

$$a''_{43} = \left.\frac{\partial B_4}{\partial \dot{\theta}_3}\right|_{\bar{x}} = 0.0$$

$$a''_{44} = \left.\frac{\partial B_4}{\partial \dot{\theta}_4}\right|_{\bar{x}} = -4.64545\beta_4$$

$$a''_{45i} = \left.\frac{\partial B_4}{\partial \dot{\varphi}_{1i}}\right|_{\bar{x}} = -\frac{4}{\eta_1^2} J_2 (\sum_{j=1}^{M} \psi'_{1j} \dot{\bar{\varphi}}_{1j})\psi'_{1i}(\sum_{j=1}^{M} \psi'_{1j} \bar{\varphi}_{1j}) \qquad (i=1, \ldots, M)$$

$$a''_{46i} = \left.\frac{\partial B_4}{\partial \dot{\varphi}_{2i}}\right|_{\bar{x}} = 0.0 \qquad (i=1, \ldots, M)$$

$$a''_{51n} = \left.\frac{\partial B_{5n}}{\partial \dot{\theta}_1}\right|_{\bar{x}} = -\frac{1}{\eta_1}\psi'_{1n}\{2[(\frac{1}{2}\lambda_2 L_2 + m_p)L_1 L_2 + \lambda_2 \sum_{i=1}^{M} \psi_{1i} \bar{\varphi}_{1i} \sum_{i=1}^{M} \bar{\varphi}_{2i} K_{2i}]\,\dot{\theta}_1$$
$$\sin(\bar{\theta}_2 + \bar{\alpha}_{1e}) + (\lambda_2 L_2 + 2m_p)L_2 \sum_{i=1}^{M} \psi_{1i}\,\dot{\bar{\varphi}}_{1i} \sin(\bar{\theta}_2 + \bar{\alpha}_{1e})\} + 2(\lambda_2 \sum_{i=1}^{M} \dot{\bar{\varphi}}_{2i} K_{2i}$$
$$+ m_p \sum_{i=1}^{M} \psi_{2i}\,\dot{\bar{\varphi}}_{2i})\psi_{1n}\sin(\bar{\theta}_2 + \bar{\alpha}_{1e}) + (\lambda_2 L_2 + 2m_p)L_2 \psi_{1n}(\dot{\theta}_1 + \dot{\bar{\theta}}_2 + \dot{\bar{\alpha}}_{1e})\sin(\bar{\theta}_2 + \bar{\alpha}_{1e})$$
$$\frac{1}{\eta_1}\psi'_{1n}\{2[\lambda_2 \sum_{i=1}^{M} \bar{\varphi}_{2i} K_{2i} + m_p \sum_{i=1}^{M} \psi_{2i} \bar{\varphi}_{2i})L_1 - (\frac{1}{2}\lambda_2 L_2 + m_p)L_2 \sum_{i=1}^{M} \psi_{1i} \bar{\varphi}_{1i}]\,\dot{\theta}_1$$
$$\cos(\bar{\theta}_2 + \bar{\alpha}_{1e}) + 2(\lambda_2 \sum_{i=1}^{M} \bar{\varphi}_{2i} K_{2i} + m_p \sum_{i=1}^{M} \psi_{2i} \bar{\varphi}_{2i}) \sum_{i=1}^{M} \psi_{1i}\,\dot{\bar{\varphi}}_{1i} \cos(\bar{\theta}_2 + \bar{\alpha}_{1e})\} +$$
$$2(\lambda_2 \sum_{i=1}^{M} \bar{\varphi}_{2i} K_{2i} + m_p \sum_{i=1}^{M} \psi_{2i} \bar{\varphi}_{2i})\psi_{1n}(\dot{\theta}_1 + \dot{\bar{\theta}}_2 + \dot{\bar{\alpha}}_{1e})\cos(\bar{\theta}_2 + \bar{\alpha}_{1e}) - \frac{2}{\eta_1}\psi'_{1n}$$

$$(\lambda_2 \sum_{i=1}^{M}\sum_{j=1}^{M} \bar{\varphi}_{2i}\,\dot{\bar{\varphi}}_{2j} N_{2ij} + m_p \sum_{i=1}^{M} \psi_{2i}\bar{\varphi}_{2i} \sum_{j=1}^{M} \psi_{2j}\,\dot{\bar{\varphi}}_{2j}) + 2\lambda_1\,\dot{\bar{\theta}}_1 \sum_{i=1}^{M} \bar{\varphi}_{1i} N_{1ni} +$$

$$2(m_{r2} + \lambda_2 L_2 + m_{h2} + m_p)\psi_{1n}\,\dot{\bar{\theta}}_1 \sum_{i=1}^{M} \psi'_{1i}\bar{\varphi}_{1i} \qquad (n=1, \ldots, M)$$

$$a''_{52n} = \left.\frac{\partial B_{5n}}{\partial \dot{\theta}_2}\right|_{\bar{x}} = 2(\lambda_2 \sum_{i=1}^{M} \dot{\bar{\varphi}}_{2i} K_{2i} + m_p \sum_{i=1}^{M} \psi_{2i}\,\dot{\bar{\varphi}}_{2i})\psi_{1n}\sin(\bar{\theta}_2 + \bar{\alpha}_{1e}) + (\lambda_2 L_2 + 2m_p)$$

$$L_2\psi_{1n}(\dot{\bar{\theta}}_1 + \dot{\bar{\theta}}_2 + \dot{\bar{\alpha}}_{1e})\sin(\bar{\theta}_2 + \bar{\alpha}_{1e}) + 2(\lambda_2 \sum_{i=1}^{M} \bar{\varphi}_{2i} K_{2i} + m_p \sum_{i=1}^{M} \psi_{2i}\bar{\varphi}_{2i},$$

$$\psi_{1n}(\dot{\bar{\theta}}_1 + \dot{\bar{\theta}}_2 + \dot{\bar{\alpha}}_{1e})\cos(\bar{\theta}_2 + \bar{\alpha}_{1e}) - \frac{2}{\eta_1}\psi'_{1n}(\lambda_2 \sum_{i=1}^{M}\sum_{j=1}^{M} \bar{\varphi}_{2i}\,\dot{\bar{\varphi}}_{2j} N_{2ij} +$$

$$m_p \sum_{i=1}^{M} \psi_{2i}\bar{\varphi}_{2i} \sum_{j=1}^{M} \psi_{2j}\,\dot{\bar{\varphi}}_{2j}) \qquad (n=1, \ldots, M)$$

$$a''_{53n} = \left.\frac{\partial B_{53n}}{\partial \dot{\theta}_3}\right|_{\bar{x}} = 0.0 \qquad (n=1, \ldots, M)$$

$$a''_{54n} = \left.\frac{\partial B_{53n}}{\partial \dot{\theta}_4}\right|_{\bar{x}} = 0.0 \qquad (n=1, \ldots, M)$$

$$a''_{55ni} = \left.\frac{\partial B_{5n}}{\partial \dot{\varphi}_{1i}}\right|_{\bar{x}} = \frac{1}{\eta_1}\psi'_{1n}[(\lambda_2 L_2 + 2m_p)L_2\psi_{1i}\,\dot{\bar{\theta}}_1 \sin(\bar{\theta}_2 + \bar{\alpha}_{1e}) + 2(\lambda_2 \sum_{j=1}^{M} \bar{\varphi}_{2j} K_{2j} +$$

$$m_p \sum_{j=1}^{M} \psi_{2j}\bar{\varphi}_{2j})\psi_{1i}\,\dot{\bar{\theta}}_1 \cos(\bar{\theta}_2 + \bar{\alpha}_{1e})] + 2\{[\lambda_2 \sum_{j=1}^{M} \dot{\bar{\varphi}}_{2j} K_{2j} + m_p \sum_{j=1}^{M} \psi_{2j}\bar{\varphi}_{2j} + (\frac{1}{2}\lambda_2 L_2$$

$$+m_p)L_2(\dot{\bar{\theta}}_1 + \dot{\bar{\theta}}_2 + \dot{\bar{\alpha}}_{1e})]\sin(\bar{\theta}_2 + \bar{\alpha}_{1e}) + 2(\lambda_2 \sum_{j=1}^{M} \bar{\varphi}_{2j} K_{2j} + m_p \sum_{j=1}^{M} \psi_{2j}\bar{\varphi}_{2j})$$

$$(\dot{\bar{\theta}}_1 + \dot{\bar{\theta}}_2 + \dot{\bar{\alpha}}_{1e})\cos(\bar{\theta}_2 + \bar{\alpha}_{1e})\psi_{1n} + \lambda_2 \sum_{j=1}^{M}\sum_{k=1}^{M} \bar{\varphi}_{2j}\,\dot{\bar{\varphi}}_{2k} N_{2jk} + m_p \sum_{j=1}^{M} \psi_{2j}\bar{\varphi}_{2j}$$

$$\sum_{k=1}^{M} \psi_{2j}\,\dot{\bar{\varphi}}_{2k}\} \left.\frac{\partial\,\dot{\alpha}}{\partial\,\dot{\varphi}_{1i}}\right|_{\bar{x}} + \frac{4}{\eta_1^2}\psi'_{1i}(\sum_{j=1}^{M} \psi'_{1j}\,\dot{\bar{\varphi}}_{1j})(\sum_{j=1}^{M} \psi'_{1j}\bar{\varphi}_{1j})\{\frac{1}{\eta_1}\psi'_{1n}[I_{h2} + (\frac{1}{3}\lambda_2 L_2$$

$$+m_p)L_2^2] + \psi_{1n}[(\frac{1}{2}\lambda_2 L_2 + m_p)L_2\cos(\bar{\theta}_2 + \bar{\alpha}_{1e}) - (\lambda_2 \sum_{j=1}^{M} \bar{\varphi}_{2j} K_{2j} + m_p \sum_{j=1}^{M} \psi_{2j}\bar{\varphi}_{2j})$$

$$\sin(\bar{\theta}_2 + \bar{\alpha}_{1e})]\} + \frac{4}{\eta_1^3}\psi'_{1i}(\sum_{j=1}^{M} \psi'_{1j}\,\dot{\bar{\varphi}}_{1j})(\sum_{j=1}^{M} \psi'_{1j}\bar{\varphi}_{1j})\psi'_{1n}(I_p + I_{r2} + J_2) -$$

$$\beta_1 I_1 G_{1ni} \qquad (i=1,\ldots,M;n=1,\ldots,M)$$

$$a''_{56ni} = \left.\frac{\partial B_{5n}}{\dot{\varphi}_{2i}}\right|_{\bar{x}} = 2(\lambda_2 K_{2i} + m_p\psi_{2i})\psi_{1n}(\dot{\bar{\theta}}_1 + \dot{\bar{\theta}}_2 + \dot{\bar{\alpha}}_{1e})\sin(\bar{\theta}_2 + \bar{\alpha}_{1e}) - \frac{2}{\eta_1}\psi'_{1n}$$

$$(\lambda_2 \sum_{j=1}^{M} \bar{\varphi}_{2j} N_{2ij} + m_p\psi_{2i} \sum_{j=1}^{M} \psi_{2j}\bar{\varphi}_{2j})(\dot{\bar{\theta}}_1 + \dot{\bar{\theta}}_2 + \dot{\bar{\alpha}}_{1e}) +$$

$$\frac{4}{\eta_2^2}(\sum_{j=1}^{M} \psi'_{2j}\,\dot{\bar{\varphi}}_{2j})(\sum_{j=1}^{M} \psi'_{2j}\bar{\varphi}_{2j})\psi'_{2i}\frac{1}{\eta_1}\psi'_{1n}I_p \qquad (i=1,\ldots,M;n=1,\ldots,M)$$

$$a''_{61n} = \left.\frac{\partial B_{6n}}{\dot{\theta}_1}\right|_{\bar{x}} = 2(\lambda_2 K_{2i} + m_p\psi_{2i})[\dot{\bar{\theta}}_1 \sum_{i=1}^{M} \psi_{1i}\bar{\varphi}_{1i}\cos(\bar{\theta}_2 + \bar{\alpha}_{1e}) - (L_1\,\dot{\bar{\theta}}_1 + \sum_{i=1}^{M} \psi_{1i}\,\dot{\bar{\varphi}}_{1i})$$

$$\sin(\bar{\theta}_2+\bar{\alpha}_{1e})]+2(\lambda_2\sum_{i=1}^{M}\bar{\varphi}_{2i}N_{2ni}+m_p\psi_{2n}\sum_{i=1}^{M}\psi_{2i}\bar{\varphi}_{2i})(\dot{\bar{\theta}}_1+\dot{\bar{\theta}}_2+\dot{\bar{\alpha}}_{1e}) \quad (n=1,\ldots,M)$$

$$a''_{62n}=\left.\frac{\partial B_{6n}}{\partial\dot{\theta}_2}\right|_{\bar{x}}=2(\lambda_2\sum_{i=1}^{M}\bar{\varphi}_{2i}N_{2ni}+m_p\psi_{2n}\sum_{i=1}^{M}\psi_{2i}\bar{\varphi}_{2i})(\dot{\bar{\theta}}_1+\dot{\bar{\theta}}_2+\dot{\bar{\alpha}}_{1e}) \quad (n=1,\ldots,M)$$

$$a''_{63n}=\left.\frac{\partial B_{6n}}{\partial\dot{\theta}_3}\right|_{\bar{x}}=0.0 \qquad (n=1,\ldots,M)$$

$$a''_{64n}=\left.\frac{\partial B_{6n}}{\partial\dot{\theta}_4}\right|_{\bar{x}}=0.0 \qquad (n=1,\ldots,M)$$

$$a''_{65ni}=\left.\frac{\partial B_{6n}}{\partial\dot{\varphi}_{1i}}\right|_{\bar{x}}=-2(\lambda_2K_{2n}+m_p\psi_{2n})\,\dot{\bar{\theta}}_1\,\psi_{2i}\sin(\bar{\theta}_2+\bar{\alpha}_{1e})+2(\lambda_2\sum_{j=1}^{M}\bar{\varphi}_{2j}N_{2nj}+$$

$$m_p\psi_{2n}\sum_{j=1}^{M}\psi_{2j}\bar{\varphi}_{2j})(\dot{\bar{\theta}}_1+\dot{\bar{\theta}}_2+\dot{\bar{\alpha}}_{1e})\left.\frac{\partial\dot{\alpha}}{\partial\dot{\varphi}}\right|_{\bar{x}}+\frac{4}{\eta_1^2}(\sum_{j=1}^{M}\psi'_{1j}\,\dot{\bar{\varphi}}_{1j})(\sum_{j=1}^{M}\psi'_{1j}\bar{\varphi}_{1j})$$

$$\psi'_{1i}(\lambda_2M_{2n}+m_pL_2\psi_{2n}+\frac{1}{\eta_1}I_p\psi'_{2n}) \qquad (i=1,\ldots,M;n=1,\ldots,M)$$

$$a''_{66ni}=\left.\frac{\partial B_{6n}}{\partial\dot{\varphi}_{2i}}\right|_{\bar{x}}=\frac{4}{\eta_2^2}(\sum_{j=1}^{M}\psi'_{2j}\,\dot{\bar{\varphi}}_{2j})(\sum_{j=1}^{M}\psi'_{2j}\bar{\varphi}_{2j})\psi'_{2n}I_p\psi'_{2i}-\beta_2I_2G_{2ni} \quad i=1,\ldots,M;n=1,\ldots,M$$

Elements of Matrix $\tilde{A}$:

$$\tilde{a}_{11} = \left.\frac{\partial m_{11}}{\partial \theta_2}\right|_{\bar{x}} \dot{\bar{\theta}}_2 + \sum_{j=1}^{M} \left.\frac{\partial m_{11}}{\partial \varphi_{1j}}\right|_{\bar{x}} \dot{\bar{\varphi}}_{1j} + \sum_{j=1}^{M} \left.\frac{\partial m_{11}}{\partial \varphi_{2j}}\right|_{\bar{x}} \dot{\bar{\varphi}}_{2j}$$

with

$$\left.\frac{\partial m_{11}}{\partial \theta_2}\right|_{\bar{x}} = -[(\lambda_2 L_2 + 2m_p)L_1 L_2 + 2\lambda_2 \sum_{j=1}^{M} \psi_{1j}\bar{\varphi}_{1j} \sum_{j=1}^{M} \bar{\varphi}_{2j}K_{2j}]\sin(\bar{\theta}_2 + \bar{\alpha}_{1e}) +$$
$$\lambda_2(L_2^2 \sum_{j=1}^{M} \psi_{1j}\bar{\varphi}_{1j} - 2L_1 \sum_{j=1}^{M} \bar{\varphi}_{2j}K_{2j})\cos(\bar{\theta}_2 + \bar{\alpha}_{1e})$$

$$\left.\frac{\partial m_{11}}{\partial \varphi_{1j}}\right|_{\bar{x}} = -\{[(\lambda_2 L_2 + 2m_p)L_1 L_2 + 2\lambda_2 \sum_{k=1}^{M} \psi_{1k}\bar{\varphi}_{1k} \sum_{k=1}^{M} \bar{\varphi}_{2k}K_{2k}]\sin(\bar{\theta}_2 + \bar{\alpha}_{1e}) + \lambda_2$$
$$(L_2^2 \sum_{k=1}^{M} \psi_{1k}\bar{\varphi}_{1k} - 2L_1 \sum_{k=1}^{M} \bar{\varphi}_{2k}K_{2k})\cos(\bar{\theta}_2 + \bar{\alpha}_{1e})\} \left.\frac{\partial \alpha_{1e}}{\partial \varphi_{1j}}\right|_{\bar{x}} +$$
$$\lambda_2 \psi_{1j}[2(\sum_{k=1}^{M} \bar{\varphi}_{2k}K_{2k})\cos(\bar{\theta}_2 + \bar{\alpha}_{1e}) + L_2^2 \sin(\bar{\theta}_2 + \bar{\alpha}_{1e})]$$

$$\left.\frac{\partial m_{11}}{\partial \varphi_{2j}}\right|_{\bar{x}} = -2\lambda_2 K_{2j}[L_1 \sin(\bar{\theta}_2 + \bar{\alpha}_{1e}) - \sum_{k=1}^{M} \psi_{1k}\bar{\varphi}_{1k}\cos(\bar{\theta}_2 + \bar{\alpha}_{1e})]$$

$$\tilde{a}_{12} = \left.\frac{\partial m_{12}}{\partial \theta_2}\right|_{\bar{x}} \dot{\bar{\theta}}_2 + \sum_{j=1}^{M} \left.\frac{\partial m_{12}}{\partial \varphi_{1j}}\right|_{\bar{x}} \dot{\bar{\varphi}}_{1j} + \sum_{j=1}^{M} \left.\frac{\partial m_{12}}{\partial \varphi_{2j}}\right|_{\bar{x}} \dot{\bar{\varphi}}_{2j}$$

with

$$\left.\frac{\partial m_{12}}{\partial \theta_2}\right|_{\bar{x}} = -[(\frac{1}{2}\lambda_2 L_2 + m_p)L_1 L_2 + \lambda_2 \sum_{j=1}^{M} \psi_{1j}\bar{\varphi}_{1j} \sum_{j=1}^{M} \bar{\varphi}_{2j}K_{2j}]\sin(\bar{\theta}_2 + \bar{\alpha}_{1e}) +$$
$$\lambda_2(\frac{1}{2}L_2^2 \sum_{j=1}^{M} \psi_{1j}\bar{\varphi}_{1j} - L_1 \sum_{j=1}^{M} \bar{\varphi}_{2j}K_{2j})\cos(\bar{\theta}_2 + \bar{\alpha}_{1e})$$

$$\left.\frac{\partial m_{12}}{\partial \varphi_{1j}}\right|_{\bar{x}} = -\{[(\frac{1}{2}\lambda_2 L_2 + m_p)L_1 L_2 + \lambda_2 \sum_{k=1}^{M} \psi_{1k}\bar{\varphi}_{1k} \sum_{k=1}^{M} \bar{\varphi}_{2k}K_{2k}]\sin(\bar{\theta}_2 + \bar{\alpha}_{1e}) +$$
$$\lambda_2(\frac{1}{2}L_2^2 \sum_{k=1}^{M} \psi_{1k}\bar{\varphi}_{1k} - L_1 \sum_{k=1}^{M} \bar{\varphi}_{2k}K_{2k})\cos(\bar{\theta}_2 + \bar{\alpha}_{1e})\} \left.\frac{\partial \alpha_{1e}}{\partial \varphi_{1j}}\right|_{\bar{x}} +$$
$$\lambda_2 \psi_{1j}[\sum_{k=1}^{M} \bar{\varphi}_{2k}K_{2k})\cos(\bar{\theta}_2 + \bar{\alpha}_{1e}) + \frac{1}{2}L_2^2 \sin(\bar{\theta}_2 + \bar{\alpha}_{1e})]$$

$$\left.\frac{\partial m_{12}}{\partial \varphi_{2j}}\right|_{\bar{x}} = -\lambda_2 K_{2j}[L_1 \sin(\bar{\theta}_2 + \bar{\alpha}_{1e}) - \sum_{k=1}^{M} \psi_{1k}\bar{\varphi}_{1k}\cos(\bar{\theta}_2 + \bar{\alpha}_{1e})] + 2\lambda_2 \sum_{k=1}^{M} \bar{\varphi}_{2k}N_{2jk}$$

$$\tilde{a}_{13} = 0.0$$

$$\tilde{a}_{14} = 0.0$$

$$\tilde{a}_{15i} = \left.\frac{\partial m_{15i}}{\partial \theta_2}\right|_{\bar{x}} \dot{\bar{\theta}}_2 + \sum_{j=1}^{M} \left.\frac{\partial m_{15i}}{\partial \varphi_{1j}}\right|_{\bar{x}} \dot{\bar{\varphi}}_{1j} + \sum_{j=1}^{M} \left.\frac{\partial m_{15i}}{\partial \varphi_{2j}}\right|_{\bar{x}} \dot{\bar{\varphi}}_{2j} \qquad (i=1, \ldots, M)$$

with

$$\left.\frac{\partial m_{15l}}{\partial \theta_2}\right|_{\bar{x}} = -\psi_{1l}[(\frac{1}{2}\lambda_2 L_2 + m_p)L_2 \sin(\bar{\theta}_2 + \bar{\alpha}_{1e}) + \lambda_2 \sum_{j=1}^{M} \bar{\varphi}_{2j} K_{2j} \cos(\bar{\theta}_2 + \bar{\alpha}_{1e})] - \frac{1}{\eta_1}\psi'_{1l}$$

$$[(\frac{1}{2}\lambda_2 L_2 + m_p)L_1 L_2 \sin(\bar{\theta}_2 + \bar{\alpha}_{1e}) + (\lambda_2 \sum_{k=1}^{M} \bar{\varphi}_{2k} K_{2k} + m_p \sum_{k=1}^{M} \psi_{2j}\bar{\varphi}_{2k}) L_1 \cos(\bar{\theta}_2 + \bar{\alpha}_{1e}) +$$

$$\lambda_2 \sum_{k=1}^{M} \psi_{1k}\bar{\varphi}_{1k} \sum_{k=1}^{M} \bar{\varphi}_{2k} K_{2k} \sin(\bar{\theta}_2 + \bar{\alpha}_{1e})]$$

$$\left.\frac{\partial m_{15l}}{\partial \varphi_{1j}}\right|_{\bar{x}} = \left.\frac{\partial m_{15l}}{\partial \theta_2} \bullet \frac{\partial \alpha_{1e}}{\partial \varphi_{1j}}\right|_{\bar{x}} + \frac{1}{\eta_1}\lambda_2 \psi'_{1l}\psi_{1j} \sum_{k=1}^{M} \bar{\varphi}_{2k} K_{2k} \cos(\bar{\theta}_2 + \bar{\alpha}_{1e}) + \left.\frac{\partial}{\partial \varphi_{1l}}(\frac{1}{\eta_1})\right|_{\bar{x}} \psi'_{1l}$$

$$[I_{h2} + (\frac{1}{3}\lambda_2 L_2 + m_p)L_2^2 + (\frac{1}{2}\lambda_2 L_2 + m_p)L_1 L_2 \cos(\bar{\theta}_2 + \bar{\alpha}_{1e}) - (\lambda_2 \sum_{k=1}^{M} \bar{\varphi}_{2k} K_{2k} +$$

$$m_p \sum_{k=1}^{M} \psi_{2k}\bar{\varphi}_{2k}) L_1 \sin(\bar{\theta}_2 + \bar{\alpha}_{1e}) + \lambda_2 \cos(\bar{\theta}_2 + \bar{\alpha}_{1e}) \sum_{k=1}^{M} \psi_{1k}\bar{\varphi}_{1k} \sum_{k=1}^{M} \bar{\varphi}_{2k} K_{2k}$$

$$\sin(\bar{\theta}_2 + \bar{\alpha}_{1e}) + I_{r2} + I_p + J_2]$$

$$\left.\frac{\partial m_{15l}}{\partial \varphi_{2j}}\right|_{\bar{x}} = -\lambda_2 K_{2j}\psi_{1l} \sin(\bar{\theta}_2 + \bar{\alpha}_{1e}) + \frac{1}{\eta_1}\psi'_{1l}[\lambda_2 K_{2j} \cos(\bar{\theta}_2 + \bar{\alpha}_{1e}) \sum_{k=1}^{M} \psi_{1k}\bar{\varphi}_{1k} -$$

$$(\lambda_2 K_{2j} + m_p \psi_{2j}) L_1 \sin(\bar{\theta}_2 + \bar{\alpha}_{1e})]$$

$$\tilde{a}_{16l} = \left.\frac{\partial m_{16l}}{\partial \theta_2}\right|_{\bar{x}} \dot{\bar{\theta}}_2 + \sum_{j=1}^{M} \left.\frac{\partial m_{16l}}{\partial \varphi_{1j}}\right|_{\bar{x}} \dot{\bar{\varphi}}_{1j} + \sum_{j=1}^{M} \left.\frac{\partial m_{16l}}{\partial \varphi_{2j}}\right|_{\bar{x}} \dot{\bar{\varphi}}_{2j} \qquad (i=1, \ldots, M)$$

with

$$\left.\frac{\partial m_{16l}}{\partial \theta_2}\right|_{\bar{x}} = -\lambda_2 K_{2l}[L_1 \sin(\bar{\theta}_2 + \bar{\alpha}_{1e}) - \sum_{k=1}^{M} \psi_{1k}\bar{\varphi}_{1k} \cos(\bar{\theta}_2 + \bar{\alpha}_{1e})] - m_p \psi_{2l} L_1 \sin(\bar{\theta}_2 + \bar{\alpha}_{1e})$$

$$\left.\frac{\partial m_{16l}}{\partial \varphi_{1j}}\right|_{\bar{x}} = \left.\frac{\partial m_{16l}}{\partial \theta_2} \bullet \frac{\partial \alpha_{1e}}{\partial \varphi_{1j}}\right|_{\bar{x}} + \lambda_2 \psi_{1j} K_{2l} \sin(\bar{\theta}_2 + \bar{\alpha}_{1e})$$

$$\left.\frac{\partial m_{16l}}{\partial \varphi_{2j}}\right|_{\bar{x}} = \left.\frac{\partial}{\partial \varphi_{2j}}(\frac{1}{\eta_2})\right|_{\bar{x}} I_p \psi'_{2l}$$

$$\tilde{a}_{21} = \left.\frac{\partial m_{21}}{\partial \theta_2}\right|_{\bar{x}} \dot{\bar{\theta}}_2 + \sum_{j=1}^{M} \left.\frac{\partial m_{21}}{\partial \varphi_{1j}}\right|_{\bar{x}} \dot{\bar{\varphi}}_{1j} + \sum_{j=1}^{M} \left.\frac{\partial m_{21}}{\partial \varphi_{2j}}\right|_{\bar{x}} \dot{\bar{\varphi}}_{2j}$$

with

$$\left.\frac{\partial m_{21}}{\partial \theta_2}\right|_{\bar{x}} = -[(\frac{1}{2}\lambda_2 L_2 + m_p)L_1 L_2 + \lambda_2 \sum_{k=1}^{M} \psi_{1k}\bar{\varphi}_{1k} \sum_{k=1}^{M} \bar{\varphi}_{2k} K_{2k}] \sin(\bar{\theta}_2 + \bar{\alpha}_{1e}) -$$

$$\lambda_2 L_1 \sum_{k=1}^{M} \bar{\varphi}_{2k} K_{2k} \cos(\bar{\theta}_2 + \bar{\alpha}_{1e})$$

$$\left.\frac{\partial m_{21}}{\partial \varphi_{1j}}\right|_{\bar{x}} = \left.\frac{\partial m_{21}}{\partial \theta_2} \bullet \frac{\partial \alpha_{1e}}{\partial \varphi_{1j}}\right|_{\bar{x}} + \lambda_2 \psi_{1j} \sum_{k=1}^{M} \bar{\varphi}_{2k} K_{2k} \cos(\bar{\theta}_2 + \bar{\alpha}_{1e})$$

$$\left.\frac{\partial m_{21}}{\partial \varphi_{2j}}\right|_{\bar{x}} = \lambda_2 K_{2j}[\sum_{k=1}^{M} \psi_{1k}\bar{\varphi}_{1j} \cos(\bar{\theta}_2 + \bar{\alpha}_{1e}) - L_1 \sin(\bar{\theta}_2 + \bar{\alpha}_{1e})]$$

$$\tilde{a}_{22} = \sum_{j=1}^{M} \left.\frac{\partial m_{22}}{\partial \varphi_{2j}}\right|_{\bar{x}} \dot{\bar{\varphi}}_{2j}$$

with

$$\left.\frac{\partial m_{22}}{\partial \varphi_{2j}}\right|_{\bar{x}} = 2\lambda_2 \sum_{k=1}^{M} \bar{\varphi}_{2k} N_{2jk} + 2m_p \psi_{2j} \sum_{k=1}^{M} \psi_{2k} \bar{\varphi}_{2i}$$

$$\tilde{a}_{23} = 0.0$$

$$\tilde{a}_{24} = 0.0$$

$$\tilde{a}_{25i} = \left.\frac{\partial m_{25i}}{\partial \theta_2}\right|_{\bar{x}} \dot{\bar{\theta}}_2 + \sum_{j=1}^{M} \left.\frac{\partial m_{25i}}{\partial \varphi_{1j}}\right|_{\bar{x}} \dot{\bar{\varphi}}_{1j} + \sum_{j=1}^{M} \left.\frac{\partial m_{25i}}{\partial \varphi_{2j}}\right|_{\bar{x}} \dot{\bar{\varphi}}_{2j} \qquad (i=1, \ldots, M)$$

with

$$\left.\frac{\partial m_{25i}}{\partial \theta_2}\right|_{\bar{x}} = -\psi_{1i}[(\frac{1}{2}\lambda_2 L_2 + m_p)L_2 \sin(\bar{\theta}_2 + \bar{\alpha}_{1e}) - (\lambda_2 \sum_{k=1}^{M} \bar{\varphi}_{2k} K_{2k} + m_p \sum_{k=1}^{M} \psi_{2k} \bar{\varphi}_{2k}) \cos(\bar{\theta}_2 + \bar{\alpha}_{1e})]$$

$$\left.\frac{\partial m_{25i}}{\partial \varphi_{1j}}\right|_{\bar{x}} = \frac{\partial m_{25i}}{\partial \theta_2} \bullet \left.\frac{\partial \alpha_{1e}}{\partial \varphi_{1j}}\right|_{\bar{x}} + \left.\frac{\partial}{\partial \varphi_{1j}}(\frac{1}{\eta_1})\right|_{\bar{x}} \psi'_{1i}[I_{h2} + \lambda_2 \sum_{k=1}^{M}\sum_{l=1}^{M} \bar{\varphi}_{2k}\bar{\varphi}_{2l} N_{2kl} + (\frac{1}{3}\lambda_2 L_2 + m_p)L_2^2 + I_p]$$

$$\left.\frac{\partial m_{25i}}{\partial \varphi_{2j}}\right|_{\bar{x}} = -\psi_{1i}(\lambda_2 K_{2j} + m_p \psi_{2j}) \sin(\bar{\theta}_2 + \bar{\alpha}_{1e}) + \frac{2}{\eta_1}\lambda_2 \psi'_{1i} \sum_{k=1}^{M} \bar{\varphi}_{2k} N_{2jk}$$

$$\tilde{a}_{26i} = \sum_{j=1}^{M} \left.\frac{\partial m_{26i}}{\partial \varphi_{2j}}\right|_{\bar{x}} \dot{\bar{\varphi}}_{2j} \qquad (i=1, \ldots, M)$$

with

$$\left.\frac{\partial m_{26i}}{\partial \varphi_{2j}}\right|_{\bar{x}} = \left.\frac{\partial}{\partial \varphi_{2j}}(\frac{1}{\eta_2})\right|_{\bar{x}} I_p \psi'_{2i}$$

$$\tilde{a}_{31} = 0.0$$

$$\tilde{a}_{32} = 0.0$$

$$\tilde{a}_{33} = 0.0$$

$$\tilde{a}_{34} = 0.0$$

$$\tilde{a}_{35i} = 0.0 \qquad (i=1, \ldots, M)$$

$$\tilde{a}_{36i} = 0.0 \qquad (i=1, \ldots, M)$$

$$\tilde{a}_{41} = 0.0$$

$$\tilde{a}_{42} = 0.0$$

$$\tilde{a}_{43} = 0.0$$

$$\tilde{a}_{44} = 0.0$$

$$\tilde{a}_{45i} = \sum_{j=1}^{M} \left.\frac{\partial m_{45i}}{\partial \varphi_{1j}}\right|_{\bar{x}} \dot{\bar{\varphi}}_{1j} \qquad (i=1, \ldots, M)$$

with

$$\left.\frac{\partial m_{45i}}{\partial \varphi_{1j}}\right|_{\bar{x}} = \left.\frac{\partial}{\partial \varphi_{1j}}\left(\frac{1}{\eta_1}\right)\right|_{\bar{x}} J_2 \psi'_{1i}$$

$$\tilde{a}_{46i} = 0.0 \qquad (i=1, \ldots, M)$$

$$\tilde{a}_{51n} = \left.\frac{\partial m_{51n}}{\partial \theta_2}\right|_{\bar{x}} \dot{\bar{\theta}}_2 + \sum_{j=1}^{M} \left.\frac{\partial m_{51n}}{\partial \varphi_{1j}}\right|_{\bar{x}} \dot{\bar{\varphi}}_{1j} + \sum_{j=1}^{M} \left.\frac{\partial m_{51n}}{\partial \varphi_{2j}}\right|_{\bar{x}} \dot{\bar{\varphi}}_{2j} \qquad (n=1, \ldots, M)$$

with

$$\left.\frac{\partial m_{51n}}{\partial \theta_2}\right|_{\bar{x}} = -\psi_{1n}[(\tfrac{1}{2}\lambda_2 L_2 + m_p)L_2 \sin(\bar{\theta}_2 + \bar{\alpha}_{1e}) + (\lambda_2 \sum_{k=1}^{M} \bar{\varphi}_{2k} K_{2k} + m_p \sum_{k=1}^{M} \psi_{2k}\bar{\varphi}_{2k})$$
$$\cos(\bar{\theta}_2 + \bar{\alpha}_{1e})] - \frac{1}{\eta_1}\psi'_{1n}\{[(\tfrac{1}{2}\lambda_2 L_2 + m_p)L_1 L_2 + \lambda_2 \sum_{k=1}^{M} \psi_{1k}\bar{\varphi}_{1k} \sum_{k=1}^{M} \bar{\varphi}_{2k} K_{2k}]$$
$$\sin(\bar{\theta}_2 + \bar{\alpha}_{1e}) + \lambda_2 (L_1 \sum_{k=1}^{M} \bar{\varphi}_{2k} K_{2k} - \tfrac{1}{2} L_2^2 \sum_{k=1}^{M} \psi_{1k}\bar{\varphi}_{1k})\cos(\bar{\theta}_2 + \bar{\alpha}_{1e})\}$$

$$\left.\frac{\partial m_{51n}}{\partial \varphi_{1j}}\right|_{\bar{x}} = \frac{\partial m_{51n}}{\partial \theta_2} \bullet \left.\frac{\partial \alpha_{1e}}{\partial \varphi_{1j}}\right|_{\bar{x}} + \left.\frac{\partial}{\partial \varphi_{1j}}\left(\frac{1}{\eta_1}\right)\right|_{\bar{x}} \psi'_{1n}\{I_{h2} + I_{r2} + I_p + J_2 + (\tfrac{1}{3}\lambda_2 L_2 + m_p)L_2^2 +$$
$$+[(\tfrac{1}{2}\lambda_2 L_2 + m_p)L_1 L_2 + \lambda_2 \sum_{k=1}^{M} \psi_{1k}\bar{\varphi}_{1k} \sum_{k=1}^{M} \bar{\varphi}_{2k} K_{2k}]\cos(\bar{\theta}_2 + \bar{\alpha}_{1e}) - \lambda_2 (L_1 \sum_{k=1}^{M} \bar{\varphi}_{2k} K_{2k} -$$
$$\tfrac{1}{2} L_2^2 \sum_{k=1}^{M} \psi_{1k}\bar{\varphi}_{1k})\sin(\bar{\theta}_2 + \bar{\alpha}_{1e}) + \lambda_2 \sum_{k=1}^{M}\sum_{l=1}^{M} \bar{\varphi}_{2k}\bar{\varphi}_{2l} N_{2kl}\} + \frac{1}{\eta_1}\psi'_{1n}\psi_{1j}\lambda_2[\sum_{k=1}^{M} \bar{\varphi}_{2k} K_{2k}$$
$$\cos(\bar{\theta}_2 + \bar{\alpha}_{1e}) + \tfrac{1}{2} L_2^2 \sin(\bar{\theta}_2 + \bar{\alpha}_{1e})]$$

$$\left.\frac{\partial m_{51n1}}{\partial \varphi_{2j}}\right|_{\bar{x}} = -\psi_{1n}(\lambda_2 K_{2j} + m_p \varphi_{2j})\sin(\bar{\theta}_2 + \bar{\alpha}_{1e}) + \frac{1}{\eta_1}\psi'_{1n}[\lambda_2 K_{2i} \sum_{k=1}^{M} \psi_{1k}\bar{\varphi}_{1j}\cos(\bar{\theta}_2 + \bar{\alpha}_{1e}) -$$
$$\lambda_2 L_1 K_{2j}\sin(\bar{\theta}_2 + \bar{\alpha}_{1e}) + 2\lambda_2 \sum_{k=1}^{M} \bar{\varphi}_{2k} N_{2jk}]$$

$$\tilde{a}_{52n} = \left.\frac{\partial m_{52n}}{\partial \theta_2}\right|_{\bar{x}} \dot{\bar{\theta}}_2 + \sum_{j=1}^{M} \left.\frac{\partial m_{52n}}{\partial \varphi_{1j}}\right|_{\bar{x}} \dot{\bar{\varphi}}_{1j} + \sum_{j=1}^{M} \left.\frac{\partial m_{52n}}{\partial \varphi_{2j}}\right|_{\bar{x}} \dot{\bar{\varphi}}_{2j} \qquad (n=1, \ldots, M)$$

with

$$\left.\frac{\partial m_{52n}}{\partial \theta_2}\right|_{\bar{x}} = -\psi_{1n}[(\tfrac{1}{2}\lambda_2 L_2 + m_p)L_2 \sin(\bar{\theta}_2 + \bar{\alpha}_{1e}) + (\lambda_2 \sum_{k=1}^{M} \bar{\varphi}_{2k} K_{2k} + m_p \sum_{k=1}^{M} \psi_{2k}\bar{\varphi}_{2k})$$
$$\cos(\bar{\theta}_2 + \bar{\alpha}_{1e})]$$

$$\left.\frac{\partial m_{52n}}{\partial \varphi_{1j}}\right|_{\bar{x}} = \frac{\partial m_{52n}}{\partial \theta_2} \bullet \left.\frac{\partial \alpha_{1e}}{\partial \varphi_{1j}}\right|_{\bar{x}} + \left.\frac{\partial}{\partial \varphi_{1j}}\left(\frac{1}{\eta_1}\right)\right|_{\bar{x}} \psi'_{1n}[I_{h2} + I_p + (\tfrac{1}{3}\lambda_2 L_2 + m_p)L_2^2 +$$
$$m_p \sum_{k=1}^{M} \psi_{2k}\bar{\varphi}_{2k} \sum_{l=1}^{M} \psi_{2l}\bar{\varphi}_{2l}$$

$$\left.\frac{\partial m_{52n}}{\partial \varphi_{2j}}\right|_{\bar{x}} = -\psi_{1n}(\lambda_2 K_{2j} + m_p \psi_{2j})\sin(\bar{\theta}_2 + \bar{\alpha}_{1e}) + \frac{2}{\eta_1}\psi'_{1n}\psi_{2j} m_p \sum_{k=1}^{M} \psi_{2k}\bar{\varphi}_{2k}$$

$$\tilde{a}_{53n} = 0.0 \qquad (n=1, \ldots, M)$$

$$\tilde{a}_{54n} = \sum_{j=1}^{M} \left.\frac{\partial m_{54n}}{\partial \varphi_{1j}}\right|_{\bar{x}} \dot{\bar{\varphi}}_{1j} \qquad (n=1, \ldots, M)$$

with

$$\left.\frac{\partial m_{54n}}{\partial \varphi_{1j}}\right|_{\bar{x}} = \left.\frac{\partial}{\partial \varphi_{1j}}\left(\frac{1}{\eta_1}\right)\right|_{\bar{x}} \psi'_{1n} J_2$$

$$\tilde{a}_{55ni} = \left.\frac{\partial m_{55ni}}{\partial \theta_2}\right|_{\bar{x}} \dot{\bar{\theta}}_2 + \sum_{j=1}^{M} \left.\frac{\partial m_{55ni}}{\partial \varphi_{1j}}\right|_{\bar{x}} \dot{\bar{\varphi}}_{1j} + \sum_{j=1}^{M} \left.\frac{\partial m_{55ni}}{\partial \varphi_{2j}}\right|_{\bar{x}} \dot{\bar{\varphi}}_{2j} \qquad (i=1,...,M; n=1,...,M)$$

with

$$\left.\frac{\partial m_{55ni}}{\partial \theta_2}\right|_{\bar{x}} = \frac{1}{\eta_1}(\psi_{1i}\psi'_{1n} + \psi'_{1i}\psi_{1n})[(\frac{1}{2}\lambda_2 L_2 + m_p)L_2 \sin(\bar{\theta}_2 + \bar{\alpha}_{1e}) + (\lambda_2 \sum_{j=1}^{M} \bar{\varphi}_{2j} K_{2j} + m_p \sum_{k=1}^{M} \psi_{2k}\bar{\varphi}_{2k})\cos(\bar{\theta}_2 + \bar{\alpha}_{1e})]$$

$$\left.\frac{\partial m_{55ni}}{\partial \varphi_{1j}}\right|_{\bar{x}} = \left.\frac{\partial m_{55ni}}{\partial \theta_2} \bullet \frac{\partial \alpha_{1e}}{\partial \varphi_{1j}}\right|_{\bar{x}} + \left.\frac{\partial}{\partial \varphi_{1i}}\left(\frac{1}{\eta_1^2}\right)\right|_{\bar{x}} \psi'_{1i}\psi'_{1n}[I_{h2} + I_{r2} + I_p + J_2 + (\frac{1}{3}\lambda_2 L_2 + m_p)L_2^2 + \lambda_2 \sum_{k=1}^{M}\sum_{l=1}^{M} \bar{\varphi}_{2k}\bar{\varphi}_{2l} N_{2kl} + m_p \sum_{k=1}^{M} \psi_{2k}\bar{\varphi}_{2k} \sum_{l=1}^{M} \psi_{2l}\bar{\varphi}_{2l}] + \left.\frac{\partial}{\partial \varphi_{1j}}\left(\frac{1}{\eta_1}\right)\right|_{\bar{x}} (\psi_{1i}\psi'_{1n} + \psi'_{1i}\psi_{1n})$$
$$[(\frac{1}{2}\lambda_2 L_2 + m_p)L_2 \cos(\bar{\theta}_2 + \bar{\alpha}_{1e}) - (\lambda_2 \sum_{j=1}^{M} \bar{\varphi}_{2j} K_{2j} + m_p \sum_{k=1}^{M} \psi_{2k}\bar{\varphi}_{2k})\sin(\bar{\theta}_2 + \bar{\alpha}_{1e})]$$

$$\left.\frac{\partial m_{55ni}}{\partial \varphi_{2j}}\right|_{\bar{x}} = \frac{2}{\eta_1^2}\psi'_{1i}\psi'_{1n}(\lambda_2 \sum_{k=1}^{M} \bar{\varphi}_{2k} N_{2jk} + m_p \psi_{2l} \sum_{k=1}^{M} \psi_{21k}\bar{\varphi}_{21k}) - \frac{1}{\eta_1}(\psi_{1i}\psi'_{1n} + \psi'_{1i}\psi_{1n}) \cdot (\lambda_2 K_{2j} + m_p \psi_{2j})\sin(\bar{\theta}_2 + \bar{\alpha}_{1e})$$

$$\tilde{a}_{56ni} = \left.\frac{\partial m_{56ni}}{\partial \theta_2}\right|_{\bar{x}} \dot{\bar{\theta}}_2 + \sum_{j=1}^{M} \left.\frac{\partial m_{56ni}}{\partial \varphi_{1j}}\right|_{\bar{x}} \dot{\bar{\varphi}}_{1j} + \sum_{j=1}^{M} \left.\frac{\partial m_{56ni}}{\partial \varphi_{2j}}\right|_{\bar{x}} \dot{\bar{\varphi}}_{2j} \qquad (i=1,...,M; n=1,...,M)$$

with

$$\left.\frac{\partial m_{56ni}}{\partial \theta_2}\right|_{\bar{x}} = -(\lambda_2 K_{2i} + m_p \psi_{2i})\psi_{1n}\sin(\bar{\theta}_2 + \bar{\alpha}_{1e})$$

$$\left.\frac{\partial m_{56ni}}{\partial \varphi_{1j}}\right|_{\bar{x}} = \left.\frac{\partial m_{56ni}}{\partial \theta_2} \bullet \frac{\partial \alpha_{1e}}{\partial \varphi_{1j}}\right|_{\bar{x}} + \left.\frac{\partial}{\partial \varphi_{1j}}\left(\frac{1}{\eta_1}\right)\right|_{\bar{x}} \psi'_{1n}(\lambda_2 M_{2i} + m_p L_2 \psi_{2i} + \frac{1}{\eta_2}\psi'_{2i} I_p)$$

$$\left.\frac{\partial m_{56ni}}{\partial \varphi_{2j}}\right|_{\bar{x}} = \left.\frac{\partial}{\partial \varphi_{2j}}\left(\frac{1}{\eta_2}\right)\right|_{\bar{x}} \frac{1}{\eta_1} I_p \psi'_{2i}\psi'_{1n}$$

$$\tilde{a}_{61n} = \left.\frac{\partial m_{61n}}{\partial \theta_2}\right|_{\bar{x}} \dot{\bar{\theta}}_2 + \sum_{j=1}^{M} \left.\frac{\partial m_{61n}}{\partial \varphi_{1j}}\right|_{\bar{x}} \dot{\bar{\varphi}}_{1j} + \sum_{j=1}^{M} \left.\frac{\partial m_{61n}}{\partial \varphi_{2j}}\right|_{\bar{x}} \dot{\bar{\varphi}}_{2j} \qquad (n=1, ..., M)$$

with

$$\left.\frac{\partial m_{62n1}}{\partial \theta_2}\right|_{\bar{x}} = -(\lambda_2 K_{2n} + m_p \psi_{2n})L_1 \sin(\bar{\theta}_2 + \bar{\alpha}_{1e}) + \lambda_2 K_{2n} \sum_{k=1}^{M} \psi_{1k}\bar{\varphi}_{1k}\cos(\bar{\theta}_2 + \bar{\alpha}_{1e})$$

$$\left.\frac{\partial m_{61n}}{\partial \varphi_{1j}}\right|_{\bar{x}} = \left.\frac{\partial m_{61n}}{\partial \theta_2} \bullet \frac{\partial \alpha_{1e}}{\partial \varphi_{1j}}\right|_{\bar{x}} + \lambda_2 \psi_{1j} K_{2n}\sin(\bar{\theta}_2 + \bar{\alpha}_{1e})$$

$$\left.\frac{\partial m_{61n}}{\partial \varphi_{2j}}\right|_{\bar{x}} = \left.\frac{\partial}{\partial \varphi_{2j}}\left(\frac{1}{\eta_2}\right)\right|_{\bar{x}} I_p \psi'_{2n}$$

$$\tilde{a}_{62n} = \sum_{j=1}^{M} \left.\frac{\partial m_{62n}}{\partial \varphi_{2j}}\right|_{\bar{x}} \ddot{\varphi}_{2j} \qquad (n=1, \ldots, M)$$

with

$$\left.\frac{\partial m_{62n}}{\partial \varphi_{2j}}\right|_{\bar{x}} = \left.\frac{\partial}{\partial \varphi_{2j}}\left(\frac{1}{\eta_2}\right)\right|_{\bar{x}} \psi'_{2n} I_p$$

$$\tilde{a}_{63n} = 0.0 \qquad (n=1, \ldots, M)$$

$$\tilde{a}_{64n} = 0.0 \qquad (n=1, \ldots, M)$$

$$\tilde{a}_{65ni} = \left.\frac{\partial m_{65ni}}{\partial \theta_2}\right|_{\bar{x}} \ddot{\theta}_2 + \sum_{j=1}^{M} \left.\frac{\partial m_{65ni}}{\partial \varphi_{1j}}\right|_{\bar{x}} \ddot{\varphi}_{1j} + \sum_{j=1}^{M} \left.\frac{\partial m_{65ni}}{\partial \varphi_{2j}}\right|_{\bar{x}} \ddot{\varphi}_{2j} \qquad (i=1,\ldots,M;n=1,\ldots,M)$$

with

$$\left.\frac{\partial m_{65ni}}{\partial \theta_2}\right|_{\bar{x}} = -(\lambda_2 K_{2n} + m_p \psi_{2n}) \psi_{1i} \sin(\bar{\theta}_2 + \bar{\alpha}_{1e})$$

$$\left.\frac{\partial m_{65ni}}{\partial \varphi_{1j}}\right|_{\bar{x}} = \frac{\partial m_{65ni}}{\partial \theta_2} \bullet \left.\frac{\partial \alpha_{1e}}{\partial \varphi_{1j}}\right|_{\bar{x}} + \left.\frac{\partial}{\partial \varphi_{1j}}\left(\frac{1}{\eta_1}\right)\right|_{\bar{x}} \psi'_{1i}(\lambda_2 M_{2n} + m_p L_2 \psi_{2n} + \frac{1}{\eta_2}\psi'_{2n} I_p)$$

$$\left.\frac{\partial m_{65ni}}{\partial \varphi_{2j}}\right|_{\bar{x}} = \left.\frac{\partial}{\partial \varphi_{2j}}\left(\frac{1}{\eta_2}\right)\right|_{\bar{x}} \frac{1}{\eta_1} I_p \psi'_{1i} \psi'_{2n}$$

$$\tilde{a}_{66ni} = \sum_{j=1}^{M} \left.\frac{\partial m_{66ni}}{\partial \varphi_{2j}}\right|_{\bar{x}} \ddot{\varphi}_{2j} \qquad (i=1,\ldots,M;n=1,\ldots,M)$$

with

$$\left.\frac{\partial m_{66ni}}{\partial \varphi_{2j}}\right|_{\bar{x}} = \left.\frac{\partial}{\partial \varphi_{2j}}\left(\frac{1}{\eta_2^2}\right)\right|_{\bar{x}} \psi'_{2n} \psi'_{2i} I_p$$

PROOF OF THE INTERNAL POWER BALANCING PROPERTY FOR MODIFIED STATE TRANSFORMATION

With the state transformation of

$$\gamma = R_2 R_1 z,$$

system (6.5) becomes

$$\dot{\gamma} = \tilde{A}\gamma + \tilde{B}u \tag{D.1a}$$

$$y = \tilde{C}\gamma \tag{D.1b}$$

where

$$\tilde{A} = \begin{bmatrix} A_1 & 0 & \cdots & 0 \\ 0 & A_2 & \cdots & 0 \\ \vdots & \vdots & \ddots & \vdots \\ 0 & 0 & \cdots & A_n \end{bmatrix}, \quad \tilde{B} = \begin{bmatrix} B_1 \\ B_2 \\ \vdots \\ B_n \end{bmatrix}, \quad \tilde{C} = \begin{bmatrix} C_1 & C_2 & \cdots & C_n \end{bmatrix} \tag{D.2}$$

and

$$A_i = \begin{bmatrix} 0 & 1 \\ -\omega_i^2 & 0 \end{bmatrix}, \quad B_i = \begin{bmatrix} 0 \\ b_i \end{bmatrix}, \quad C_i = \begin{bmatrix} c_i & 0 \end{bmatrix}. \tag{D.3}$$

With the submatrices A_i and B_i (i=1,2, ..., n) given by (D.3), we have

$$e^{A_i\tau}B_i=\begin{bmatrix}\cos(\omega_i\tau) & \frac{1}{\omega_i}\sin(\omega_i\tau)\\ -\omega_i\sin(\omega_i\tau) & \cos(\omega_i\tau)\end{bmatrix}\begin{bmatrix}0\\ b_i\end{bmatrix}=\begin{bmatrix}\frac{b_i}{\omega_i} & 0\\ 0 & b_i\end{bmatrix}\begin{bmatrix}\sin(\omega_1\tau)\\ \cos(\omega_1\tau)\end{bmatrix}. \qquad (D.4)$$

The system power matrix P_s becomes

$$P_s=\lim_{t\to\infty}\frac{2}{t}\int_0^t e^{\tilde{A}\tau}\tilde{B}\tilde{B}^T e^{\tilde{A}^T\tau}d\tau \qquad (D.5)$$

$$=M\left(\lim_{t\to\infty}\frac{2}{t}\int_0^t\begin{bmatrix}\sin(\omega_1\tau)\\ \cos(\omega_1\tau)\\ \vdots\\ \sin(\omega_n\tau)\\ \cos(\omega_n\tau)\end{bmatrix}\begin{bmatrix}\sin(\omega_1\tau) & \cos(\omega_1\tau) & \cdots & \sin(\omega_n\tau) & \cos(\omega_n\tau)\end{bmatrix}dt\right)M^T$$

where

$$M=\text{diag}\left[\frac{b_1}{\omega_1},b_1,\cdots,\frac{b_n}{\omega_n},b_n\right].$$

According to the orthogonality of trigonometric functions, it is obvious that the limit of the integral in the brace in equation (D.5) is the identity matrix of dimension $2n$x$2n$. Therefore

$$P_s=MM^T=\text{diag}\left(\frac{b_1^2}{\omega_1^2},b_1^2,\cdots,\frac{b_n^2}{\omega_n^2},b_n^2\right).$$

Similarly we have the output power matrix P_o

$$P_o=\text{diag}\left(c_1^2,\frac{c_1^2}{\omega_1^2},\cdots,c_n^2,\frac{c_n^2}{\omega_n^2}\right).$$

Using the transformation matrix R_3 defined by equation (6.11), we see that

$$\hat{P}_s=R_3^{-1}P_sR_3^{-T}=\text{diag}\left(\frac{|b_1c_1|}{\omega_1},\frac{|b_1c_1|}{\omega_1},\cdots,\frac{|b_nc_n|}{\omega_n},\frac{|b_nc_n|}{\omega_n}\right)=R_3^TP_oR_3=\hat{P}_o \qquad (D.6)$$

which indicates the system is internally power balanced. This completes the proof.

STABILITY ANALYSIS

Using equations (7.4) and (7.6), we have

$$\begin{aligned} e(k+1) &= x_p^*(k+1) - x_p(k+1) \\ &= A_p x_p^*(k) + B_p u_p^*(k) - A_p x_p(k) - B_p u_p(k) \\ &= A_p[x_p^*(k) - x_p(k)] - B_p \tilde{K}_e C_p e(k) + B_p \tilde{K}_e C_p e(k) + B_p[u_p^*(k) - u_p(k)] \\ &= \tilde{A}_p e(k) + B_p z(k) \end{aligned}$$

where

$$\tilde{A}_p = A_p - B_p \tilde{K}_e H_p$$

$$z = u_p^*(k) - u_p(k) + \tilde{K}_e C_p e(k).$$

Therefore

$$e^T(k+1)Pe(k+1) = e^T(k)\tilde{A}_p^T P \tilde{A}_p e(k) + 2e^T(k)\tilde{A}_p^T P B_p z(k) + z^T(k) B_p^T P B_p z(k).$$

With equation (7.14c) the trace terms in ΔV given in equation (7.12) can be expressed as

$$\begin{aligned} \Delta_{trace} &= Tr\{S[K_I(k) - \tilde{K} + v(k)r^T(k)T]T^{-1}[K_I(k) - \tilde{K} + vr^T T]^T S^T]\} \\ &\quad - Tr\{[S(K_I(k) - \tilde{K})T^{-1}(K_I(k) - \tilde{K})^T S^T]\} \\ &= Tr\{S(K_I(k) - \tilde{K})T^{-1}(K_I(k) - \tilde{K})^T S^T + 2Sv_k r_k^T T T^{-1}(K_I(k) - \tilde{K})^T S^T \\ &\quad + Sv_k r_k^T T T^{-1} T r_k v_k^T S^T - S(K_I(k) - \tilde{K})^T S^T\} \end{aligned}$$

$$= Tr\{Sv_K r_k^T Tr_k v_k^T S^T + 2Sv_k r_k^T (K_I(k) - \bar{K})^T S^T\}$$

$$= Tr[Sv_k v_k^T S^T r_k^T Tr_k + 2r_k^T (K_I(k) - \bar{K})^T S^T Sv_k]$$

$$v_k^T S^T Sv_k r_k^T Tr_k + 2v_k^T S^T S(K_I(k) - \bar{K}) r_k .$$

Equation (7.12) now becomes

$$\Delta V = e^T(k)\tilde{A}_p^T P\tilde{A}_p e(k) + 2e^T(k)\tilde{A}_p^T PB_p z(k) + z^T(k)B_p^T PB_p z(k)$$

$$+v_k^T S^T Sv_k r_k^T Tr_k + 2v_k^T S^T S(K_I(k) - \bar{K}) r_k - e^T(k)Pe(k).$$

By assuming the transfer matrix $J + C_p(zI - A_p + B_p\bar{K}H_p)^{-1}B_p$ being strictly positive real, it follows that

$$\tilde{A}_p^T P\tilde{A}_p - P = -LL^T < 0$$

$$\tilde{A}_p^T PB_p = H_p - LW$$

$$W^T W = J + J^T - B_p^T PB_p$$

and

$$e^T(k)\tilde{A}_p^T P\tilde{A}_p e(k) = e^T(k)Pe(k) - e^T(k)LL^T e(k)$$

$$2e^T(k)\tilde{A}_p^T PB_p z(k) = 2e^T(k)C_p z(k) - 2e^T(k)LWz(k)$$

$$z^T(k)B_p^T PB_p z(k) = z^T(k)Jz(k) + z^T(k)J^T z(k) - z^T(k)W^T Wz(k).$$

Therefore

$$\Delta V = -(L^T e_k + Wz_k)^T (L^T e_k + Wz_k) + e_k^T Pe_k + 2e_k^T C_p z_k + 2z_k^T Jz_k +$$

$$v_k^T S^T Sv_k r_k^T Tr_k 2v_k^T S^T S(K_I(k) - \bar{K}) r_k - e_k^T Pe_k$$

Using equations (7.14f), (7.17), (7.13), and (7.14a) and defining

$$\bar{K} = [\bar{K}_e \quad S_{21} \quad S_{22}],$$

we have

$$z(k) = \bar{K}r_k - [v_k r_k^T \bar{T} + K_I(k)] r_k$$

$$= [\bar{K} - K_I(k)] r_k - v_k r_k^T \bar{T} r_k$$

or

$$[K_I(k) - \bar{K}] r_k = -z(k) - v_k r_k^T \bar{T} r_k .$$

Hence

$$\Delta V = -(L^T e_k + W z_k)^T (L^T e_k + W z_k) + 2 e_k^T C_p z_k + 2 z_k^T J z_k -$$
$$2 v_k^T S^T S z_k - v_k^T S^T S v_k r_k^T (2\bar{T} - T) r_k .$$

With the choice of $v_k = F e_k + G z_k$,

$$\Delta V = -(L^T e_k + W z_k)^T (L^T e_k + W z_k) + 2 e_k^T C_p z_k + 2 z_k^T J z_k$$
$$-2(F e_k + G z_k)^T S^T S z_k - v_k^T S^T S v_k r_k^T (2\bar{T} - T) r_k$$
$$= -(L^T e_k + W z_k)^T (L^T e_k + W z_k) - v_k^T S^T S v_k r_k^T (2\bar{T} - T) r_k$$
$$-2 z_k^T (S^T S G - J) z_k + 2 e_k^T (C_p - F^T S^T S) z_k$$

which is negative definite in $z(k)$ if

$$S^T S G > J$$

$$F = (S^T S)^{-1} C_p^{\,T}$$

and

$$2\bar{T} - T \geq 0$$

[1] Naganathan, G. and Soni, A.H., "Coupling Effects of Kinematics and Flexibility in Manipulators", *International Journal of Robotics Research*, Vol.6, No.1, 1987, pp.75-84.

[2] Huang, Y. and Lee, C.S.G., "Generalization of Newton-Euler Formulation of Dynamic Equations to Nonrigid Manipulators", *Journal of Dynamic System*, Measurement, and Control, Vol.110, 1988, pp.308-315.

[3] Marino, R. and Nicosia, S., "Singular Perturbation Techniques in the Adaptive Control of Elastic Robots", *1st IFAC Symp. on Robot Control*, 1985, pp.95-100

[4] Spong, M.W., "Modelling and Control of Elastic Joint Robots", *Journal of Dynamic System, Measurement, and Control*, Vol.109, 1987, pp.310-319.

[5] Nebot, E.M., Lee, K.F., and Brubaker, T.A., "Experiments on a Single Link Flexible Manipulator", *Proceedings of the USA-Japan Symp. on Flexible Automations*, 1988, pp.391-398

[6] Yuan, B.S., Lee, J.W., and Book, W.J., "Dynamic Analysis and Control of Lightweight Arms with a Parallel Mechanism", *Proceedings of the USA-Japan Symp. on Flexible Automations*, 1988, pp.369-374.

[7] Korolov, V.V. and Chen, Y.H., "Controller Design Robust to Frequency Variation in a One-Link Flexible Robot Arm", *Journal of Dynamic System, Measurement, and Control*, Vol.111, 1989, pp.9-14.

[8] Siciliano, B. and Book, W.J., "A Singular Perturbation Approach to Control of Lightweight Flexible Manipulators", *The International Journal of Robotics Research*, Vol.7, No.4, 1988, pp.79-90.

[9] Fan, G.W. and Castelazo, I.A., "Force Control in Flexible Manipulators", *Proceedings of the USA-Japan Symp. on Flexible Automations*, 1988, pp.361-368.

[10] Wang, W.J. and Hsu, C.F., "A Position Controller of a One-Link Flexible Robot Arm", *Journal of the Chinese Institute of Engineers*, Vol.12, No.3, 1989, pp.285-291.

[11] Cannon, R.H. and Schmitz, E., "Initial Experiments on the End-Point Control of a Flexible One-Link Robot", *The International Journal of Robotics Research*, Vol.3, 1984, pp.62-75.

[12] Carusone, J., Buchan, K.S., and D'Eleuterio, G.M.T., "End-Effector Tracking Control for Structurally Flexible Manipulators", *Proceedings of American Control Conference*, 1989, pp.1389-1396.

[13] Chassiakos, A.G. and Bekey, G.A., " Pointwise Control of a Flexible Manipulator Arm", *1st IFAC Symp. on Robot Control*, 1985, pp.181-185.

[14] Benati, M. and Morro, A., "Dynamics of Chain of Flexible Links", *Journal of Dynamic Systems, Measurement, and Control*, Vol.110, 1988, pp.410-415.

[15] Ramakrishnan, S., "Experimental Identification and Control of the Tip Position of a Flexible, Single Link Manipulator", Ph.D. Thesis, University of California, Berkeley, 1985.

[16] Hastings, G.G., "Controlling Flexible Manipulators, an Experimental Investigation", Ph.D. Thesis, Georgia Institute of Technology, 1986.

[17] Kojima, H., "Dynamic Characteristics of a One-Link Flexible Robot Arm with Variable Cross Section and Viscous Damping", *Proceedings of the USA-Japan Symp. on Flexible Automations*, 1988, pp.383-389.

[18] Oakley, C.M. and Cannon, R.H., "End-Point Control of a Two-Link Manipulator with a Very Flexible Forearm: Issues and Experiments", *Proceedings of American Control Conference*, 1989, pp.1381-1388.

[19] Chalhoub, N.G., "Control of a Leadscrew Driven Flexible Robot Arm", Ph.D. Thesis, The University of Michigan, 1986.

[20] Naganathan, G. and Soni, A.H., "Non-linear Flexibility Studies for Spatial Manipulators", *Proceedings of IEEE 1986 International Conference on Robotics and Automation.*, 1986

[21] Nicosia, S., Tomei, P., and Tornambe, A., "Dynamic Modelling of Flexible Robot Manipulators", *Proceedings of IEEE 1986 International Conference on Robotics and Automation*, 1986, pp.365-372.

[22] Low, K.H., and Vidyasagar, M., "Dynamics Study of Flexible Manipulators with Open and Closed Chain Mechanisms", *Modelling and Control of Robotic Manipulators and Manufacturing Process*, The Winter Annual Meeting of ASME, 1987, DSC-Vol.6, pp.277-286.

[23] Wang, D. and Vidyasagar, M., "Transfer Functions for a Single Flexible Link", *Proceedings of IEEE International Conference on Robotics and Automation*, Vol.2, 1989, pp.1042-1047.

[24] Bayo, E., Papadopoulos, P., and Stubbe, J., "Inverse Dynamics and Kinematics of Multi-Link Elastic Robots: An Iterative Frequency Domain Approach", *The International Journal of Robotics Research*, Vol.8, 1989, pp.49-62.

[25] Bayo, E. and Moulin, H., "An Efficient Computation of the Inverse Dynamics of Flexible Manipulators in the Time Domain", *Proceedings of 1989 IEEE International Conference on Robotics and Automation*, Vol.2, 1989, pp.710-715.

[26] Cyril, X., Angeles, J., and Misra, A.K., "Flexible-Link Robotic Manipulator Dynamics", *Proceedings of American Control Conference*, 1989, pp.2346-2351.

[27] Everett, L.J., "An Extension of Kane's Method for Deriving Equations of Motion of Flexible Manipulators", *Proceedings of IEEE International Conference on Robotics and Automation*, 1989, Vol.2, pp.716-721.

[28] Oakley, C.M. and Cannon, R.H., "Equations of Motion for an Experimental Planar Two-Link Flexible Manipulator", *Robotics Research*, Presented at the Winter Annual Meeting of the ASME, 1989, DSC-Vol.14, pp.267-278.

[29] Yuh, J., Young, T., and Baek, Y.S., "Modelling of a Flexible Link Having a Prismatic Joint in Robot Mechanism -- Experimental Verification",

Proceedings of IEEE International Conference on Robotics and Automation, 1989, Vol.2, pp.722-727.

[30] Bellezza, F., Lanari, L., and Ulivi, G., "Exact Modelling of the Flexible Slewing Link", *Proceeding of 1990 IEEE International Conference on Robotics and Automation*, 1990, pp.734-739.

[31] Cheng, L.W. and Gannon, K.P., "A Dynamic Model on a Single-Link Flexible Manipulator", *Journal of Vibration and Acoustics*, Transactions of ASME, Vol.112, 1990, pp.138-143.

[32] Chang, L.-W. and Hamilton, J.F., "The Kinematics of Robotic Manipulators with Flexible Links Using an Equivalent Rigid Link System (ERLS) Model", *Journal of Dynamic Systems, Measurement, and Control*, Vol.113, 1991, pp.48-53.

[33] Chang, L.-W. and Hamilton, J.F., "Dynamics of Robotic Manipulators with Flexible Links", *Journal of Dynamic Systems, Measurement, and Control*, Vol.113, 1991, pp.54-59.

[34] Choura, S., Jayasuriya, S., and Medick, M.A., "On the Modelling, and Open-Loop Control of a Rotating Thin Flexible Beam", *Journal of Dynamic Systems, Measurement, and Control*, Vol.113, 1991, pp.26-33.

[35] Fukuda, T. and Arakawa, A., "Decoupled Vibration Control of 3D Robotic Arm with Flexible Links", *Proceedings of the USA-Japan Symp. on Flexible Automations*, 1988, pp.415-421.

[36] Dado, M.H. and Soni, A.H., "A Dynamic Analysis Tool for Flexible Robotic Manipulators", *Proceedings of the USA-Japan Symp. on Flexible Automations*, 1988, pp.399-405.

[37] Low, K.H. and Vidyasagar, M., "A Lagrangian Formulation of the Dynamic Model for Flexible Manipulator Systems", *Journal of Dynamic Systems, Measurement, and Control*, Vol.110, 1988, pp.175-181.

[38] Lin, L.C. and Yuan, K., "A Lagrange-Euler-Assumed Modes Approach to Modeling Flexible Robotic Manipulators", *Journal of Chinese Institute of Engineers*, Vol.11, No.4, 1988, pp.335-347.

[39] Dado, M. and Soni, S., "A Generalized Approach for Forward and Inverse Dynamics of Elastic Manipulator", *Proceedings IEEE 1986 International Conference on Robotics and Automation*, 1986, pp.359-364.

[40] Yang, G.-B. and Donath, M., "Dynamic Model of a Two-Link Robot Manipulator with Both Structural and Joint Flexibility", *Symposium on Robotics*, the Winter Annual Meeting of the ASME, DSC-Vol.11, 1988, pp.37-44.

[41] Baker, W.E., Woolam, W.E., and Young, D., "Air and Internal Damping of Thin Cantilever Beams", *Int. J. Mech. Sci. Pergamon Press Ltd.*, Vol.9, 1967, pp.743-766.

[42] Zhang, W., "Internal Damping Problem in Cantilever Beam", *International Journal of Robotics and Automation*, Vol.6, No.4, 1991, pp.236-241.

[43] Kataoka, M., Ohno, S., and Suzuki, T., "Forced Torsional Vibration of a Two Degree of Freedom System with a Clearance", *Bulletin of JSME*, Vol.29, No.256, 1986, pp.3491-3498.

[44] Hunt, K.H. and Crossley, F.R.E., "Coefficient of Restitution Interpreted as Damping in Vibroimpact", *Journal of Applied Mechanics*, 1975, pp.440-445.

[45] Moore, B., "Principal Component Analysis in Linear Systems: Controllability, Observability, and Model Reduction", *IEEE Transactions on Automatic Control*, Vol. AC-26, No.1, 1981, pp.17-32.

[46] Shokoohi, S., Silverman, L.M., and Van Dooren, P.M., "Linear Time-Variable Systems: Balancing and Model Reduction", *IEEE Transactions on Automatic Control*, Vol.AC-28, No.8, 1983, pp.810-822.

[47] Kung, S.Y. and Lin, D.W., "Optimal Hankel-Norm Model Reductions: Multivariable Systems", *IEEE Transactionson Automatic Control*, Vol.AC-26, No.4, 1981, pp.832-852.

[48] Tsujisawa, T. and Book, W.J., "A Reduced Order Model Derivation for Lightwieght Arms with a Parallel Mechanism", *Proceedings of IEEE International Conference on Robotics and Automation*, 1989, pp.728-735.

[49] Hastings, G.G., Dorsey, J.F., and Book, W.J., "Application of Balanced Realizations to Estimate Model Order Requirements for Flexible Manipulators", *Modelling and Control of Robotic Manipulators and Manufacturing Processes*, Presented at the Winter Annual Meeting of the ASME, DSC-Vol.6, 1987, pp.323-327.

[50] Tsujisawa, T. and Book, W.J., "A Reduced Order Model Derivation for Lightweight Arms with a Parallel Mechanism", *Proceedings of IEEE International Conference on Robotics and Automation*, Vol.2, 1989, pp.728-735.

[51] Fowler, T.B., "A Time-Domain Solution Approach to Model Reduction", *IEEE Transactions on Circuits and Systems*, Vol.35, No.8, 1988, pp.1020-1024.

[52] Safonov, M.G., Chiang, R.Y., and Limebeer, D.J.N., "Optimal Hankel Model Reduction for Nonminimal Systems", *IEEE Transactions on Automatic Control*, Vol.35, No.4, 1990, pp.496-502.

[53] Rovner, D.M. and Cannon, R.H., "Experiments toward On-Line Identification and Control of a Very Flexible One-Link Manipulator", *The International Journal of Robotics Research*, Vol.6, No.4, 1987, pp.3-19

[54] Barbieri, E. and Figueroa, F., "Optimal Strategies for Self Motion Control in Redundant Flexible Manipulators", *Robotics Research*, Presented at the Winter Annual Meeting of the ASME, DSC-Vol.14, 1989, pp.255-260.

[55] Yuan, B.S., Huggins, J.D., and Book, W.J., "Small Motion Experiments on a Large Flexible Arm with Strain Feedback", *Proceedings of 1989 American Control Conference*, 1989, pp.2091-2095.

[56] Schmitz, E., "Modelling and Control of a Planar Manipulator with an Elastic Forearm", *Proceedings of IEEE International Conference on Robotics and Automation*, Vol.2, 1989, pp.894-899.

[57] Wang, W.-S. and Liu, C.-H., "Implementation of H_2 Optimal Controller for a Single Link Flexible-Joint Robot", *Proceedings of IEEE International Conference on Robotics and Automation*, 1990, pp.1438-1443.

[58] Cetinkunt, S. and Wu, S.J., "Output Predictive Control of a Single-Link Flexible Arm", *International Journal of Control*, Vol.53, No.2, 1991, pp.311-333.

[59] Alder, L.J. and Rock, S.M., "Control of a Flexible Robotic Manipulator with Unknown Payload Dynamics: Inial Experiments", *Modelling and Control of Compliant and Rigid Motion Systems*, Presented at the Winter Annual Meeting of the ASME, DSC-Vol. 31, 1991, pp.61-66.

[60] Nathan, P.J. and Singh, S.N., "Variable Structure Control of a Robotic Arm with Flexible Links", *Proceedings of IEEE International Conference on Robotics and Automation*, Vol.2, 1989, pp.882-887.

[61] Meldrum, D.R. and Balas, M.J., "Direct Adaptive Control of Flexible Remote Manipulator Arm", *Robotics and Manufacturing Automation*, Presented at the Winter Annual Meeting of the ASME, 1985, pp.115-119.

[62] Yuan, B.-S. and Book, W.J., "A Robust Scheme for Direct Adaptive Control of Flexible Arms", *Modelling and Control of Robotic Manipulators and Manufacturing Processes*, Presented at the Winter Annual Meeting of the ASME, DSC-Vol.6, 1987, pp.261-268.

[63] Yuan, B.S., Book, W.J., and Huggins, J.D., "Decentralized Adaptive Control of a Two Degree of Freedom Flexible Arm", *Robotics Research*, Presented at the Winter Annual Meeting of the ASME, DSC-Vol.14, 1989, pp.247-253.

[64] Book, W.J. and Lee, S.H., "Vibration Control of a Large Flexible Manipulators by a Small Robotic Arm", *Proceedings of American Control Conference*, 1989, pp.1377-1380.

[65] Lee, J.D., Haynes, L.S., Wang, B.L., and Tsai, K.-H., "Control of Flexible Robot Arm", *Modelling and Control of Robotic Manipulators and Manufacturing Processes*, Presented at the Winter Annual Meeting of the ASME, DSC-Vol.6, 1987, pp.241-251.

[66] Lin, S.-H., Tosunoglu, S., and Tesar, D., "Control of Multi-Link Robotic Manipulators with Compliant Joints", *Robotics Research*, Presented at the Winter Annual Meeting of the ASME, DSC-Vol.14, 1989, pp.299-307.

[67] Lin, L.-C. and Yuan, K., "Feedback Linearization and Linear Stabilization Control of Flexible Robots", *Journal of the Chinese Institute of Engineers*, Vol.13, No.1, 1990, pp.11-24.

[68] Yuan, King and Lin, L.-C., "Motor-Based Control of Manipulators with Flexible Joints and Links", *Proceedings of 1990 IEEE International Conference on Robotics and Automation*, 1990, pp.1809-1814.

[69] Rattan, K.S., Feliu, V., and Brown, H.B., "Tip Position Control of Flexible Arms Using a Control Law Partitioning Scheme", *Proceedings of 1990 IEEE International Conference on Robotics and Automation*, 1990, pp.1803-1808.

[70] Siciliano, B., Calise, A.J., and Prasad, J.V.R., "Two-Time Scale Stabilization of a Flexible Arm with Output Feedback", *Proceedings of American Control Conference*, 1989, pp.2377-2382.

[71] Mills, J.K., "Control of Robotic Manipulators with Flexible Joints during Constrained Motion Task Execution", *Proceedings of the 26th Conference on Decision and Control*, 1989, pp.1676-1681.

[72] Montgomery, R.C., Ghosh, D., and Kenny, S., "Analytic and Simulation Studies on the Use of Torque-Wheel Actuators for the Control of Flexible Robotic Arms", *Modelling and Control of Compliant and Rigid Motion Systems*, Presented at the Winter Annual Meeting of the ASME, DSC-Vol.31, 1991, pp.55-60.

[73] Jumarie, G., "Tracking Control of Flexible Robot Manipulators with Active Inertia Links", *Robotica*, International Journal of Information Education and Research in Robotics and Artificial Intelligence, Vol.8, 1990, pp.73-80.

[74] Tzou, H.S. and Wan G.C., "Distributed Structural Dynamics Control of Flexible Manipulators - I. Structural Dynamics and Distributed Viscoelastic Actuator", *Computers and Structures*, Vol. 35, No.6, 1990, pp.669-677.

[75] Tzou, H.S. and Wan G.C., "Distributed Structural Dynamics Control of Flexible Manipulators - II. Distributed Sensor and Active Electromechanical Actuator", *Computers and Structures*, Vol. 35, No.6, 1990, pp.679-687.

[76] Tsujio, S., "A New Approach to Inverse Dynamics of Flexible Manipulator Arms", *Proceedings of the USA-Japan Symp. on Flexible Automations*, 1988, pp.375-382.

[77] Zalucky, A. and Hardt, D.E., "Active Control of Robot Structure Deflections", *Robotics Research and Advanced Applications*, Presented at the Winter Annual Meeting of the ASME, 1982, pp.83-100.

[78] Asada, H., Ma, Z.-D., and Park, J.-H., "Inverse Dynamics of Flexible Robot Arms for Trajectory Control", *Modelling and Control of Robotic Manipulators and Manufacturing Processes*, The Winter Annual Meeting of the ASME, DSC-Vol.6, 1987, pp.329-336.

[79] Asada, H. and Ma, Z.-D., "Inverse Dynamics of Flexible Robot Arms - Part I: Modelling, Linearization and analysis", *Symposium on Robotics*, The Winter Annual Meeting of the ASME, DSC-Vol.11, 1988, pp.45-60.

[80] Asada, H., Ma, Z.-D., "Inverse Dynamics of Flexible Robots", *Proceedings of American Control Conference*, 1989, pp.2352-2359.

[81] Asada, H., Ma, Z.-D., and Park, J.-H., "Inverse Dynamics of Flexible Robots: Feasible Solutions and Arm Design Guidelines", *Robotics Research*, Presented at the Winter Annual Meeting if the ASME, DSC-Vol.14, 1989, pp.279-287.

[82] Asada, H., Ma, Z.-D., and Tokumaru, H., "Inverse Dynamics of Flexible Robot Arms: Modelling and Computation for Trajectory Control", *Journal of Dynamic Systems, Measurement, and Control*, Vol.112, 1990, pp.177-185.

[83] Wang, D. and Vidyasagar, M.,"Passive Control of a Single Flexible Link", *Proceedings of IEEE International Conference on Robotics and Automation*, 1990, pp.1432-1437.

[84] Wang, D. and Vidyasagar, M., "Control of a Class of Manipulators with a Single Flexible Link - Part I: Feedback Linearization", *Journal of Dynamic Systems, Measurement, and Control*, Vol.113, 1991, pp.655-661.

[85] Wang, D. and Vidyasagar, M., "Control of a Class of Manipulators with a Single Flexible Link - Part II: Observer-Controller Stabilization", *Journal of Dynamic Systems, Measurement, and Control*, Vol.1991,113, pp.662-668.

[86] Choi, S.B., Thompson, B.S., and Gandhi, M.V., "Modelling and Control of a Single-Link Flexible Manipulator Featuring a Graphite-Epoxy Composite Arm", *Proceedings of 1990 IEEE International Conference on Robotics and Automation*, 1990, pp.1450-1455.

[87] Castelazo, I.A. and Lee, H., "Nonlinear Compensation for Flexible Manipulators", *Journal of Dynamic systems, Measurement, and Control*, Vol.112, 1990, pp.62-68.

[88] Yurkovich, S., Tzes, A.P., Lee, I., and Hillsley, K.L., "Control and System Identification of a Two-Link Flexible Manipulator", *Proceedings of 1990 IEEE International Conference on Robotics and Automation*, 1990, pp.1626-1631.

[89] Hashimoto, H., Hasegawa, K., and Harashima, F., "A Discrete-Model Reference Adaptive Control of a Flexible Arm Using End-Point Position Sensing-Considerations on Sampling Period and Adaptation", *Proceedings of the USA-Japan Symp. on Flexible Automations*, 1988, pp.407-414.

[90] Morimoto, Y., Inamura, T., and Mizoguchi, K., "Dynamic Control of a Flexible Robot Arm by Using Experimental Modal Analysis", *Modelling and Control of Robotic Manipulators and Manufacturing Processes*, the Winter Annual Meeting of the ASME, DSC-Vol.6, 1987, pp.337-343.

[91] Krzyzak, A. and Sasiadek, J., "Displacement Identification of Flexible Manipulator Arm Using Hammerstein Model", *Proceedings of American Control Conference*, 1989, pp.2360-2363.

[92] Chen, J.-S. and Meng, C.-H., "Experiments on the Payload-Adaptive of a Flexible One-Link Manipulator with Unknown Payload", *Proceedings of 1990 IEEE International Conference on Robotics and Automation*, 1990, pp.1614-1619.

[93] Cetinkunt, S. and Wu, S., "Tip Position Control of a Flexible One Arm Robot with Predictive Adaptive Output Feedback Implemented with Lattice Filter Parameter Identifier", *Proceedings of 1990 IEEE International Conference on Robotics and Automation*, 1990, pp.1620-1625.

[94] Whitney, D.E., Book, W.J., and Lynch, P.M., "Design and Control Considerations for Industrial and Space Manipulators", *Proceedings of the Joint Automatic Control Conference*, 1974, pp.591-598.

[95] Chretien, J.P., "SECAFLEX: An Experimental Set-up for the study of Active Control of Flexible Structures", *Proceedings of American Control Conference*, 1989, pp.1397-1402.

[96] Vidyasagar, M. and Morris, K.A., "An Analysis of Euler-Bernoulli Beams from the Standpoint of Controller Design", *Modelling and Control of Robotic Manipulators and Manufacturing Processes*, Presented at the Winter Annual Meeting of the ASME, DSC-Vol.6, 1987, pp.297-305.

[97] Morris, K.A. and Vidyasagar, M., "Modelling of Beam vibrations for the Purpose of Controller Design", *Symposium on Robotics*, the Winter Annual Meeting of ASME, DSC-Vol.11, 1988, pp.17-26.

[98] Rivin, E.I., Holbrook, R., Bhatt, S., and Bhattacharyya, A., "A High Stiffness/Low Inertia Revolute Link for Robotic Manipulators", *Modelling and Control of Robotic Manipulators and Manufacturing Process*, The Winter Annual Meeting of ASME, DSC-Vol.6, 1987, pp.253-259.

[99] Nebot, E.M., Lee, G.K.F., and Brubaker, T., "Experimental Test-Bed for a Single Link Flexible Manipulator", *Proceedings of American Control Conference*, 1989, pp.2096-2101.

[100] Cetinkunt, S. and Book, W.J., "Performance Limitations of Joint Variable-Feedback Controllers due to Manipulator Structural Flexibility", *IEEE Transactions on Robotics and Automation*, Vol.6, No.2, 1990, pp.219-231.

[101] Chiou, B.C. and Shahinpoor, M., "Stability Considerations for a Two-Link Force-Controlled Flexible Manipulator", *Proceedings of 1990 IEEE International Conference on Robotics and Automation*, 1990, pp.728-733.

[102] Serna, M.A. and Bayo, E., "Trajectory Planning for Flexible Manipulators", *Proceedings of 1990 IEEE International Conference on Robotics and Automation*, 1990, pp.910-915

[103] Park, J.-H. and Asada, H., "Design and Control of Minimum-Phase Flexible Arms with Torque transmission Mechanisms", *Proceedings of 1990 IEEE International Conference on Robotics and Automation*, 1990, pp.1790-1795.

[104] Cotsaftis, M., "Direct Stability and Control of Deformable and Compliant N-Link Robotic Systems", *Modelling and Control of Compliant and Rigid Motion Systems*, Presented at the Winter Annual Meeting of the ASME, DSC-Vol.31, 1991, pp.39-45.

[105] Thomson, W.T., *Theory of Vibration with Applications*, Prentic-Hall, Inc. 1981.

[106] Hurty, W.C. and Rubinstein, M.F., *Dynamics of Structures*, Prentic-Hall, Inc. 1964.

[107] Kenjo, T. and Nagamori, S., *Permanent-Magnet and Brushless DC Motors*, Clarendon Press, Oxford, 1985.

[108] Han, Y., Li, Z., Liu, M., Sinha, N.K., and Elbestawi, M.A., "Power Balancing and Model Reduction of Linear Conservative Mechanical Systems", *Internal Report*, Dept. of Electrical and Computer Engineering, McMaster University, 1993.

[109] Rozsa, P., Sinha, N.K., Han, Y., and Li, Z., "System Energy Matrix, Output Energy Matrix and Their Application to Model Reduction", *Internal Report*, Dept. of Electrical and Computer Engineering, McMaster University, 1993.

[110] Landau, Y.D., *Adaptive Control: The Model Reference Approach*, Marcell Dekker, Inc. 1979.

[111] Sobel, K.M., *Model Reference Adaptive Control for Multi-Input Multi-Output Systems*, Ph.D. Thesis, Departmental of Computer and Systems Engineering, Rensselaer Polytechnic Institute, 1980.

[112] O'Brien, M.J. and Broussard, R., "Feedforward Control to Track the Output of A Forced Model", *17th IEEE Conference on Desicion and Control*, 1979, pp.1149-1155.

[113] Anderson, D.O. and Moore, J.B., "Linear System Optimization with Prescribed Degree of Stability", *Proceedings of IEE*, Vol.116, No.12, 1969, pp.2083-2087.